Quantum interference phenomena in transport through molecules and multiple quantum dots

D I S S E R T A T I O N

zur Erlangung des
DOKTORGRADES DER NATURWISSENSCHAFTEN (DR. RER. NAT.)
der Naturwissenschaftlichen Fakultät II - Physik
der Universität Regensburg

vorgelegt von
GEORG BEGEMANN *aus* ***REGENSBURG***
im September 2009

Quantum interference phenomena in transport
through molecules and multiple quantum dots

DISSERTATION

Die Arbeit wurde angeleitet von:
Prof. Dr. Milena Grifoni

Promotionsgesuch eingereicht am:
31.07.2009

Prüfungsausschuß:

Vorsitz:	
Erstgutachten:	Prof. Dr. Milena Grifoni
Zweitgutachten:	Prof. Dr. Jens Paaske
Weiterer Prüfer:	

Contents

Chapter 1

Introduction

1.1 Interference of massive particles

Self interference of massive particles is fascinating. In the 1960s, Richard Feynman [1] described it as a phenomenon "which has in it the heart of quantum mechanics," and it didn't lose any of its attraction up to the present day. In fact, when the journal *Physics World* recently asked for suggestions for the most beautiful experiment ever in science [2], Young's original double-slit experiment to demonstrate interference with light from 1804 [3] was ranked among the top 5, but its application to electrons in vacuum [4] was cited more often than any other. In this experiment, a beam of electrons is shot through an apparatus containing an electron biprism which acts as an effective double slit and the electrons are detected at an observation plane. In later experiments, only one electron was in the apparatus at a time [5, 6]. The beauty of these experiments lies in the fact that one can actually observe the emergence of the interference pattern in time as the electrons hit the observation screen one by one. Every electron is detected before the next electron enters the apparatus, such that interactions between the electrons can be excluded as a possible explanation. After 10 or even few 100 electrons, the observed pattern looks more or less random, but after a few thousand electrons, a clear modulation in the intensity on the screen can be seen as a manifestation of single particle interference (Figure 1.1). Since then, particle interference has been demonstrated with neutrons, atoms [7, 8] and molecules as large as carbon-60 [9] and carbon-70 [10]. Mesoscopic rings contacted to leads and threaded by a magnetic flux provide the solid-state analogous of the experiment described above [11, 12].

Interference of electrons in single molecule junctions is a novel effect and has some analogies to interference on double slits. It manifests itself as perfect destructive interference that causes complete blocking of the current through the junction and has been predicted for molecules with discrete rotational symmetry such as benzene or annulene rings. The symmetry assures the presence of degenerate states, to which clockwise and counter-clockwise angular momenta can be assigned, so that the two paths around the molecule exhibit a certain phase difference depending on the arrangement of the contacts. In the last years, this "intramolecular interference" has been inves-

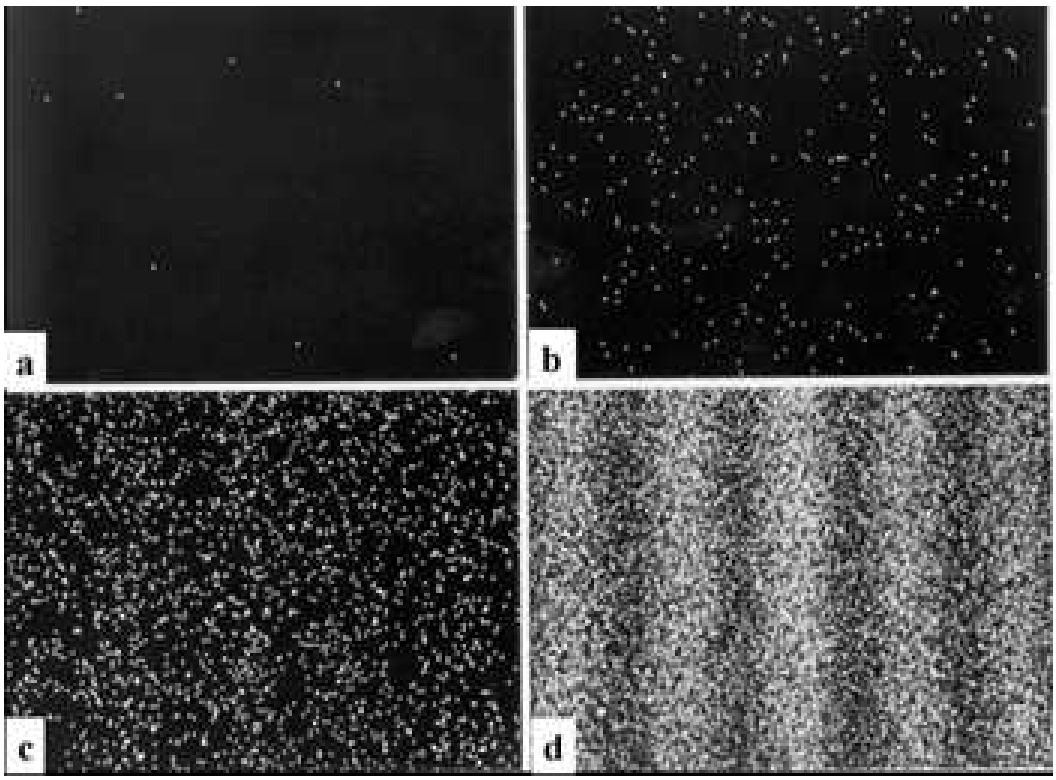

Figure 1.1: Single electron build up of interference pattern over 20 minutes. At the beginning of the experiment, bright spots indicating electrons occur at random positions. When a larger number of electrons is observed, clear interference fringes can be seen. Pattern after (a) 8 electrons; (b) 270 electrons; (c) 2000 electrons; (d) 60,000. Images taken from [6].

tigated by several groups in setups with strong lead molecule coupling, using models [13, 14] or density functional theory [15, 16] to describe the molecule and a Green's functions scattering approach that premises strong lead molecule-coupling to calculate transport properties. In the complementary situation of a molecule weakly coupled to leads, a generalized master equation approach for the reduced density matrix turns out to be more convenient to describe intra-molecular interference [17, 18, 19]. This thesis provides an overview over our work on electron interference effects such as current blocking and negative differential conductance in transport through benzene and multiple quantum dots. The use of interference to obtain control over the molecules (or quantum dots) spin degree of freedom by all-electrical means, a highly desirable property for spintronics and spin based quantum computing applications, is proposed. At this point, it is worth stating that this research on transport through molecules was not driven by the beauty of interference effects. Instead, it was (and still is) motivated by the quest for new electronic devices equipped with new functionalities and based on new materials that provide potential alternatives for the conventional metal oxide semiconductor field effect transistor (MOSFET) technology, which has opened new fields in engineering, applied and fundamental science. One of the most prominent and promising of these new fields is molecular electronics.

1.2 Molecular electronics

The central idea in molecular electronics is to establish electronic devices based on molecular films, groups of molecules or even single molecules. One of the major themes in electronics is therefore to build up electronic circuits in which molecular systems act as conducting elements and to understand or even design the current voltage characteristics of such junctions. These novel molecular building blocks can for example act as switches, gates, rectifiers or memory elements or provide new functions that need to be characterized and understood [20].
Aviram and Ratner were the first to propose a molecular rectifier based on a single organic molecule back in 1974 [21]. However, the field of molecular electronics emerged only after modern nanoscale fabrication techniques made it possible to construct single molecule junctions. In 1997, Reed et al. [22] attributed a current voltage curve measured in a break junction experiment to a single 1,4 benzene dithiol molecule. Since then, huge experimental and theoretical efforts have been made and created a diverse and rapidly growing research field.

1.2.1 Measurements of single molecules

Many experimental techniques are available to measure and control current through molecules. On one hand, there are experiments in which current through a large number of molecules organized in self-assembled, highly ordered films is measured. These films are placed on one electrode and then another electrode is placed on top of it. On the other hand, there are a number of techniques that allow to contact and

to measure the conductance of a single molecule. Since the latter are more related to the subject of this thesis, we will describe some of them here in more detail.

Scanning tunneling microscopy (STM) [23] has played a unique role in the field of molecular electronics. First, it allows to image single molecules lying on conducting substrates or different orbitals of the very same molecule with submolecular resolution. In the same setup, one can measure the current through the molecule as a function of the molecular position. The STM tip can also be used to place metal atoms in contact with a single molecule on the substrate with atomic precision. An open challenge in this approach is to reliably contact the metal atoms and to exclude effects on the conductance coming from the molecule substrate coupling [24]. In other approaches, one end of the molecule is lifted from the substrate by the tip of the STM and current through the molecule from the tip to the substrate can be directly measured. The tip can be pulled away until the contact on one end of the molecule breaks away. Afterwards the tip is lowered again until a new single molecule junction forms. Breaking and forming of contacts is observed in the current as steplike features. The repeating of this cycle (see Figure 1.2) allows the statistical analysis of many single molecule junction measurements in short times. If the STM tip and the substrate are coated with an insulating layer, the sample can be placed in an electrolyte whose surface potential can be controlled with a third electrode, acting as a gate. Metal ions can be introduced to the electrolyte, so that the current through the molecule is controlled by gate induced reversible chemical binding reactions to the metal ions [25]. Also without metal ions, potential control of the electrolyte enables to change the charge state of the molecule [26]. A gate electrode in molecular junctions is in general highly desirable, since it allows to oxidize or reduce the molecule, and three terminal devices can act as spectroscopic tools that allow to determine excitation and addition energies of the molecule.

Therefore, different techniques to fabricate molecular three terminal devices have been delveloped [27] in addition to STM. The *electromigration* technique consists in breaking a narrow and thin metalwire by a large current density to form two physically separated electrodes. The formation of the gap can be imaged using transmission electron spectroscopy. Although some control over the breaking process could be achieved by a feedback mechanism, the resulting geometry or size remains uncontrollable. Advantages of devices made by electromigration on top of Al/Al_2O_3 gate electrodes is the large gate coupling and the planar geometry (see Figure 1.3 (a)) that offers a large stability for systematic studies of effects as functions of gate voltage, magnetic field or temperature. Molecules can be deposited on the sample from solution either before the gap formation or afterwards. If the gap has about the same size as the molecule, the molecules can form chemical bonds to both electrodes. However, in general only few of the prepared samples show signatures of single molecule conductance.

A *shadow mask* technique can be used to evaporate two gold electrodes on top of a gate electrode as illustrated in Figure 1.3(b). If the tilt angle of evaporation is high there is no overlap between the source and drain shadows. Reducing the tilt angle decreases the source drain gap. The advantages of this technique include the ones of the electromigration techniques, in addition one has precise control over the gap size

[28].
Recently, it has been possible to include a gate voltage also in *mechanically controlable break junctions* (MCBJ) experiments [29]. In an MCBJ setup, a thin metallic wire with predefined break points is placed on a substrate. The hole geometry is now bended with a pushing rod so that the wire breaks, see Figure 1.3(c) . The huge advantage of this approach is that the distance of the emerging gap can be controlled with picometer (!) resolution by the pushing rod. The gate coupling, however, is typically orders of magnitude smaller than in the techniques with planar configuration, which makes it difficult to access several charge states of the molecule.
In Figure 1.3(d) a sketch of the *dimer contacting scheme* reported by Dadosh et al. [30] is depicted. In this approach, a dimer structure consisting of two colloidal gold particles connected by a dithiolated molecule is synthesized in solution. This dimer structure can be trapped electrostatically between two gold electrodes (with a gap much larger than the actual size of the molecule) on top of a gate electrode. The advantage of this approach is that it allows to fabricate single molecule devices with high certainty and well defined contacts to the molecule. However, the gold particles screen the gate potential efficiently, and spectroscopic features of the gold particles are sometimes superimposed on the conduction characteristics of the molecule.
With all these methods, molecular junctions have been realized and current-voltage characteristics could be assigned to a single or very few molecules. However, there are a number of problems that have to be overcome to assure future success of the whole field. First of all, the placement of the molecule inside the nanogap between the contacts is basically uncontrolled. A large number of samples have to be prepared to obtain at least a few where the formation of a molecular junction can be identified. Related to this is the problem that the conductance of a molecule depends crucially on its local environment. Still, there is a lack of a technique that can provide reliable and well defined molecule-electrode contacts. Although the molecules themselves can be produced identically in large numbers, visions of building millions of atomically identical electronic devices seem to be doomed because they cannot be fabricated in a controlled way. In this sense there is still a long way to go, or as Fang Chen put it in the summary of her recent review article [24]:

> Future techniques that can fabricate molecular junctions with molecule-electrode contacts that are well defined on the atomic scale and that can characterize the atomic-scale structures of the molecule-electrodes contacts will contribute enormously to the field of molecular electronics.

1.2.2 Theoretical approaches

Similar to the variety of experimental techniques, also a number of theoretical concepts to describe transport through molecular devices have been developed. One one hand, numerical approaches to transport based on the combination of *ab initio* methods like density functional theory (DFT) with nonequilibrium Green's function techniques have become standard to study transport at the nanoscale [31, 32]. These methods

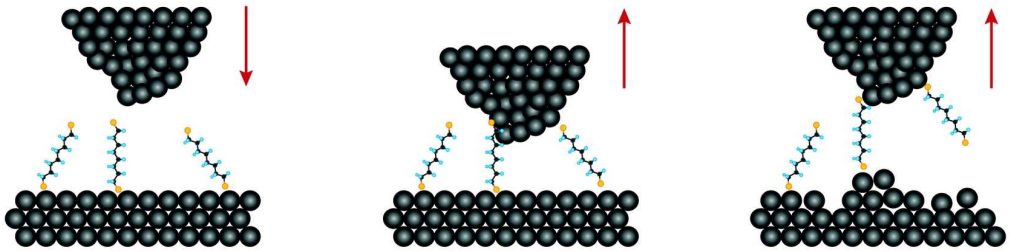

Figure 1.2: Forming and breaking of a molecular junction with an STM tip. The tip is pushed into contact with molecules adsorbed on an electrode. Pulling away the tip subsequently breaks molecular bridges which can be seen as steps in the current. Image taken from [24].

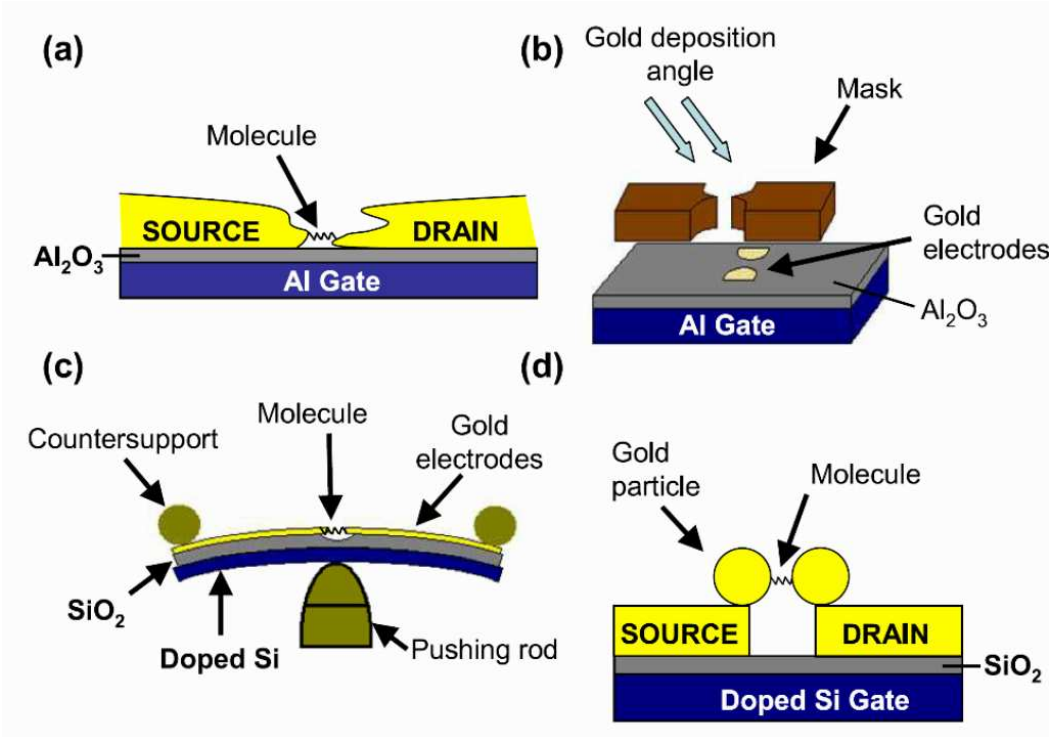

Figure 1.3: Schematic images of different molecular three-terminal device techniques (see text). (a) Electromigrated thin metal wire. (b) Angle evaporation technique. (c) Gate mechanical break junction. (d) The dimer contacting scheme. Image taken from [27].

take into account not only the molecule itself, but also the atomistic structure of lead-molecule interfaces. They are appropriate to investigate quantum transport through molecular bridges strongly coupled to leads. Complex structures with a large number of atoms can be described. However, they fail to describe transport through a molecule weakly coupled to leads, since they are not able to account for effects arising from Coulomb interaction properly. In nanoscale objects with a small number of electrons, this interaction provides the dominant energy scale and therefore plays a crucial role. That is why, on the other hand, approaches to transport are used that explicitly incorporate the Coulomb interaction in the molecule. Powerful many-body techniques such as the numerical renormalization group (NRG) or the density matrix renormalization group (DMRG) scheme have been developed and applied to the problem of quantum transport. They can treat a broad parameter regime ranging from weak and to lead-molecule coupling. However, only very simple models with a limited number of degrees of freedom can be investigated with these techniques because of the complexity and the rather large computational costs of these methods.
In semi-quantitative approaches, a realistic model for the molecule that includes the degrees of freedom relevant for a particular molecule and transport situation is considered. Specific features in the current voltage characteristics such as Coulomb blockade, spin blockade, the Franck-Condon effect or negative differential conductance are related to very different excitations, that can be of electronic or vibrational nature. In the weak lead-molecule tunneling limit, one calculates the eigenstates of the model for the isolated molecule and essentially considers them unperturbed by the contact to the leads. With this approach, one tries to cope with the complexity of real molecules as well as with the Coulomb interaction, at the cost of a limited ability to describe intermediate or strong lead-molecule coupling. At the simplest level, transport is described in terms of transition rates between molecular states, where the lead-molecule coupling is treated perturbatively, yielding so called Pauli rate equations. In more general approaches, also coherences between molecular states are taken into account. In chapter 3, we provide a technical derivation of the equations for the latter case. The application to molecular systems includes e.g. the works [33, 34, 35, 36, 37]. Drawbacks of such approaches are that details of the lead-molecule interface can usually not be taken into account and these models can have a large number of parameters, which in general is not desirable.
Thus, the main challenges in molecular electronics are on the experimental side to provide well defined molecule-electrode contacts, and on the theoretical side to improve the limited correspondence between experimental and theoretical studies. Of course, the support of new ideas to drive the design of molecular junctions with novel functionalities is a main task for all scientists working in the field.

1.3 Spintronics and spin-qubit applications

Until recently, the spin of the electrons was ignored in mainstream charge-based electronics. In spintronics, the spin degree of freedom is either brought into play in combination with the charge of the electrons or used exclusively in new devices, that have

many potential advantages such as nonvolatility, increased data processing speed, decreased electric power consumption and increased integration densities. To realize such devices, technical issues such as spin injection or the control, manipulation and detection of spin polarization and spin currents have to be resolved [38, 39]. Within this work, we address possible solutions of some of these tasks.
In particular, quantum dots can be used for spin-based quantum computation. The unit of information in quantum computing, a quantum bit (qubit) can be formed in principle by any quantum mechanical two level system. In analogy to the classical bit, two states, denoted as $|0\rangle$ and $|1\rangle$ are required. The possibility to form coherent superpositions of these basis states allows the application of new algorithms that exceed classical algorithms in performance by far (polynomial instead of exponential scaling) for some problems [40]. In spin based qubits, the two possible values of the S_z component of the electron spin form the basis. In quantum dots (based on single molecule junctions or made from other materials), the electron number can be precisely controlled and, more important, they provide the possibility of coherent manipulation of single spins, the essential mechanism in spin based quantum bits. Electric control of the spin is particularly appealing, because electric fields are easy to generate locally in contrast to magnetic fields [41]. It can be realized either via a mechanism that takes advantage of the spin orbit-coupling [41, 42, 43, 44, 45] or of tunneling-induced spin splitting in the Kondo regime [46].
In this thesis, we propose a new mechanism for all-electric spin control that relies on the current blocking occurring in single molecule based quantum dots due to interference between degenerate states [19].

1.4 Thesis outline

The outline of this thesis is as follows: In chapter 2, we introduce the Pariser-Parr-Pople model for conjugated molecules and adopt it to the physics of benzene. The numerical treatment of the model is described shortly. In chapter 3, we discuss elementary physics in quantum dots and we introduce the theoretical framework based on a generalized master equation (GME) for the reduced density matrix to describe transport through quantum dots or molecules weakly coupled to leads. In chapter 4, we present the results of our transport calculations for benzene. The concept of interference single electron transistors (ISETs) is introduced. We also discuss the robustness of interference effects. In chapter 5, we propose the use of interference blockade in ISETs to obtain control over the molecules (or quantum dots) spin degree of freedom by all-electrical means. In chapter 6, we leave the sequential tunneling regime and develop a simple theory based on the T-matrix formalism to describe cotunneling processes in quantum dots.

Chapter 2

The Pariser-Parr-Pople (PPP) model for conjugated molecules

In transport through molecules, signatures in the current or differential conductance are directly related to the electronic spectrum of the isolated molecule. The full Hamiltonian of such a molecule, however, is by far too complicated to deal with analytically, and therefore simpler models have to be derived, reflecting the relevant properties of the molecule.
In the 1950s, Pariser and Parr [47] and Pople [48] developed a model for the π-electron system of hydrocarbon molecules. It was derived starting from the complete many-body Hamiltonian and using a set of systematic approximations to separate the electronic from the nuclear motion and subsequently eliminate the σ-part of the electronic system, which is considered to determine the backbone of the molecule and not to participate in transport. Linderberg and Öhrn rederived this model in second quantization in 1968 [49]. Recently [33], Hettler et al. were the first to use this model to calculate the I-V-characteristics of a benzene junction.

2.1 Derivation of the Pariser-Parr-Pople model

In the following, we give a short overview of the derivation of the Pariser-Parr-Pople (PPP) model for benzene.
The general Hamiltonian for a molecule is

$$H = T^n(\{\mathbf{R}_\alpha\}) + T^e(\{\mathbf{r}_i\}) + V^{n-n}(\{\mathbf{R}_\alpha\}) + V^{e-n}(\{\mathbf{R}_\alpha\},\{\mathbf{r}_i\}) + V^{e-e}(\{\mathbf{r}_i\}), \quad (2.1)$$

where $\{\mathbf{R}_\alpha\},\{\mathbf{r}_i\}$ denotes the set of coordinates for the nuclei and for the electrons, respectively. T^n, T^e are the kinetic parts of the nuclei and electrons, and V^{n-n}, V^{e-n} and V^{e-e} are the potential terms due to the Coulomb interaction between the nuclei and electrons. We separate the motion of the nuclei from the electronic problem (Born-Oppenheimer approximation) by factorizing the wavefunction in an electronic and a nuclear part:

$$\Psi(\{\mathbf{R}_\alpha\},\{\mathbf{r}_i\}) = \chi(\{\mathbf{R}_\alpha\})\phi(\{\mathbf{R}_\alpha\},\{\mathbf{r}_i\}). \quad (2.2)$$

In particular, we assume that $T^n(\{\mathbf{R}_\alpha\})\phi(\{\mathbf{R}_\alpha\},\{\mathbf{r}_i\}) \approx 0$ and therefore an effective (so called Born-Oppenheimer) Hamiltonian for the electronic problem can be derived that does not contain T^n. Moreover, we have to consider the specific form of the molecular system to be investigated. Within the PPP-model, the focus is on molecules which consist of carbon and hydrogen atoms. We consider the inner core electrons of carbon as strongly bound to the nuclei. We thus forget about their dynamics and concentrate on the four valence electrons of carbon. Three of them are in sp^2-hybrid orbitals in one plane, symmetrically arranged so that the angle between two orbitals is 120 degrees. These orbitals point in the direction of the neighboring (either carbon or hydrogen) atom and overlap with the corresponding orbital of this atom. Such molecular bonds between s- and p-hybrid orbitals, where the orbitals point along the connecting axis, are called σ-bonds, the electrons in the orbitals σ-electrons. The one remaining valence electron is in a p-orbital perpendicular to the molecular plane. Orbitals of neighboring atoms also overlap to form bonds, but the binding is different and is called π-bond. Accordingly, we call these electrons π-electrons. In the PPP-model, the σ-electrons together with the core electrons play the role of screening the Coulomb interactions between the π-electrons and between the π-electrons and the nuclei, which are dressed with the $1s$ core electrons and with the σ-electrons. The electronic problem we are dealing with then reads

$$[T^\pi + V^{\pi-ion} + V^{\pi-\pi} + V^{ion-ion}]\ \tilde{\phi}(\{\mathbf{R}_\alpha\},\{\mathbf{r}_i\}) = E_{el}\ \tilde{\phi}(\{\mathbf{R}_\alpha\},\{\mathbf{r}_i\}), \tag{2.3}$$

where $V^{\pi-ion}$, $V^{\pi-\pi}$ and $V^{ion-ion}$ are effective potentials that model the interaction between π-electrons and the ions, which consist of the nuclei plus the core and σ-electrons. The positions of the nuclei $\{\mathbf{R}_\alpha\}$ enter only as parameters in $\tilde{\phi}$. The Hamiltonian in equation (2.3) provides thus a model for the π-electron system of the molecule in the limit of one p_z-orbital per carbon atom, which can be occupied by at most two electrons with opposite spins (see Figure 2.1). In general, the explicit form of the effective potentials is not taken into account in π-electron models. Instead they are parametrized to fit experiments (see section 2.2). In second quantization, this Hamiltonian for the many-electron problem of the molecule can be written as

$$\begin{aligned} H = &\sum_{i,j=1}^{M}\sum_{\sigma}\left(T^\pi_{ij\sigma}d^\dagger_{i\sigma}d_{j\sigma} + V^{\pi-ion}_{ij\sigma}d^\dagger_{i\sigma}d_{j\sigma}\right) \\ &+\sum_{ij}\sum_{\sigma\sigma'}V^{\pi-\pi}_{ijkl\sigma\sigma'}d^\dagger_{i\sigma}d^\dagger_{j\sigma'}d_{k\sigma'}d_{l\sigma} + V^{ion-ion}, \end{aligned} \tag{2.4}$$

where $d^\dagger_{i\sigma}$, $d_{j\sigma}$ are creation or annihilation operators for π-electrons on site i or j and $\sigma = \uparrow, \downarrow$ is the spin degree of freedom. M is the number of carbon atoms or sites.
In the spirit of the jellium model, we now approximate each ion to be a hole with the same spatial symmetry as the electron. More explicitly, we define the charge density operator $\rho(\mathbf{r})$ to be

$$\rho(\mathbf{r}) = \sum_{i,j=1}^{M}\left[\sum_{\sigma} p_z^*(\mathbf{r}-\mathbf{R}_j)p_z(\mathbf{r}-\mathbf{R}_i)d^\dagger_{j\sigma}d_{i\sigma} - |p_z(\mathbf{r}-\mathbf{R}_i)|^2\delta_{ij}\right], \tag{2.5}$$

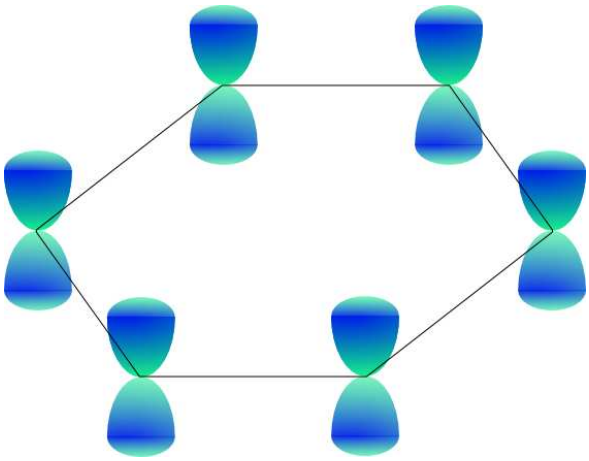

Figure 2.1: The relevant orbitals for the PPP-model in benzene

where the second term describes holes at the positions $\mathbf{R}_i$ with the spatial structure of p_z-orbitals in carbon atoms. We can thus rewrite the Hamiltonian (2.4) in the approximated form:

$$H = T + V,$$

where T is the kinetic term and

$$V = \int\int d\mathbf{r}_1\, d\mathbf{r}_2 \rho(\mathbf{r}_1) \frac{e^2}{4\pi\epsilon_0 |\mathbf{r}_1 - \mathbf{r}_2|} \rho(\mathbf{r}_2). \tag{2.6}$$

The definition of V includes in principle multicentered integrals. In the approximation of two center integrals we obtain the Pariser-Parr-Pople (PPP) Hamiltonian for an isolated molecule:

$$\begin{aligned} H &= b \sum_{i=1}^{M} \sum_{\sigma} \left(d_{i\sigma}^{\dagger} d_{i+1\sigma} + d_{i+1\sigma}^{\dagger} d_{i\sigma} \right) + U \sum_{i=1}^{M} \left(n_{i\uparrow} - \frac{1}{2} \right) \left(n_{i\downarrow} - \frac{1}{2} \right) \\ &\quad + \frac{1}{2} \sum_{i \neq j} V_{ij} \left(n_{i\uparrow} + n_{i\downarrow} - 1 \right) \left(n_{j\uparrow} + n_{j\downarrow} - 1 \right), \end{aligned} \tag{2.7}$$

where we have introduced the parameters b, U and V_{ij}. Additionally $n_{i\sigma} = d_{i\sigma}^{\dagger} d_{i\sigma}$ is the electron number operator for the orbital on site i with spin σ. The single-particle contribution b is defined as

$$\begin{aligned} b &= \int\int d\mathbf{r}_1 d\mathbf{r}_2 \frac{e^2}{4\pi\epsilon_0} \frac{p_z^*(\mathbf{r}_1) p_z(\mathbf{r}_1 + \mathbf{d}) \left(|p_z(\mathbf{r}_2)|^2 + |p_z(\mathbf{r}_2 + \mathbf{d})|^2 \right)}{|\mathbf{r}_1 - \mathbf{r}_2|} \\ &\quad + \int d\mathbf{r}_1 p_z^*(\mathbf{r}_1) \frac{(-\bigtriangledown)^2 \hbar^2}{2m} p_z(\mathbf{r}_1 + \mathbf{d}), \end{aligned} \tag{2.8}$$

where $\mathbf{d}$ is the vector pointing to the next neighboring site. If two electrons are on the same site, they must have different spin due to the Pauli principle. This is why the

on-site Coulomb interaction (the U-term) only involves electrons with opposite spin. It reads

$$U = \int\int d\mathbf{r}_1 d\mathbf{r}_2 \frac{e^2}{4\pi\epsilon_0} \frac{|p_z(\mathbf{r}_1)|^2 |p_z(\mathbf{r}_2)|^2}{|\mathbf{r}_1 - \mathbf{r}_2|}. \tag{2.9}$$

Finally, the intersite Coulomb interaction (V_{ij}-term) is between electrons on different sites independent of the electron spin. It has the form

$$V_{ij} = \int\int d\mathbf{r}_1 d\mathbf{r}_2 \frac{e^2}{4\pi\epsilon_0} \frac{|p_z(\mathbf{r}_1)|^2 |p_z(\mathbf{r}_2 + \mathbf{d}_{ij})|^2}{|\mathbf{r}_1 - \mathbf{r}_2|}, \tag{2.10}$$

where $|\mathbf{d}_{ij}|$ is the distance of two carbon atoms and can be estimated by the $C-C$ bond length ($1.4\mathring{A}$) and the geometry of the molecule. In this work, we want to calculate transport properties of the molecule in a three terminal setup. Therefore, we include the effect of a gate electrode into this model. The energy shift due to the gate is assumed to be linear in the gate voltage and proportional to the number of electrons N on the system:

$$H_{gate} = N\left(\mu_0 - e\kappa V_g\right) = \xi \sum_{i=1}^{M} \sum_{\sigma} d_{i\sigma}^{\dagger} d_{i\sigma}, \tag{2.11}$$

where κ is a conversion factor, and the zero of ξ is defined as the point where the gate voltage is equal to the equilibrium chemical potential μ_0 of the leads. Eventually, we arrive at the final definition for the PPP-Hamiltonian $H_{\mathrm{PPP}} = H + H_{gate}$:

$$\begin{aligned} H_{\mathrm{PPP}} &= \xi \sum_{i=1}^{M} \sum_{\sigma} d_{i\sigma}^{\dagger} d_{i\sigma} + b \sum_{i=1}^{M} \sum_{\sigma} \left(d_{i\sigma}^{\dagger} d_{i+1\sigma} + d_{i+1\sigma}^{\dagger} d_{i\sigma}\right) \\ &+ U \sum_{i=1}^{M} \left(n_{i\uparrow} - \frac{1}{2}\right)\left(n_{i\downarrow} - \frac{1}{2}\right) + \frac{1}{2} \sum_{i \neq j} V_{ij} \left(n_{i\uparrow} + n_{i\downarrow} - 1\right)\left(n_{j\uparrow} + n_{j\downarrow} - 1\right). \end{aligned} \tag{2.12}$$

In solid state theory, a formally equivalent Hamiltonian with nearest neighbor hopping, on-site and intersite Coulomb interaction is also known as the extended Hubbard model.

2.2 The parameters of H_{PPP}

Typically, the parameters b and U are not explicitly calculated. Instead, the parametrization of the PPP model is optimized by fitting its prediction to the known experimental excitation energies of benzene in the gas phase. Bursill et al. [50] estimated U and b to be 10.06eV and -2.539eV, respectively. Other groups find slightly different values [51, 52], but in the same order of magnitude. For the intersite interaction, an interpolation between long range $1/r$ behavior and short range behavior which models the shape of the atomic orbitals is made. One example of such an interpolation is the Ohno parametrization [53]

$$V_{ij} = \frac{U}{\sqrt{1 + \alpha |\mathbf{d}_{ij}|^2}}, \tag{2.13}$$

where $\alpha = \left(\frac{4\pi\epsilon_0 U}{e^2}\right)^2$, thus ensuring that $V_{ij} \to \frac{e^2}{4\pi\epsilon_0 |\mathbf{d}|_{ij}}$ as $|\mathbf{d}_{ij}| \to \infty$.
Experiments on organic molecules have shown that the so-called addition energy, which is the difference between the ionization potential and the electron affinity, is heavily reduced in single-molecule junctions compared to its gas phase value [54, 55, 28]. This observation is attributed to a screening of the Coulomb repulsion on the molecule due to the polarizable environment, namely the metallic leads and also the dielectric substrate that forms the base in many single-molecule junctions. Kaasbjerg et al. gave a quantitative estimate of this effect for an OPV-5 molecule in a single molecule junction, and showed that the reduction of the addition energy is not only due to this effect, but also due to a closing of the HOMO-LUMO gap in polarizable environments [56]. Accordingly, we expect a reduction of the parameters of H_{PPP} compared to their gas phase value, in particular of the on-site interaction U.

2.3 Numerical diagonalization of H_{PPP}

Since for every site there are four different possible configurations ($|0\rangle$, $|\uparrow\rangle$, $|\downarrow\rangle$, $|\uparrow\downarrow\rangle$), the Fock space has the dimension 4^M ($= 4096$ for benzene), which requires in general a numerical treatment. In this section, we describe briefly how to represent both the states and the operators in an organized and manageable way that allows book-keeping of the states and can be implemented numerically. Any state in the localized basis can be written as a series of creation operators acting on the vacuum state $|0\rangle$. The anti-symmetry of this wave-function is assured by the fermionic commutation relations of the operators. The ordering of the operators has to be established to define the states uniquely. Conventionally, we order the operators first by their spin index and then by their site index, so that for a generic state with three spin up and three spin down electrons

$$d^\dagger_{i\uparrow} d^\dagger_{j\uparrow} d^\dagger_{k\uparrow} d^\dagger_{i'\downarrow} d^\dagger_{j'\downarrow} d^\dagger_{k'\downarrow} |0\rangle, \tag{2.14}$$

$i < j < k$ and $i' < j' < k'$. This state can be as well represented in occupation number representation (see Table 2.1) as a vector with $2M$ entries $v_{i\sigma}$, where the first M entries $n_{i\uparrow}$ correspond to the spin up orbitals at site 1 to M and the entries $M+1$ to $2M$ to the spin down orbitals. $n_{i\sigma}$ can either be 1, if there is an electron created in this orbital, or 0 if there is no electron. The above state (let's say for example $M = 6$, $\{i, j, k\} = \{2, 3, 5\}$ and $\{i', j', k'\} = \{1, 3, 5\}$), would have $n_{2\uparrow} = n_{3\uparrow} = n_{5\uparrow} = 1$ and $n_{1\downarrow} = n_{3\downarrow} = n_{5\downarrow} = 1$. In Dirac notation it would read $|011010101010\rangle$. The states can most easily be labeled with a unique key number by transforming the "binary" number $n_{1\uparrow} \ldots n_{6\uparrow} n_{1\downarrow} \ldots n_{6\downarrow} = 011010101010$ into an decimal number, in this case

$$0 \cdot 2^0 + 2^1 + 0 \cdot 2^2 + 2^3 + 0 \cdot 2^4 + 2^5 + 0 \cdot 2^6 + 2^7 + 0 \cdot 2^8 + 2^9 + 2^{10} + 0 \cdot 2^{11} = 1706. \tag{2.15}$$

In this way, every state in the localized basis can be encoded in an integer number from 0 to $4^M - 1 = 2^{2M} - 1$. This number can be used for book-keeping. The impact of any operator that consists of combinations of creation and annihilation operators on these states can easily be described, just by taking into account the fermionic commutation relations, so that we obtain the matrix representation of these operators (e.g. H_{PPP},

Slater determinant:	$d^\dagger_{2\uparrow} d^\dagger_{3\uparrow} d^\dagger_{5\uparrow} d^\dagger_{1\downarrow} d^\dagger_{3\downarrow} d^\dagger_{5\downarrow} \lvert 0\rangle$					
occupation numbers:						
site i:	1	2	3	4	5	6
$n_{i\uparrow}$:	0	1	1	0	1	0
$n_{i\downarrow}$:	1	0	1	0	1	0
binary:	011010101010					
key:	1706					

Table 2.1: Different representations of a localized state

$d^\dagger_{i\sigma}$, $d_{i\sigma}$) in the localized basis. Since the Hamiltonian conserves the particle number and the z-component of the spin, it is convenient to sort the states according to these quantum numbers, to obtain a block structure in the matrices. Afterwards, the Hamiltonian can be diagonalized with the help of standard software packages (Matlab, LAPACK, etc.) and all other operators are transformed to the eigenbasis.

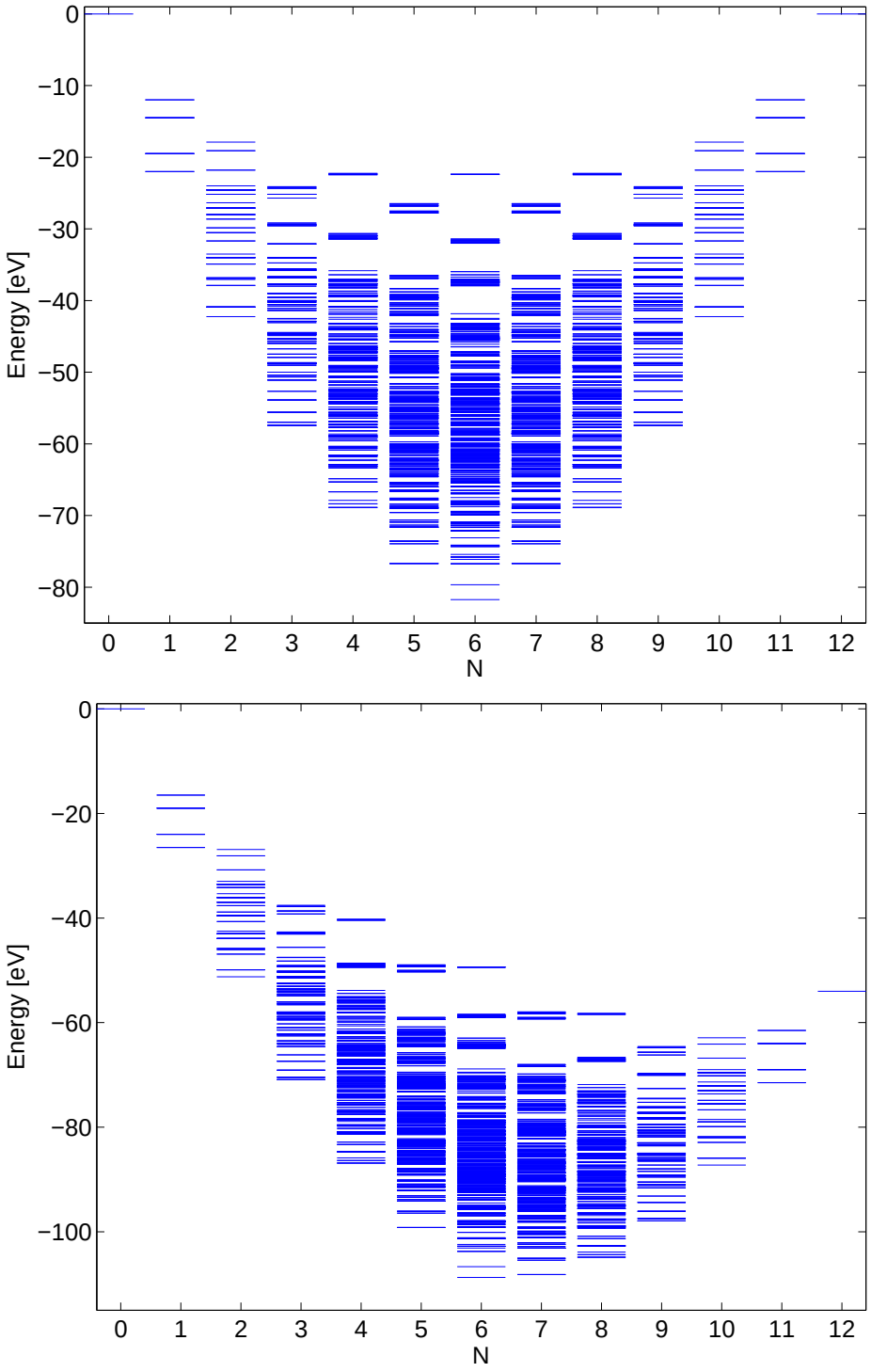

Figure 2.2: Spectrum of H_{PPP} calculated for the parameters $U = 10eV$, $b = -2.5eV$. Only nearest-neighbor intersite interaction is taken into account with the value $V = 6eV$. The states are sorted according to their particle number on the x-axis. For $N = 6$, the π-electron system is filled and the molecule is neutral. Upper panel: Spectrum for $\xi = 0$. Lower panel: Spectrum for $\xi = -4.5eV$. This demonstrates the influence of a gate electrode on the spectrum of the molecule. The energies of states with different particle numbers are shifted with respect to each other.

Chapter 3

Transport through interacting quantum dots

Quantum dots are small electronic islands in which the motion of the electrons is confined in all three spatial directions. Due to the small (nanometer) length scales, the Coulomb interaction between the electrons becomes important and gives rise to intricate effects in experiments where electron transport through the island is studied. In this chapter, we introduce the physics of Coulomb-blockade in quantum dots, which is needed to understand the results of this work discussed in later chapters.
Quantum dots have been realized in several different ways, for example in semiconductor heterostructures, where metallic electrodes could be defined on top of a two dimensional electron gas, or in other approaches, where carbon nanotubes or single molecules were used to bridge the gap between two leads. Molecules are characterized by a discrete vibrational spectrum, which can serve as a fingerprint of the molecule in the current-voltage characteristics obtained in single-molecule junctions [55]. However, the interplay between electronic and vibrational degrees of freedom is not the topic of this thesis. Instead, we focus on transport through nanoscale objects with a rather complex electronic spectrum (see e.g. Figure 2.2) that can be attributed either to a molecule or for example to a complex multiple quantum dot structure, and discuss effects arising from the electronic problem only.

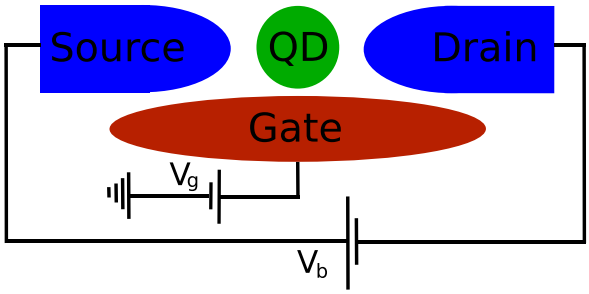

Figure 3.1: Sketch of a quantum dot setup. The quantum dot (QD) is weakly contacted to source and drain leads and capacitively coupled to a gate electrode.

3.1 Quantum dot physics

3.1.1 Sequential tunneling - Coulomb blockade

In a typical setup, one has source and drain leads with a continuous density of states weakly coupled to central conducting system with a discrete energy spectrum, usually called "quantum dot," the latter capacitively coupled to a gate electrode, see Figure 3.1. Weak coupling means that electrons can tunnel between leads and dot, but it implies also that the time between two tunneling events is large compared to the duration of a tunneling event, so that the number of electrons N on the dot is well defined. This regime is called sequential tunneling regime. Quantum dot devices are often called "single electron transistors", because the underlying physics can be understood in terms of single electron tunneling events. This is not to say that quantum dots can be described within a single-particle picture, because the Coulomb interaction, which is an archetypal example of a many-body interaction, plays a crucial role in these systems.
To understand if a tunneling process is possible, we have to take into account Pauli's exclusion principle and to analyze the energetics of the overall system before and after the tunneling. Essentially, the energy is conserved by the tunneling.
We label the states in the spectrum of the dot with the particle number N and with a running index $i = 0, 1, 2...$ for each particle number, so that E_0^N is the N-particle ground state, E_1^N is the first excited state, and so on. Consider now the situation where the dot is in the N-electron ground state before the tunneling event. The (non-interacting) leads are filled with electrons up to their Fermi energy $E_{s/d}^F$ which coincides with the electrochemical potential $\mu_{s/d}$ at zero temperature. An electron with energy $\epsilon \leq E_\alpha^F$ from lead α can tunnel in the $N+1$-particle ground state on the dot, when the condition $E_0^{N+1} - \epsilon = E_0^N$ is fulfilled. It is now convenient to introduce the $N+1$-particle chemical potential of the dot as $\mu^{N+1} = E_0^{N+1} - E_0^N$. The condition for adding one more electron in a quantum dot with N-particles from a lead with Fermi energy E_α^F reads then

$$E_\alpha^F \geq \mu^{N+1}. \tag{3.1}$$

To realize electron transport through a quantum dot, electrons must be able to tunnel onto the dot from one lead (lets say source) and to tunnel out into some unoccupied state in the other (drain) lead. Under the constrictions that the tunneling out process requires unoccupied states above the Fermi energy in the leads, and that the tunneling process is elastic, we find the condition to go from the $N+1$- to the N-particle ground state by tunneling out in the drain as $\mu^{N+1} \geq E_d^F$. The leads will relax into the thermal equilibrium configuration very fast, in any case before the next tunneling event will take place. The condition to transport an electron from source to drain lead at zero temperature therefore reads

$$E_s^F \geq \mu^{N+1} \geq E_d^F. \tag{3.2}$$

If this condition is fullfilled, one can speak of a transport channel available in the bias window. A sketch of the chemical potentials of leads and dot in a blockade situation and at resonance where current can flow is given in Figure 3.2.

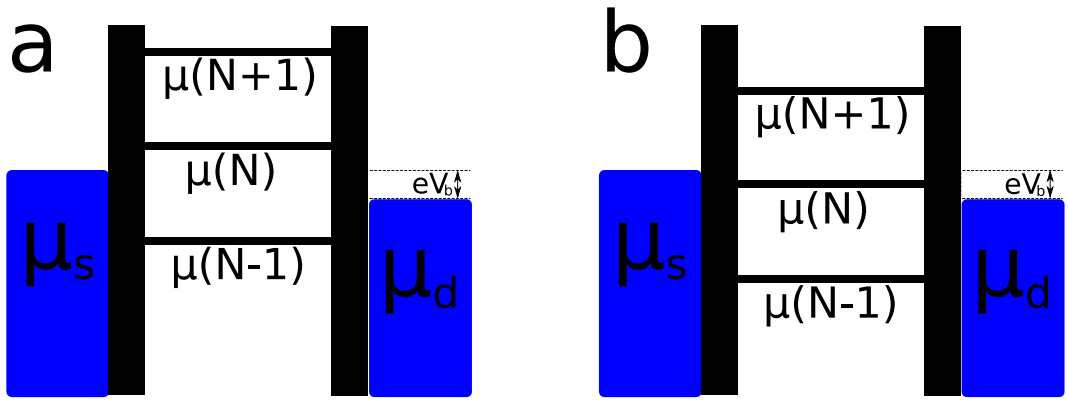

Figure 3.2: Sketch of the electrochemical potentials of leads and dot. In a blockade situation, the N-particle chemical potentials of the dot are not in the transport window between μ_s and μ_d (panel a). This can be achieved by varying a gate voltage (panel b). In this situation, current from the source to the drain lead can flow as a series of sequential tunneling events where the electron number on the dot changes back and forth between N and $N-1$.

As it can be seen from the definition of H_{gate} in equation (2.11), the chemical potential of the dot is linear in the gate voltage V_g. The Fermi energy of the leads, on the other hand, can be shifted by the bias voltage V_b. For convenience, we always split the bias symmetrically, such that the Fermi energy of the source is by $\mu_0 + \frac{V_\mathrm{b}}{2}$, the one of the drain by $\mu_0 - \frac{V_\mathrm{b}}{2}$. Thus, the conditions $E_s^F = \mu^{N+1}$ and $\mu^{N+1} = E_d^F$ can be represented by two lines with slope $\pm 2\kappa V_\mathrm{g}$ that cross each other at the point

$$V_\mathrm{g} = \frac{E_0^{N+1}(\xi = 0) - E_0^N(\xi = 0)}{e\kappa}, \quad V_\mathrm{b} = 0 \tag{3.3}$$

in a V_b-V_g-plot. Together with similar conditions from situations where the dot is filled with a different number of electrons, one gets a diamond-shaped pattern. Inside the diamonds, transport is blocked and the electron number can not change. On the outside, current can flow as a series of sequential tunneling events that change the number of electrons on the dot by ± 1. The current-voltage characteristics of quantum dots are typically presented in such "charge stability diagrams," where the current is color-coded and plotted against both gate and bias voltage. Very often the differential conductance dI/dV is plotted instead of the current. The resulting graph is called "stability diagram." The width of a diamond on the V_g-axis depends on the gate coupling factor κ. However, since also the slope of the lines depends on this factor, the height of the diamonds depends on the energy spectrum of the quantum dot only and not on external coupling parameters. In particular, the N-particle addition energy U^N can be assigned to the height of the N-particle diamond divided by the charge quantum e. U^N is defined as the difference of the ionization potential $\mathrm{IP} = E_0^{N-1} - E_0^N = -\mu^N$ and the electron affinity $\mathrm{EA} = E_0^N - E_0^{N+1} = -\mu^{N+1}$ and can be expressed as

$$U^N = \mathrm{IP} - \mathrm{EA} = E_0^{N+1} + E_0^{N-1} - 2E_0^N. \tag{3.4}$$

In this way, current measurements as a function of both gate and bias voltage act as spectroscopic tool and provide detailed information about the central quantum dot system. The fact that $\mu^{N+1} > \mu^N$ and that one therefore sees consecutive diamonds in the stability diagram is a consequence of the Coulomb repulsion of the electrons. That is why the diamond structures we discussed above are referred to as Coulomb diamonds. The energy needed to fill the quantum dot with one more electron is called addition energy.
Within the so-called "constant interaction model", the addition energy is associated with the charging of a capacitor and given by the classical expression

$$E_C = \frac{e^2}{2C}, \tag{3.5}$$

where C is the capacitance of the device. As such E_C is known as charging energy. This model yields a diamond structure where all diamonds have the same height and width, given that the single-particle level spacing $\Delta(N)$ is negligible compared to E_C. It works well for metallic and semiconducting quantum dots containing a large number of electrons. Sometimes, e.g. for nanotubes, this model is extended to incorporate also the discreteness of the single particle level spacing, which yields diamonds of different sizes $E_C + \Delta(N)$. In benzene however, the complicated interplay between electron hopping, on-site and intersite electron interaction makes it impossible to estimate the electronic spectrum just by taking into account the constant interaction model on top of the single-particle spectrum. We find that apart from the particle-hole symmetry, no regularities in the diamonds can be observed and that all the diamonds have different sizes. We keep in mind though, that Coulomb interaction and charging of the molecule leads to the characteristic diamond pattern.
At zero temperature, the chemical potential in the leads coincides with the energy of the highest occupied state, the Fermi energy. At finite temperatures, this is no longer true, since there are occupied states in the leads in an energy range of a few k_BT above the chemical potential and unoccupied states in the same range below the chemical potential. To observe Coulomb blockade effects, the temperature must be so small that the energy scale k_BT associated with the temperature is much smaller than the addition energies U^N. If this is true, it is convenient to express the condition for transport not in terms of the Fermi energy, but in terms of the chemical potential of the leads:

$$\mu_s \gtrsim \mu^{N+1} \gtrsim \mu_d, \tag{3.6}$$

where the $\gtrsim$ symbol indicates that the onset of transport is already a few k_BT before the actual resonance. At zero temperature, the current-voltage curve would increase step-like ("Coulomb staircase") when a new channel enters the bias window, resulting in $\delta-$like peaks in the differential conductance. At finite temperatures these steps are smeared out (the peaks in the dI/dV are broadened) over an energy range of $\sim k_BT$.
So far, only ground state transitions have been considered. Of course, a sequential tunneling process can as well involve one or more excited states. Again, one has to compare the energies of the system before and after the tunneling. Defining a generalized $N+1$-particle chemical potential as $\mu_{ij}^{N+1} = E_i^{N+1} - E_j^N$, one finds that

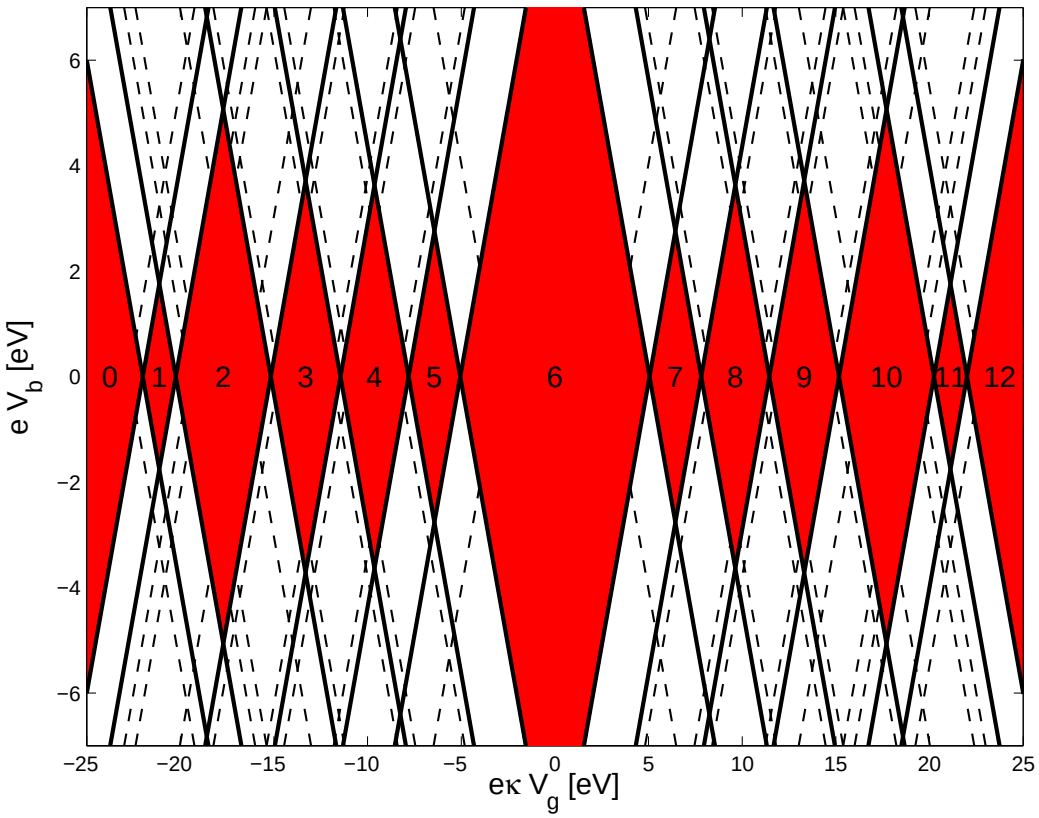

Figure 3.3: Charge stability diagram obtained for benzene with the parameters as used in Figure 2.2. Only ground states and first excited states are included. Ground state transitions mark the borders of the the red diamonds. Inside, no current can flow and the charge on the dot is stable. The six-electron diamond around zero gate voltage, corresponding to the neutral molecule, is by far the largest.

a tunneling process from an N-particle state with energy E_j^N to an $N+1$-particle state with energy E_i^{N+1} is possible if $\mu_s \gtrsim \mu_{ij}^{N+1}$ and the reverse process is possible if $\mu_{ij}^{N+1} \gtrsim \mu_d$. In stability diagrams, one can therefore see additional lines indicating peaks in the dI/dV that correspond to transitions between excited states. These lines cross the borders of the charge diamonds, however, they are not seen inside, because inside the diamonds only groundstates can be populated. This can be understood by the following argument: Imagine that one has prepared the quantum dot in an excited N-particle state with energy E_j^N and the bias voltage is zero, meaning that $\mu_s = \mu_d = \mu_0$. Now, after two consecutive tunneling events (from E_j^N to $E_i^{N\pm1}$ and then from $E_i^{N\pm1}$ to $E_{j'}^N$), the dot will be in a state with energy $E_{j'}^N$, with $j' \leq j$. This follows from the conditions (for the case from going to $N+1$) $\mu_s \geq \mu_{ij}^{N+1}$ and then $\mu_s \leq \mu_{ij'}^{N+1}$, which implies $\mu_{ij'}^{N+1} \geq \mu_{ij}^{N+1}$ and therefore $j' \leq j$. In general, tunneling events can only decrease the energy of the central system with respect to the Fermi energy of the leads. In other words, even if the quantum dot is in an excited state at some initial time, consecutive tunneling events that do not contribute to the stationary current (one can also think of other relaxation processes) will bring it into the ground state, from where sequential tunneling is energetically forbidden at small bias values. Only if the bias is high enough so that current can flow, this will lead to a finite average population of excited states if the condition $\mu_s \geq \mu_{ij}^{N+1}$ is fulfilled, and the lines indicating this condition in the stability diagram will be observed in a measurement.
The charge stability diagram of benzene with the parameters as in Figure 2.2 is shown in Figure 3.3. For clarity, only groundstate transitions and groundstate-first excited state transitions are taken into account. The latter are only visible outside the stable Coulomb diamonds.

3.1.2 Cotunneling

When the coupling between quantum dots and leads becomes stronger, the time between two tunneling events decreases. At some point, two or more tunneling events overlap, and these so-called cotunneling events cannot be regarded as consecutive individual tunneling processes. In a cotunneling process, an electron tunnels in or out the dot, leaving the dot in an intermediate virtual state, which can have a higher energy than the initial state. From this intermediate state, the dot changes back into the state where it was before or to any other energetically accessible state. Cotunneling of two electrons can leave the number of electrons on the quantum dot unchanged, or change it by ± 2. Furthermore, cotunneling can be either elastic or inelastic. Elastic means that the energies of the initial and final electron states in the leads are the same, inelastic means that these energies are different. In the latter case, this energy has been transferred to the dot and leaves it in an excited state. In quantum dots, this energy transfer can only be in discrete amounts given by the dots' spectrum. In transport experiments, inelastic cotunneling events can be observed as horizontal lines in the stability diagrams inside the Coulomb diamonds at bias values that correspond to the excitation energy. A more detailed introduction to cotunneling in interacting mesoscopic systems can be found in the textbook by Bruus and Flensberg [57].

3.1.3 The Kondo effect

For even larger dot-lead coupling, the Kondo effect can be observed in quantum dots. It is an interesting many-body phenomenon, widely studied in condensed matter physics, which arises from the interplay between delocalized and localized electrons. It was first used by Jun Kondo in 1964 to explain the low-temperature resistivity minimum observed in certain magnetic alloys [58]. He explained that particular feature in terms of an anti-ferromagnetic exchange interaction between the spins of the delocalized conduction electrons and the spins of the electrons localized at the magnetic impurities. The Kondo effect has created enormous attention since, with the help of modern nano fabrication methods, it was observed in quantum dot structures with intermediate dot-lead coupling [59]. In quantum dots in the Coulomb blockade regime filled with an odd number of electrons, the interaction of the delocalized lead electrons with the unpaired spin on the dot leads to a sharp conductance peak at zero bias when the temperature is lower than a characteristic energy scale, the Kondo temperature T_K, which is related to the dot-lead coupling strength and to some intrinsic properties of the leads like the density of states and the width of the conduction band. It has been observed in a variety of quantum dots made out of a wide class of materials, e.g in semiconducting [59], nanotube [60] and single-molecule [61] quantum dots.

A series of tutorial articles on different aspects of Coulomb blockade physics can be found in the book edited by Grabert and Devoret [62]. A recent review on single-electron effects in transport through nanoscale devices like quantum dots or single molecule junctions is e.g. [63]. In Figure 3.4, the results of a measurement on a single-walled carbon nanotube (SWCNT) quantum dot [64] are shown. Coulomb diamonds as features of sequential tunneling as well as cotunneling lines and Kondo resonances can be clearly seen.

3.2 Model Hamiltonian

After having provided some ideas of the phenomenology of quantum dots in the previous section, we want to give a more qualitative description of the current-voltage characteristics. To do so, we introduce the Hamiltonian of the overall system as

$$H = H_{\mathrm{QD}} + H_{\mathrm{leads}} + H_{\mathrm{T}}, \tag{3.7}$$

where H_{QD} describes the quantum dot structure. In the case of a benzene junction $H_{\mathrm{QD}} = H_{\mathrm{PPP}}$. The effect of the gate voltage is already incorporated in H_{QD} (see chapter 2). H_{leads} describes both the source and drain contact as a Fermi gas of noninteracting particles

$$H_{\mathrm{leads}} = \sum_{\alpha\, k\, \sigma} (\epsilon_k - \mu_\alpha) c^\dagger_{\alpha k\sigma} c_{\alpha k\sigma}, \tag{3.8}$$

where $\alpha = L, R$ stands for the left or right lead. As a convention, we identify the source with the left and the drain with the right lead and, and in particular $\mu_{\mathrm{s}} = \mu_L$,

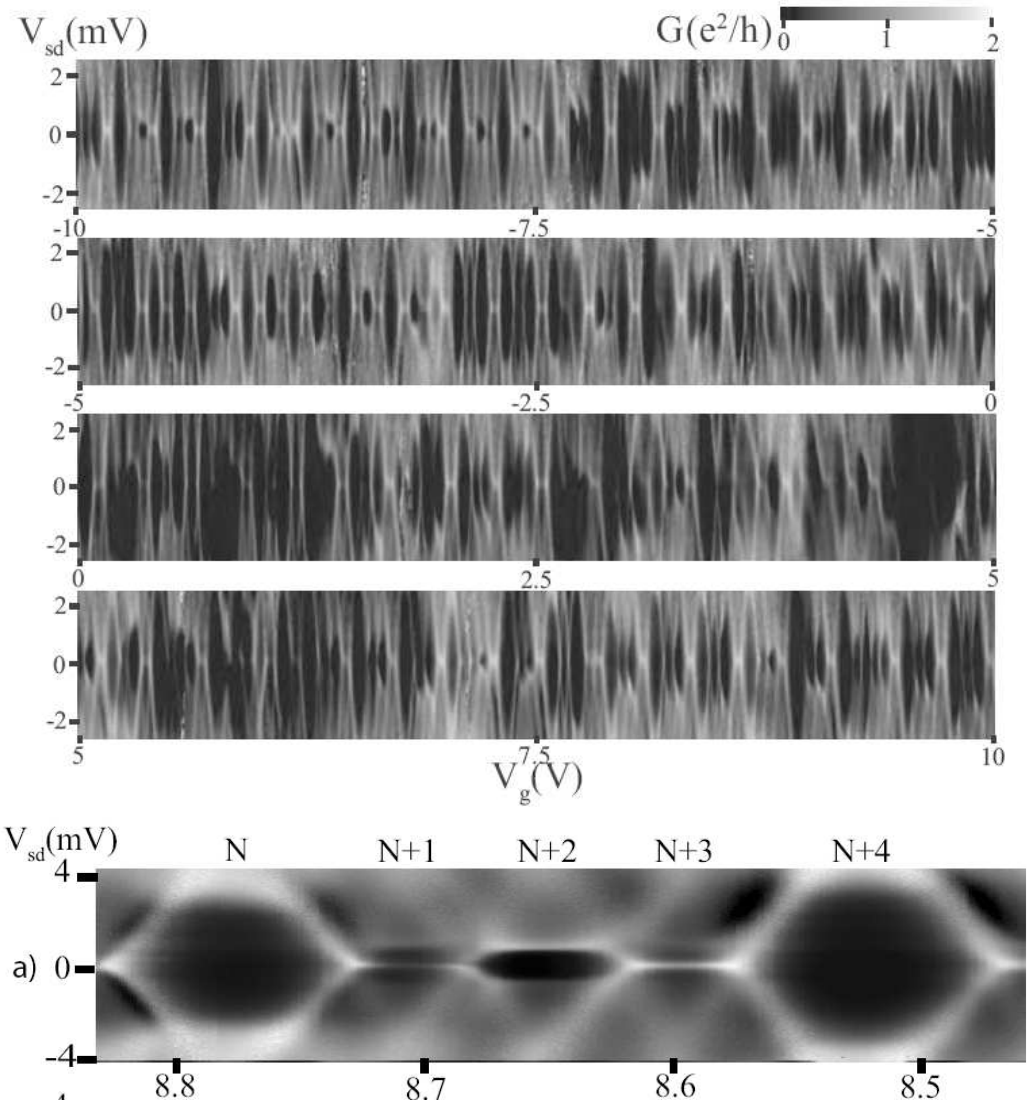

Figure 3.4: Bias spectroscopy plot of a single-walled carbon nanotube (SWCNT) quantum dot for $-10V < V_g < 10V$ (upper panel) that shows clear features of sequential tunneling, cotunneling and the Kondo effect. The Coulomb diamonds are seen for almost every added electron (285), and 88 odd-occupancy diamonds exhibit a zero bias Kondo resonance. Lower panel: blow-up of five Coulomb diamonds that show inelastic cotunneling and for odd occupancy Kondo resonances. Experiment by Holm et al. [64].

$\mu_{\mathrm{d}} = \mu_R$. The chemical potentials μ_α of the leads depend on the applied bias voltage $\mu_{\mathrm{s,d}} = \mu_0 \pm e\frac{V_{\mathrm{b}}}{2}$, so that the difference in the chemical potentials of the leads is given by the bias voltage $\mu_{\mathrm{s}} - \mu_{\mathrm{d}} = eV_{\mathrm{b}}$. In the following we will measure the energy starting from the equilibrium chemical potential of the leads $\mu_0 = 0$. The coupling to source and drain leads is described by the tunneling Hamiltonian

$$H_{\mathrm{T}} = t \sum_{\alpha k\sigma} \left(d^\dagger_{\alpha\sigma} c_{\alpha k\sigma} + c^\dagger_{\alpha k\sigma} d_{\alpha\sigma} \right), \tag{3.9}$$

where we define $d^\dagger_{\alpha\sigma}$ as the creator of the electron with spin quantum number $\sigma = \pm\frac{1}{2}$ in the carbon atom (in case of a molecular junction) or quantum dot (in case of coupled multiple quantum dots) which is closest to the lead α. To avoid confusion with the reduced density matrix $\sigma(t)$ introduced in the next section, we will use from now on the letter τ for the quantum number of the operator S_z.

3.3 Generalized master equation - The dynamics of the reduced density matrix

The electron dynamics of the quantum dot is obtained by solving the equation of motion for the reduced density matrix (RDM). In this section, we give a derivation of this generalized master equation (GME), mainly following [17, 18, 65, 66] and the textbook of Blum [67]. Our starting point is the Liouville equation for the time evolution of the density matrix $\rho(t)$ of the overall system consisting of the leads and the dot. The tunneling Hamiltonian H_{T} is treated as a perturbation. We calculate the time dependence of $\rho(t)$ in the interaction picture, i.e. we define

$$\rho^I(t) = U_I(t, t_0)\rho(t_0)U_I^\dagger(t, t_0), \tag{3.10}$$

with the time evolution operator $U_I(t, t_0)$, given by

$$U_I(t, t_0) = \exp\left(\frac{i}{\hbar}\left(H_{\mathrm{QD}} + H_{\mathrm{leads}}\right)(t - t_0)\right) \exp\left(-\frac{i}{\hbar}\left(H_{\mathrm{QD}} + H_{\mathrm{leads}} + H_{\mathrm{T}}\right)(t - t_0)\right), \tag{3.11}$$

and t_0 being some reference time. Using (3.11) and (3.10) the equation of motion becomes

$$i\hbar\frac{\partial\rho^I(t)}{\partial t} = \left[H^I_{\mathrm{T}}(t), \rho^I(t)\right], \tag{3.12}$$

with $H^I_{\mathrm{T}}(t) = \exp\left(\frac{i}{\hbar}\left(H_{\mathrm{QD}} + H_{\mathrm{leads}}\right)(t - t_0)\right) H_{\mathrm{T}} \exp\left(-\frac{i}{\hbar}\left(H_{\mathrm{QD}} + H_{\mathrm{leads}}\right)(t - t_0)\right)$. By integrating over time, we get

$$\rho^I(t) = \rho^I(t_0) - \frac{i}{\hbar}\int_{t_0}^{t} dt_1 \left[H^I_{\mathrm{T}}(t_1), \rho^I(t_1)\right], \tag{3.13}$$

and reinserting (3.13) into (3.12) yields

$$\dot\rho^I(t) = -\frac{i}{\hbar}\left[H^I_{\mathrm{T}}(t), \rho^I(t_0)\right] + \left(\frac{i}{\hbar}\right)^2 \int_{t_0}^{t} dt_1 \left[H^I_{\mathrm{T}}(t), \left[H^I_{\mathrm{T}}(t_1), \rho^I(t_1)\right]\right]. \tag{3.14}$$

The dynamics of electron transport is determined by the chemical potentials of the two leads, but more notably by the configuration of the central system. That is why, from now on, we treat the time evolution of the reduced density matrix (RDM) $\sigma = \mathrm{Tr}_{\mathrm{leads}}\{\rho^{\mathrm{I}}(t)\}$, which is formally obtained from (3.14) by tracing out the lead degrees of freedom: $\dot{\sigma} = \mathrm{Tr}_{\mathrm{leads}}\{\dot{\rho}^{\mathrm{I}}\}$. The trace over lead states in equation (3.14) reads

$$\dot{\sigma}(t) = -\left(\frac{1}{\hbar}\right)^2 \int_{t_0}^{t} dt_1 \mathrm{Tr}_{\mathrm{leads}}\left[H_{\mathrm{T}}^I(t), \left[H_{\mathrm{T}}^I(t_1), \rho^I(t_1)\right]\right]. \tag{3.15}$$

The first term in equation (3.14) drops out, because leads and dot can be seen at as statistically independent at time t_0, which is natural if H_{T} is switched on a that time. Under the trace, the product $H_{\mathrm{T}}^I(t)\rho^I(t_0)$ vanishes, because H_{T} changes the number of particles in the leads. Up to this point, the equation is exact.
To simplify equation (3.15), several well defined approximations can be made. First, the leads can be considered as large, macroscopic objects compared to the dot. The influence of the central system on the leads is only marginal, because of the difference in size and the tunneling between leads and dot is weak. From now on, we treat the leads as reservoirs which stay in thermal equilibrium and we write the density matrix of the overall system as a product of the system and leads density matrices

$$\rho^I(t) = \sigma(t)\rho_{\mathrm{leads}} = \sigma(t) \otimes \rho_{\mathrm{s}}\rho_{\mathrm{d}}, \tag{3.16}$$

where ρ_{s} and ρ_{d} are time independent and given by the thermal equilibrium expression

$$\rho_{\mathrm{s/d}} = \frac{\exp\left(-\beta\left(H_{\mathrm{s/d}} - \mu_{\mathrm{s/d}}N_{\mathrm{s/d}}\right)\right)}{Z_{\mathrm{s/d}}}, \tag{3.17}$$

with $\beta = \frac{1}{k_{\mathrm{B}}T}$ the inverse temperature. It can be formally shown that the factorization (3.16) corresponds to a second order treatment in the perturbation H_{T} [67].
Second, we see that equation (3.15) is nonlocal in time, which means that $\dot{\sigma}(t)$ at the time t depends on $\sigma(t_1)$ at all times between t_0 and t. An equation local in time is obtained by introducing the Markov approximation which replaces $\rho^I(t_1) = \sigma^I(t_1) \otimes \rho_{\mathrm{s}}\rho_{\mathrm{d}}$ by $\sigma^I(t) \otimes \rho_s\rho_d$. This means, that the time evolution of $\sigma^I(t)$ is determined by $\sigma^I(t)$ at the same time only. This approximation is motivated by the following argument: Equation (3.15) contains two-time correlation function of the form $\mathrm{Tr}_{\mathrm{leads}}\{\rho_{\mathrm{leads}} \prod B_{\mathrm{leads}}\}$, where $\prod B_{\mathrm{leads}}$ is a product of two lead operators at different times. These correlation functions rapidly decay on the time scale of the dot dynamics so that they can be replaced by δ-functions [37]. In particular the Markov approximation becomes exact in the stationary limit ($t \to \infty$) we will focus on. Since we are interested in the long term behavior of the system, we set $t_0 \to -\infty$, replace $t1$ by $t - t_2$ and finally obtain the generalized master equation

$$\dot{\sigma}(t) = -\left(\frac{1}{\hbar}\right)^2 \int_{0}^{\infty} dt_2 \mathrm{Tr}_{\mathrm{leads}}\left[H_{\mathrm{T}}^I(t), \left[H_{\mathrm{T}}^I(t - t_2), \sigma^I(t)\rho_{\mathrm{leads}}\right]\right]. \tag{3.18}$$

The reduced density operator σ is defined on the Fock space of the quantum dot, yet we can neglect coherences (off-diagonal elements of the density matrix) between

states with different particle number, since they are decoupled from the dynamics of the populations. Coherences between states with same number of particles but with different energy can be neglected, when their energy difference is larger than the lead-dot coupling strength. Under this conditon, they are irrelevant due to their fast fluctuation compared to the dynamics of the system. If two states are either exactly degenerate or their energy difference is large, then the secular approximation can be applied, meaning that only coherences between degenerate states are kept. In case of quasi degenerate states, where the energy difference is smaller than the lead-dot coupling strength, also coherences between these states must be taken into account. We will discuss such cases in chapter 4.
Here, we show the GME for the case where the secular approximation is valid. To proceed, we project equation (3.18) into the subspace of N-particle and energy E. To do so, we introduce the projection operator $\mathcal{P}_{\mathrm{NE}} := \sum_{\ell\tau} |N\,E\,\ell\,\tau\rangle\langle N\,E\,\ell\,\tau|$. The sum runs over the orbital and spin quantum numbers ℓ and τ, respectively. We find for the block of the density matrix with energy E and particle number N, $\sigma^{\mathrm{NE}} = \mathcal{P}_{\mathrm{NE}}\,\sigma\,\mathcal{P}_{\mathrm{NE}}$ the GME

$$\begin{aligned}\dot{\sigma}^{\mathrm{NE}} \;=\; & -\sum_{\alpha\tau}\frac{\Gamma_\alpha}{2}\Bigg\{\mathcal{P}_{\mathrm{NE}}d_{\alpha\tau}\left[f_\alpha^+(H_{\mathrm{QD}}-E)-\frac{i}{\pi}\,p_\alpha(H_{\mathrm{QD}}-E)\right]d_{\alpha\tau}^\dagger\,\sigma^{\mathrm{NE}}+ \\ & +\mathcal{P}_{\mathrm{NE}}d_{\alpha\tau}^\dagger\left[f_\alpha^-(E-H_{\mathrm{QD}})-\frac{i}{\pi}\,p_\alpha(E-H_{\mathrm{QD}})\right]d_{\alpha\tau}\,\sigma^{\mathrm{NE}}+H.c.\Bigg\} \\ & +\sum_{\alpha\tau\mathrm{E}'}\Gamma_\alpha\mathcal{P}_{\mathrm{NE}}\Big\{d_{\alpha\tau}^\dagger f_\alpha^+(E-E')\,\sigma^{\mathrm{N-1E}'}d_{\alpha\tau}+d_{\alpha\tau}f_\alpha^-(E'-E)\,\sigma^{\mathrm{N+1E}'}d_{\alpha\tau}^\dagger\Big\}\mathcal{P}_{\mathrm{NE}},\end{aligned} \tag{3.19}$$

where $\Gamma_{\mathrm{L,R}} = \frac{2\pi}{\hbar}|t_{\mathrm{L,R}}|^2\mathcal{D}_{\mathrm{L,R}}$ are the bare transfer rates with the constant densities of states of the leads $\mathcal{D}_{\mathrm{L,R}}$. Terms describing sequential tunneling from and to the lead α are proportional to the Fermi functions $f_\alpha^+(x) := f(x-\mu_\alpha)$ and $f_\alpha^-(x) := 1-f_\alpha^+(x)$, respectively. Still in the sequential tunneling limit, but only in the equations for the coherences, one finds also terms proportional to the function $p_\alpha(x) = -\mathrm{Re}\psi\left[\frac{1}{2}+\frac{i\beta}{2\pi}(x-\mu_\alpha)\right]$, where ψ is the digamma function. These terms are sometimes called energy non-conserving terms, because they describe virtual transitions to states that are not energetically accessible. In contrast, the terms proportional to the Fermi function reflect exactly the condition in equation (3.6) that was derived using energy conservation. Both the Fermi functions and the digamma function result from the trace over the leads degrees of freedom [65, 67, 68].
A closer analysis of the master equation allows also to formulate an expression for the current operator. We start from the definition of the time derivative of the charge on the quantum dot:

$$\frac{d}{dt}\langle Q\rangle = \mathrm{Tr}\left\{\hat{N}\dot{\sigma}\right\} = \langle\, I_{\mathrm{L}} + I_{\mathrm{R}}\,\rangle \tag{3.20}$$

where $Q = \sum_{i\tau} d_{i\tau}^\dagger d_{i\tau}$ is the operator of the charge on the quantum dot, $\hat{N}$ is the particle number operator and $I_{\mathrm{L,R}}$ are the current operators at the left(right) contact.

Conventionally, in the definition of $I_{\mathrm{L,R}}$ we assume the current to be positive when it is increasing the charge on the molecule. Thus, in the stationary limit, $\langle\, I_{\mathrm{L}} + I_{\mathrm{R}} \,\rangle$ is zero. We write this expression in the basis of the subspaces of N particles and energy E:

$$\langle\, I_{\mathrm{L}} + I_{\mathrm{R}} \,\rangle = \sum_{\mathrm{NE}} \mathrm{Tr}\left\{\hat{N}\mathcal{P}_{\mathrm{NE}}\dot{\sigma}\mathcal{P}_{\mathrm{NE}}\right\} = \sum_{\mathrm{NE}} \mathrm{Tr}\left\{N\dot{\sigma}^{\mathrm{NE}}\right\}. \tag{3.21}$$

Further we insert (3.19) in (3.21) and take advantage of the cyclic properties of the trace to find :

$$\begin{aligned}\langle\, I_{\mathrm{L}} + I_{\mathrm{R}} \,\rangle = \\ \sum_{\mathrm{NE}}\sum_{\alpha\tau} N\Gamma_\alpha \mathrm{Tr}\Big\{ &- \left[f_\alpha^+(H_{\mathrm{QD}} - E)d_{\alpha\tau}^\dagger \sigma^{\mathrm{NE}} d_{\alpha\tau} + f_\alpha^-(E - H_{\mathrm{QD}})d_{\alpha\tau}\sigma^{\mathrm{NE}} d_{\alpha\tau}^\dagger\right] \\ &+ \sum_{\mathrm{E}'} \mathcal{P}_{\mathrm{NE}}\left[f_\alpha^+(E-E')d_{\alpha\tau}^\dagger \sigma^{\mathrm{N-1E'}} d_{\alpha\tau} + f_\alpha^-(E'-E)d_{\alpha\tau}\sigma^{\mathrm{N+1E'}} d_{\alpha\tau}^\dagger\right]\Big\}.\end{aligned} \tag{3.22}$$

Notice that the energy non-conserving contributions drop from the expression of the current operator. Still they contribute to the average current, because they determine the solution of the GME, which is entering in the current formula in any case. Since E and E' are dummy variables, we can switch them in the summands containing E'. Applying the relation:

$$\sum_{\mathrm{NE}'} \mathrm{Tr}\left\{\mathcal{P}_{\mathrm{NE}'}\, g(E')\right\} = \mathrm{Tr}\left\{g(H_{\mathrm{QD}})\right\},$$

where $g(E')$ is a generic function, we substitute E' with H_{QD} in equation (3.23). Further we can conveniently rearrange the sum over N, arriving at the expression for the current:

$$\begin{aligned}\langle\, I_{\mathrm{L}} + I_{\mathrm{R}} \,\rangle = &\sum_{\mathrm{NE}}\sum_{\alpha\tau}\Gamma_\alpha \mathrm{Tr} \\ \Big\{ &d_{\alpha\tau}^\dagger \sigma^{\mathrm{NE}} d_{\alpha\tau}\Big[-Nf_\alpha^+(H_{\mathrm{QD}}-E)+(N+1)f_\alpha^+(H_{\mathrm{QD}}-E)\Big] \\ &+ d_{\alpha\tau}\sigma^{\mathrm{NE}} d_{\alpha\tau}^\dagger\Big[-Nf_\alpha^-(E-H_{\mathrm{QD}})+(N-1)f_\alpha^-(E-H_{\mathrm{QD}})\Big]\Big\}.\end{aligned} \tag{3.23}$$

This relation can be further simplified in order to identify the current operators. The one corresponding to the left contact is *e.g.*

$$I_{\mathrm{L}} = \Gamma_{\mathrm{L}} \sum_{\mathrm{NE}\tau} \mathcal{P}_{\mathrm{NE}}\Big[d_{\mathrm{L}\tau} f_{\mathrm{L}}^+(H_{\mathrm{QD}} - E)d_{\mathrm{L}\tau}^\dagger - d_{\mathrm{L}\tau}^\dagger f_{\mathrm{L}}^-(E - H_{\mathrm{QD}})d_{\mathrm{L}\tau}\Big]\mathcal{P}_{\mathrm{NE}}. \tag{3.24}$$

With this relation we can calculate the stationary current as the average $\langle I_{\mathrm{L}}\rangle = \mathrm{Tr}\{\sigma_{\mathrm{stat}} I_{\mathrm{L}}\} = -\langle I_{\mathrm{R}}\rangle$, with σ_{stat} as the stationary density operator which is obtained by setting $\dot{\sigma}^{NE} = 0$ in equation (3.19) and solving the remaining equation for σ^{NE} under the condition that $\mathrm{Tr}\sigma = 1$.

3.4 GME and current in the non-secular approximation

Coherences between states with different energies can become important, when the difference in their energies has the same order of magnitude as the coupling to the leads. In this case the secular approximation cannot be applied. We report here the general expression for the generalized master equation and the associated current operator in the Born-Markov approximation and under the only further condition (exact in absence of superconductors) that coherences between states with different particle number are decoupled from the populations and vanish exactly in the stationary limit:

$$
\begin{aligned}
\dot{\sigma}^{\mathrm{N}}_{\mathrm{EE}'} \;=\; & -\frac{i}{\hbar}(E-E')\sigma^{\mathrm{N}}_{\mathrm{EE}'} + \\
& -\sum_{\alpha\tau\mathrm{F}} \frac{\Gamma_\alpha}{2}\mathcal{P}_{\mathrm{NE}} \Big\{ d^\dagger_{\alpha\tau}\left[-\frac{i}{\pi}p_\alpha(F-H_{\mathrm{QD}}) + f^-_\alpha(F-H_{\mathrm{QD}})\right] d_{\alpha\tau} + \\
& \qquad\qquad d_{\alpha\tau}\left[-\frac{i}{\pi}p_\alpha(H_{\mathrm{QD}}-F) + f^+_\alpha(H_{\mathrm{QD}}-F)\right] d^\dagger_{\alpha\tau}\Big\}\sigma^{\mathrm{N}}_{\mathrm{FE}'} \\
& -\sum_{\alpha\tau\mathrm{F}} \frac{\Gamma_\alpha}{2}\sigma^{\mathrm{N}}_{\mathrm{EF}} \Big\{ d^\dagger_{\alpha\tau}\left[+\frac{i}{\pi}p_\alpha(F-H_{\mathrm{QD}}) + f^-_\alpha(F-H_{\mathrm{QD}})\right] d_{\alpha\tau} + \\
& \qquad\qquad d_{\alpha\tau}\left[+\frac{i}{\pi}p_\alpha(H_{\mathrm{QD}}-F) + f^+_\alpha(H_{\mathrm{QD}}-F)\right] d^\dagger_{\alpha\tau}\Big\}\mathcal{P}_{\mathrm{NE}'} \\
& +\sum_{\alpha\tau\mathrm{FF}'} \frac{\Gamma_\alpha}{2}\mathcal{P}_{\mathrm{NE}} \Big\{ d^\dagger_{\alpha\tau}\sigma^{\mathrm{N}-1}_{\mathrm{FF}'} d_{\alpha\tau}\left[+\frac{i}{\pi}p_\alpha(E'-F') + f^+_\alpha(E'-F') + \right. \\
& \qquad\qquad \left. -\frac{i}{\pi}p_\alpha(E-F) + f^+_\alpha(E-F)\right] \\
& \qquad + d_{\alpha\tau}\sigma^{\mathrm{N}+1}_{\mathrm{FF}'} d^\dagger_{\alpha\tau}\left[+\frac{i}{\pi}p_\alpha(F'-E') + f^-_\alpha(F'-E') \right. \\
& \qquad\qquad \left. -\frac{i}{\pi}p_\alpha(F-E) + f^-_\alpha(F-E)\right]\Big\}\mathcal{P}_{\mathrm{NE}'}
\end{aligned}
\tag{3.25}
$$

where $\sigma^{\mathrm{N}}_{\mathrm{EE}'}$ is, differently to equation (3.19), in the Schrödinger picture. Equation (3.19) represents a special case of equation (3.25) in which all energy spacings between states with the same particle number are either zero or much larger than the level broadening $\hbar\Gamma$. Equation (3.25) is derived in the weak coupling limit and bridges all the regimes from exact degeneracies to weakly and completely broken degeneracies.

The problem of a master equation in presence of quasi-degenerate states in order to study transport through molecules has been recently addressed in the work of Schultz et al. [69]. The authors use a different approach, denoted "singular coupling limit" in the literature, to derive an equation for the density matrix in presence of quasi-degenerate states.

The current operators associated to the master equation just presented read:

$$\begin{aligned} I_\alpha = \frac{\Gamma_\alpha}{2} \sum_{\mathrm{NEF}\tau} & \mathcal{P}_{\mathrm{NE}} \\ & \Big\{ d^\dagger_{\alpha\tau} \left[+\frac{i}{\pi} p_\alpha(E - H_{\mathrm{QD}}) + f^-_\alpha(E - H_{\mathrm{QD}}) \right] d_{\alpha\tau} \\ & + d^\dagger_{\alpha\tau} \left[-\frac{i}{\pi} p_\alpha(F - H_{\mathrm{QD}}) + f^-_\alpha(F - H_{\mathrm{QD}}) \right] d_{\alpha\tau} \\ & - d_{\alpha\tau} \left[+\frac{i}{\pi} p_\alpha(H_{\mathrm{QD}} - E) + f^+_\alpha(H_{\mathrm{QD}} - E) \right] d^\dagger_{\alpha\tau} \\ & - d_{\alpha\tau} \left[-\frac{i}{\pi} p_\alpha(H_{\mathrm{QD}} - F) + f^+_\alpha(H_{\mathrm{QD}} - F) \right] d^\dagger_{\alpha\tau} \Big\} \mathcal{P}_{\mathrm{NF}}. \end{aligned} \tag{3.26}$$

Nevertheless, within the limits of derivation of the master equation, this formula can be simplified. Actually, if $E - F \leq \hbar\Gamma$, then F can be safely substituted with E in the argument of the digamma functions and of the Fermi functions, with an error of order $\frac{E-F}{k_{\mathrm{B}}T} < \frac{\hbar\Gamma}{k_{\mathrm{B}}T}$ which is negligible (the generalized master equation that we are considering is valid for $\hbar\Gamma \ll k_{\mathrm{B}}T$). The approximation $E \sim F$ breaks down only if $E - F \sim k_{\mathrm{B}}T$, but this implies $E - F \gg \hbar\Gamma$ which is the regime of validity of the secular approximation. Consequently, in this regime, terms with $E \neq F$ do not contribute to the average current because they vanish in the stationary density matrix. Ultimately we can thus reduce the current operators to the simpler form:

$$\begin{aligned} I_\alpha = \Gamma_\alpha \sum_{\mathrm{NE}\tau} \mathcal{P}_{\mathrm{NE}} \Big\{ & + d^\dagger_{\alpha\tau} \left[f^-_\alpha(E - H_{\mathrm{QD}}) \right] d_{\alpha\tau} \\ & - d_{\alpha\tau} \left[f^+_\alpha(H_{\mathrm{QD}} - E) \right] d^\dagger_{\alpha\tau} \Big\}, \end{aligned} \tag{3.27}$$

which is almost equal to the current operator corresponding to the secular approximation. The only difference is here the absence of the second projector operator that allows contributions to the current coming from coherences between different energy eigenstates.

3.5 Extension to fourth order

One can extend this so-called Bloch-Redfield approach to fourth or higher orders in H_{T} to describe cotunneling, pair tunneling and other effects [37]. A different approach to derive the GME is a real-time diagrammatic approach developed by Schoeller et al. [70, 71, 72]. Following this theory, one traces out the leads degrees of freedom at the earliest possible stage and derive a formally exact equation of motion for the reduced density matrix (RDM) of the system. Koller et al. [73] showed the equivalence of this diagrammatic approach with the Bloch-Redfield approach described above.

While these theories have the advantage of being exact to a desired order, they are rather involved and already at fourth order in H_T the number of diagrams is quite large such that a continuation to higher orders seems to be unpractical.
In this thesis, the focus is mainly on effects arising from sequential tunneling processes which correspond to second order in H_T. Cotunneling processes are described with a simpler approach based on the T-matrix formalism in chapter 6.

Chapter 4

A benzene interference single-electron transistor

Interference effects strongly affect the transport characteristics of a benzene single-electron transistor (SET) and for this reason we call it interference SET (ISET). In this chapter, we discuss transport through such a device, where the molecule is attached to the leads in two different configurations. In both cases, we assume that tunneling on and off the molecule is only possible from the p_z-orbitals localized at the atoms that are closest to source and drain leads. In PARA configuration, atoms on opposite ends of the molecule are coupled to the leads (we label them as atoms 1 and 4, counting clockwise around the molecule and starting at the atom which is closest to the source), whereas in META configuration the contact atoms are atoms 1 and 3 (see Figure (4.1)).

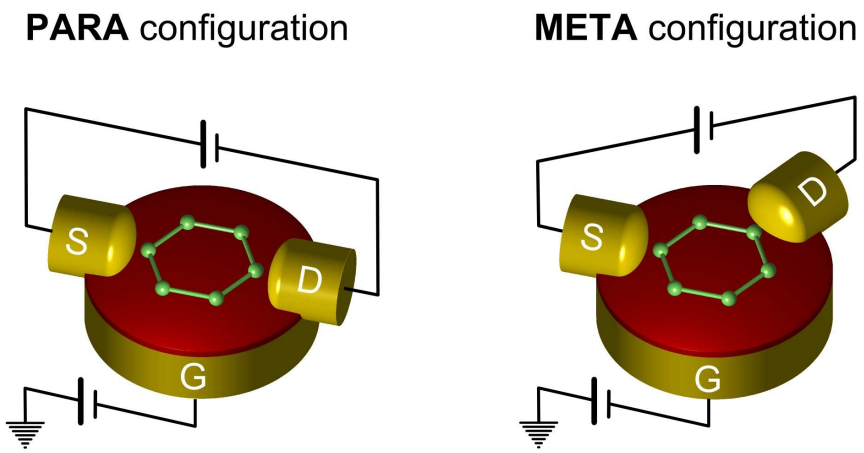

Figure 4.1: Schematic representation of the two different setups for the benzene SET. In PARA configuration, atoms on opposite ends of the molecule are coupled to the leads, whereas in META configuration the contact atoms are next-nearest neighbors.

Strong differences are visible in the stability diagrams obtained for the two configurations. Striking are the selective reduction of conductance and the appearance of regions of interference driven current blocking with associated negative differential conductance (NDC) when changing from the para to the meta configuration.
NDC and current blocking caused by interference take place any time a SET presents an N-particle non-degenerate ground state and two degenerate $N+1$-particle ground states (or two $N-1$-particle ground states) such that the ratio between the transition *amplitudes* $\gamma_{i\alpha}$ $(i = 1, 2, \quad \alpha = L, R)$ between those N- and $N+1$-particle states is different for tunneling at the left (L) and at the right (R) lead:

$$\frac{\gamma_{1L}}{\gamma_{2L}} \neq \frac{\gamma_{1R}}{\gamma_{2R}}. \tag{4.1}$$

Due to condition (4.1) there exist linear combinations of the degenerate $N+1$-particle states which are coupled to one of the leads but *not* to the other. The state which is decoupled from the right lead represents a blocking state for the current flowing $L \to R$ since electrons can populate this state by tunnelling from the left lead but cannot tunnel out towards the right lead. Viceversa the state decoupled from the left lead is a blocking state for the current $R \to L$. Typically these two blocking states are not orthogonal and thus cannot form a valid basis set together. The basis set that diagonalizes the stationary density matrix (what we call in the manuscript the "physical basis") contains at large positive biases the $L \to R$ blocking state and is thus different from the physical basis at large negative biases which necessarily contains the $R \to L$ blocking state. More generally the "physical basis" *depends continuously* on the bias. Thus only a treatment that includes coherences in the density matrix can capture the full picture at all biases. By neglecting for simplicity the spin degree of freedom, the 7-particle ground state of benzene is two times degenerate while the 6-particle one is non-degenerate. If we choose for the 7-particle states the eigenstates of the z-projection of the angular momentum we obtain the relation:

$$\frac{\gamma_{1L}}{\gamma_{2L}} = \frac{\gamma_{1R}}{\gamma_{2R}} e^{4i\phi}, \tag{4.2}$$

where ϕ is the angle between the left and the right lead. Thus in the meta configuration $(\phi = 2\pi/3)$ the condition (4.1) is fullfilled while in the para $(\phi = \pi)$ the amplitude ratios are equal. This condition implies that, in the para configuration one of the 7-particle states is decoupled from *both* leads at the same time and can thus (in first approximation) be excluded from the dynamics. In contrast, in the meta configuration, the linear combination of uniformly distributed eigenstates of the angular momentum creates states with a peculiar interference pattern. The position of their nodes allows to characterize them as different blocking states.
Notice that no asymmetry in the tunnelling *rates*, which are proportional to $|\gamma_{i\alpha}|^2$, is implied by (4.1). This fact excludes the explanation of the physics of interference SET in terms of asymmetric couplings, which is used very often to explain NDC in quantum dots. NDC can occur when the bias gets large enough so that a transport channel involving an excited state can enter in the bias window in addition to the

ground state channel. In general, the current increases in this situation. If the excited state is coupled asymetrically to source and drain leads, namely there is a large tunnel rate into the dot, but a small tunnel rate out, it will get an average population close to one and the current will actually decrease. It will decrease because it is composed of the transition rates between molecular states multiplied with the average population of the initial state, so that a redistribution of average probabilities in favor of the excited state, which can only be depopulated by a process with a small rate, leads to a smaller current. Current suppression in sequential tunneling systems always goes along with (almost) exclusive population of one particular state.
NDC and current blocking for benzene junctions have also been predicted in the work of Hettler et al. [33], but in the para configuration *and* in presence of an external electromagnetic field. In the para configuration one of the two degenerate 7-particle ground states is decoupled from the 6-particle ground state at *both* leads at the same time. More specifically, due to a selection rule derived in section 4.2, tunneling is only possible from symmetric to symmetric (with respect to the plane through the contact atoms and perpendicular to the molecule) and from anti-symmetric to anti-symmetric states in para configuration. The electromagnetic field however, couples symmetric and anti-symmetric states. The blocking situation comes about when an excited 7-particle symmetric state gets populated and decays into the anti-symmetric 7-particle ground state by emitting a photon. This state can neither be depopulated via tunneling nor decay any further and acts therefore as a blocking state.
In our work NDC occurs despite the absence of an external field and with no asymmetry in the tunnelling rates.
In the following sections, we will discuss the symmetry properties of the isolated benzene molecule and discuss the results of our transport calculations in terms of these symmetries. At the end of this chapter, we will show that the surroundings of the molecule in an SET setup will break the exact symmetry and therefore lift the exact degeneracies that give rise to the interference effects. We therefore cannot use the secular approximation any more. Our conclusion will be that also quasi-degeneracy of two states (meaning $E' - E \lesssim \Gamma$) can cause interference and NDC.

4.1 The D_{6h} point group

Benzene has a high symmetry and belongs to the D_{6h} point group. This group consists of all the symmetry operations that map the molecule onto itself and it obeys the four conditions necessary to define a group in a strict mathematical sense: the completeness of the group, the validity of the associative law, the existence of a unit element and the existence of an inverse element for each element of the group. 24 different symmetry operations can be distinguished. These are

1 unity operation, denoted as E in the Schoenflies system,

5 rotations about the symmetry axis perpendicular to the molecule by the angles $\pm\frac{2\pi}{6}$, $\pm\frac{2\pi}{3}$, and π, denoted as C_6, C_3, C_2, where in C_n the rotation angle is $\pm\frac{2\pi}{n}$,

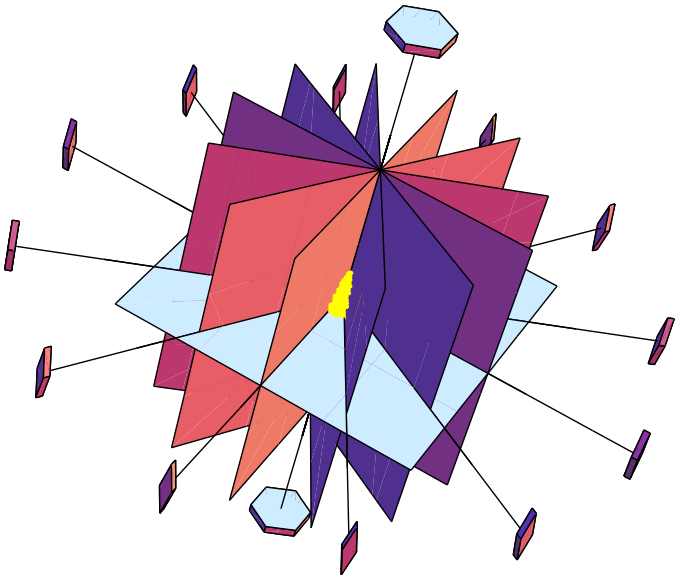

Figure 4.2: Symmetry planes and axes for the D_{6h} point group. Image generated with the *Crystal*-package for Mathematica by Jörg Enderlein [74].

1 reflection about the plane of the molecule, σ_{h},

3 reflections about planes perpendicular to the molecule and through two carbon atoms on opposite ends of the molecule, σ_{v},

3 reflections about planes perpendicular to the molecule and perpendicular to the connection of two neighboring carbon atoms, σ_{d},

3 rotations about axes lying in the molecular plane and in the plane through two carbon atoms on opposite ends of the molecule by the angle π, C_2',

3 rotations about axes lying in the molecular plane and in the plane perpendicular to the connection of two neighboring carbon atoms, C_2'',

4 improper rotations (rotations about the axis perpendicular to the molecular plane by angles of $\pm\frac{2\pi}{6}$, $\pm\frac{2\pi}{3}$, followed by an reflection about that plane), S_6 and S_3,

1 inversion i about the center of the molecule (which is actually the improper rotation S_2).

All symmetry planes and symmetry axes contain the center of the molecule. In the above list, these symmetry operations are already divided into classes, each corresponding to a physically distinct kind of symmetry operation such as rotation of π about equivalent twofold axes, or rotation of $\pm 2\pi/6$ about a six-fold axis. We make use of the mathematical power of group theory to classify the molecular orbitals by

their belonging to so-called irreducible representations of the point group. The irreducible representations completely determine the transformation of the orbitals under classes of symmetry operations and also specify their degeneracy. Group theory is employed as well for following the degeneracies of the energy levels when the symmetry of the molecule is lowered by the surroundings in a SET setup.
For strict mathematical definitions of the concepts of groups, classes, reducible and irreducible representations of groups and the conventions of the Schoenflies symmetry notation, we refer to the textbook on group theory by Dresselhaus, Dresselhaus and Jorio [75].

4.2 Symmetry of the benzene eigenstates

In this section, we will review the symmetry characteristics of the eigenstates of the interacting Hamiltonian of benzene, focusing on the symmetry operations σ_v and C_n which have a major impact on the electronic transport through the molecular ISET.
Table 4.1 shows an overview of the states of the neutral molecule (the 6 particle states) sorted by S_z and symmetries. The eigenstates of the interacting benzene molecule have either A-, B- or E-type symmetries. While orbitals having A or B symmetries can only be spin degenerate, states with an E symmetry show an additional twofold orbital degeneracy, essential for the explanation of the transport features occurring in the meta configuration.
Transport at low bias is described in terms of transitions between ground states with different particle number. Table 4.2 shows the symmetries of the ground states (and of some first excited states) of interacting benzene for all possible particle numbers. Ground state transitions occur both between orbitally non-degenerate states (with A and B symmetry), as well as between orbitally degenerate and non-degenerate states (E- to A-type states).
The interacting benzene Hamiltonian commutes with all the symmetry operations of the D_{6h} point group, thus it has a set of common eigenvectors with each operation. The element of D_{6h} of special interest for the *para* configuration is σ_v, *i.e.*, the reflection about the plane through the contact atoms and perpendicular to the molecular plane. The molecular orbitals with A and B symmetry are eigenstates of σ_v with eigenvalue ± 1, *i.e.*, they are either symmetric or antisymmetric with respect to the σ_v operation. The behavior of the $E-$type orbitals under σ_v is basis dependent, yet one can always choose a basis in which one orbital is symmetric and the other one antisymmetric.
Let us now consider the generic transition amplitude $\langle N|d_{\alpha\tau}|N+1\rangle$, where $d_{\alpha\tau}$ destroys an electron of spin τ on the contact atom closest to the α lead. It is useful to rewrite this amplitude in the form

$$\langle N|d_{\alpha\tau}|N+1\rangle = \langle N|\sigma_\mathrm{v}^\dagger \sigma_\mathrm{v} d_{\alpha\tau} \sigma_\mathrm{v}^\dagger \sigma_\mathrm{v}|N+1\rangle, \tag{4.3}$$

where we have used the property $\sigma_\mathrm{v}^\dagger \sigma_\mathrm{v} = 1$. Since in the para configuration both contact atoms lie in the mirror plane σ_v, it follows $\sigma_\mathrm{v} d_\alpha \sigma_\mathrm{v}^\dagger = d_\alpha$. If the participating

N	# ↑	# ↓	# states	# states with a certain symmetry
6	6	0	1	1 B_{1u}
	5	1	36	4 A_{1g} 2 A_{2g} 2×6 E_{2g} 4 B_{1u} 2 B_{2u} 2×6 E_{1u}
	4	2	225	16 A_{1g} 20 A_{2g} 2×36 E_{2g} 22 B_{1u} 17 B_{2u} 2×39 E_{1u}
	3	3	400	38 A_{1g} 30 A_{2g} 2×66 E_{2g} 38 B_{1u} 30 B_{2u} 2×66 E_{1u}
	2	4	225	
	1	5	36	⋮
	0	6	1	

Table 4.1: Overview of the 6 particle states of benzene, sorted by S_z and symmetry. Orbitals with A- and B-type of symmetry show no degeneracy, while E-type orbitals are doubly degenerate.

states are both symmetric under σ_{v}, equation (4.3) becomes

$$\begin{aligned}\langle N, \mathrm{sym}|\sigma_{\mathrm{v}}^{\dagger} d_{\alpha\tau}\sigma_{\mathrm{v}}|N+1, \mathrm{sym}\rangle = \\ = \langle N, \mathrm{sym}|d_{\alpha\tau}|N+1, \mathrm{sym}\rangle\end{aligned} \tag{4.4}$$

and analogously in the case where both states are antisymmetric. For states with different symmetry it is

$$\begin{aligned}\langle N, \mathrm{sym}|d_{\alpha\tau}|N+1, \mathrm{antisym}\rangle = \\ = -\langle N, \mathrm{sym}|d_{\alpha\tau}|N+1, \mathrm{antisym}\rangle = 0.\end{aligned} \tag{4.5}$$

In other terms, there is a selection rule that forbids transitions between symmetric and antisymmetric states. Further, since the ground state of the neutral molecule is symmetric, for the transport calculations in the para configuration we select the effective Hilbert space containing only states symmetric with respect to σ_{v}. Correspondingly, when referring to the N particle ground state we mean the energetically

N	Degeneracy	Energy[eV] (at $\xi = 0$)	Symmetry	Symmetry behavior under σ_{v}
0	1	0	A_{1g}	sym
1	2	-22	A_{2u}	sym
2	1	-42.25	A_{1g}	sym
3	4	-57.42	E_{1g}	2 sym, [2 antisym]
4	[3]	[-68.87]	$[A_{2g}]$	[antisym]
	2	-68.37	E_{2g}	1 sym, [1 antisym]
5	4	-76.675	E_{1g}	2 sym, [2 antisym]
6	1	-81.725	A_{1g}	sym
7	4	-76.675	E_{2u}	2 sym, [2 antisym]
8	[3]	[-68.87]	$[A_{2g}]$	[antisym]
	2	-68.37	E_{2g}	1 sym, [1 antisym]
9	4	-57.42	E_{2u}	2 sym, [2 antisym]
10	1	-42.25	A_{1g}	sym
11	2	-22	B_{2g}	sym
12	1	0	A_{1g}	sym

Table 4.2: Degeneracy, energy and symmetry of the ground states of the isolated benzene molecule for different particle numbers. We choose the on-site and inter-site Coulomb interactions to be $U = 10\,e$V, $V = 6\,e$V, and the hopping to be $b = -2.5\,e$V. Notice, however, that screening effects from the leads and the dielectric are expected to renormalize the energy of the benzene many-body states.

lowest *symmetric* state. For example in the case of 4 and 8 particle states it is the first excited state to be the *effective* ground state. In the para configuration also the orbital degeneracy of the $E-$type states is effectively cancelled due to the selection of the symmetric orbital (see Table 4.2).
Small violations of this selection rule, due *e.g.* to molecular vibrations or coupling to an electromagnetic bath, result in the weak connection of different metastable electronic subspaces. We suggest this mechanism as a possible explanation for the switching and hysteretic behavior reported in various molecular junctions. This effect is not addressed in this work.
For a simpler analysis of the different transport characteristics it is useful to introduce a unified geometrical description of the two configurations. In both cases, one lead is rotated by an angle ϕ with respect to the position of the other lead. Hence we can write the creator of an electron in the right contact atom $d^{\dagger}_{\mathrm{R}\tau}$ in terms of the creation operator of the left contact atom and the rotation operator:

$$d^{\dagger}_{\mathrm{R}\tau} = \mathcal{R}^{\dagger}_{\phi} d^{\dagger}_{\mathrm{L}\tau} \mathcal{R}_{\phi}, \tag{4.6}$$

where $\mathcal{R}_{\phi}$ is the rotation operator for the anticlockwise rotation of an angle ϕ around the axis perpendicular to the molecular plane and piercing the center of the benzene ring; $\phi = \pi$ for the para and $\phi = (2\pi/3)$ for the meta configuration.
The energy eigenstates of the interacting Hamiltonian of benzene can be classified also

in terms of their quasi-angular momentum. In particular, the eigenstates of the z-projection of the quasi angular momentum are the ones that diagonalize all operators $\mathcal{R}_\phi$ with angles multiples of $\pi/3$. The corresponding eigenvalues are phase factors $e^{-i\ell\phi}$ where $\hbar\ell$, the quasi-angular momentum of the state, is an integer multiple of $\hbar$. The discrete rotation operator of an angle $\phi = \pi$ (C_2 symmetry operation), is the one relevant for the para configuration. All orbitals are eigenstates of the C_2 rotation with the eigenvalue ± 1.
The relevant rotation operator for the meta configuration correspond to an angle $\phi = 2\pi/3$ (C_3 symmetry operation). Orbitals with an A or B symmetry are eigenstates of this operator with the eigenvalue $+1$ (angular momentum $\ell = 0$ or $\ell = 3$). Hence we can already predict that there will be no difference based on rotational symmetry between the para and the meta configuration for transitions between states involving A- and B-type symmetries. Orbitals with E symmetry however behave quite differently under the C_3 operation. They are the pairs of states of angular momenta $\ell = \pm 1$ or $\ell = \pm 2$. The diagonal form of the rotation operator on the two-fold degenerate subspace of E-symmetry reads:

$$C_3 = \begin{pmatrix} e^{-|\ell|\cdot\frac{2\pi}{3}i} & 0 \\ 0 & e^{|\ell|\cdot\frac{2\pi}{3}i} \end{pmatrix} \tag{4.7}$$

For the two-fold orbitally degenerate 7-particle ground states $|\ell| = 2$. This analysis in terms of the quasi-angular momentum makes the calculation of the fundamental interference condition (4.2) given in the introduction easier. In fact the following relation holds between the transition amplitudes of the 6 and 7 particle ground states:

$$\gamma_{\ell R} \equiv \langle 7_g \ell\tau | d^\dagger_{R\tau} | 6_g \rangle = \langle 7_g \ell\tau | \mathcal{R}^\dagger_\phi d^\dagger_{\mathrm{L}\tau} \mathcal{R}_\phi, | 6_g \rangle = e^{-i\ell\phi}\gamma_{\ell L} \tag{4.8}$$

and (4.2) follows directly.

4.3 Transport calculations

The results discussed here are obtained by solving equation (3.19) in the stationary limit $\dot{\sigma}^{NE}(t) = 0$ and using the result in the formula for the current in chapter 3. As input in equation (3.19), we need the eigenenergies of the isolated molecule described by H_{PPP}, and the matrix elements $\langle NE\ell\tau | d^\dagger_{\alpha\tau''} | N-1E'\ell'\tau' \rangle$ of the operators $d^\dagger_{\alpha\tau}$ that create an electron in a p_z-orbital at the contact atom to lead α, written in the eigenbasis of H_{PPP}. The symmetries of the eigenstates are reflected in these matrix elements. They act as transition amplitudes for the tunneling event from the state $|N-1E'\ell'\tau'\rangle$ to $|NE\ell\tau\rangle$. The sequential tunneling rates are of second order in these amplitudes.
In Figure 4.3 we present the stability diagram for the benzene ISET contacted in the para (upper panel) and meta position (lower panel). Bright ground state transition lines delimit diamonds of zero differential conductance typical for the Coulomb blockade regime, while a rich pattern of satellite lines represents the transitions between excited states. Though several differences can be noticed, most striking are the suppression of the linear conductance, the appearance of negative differential conductance

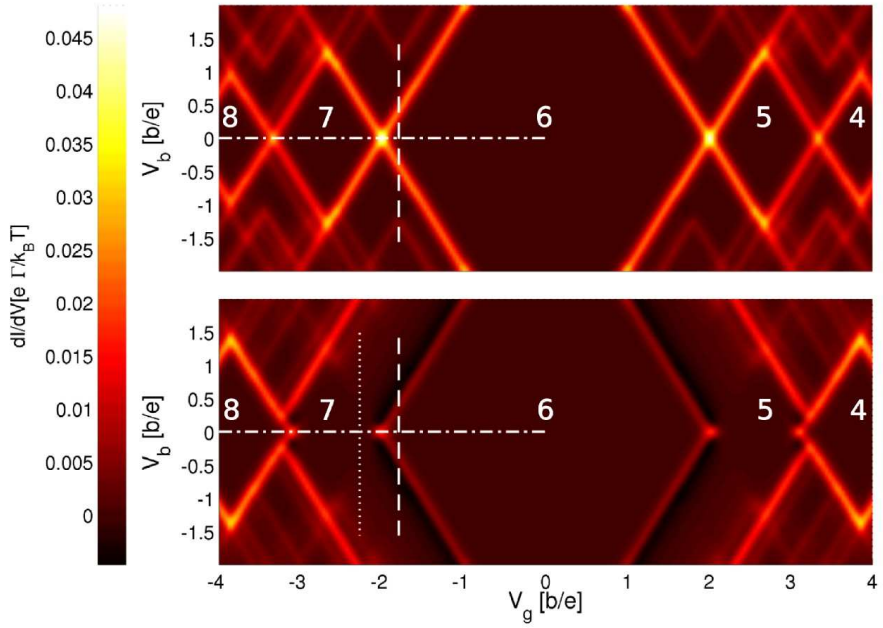

Figure 4.3: Stability diagram for the benzene ISET contacted in the para (above) and meta (below) configuration. Dot-dashed lines highlight the conductance cuts presented in Figure 4.4, the dashed lines the regions corresponding to the current traces presented in Figure 4.5 and Figure 4.7, the dotted line the region corresponding to the current trace presented in Figure 4.6. The parameters used are $U = 4|b|$, $V = 2.4|b|$, $k_{\mathrm{B}}T = 0.04|b|$, $\hbar\Gamma_{\mathrm{L}} = \hbar\Gamma_{\mathrm{R}} = 10^{-3}|b|$.

(NDC) and the strong suppression of the current at the right(left) border of the 7 (5) particle diamond when passing from the para to the meta configuration. All these features are different manifestations of the interference between orbitally degenerate states and ultimately reveal the specific symmetry of benzene.

4.3.1 Linear conductance

We study the linear transport regime both numerically and analytically. For the analytical calculation of the conductance we consider the low temperature limit where only ground states with N and $N+1$ particles have considerable occupation probabilities in a certain range of the gate voltage. Therefore only transitions between these states are relevant and we can treat just the terms of equation (3.19) with N and $N+1$ particles and the ground state energies $E_{\mathrm{g,N}}$ and $E_{\mathrm{g,N+1}}$, respectively. A closer look at (3.19) reveals that the spin coherences are decoupled from the other elements of the density matrix. Thus we can set them to zero, and write (3.19) in a block diagonal form in the basis of the ground states of N and $N+1$ particles. Additionally, since the total Hamiltonian H is symmetric in spin, the blocks of the GME with the same particle but different spin quantum number τ must be identical. Finally, since

around the resonance the only populated states are the N and $N+1$ particle states, the conservation of probability implies that:

$$1 = \sum_n \sigma^{\mathrm{N}}_{nn} + \sum_m \sigma^{\mathrm{N+1}}_{mm}, \tag{4.9}$$

where σ^{N}_{nn} is the population of the N-particle ground state and n contains the orbital and spin quantum numbers. With all these observations we can reduce (3.19) to a much smaller set of coupled differential equations, that can be treated analytically. The stationary solution of this set of equations can be derived more easily by neglecting the energy non-conserving terms in (3.19). These are contained in the elements of the GME describing the dynamics of the coherences between orbitally degenerate states. With this simplification we derive an analytical formula for the conductance close to the resonance between N and $N+1$ particle states as the first order coefficient of the Taylor series of the current in the bias:

$$G_{\mathrm{N,N+1}}(\Delta E) = 2e^2 \frac{\Gamma_{\mathrm{L}}\Gamma_{\mathrm{R}}}{\Gamma_{\mathrm{L}}+\Gamma_{\mathrm{R}}} \Lambda_{\mathrm{N,N+1}} \left[-\frac{f'(\Delta E)}{(S_{\mathrm{N+1}} - S_{\mathrm{N}}) f(\Delta E) + S_{\mathrm{N}}} \right] \tag{4.10}$$

where $\Delta E = -E_{\mathrm{g,N}} + E_{\mathrm{g,N+1}} - (\mu_0 + \kappa e V_{\mathrm{g}})$ is the energy difference between the benzene ground states with N and $N+1$ electrons diminished by a term linear in the gate voltage. The derivation of this formula is rather lengthy but not difficult and thus not given here. Interference effects are contained in the overlap factor $\Lambda_{\mathrm{N,N+1}}$:

$$\Lambda_{\mathrm{N,N+1}} = \frac{\left| \sum_{nm\tau} \langle N,n|d_{\mathrm{L}\tau}|N+1,m\rangle\langle N+1,m|d^\dagger_{\mathrm{R}\tau}|N,n\rangle \right|^2}{\sum_{nm\alpha\tau} \left| \langle N,n|d_{\alpha\tau}|N+1,m\rangle \right|^2}, \tag{4.11}$$

where n and m label the S_{N}-fold and $S_{\mathrm{N+1}}$-fold degenerate ground states with N and $N+1$ particles, respectively. In order to make the interference effects more visible we remind that $d^\dagger_{\mathrm{R}\tau} = \mathcal{R}^\dagger_\phi d^\dagger_{\mathrm{L}\tau} \mathcal{R}_\phi$, with $\phi = \pi$ for the para while $\phi = 2\pi/3$ for the meta configuration. Due to the behavior of all eigenstates of H_{ben} under discrete rotation operators with angles multiples of $\pi/3$, we can rewrite the overlap factor:

$$\Lambda_{\mathrm{N,N+1}} = \frac{\left| \sum_{nm\tau} |\langle N,n|d_{\mathrm{L}\tau}|N+1,m\rangle|^2 e^{i\phi_{nm}} \right|^2}{2\sum_{nm\tau} \left| \langle N,n|d_{\mathrm{L}\tau}|N+1,m\rangle \right|^2}, \tag{4.12}$$

where ϕ_{nm} encloses the phase factors coming from the rotation of the states $|N,n\rangle$ and $|N+1,m\rangle$.

The energy non-conserving terms neglected in (4.10) influence only the dynamics of the coherences between orbitally degenerate states. Thus, equation (4.10) provides an exact description of transport for the para configuration, where orbital degeneracy is cancelled. Even if equation (4.10) captures the essential mechanism responsible for

the conductance suppression, we have derived an exact analytical formula also for the meta configuration and we present it later on.
In Figure 4.4 we present an overview of the results of both the para and the meta configuration. A direct comparison of the conductance (including energy non-conserving terms) in the two configurations is displayed in the upper panel. The lower panel illustrates the effect of the energy non-conserving terms on the conductance in the meta configuration. The number of p_z electrons on the molecule and the symmetry of the lowest energy states corresponding to the conductance valleys are reported. The curve can be continued to negative gate voltages (notice that $b < 0$) by mirroring about $V_g = 0$ and replacing the number of electrons N by $12 - N$. The symmetries displayed in the upper panel belong to the (effective) ground states in the para configuration, the corresponding symmetries for the meta configuration are shown in the lower panel. Figure 4.4 shows that the results for the para and the meta configuration coincide for the $10 \leftrightarrow 11$ and $11 \leftrightarrow 12$ transitions. The ground states with $N = 10, 11, 12$ particles have $A-$ or $B-$type symmetries, they are therefore orbitally non-degenerate, no interference can occur and thus the transitions are invariant under configuration change. For every other transition we see a noticeable difference between the results of the two configurations (Figure 4.4). In all these transitions one of the participating states is orbitally degenerate. First we notice that the linear conductance peaks for the $7 \leftrightarrow 8$ and $8 \leftrightarrow 9$ transitions in the para configuration are *shifted* with respect to the corresponding peaks in the meta configuration. The selection of an effective symmetric Hilbert space associated to the para configuration results in different ground state energies of the 4 and 8 particle states in the two configurations, since in the para configuration the first state participating to transport (the *effective* ground state) is in reality the first excited state. This leads to a redefinition of ΔE for transitions involving these states and therefore to a change in the peak position.
In addition, the total degeneracy is reduced from 4 to 2 by cancelling the orbital degeneracy. The degeneracies $S_{\mathrm{N}}, S_{\mathrm{N+1}}$ of the participating states as well as the ground state energy are both entering the degeneracy term of equation (4.10)

$$\Delta = -\frac{f'(\Delta E)}{(S_{\mathrm{N+1}} - S_{\mathrm{N}}) f(\Delta E) + S_{\mathrm{N}}}. \tag{4.13}$$

In this term, the degeneracies give rise to two effects. First, they shift the maximum of the conductance peak away from the resonance at $\Delta E = 0$. This happens because the symmetric (with respect to $\Delta E = 0$) function $f'(\Delta E)$ is multiplied with an asymmetric, steplike function in the denominator. If the degeneracy of the $N+1$-particle state $S_{\mathrm{N+1}}$ is higher than S_{N}, the maximum will be shifted to the side where N-particles are on the quantum dot. This shift is found to be $\frac{1}{2} k_B T \ln \frac{S_{\mathrm{N+1}}}{S_{\mathrm{N}}}$, proportional to the temperature and to the logarithm of the ratio $\frac{S_{\mathrm{N+1}}}{S_{\mathrm{N}}}$. The second point is that large degeneracies, entering in the denominator, will in general lead to smaller values of Δ. The maximum value of this function Δ for the transition $6 \leftrightarrow 7$ is given in table 4.3.
The most striking effect regarding transitions with orbitally degenerate states participating is the *systematic suppression* of the linear conductance when changing from the para to the meta configuration. The suppression is appreciable despite the con-

ductance enhancement due to the energy non-conserving terms (see Figure 4.4, lower panel). Thus, we will for simplicity discard them in the following discussion.
The conductance suppression is determined by the combination of two effects: the reduction to the symmetric Hilbert space in the para configuration and the interference effects between degenerate orbitals in the meta configuration. As we can see from Table 4.3 on the example of the $6 \leftrightarrow 7$ transition peak, $\Delta_{\max}$ is higher in the para configuration but not enough to fully explain the difference between the two configurations.

	Overlap factor Λ	Degeneracy term $\Delta_{\max}$ $[1/k_{\mathrm{B}}T]$
PARA	$2C$	0,1715
META	$\frac{1}{2}C$	0,1111

Table 4.3: Overlap factor and maximum value of the degeneracy term in the para and the meta configuration for the $6 \leftrightarrow 7$ transition peak. It is $C = |\langle 6_{\mathrm{g}}|d_{\mathrm{L}\tau}|7_{\mathrm{g}}\ell\tau\rangle|^2$, where τ and ℓ are the spin and the quasi angular momentum quantum numbers, respectively. The values of $\Delta_{\max}$ are proportional to $1/k_{\mathrm{B}}T$.

The second effect determining linear transport is the interference between the E-type states, which is accounted for in the overlap factor Λ. The overlap factor is basis independent, thus we can write the transition probabilities for the $6 \leftrightarrow 7$ transition as $|\langle 6_{\mathrm{g}}|d_{\mathrm{L}\tau}|7_{\mathrm{g}}\,\ell\,\tau\rangle|^2 = C$, where τ and ℓ are the spin and the quasi-angular momentum quantum number, respectively. The transition probabilities have the same value, since all four 7 particle states are in this basis equivalent. This can be seen by taking advantage of the symmetry properties of the molecular states with respect to the σ_{v} operation and to the rotation operator R_ϕ for rotations about a discrete angle $\phi = \frac{n\pi}{3}$, as introduced in Section 4.2. The starting point is the generic relation between these two operators:

$$\mathcal{R}_\phi \sigma_{\mathrm{v}} = \sigma_{\mathrm{v}} \mathcal{R}_{-\phi}. \tag{4.14}$$

We can now apply both sides of this relation to the 7 particle ground states $|7_{\mathrm{g}}, \ell = \pm 2\rangle$:

$$\mathcal{R}_\phi \sigma_{\mathrm{v}} |7_{\mathrm{g}}, \ell = \pm 2\rangle = \sigma_{\mathrm{v}} \mathcal{R}_{-\phi} |7_{\mathrm{g}}, \ell = \pm 2\rangle. \tag{4.15}$$

The 7 particle ground states $|7_{\mathrm{g}}, \ell = \pm 2\rangle$ are eigenstates of each $\mathcal{R}_\phi$, and the corresponding eigenvalues are phase factors:

$$\mathcal{R}_\phi |7_{\mathrm{g}}, \ell = \pm 2\rangle = e^{\mp 2 \cdot i\phi} |7_{\mathrm{g}}, \ell = \pm 2\rangle. \tag{4.16}$$

Thus, equation (4.15) becomes

$$\mathcal{R}_\phi \Big(\sigma_{\mathrm{v}} |7_{\mathrm{g}}, \ell = \pm 2\rangle \Big) = e^{\pm 2 \cdot i\phi} \Big(\sigma_{\mathrm{v}} |7_{\mathrm{g}}, \ell = \pm 2\rangle \Big). \tag{4.17}$$

Yet, according to equation (4.16), this equation can only be valid if

$$\sigma_{\mathrm{v}} |7_{\mathrm{g}}, \ell = \pm 2\rangle = \lambda |7_{\mathrm{g}}, \ell = \mp 2\rangle. \tag{4.18}$$

and, since $\sigma_{\mathrm{v}}^2 = 1$, λ can only be a phase factor. For the calculation of the transition probabilities we use further the property $\sigma_{\mathrm{v}}^\dagger \sigma_{\mathrm{v}} = 1$. Since the left contact atom (atom 1) lays in the reflection plane σ_{v}, it is: $\sigma_{\mathrm{v}} d_{\mathrm{L}} \sigma_{\mathrm{v}}^\dagger = d_{\mathrm{L}}$. Also, since the symmetry of the 6 particle ground state is A_{1g}, it is: $\sigma_{\mathrm{v}}|6_{\mathrm{g}}\rangle = |6_{\mathrm{g}}\rangle$. Under these considerations, we can write for the transition probability to the state $|7_{\mathrm{g}}, \ell = 2\rangle$:

$$\begin{aligned} |\langle 6_{\mathrm{g}}|d_{\mathrm{L}}|7_{\mathrm{g}}, \ell = 2\rangle|^2 &= |\langle 6_{\mathrm{g}}|\sigma_{\mathrm{v}}^\dagger \sigma_{\mathrm{v}} d_{\mathrm{L}} \sigma_{\mathrm{v}}^\dagger \sigma_{\mathrm{v}}|7_{\mathrm{g}}, \ell = 2\rangle|^2 = \\ &= |\langle 6_{\mathrm{g}}|d_{\mathrm{L}}\sigma_{\mathrm{v}}|7_{\mathrm{g}}, \ell = 2\rangle|^2 = |\langle 6_{\mathrm{g}}|d_{\mathrm{L}}|7_{\mathrm{g}}, \ell = -2\rangle|^2 = C. \end{aligned} \tag{4.19}$$

Under the C_2 rotation the symmetric 7 particle ground state does not acquire any phase factor. Under the C_3 rotation however, the two orbitally degenerate states acquire different phase factors, namely $e^{\frac{4\pi}{3}i}$ and $e^{-\frac{4\pi}{3}i}$, respectively. Thus the overlap factors Λ for the $6 \leftrightarrow 7$ transition are:

$$\begin{aligned} \Lambda_{\mathrm{para}} &= \frac{1}{8C} \cdot |4C|^2 = 2C, \\ \Lambda_{\mathrm{meta}} &= \frac{1}{8C} \cdot \left|2Ce^{+\frac{4\pi}{3}i} + 2Ce^{-\frac{4\pi}{3}i}\right|^2 = \frac{1}{2}C. \end{aligned}$$

We see that Λ is four times larger in para configuration. The linear conductance is determined by the product between the overlap factor and the degeneracy term. It is the *destructive interference* between degenerate E-type orbitals, accounted for in the overlap factor Λ, that gives the major contribution to the strong suppression of the conductance in the meta configuration.

Analytical formula for the linear conductance including the energy non-conserving terms

In the derivation of the conductance formula (4.10) we neglected the energy non-conserving terms in the equation (3.19). Since in the GME they appear only in the dynamics of the coherences between orbitally degenerate states, equation (4.10) is exact for the para configuration, where the orbital degeneracy is cancelled. This is not the case in the meta configuration where the orbital (quasi-)degeneracy is essential for the description of interference. Thus we derived a generic analytical formula for the conductance, taking into account the energy non-conserving terms. Again, we give here just the result, because the derivation is lengthy and does not lead to new insights. It reads

$$G_{\mathrm{N,N+1}}(\Delta E) = e^2 \Gamma \Lambda_{\mathrm{N,N+1}} \Delta \left[1 + \frac{\mathrm{aux}(S_{\mathrm{N}}, S_{\mathrm{N+1}}) 12 \Lambda_{\mathrm{N,N+1}}^2 \left(f^{\pm}(\Delta E)\right)^2}{16 \Lambda_{\mathrm{N,N+1}}^2 \left(f^{\pm}(\Delta E)\right)^2 + \omega^2}\right]. \tag{4.20}$$

Here, it is $\Gamma = \Gamma_{\mathrm{L}} = \Gamma_{\mathrm{R}}$. $\Lambda_{N,N+1}$ and Δ are the overlap factor and the degeneracy term introduced in Eqs. (4.11), (4.12). The auxiliary function $\mathrm{aux}(S_{\mathrm{N}}, S_{\mathrm{N+1}})$ in the correction term is zero if there are *no* orbitally degenerate ground states involved in the transition. If one of the participating states is orbitally degenerate it is $\mathrm{aux}(S_{\mathrm{N}}, S_{\mathrm{N+1}}) = 1$. The sign in $f^{\pm}(\Delta E)$ is defined as follows: $f^{+}(\Delta E)$ has to be used

if the N particle ground state is orbitally degenerate. If instead the $N+1$ particle ground state exhibits orbital degeneracy, $f^-(\Delta E)$ has to be inserted. The energy non-conserving terms are included in the factor $\omega = \omega_{\rm L}|_{V_{\rm b}=0} = \omega_{\rm R}|_{V_{\rm b}=0}$. It is defined only if a degenerate state is participating in transport. In case that *e.g.* the N particle ground state has two degenerate orbitals $|N_{\rm g},1\rangle$, $|N_{\rm g},2\rangle$, ω_α with $\alpha = L,R$ reads

$$\begin{aligned}\omega_\alpha &= \sum_{{\rm E}',l}\left[\frac{i}{\pi}p_\alpha(E_{\rm g,N}-E')\right]\langle N_{\rm g},1|d^\dagger_{L\tau}|N-1,E'\,l\rangle\langle N-1,E'\,l|d_{L\tau}|N_{\rm g},2\rangle \quad (4.21)\\ &+\sum_{{\rm E}',l}\left[\frac{i}{\pi}p_\alpha(E'-E_{\rm g,N})\right]\langle N_{\rm g},1|d_{L\tau}|N+1,E'\,l\rangle\langle N+1,E'\,l|d^\dagger_{L\tau}|N_{\rm g},2\rangle,\end{aligned}$$

where $p_\alpha(x) = -{\rm Re}\psi\left[\frac{1}{2}+\frac{i\beta}{2\pi}(x-\mu_\alpha)\right]$ and ψ is the digamma function, as defined in Section 3.3. The presence of these terms reduces the efficiency of the destructive interference due to a renormalization of the energies of the states involved. In this expression, a particular choice of the basis is implied, such that $\langle N_{\rm g},i|d^\dagger_{L\tau}|N-1,E'\,l\rangle$, $\langle N_{\rm g},i|d_{L\tau}|N+1,E'\,l\rangle$, $i=1,2$, are real and do not depend on i. We will discuss this and the effect of renormalization on the non-linear current in chapter 5.

4.3.2 Negative differential conductance (NDC) and current blocking

Interference effects between orbitally degenerate states are also affecting non-linear transport and producing in the *meta* configuration current blocking and thus NDC at the border of the 6 particle state diamond (Figure 4.3). The upper panel of Figure 4.5 shows the current through the benzene ISET contacted in the meta configuration as a function of the bias voltage. The current is given for parameters corresponding to the white dashed line of Figure 4.3. In this region only the 6 and 7 particle ground states are populated.

At low bias the 6 particle state is mainly occupied. As the bias is raised, transitions $6 \leftrightarrow 7$ occur and current flows. Above a certain bias threshold a blocking state is populated and the current drops. For the understanding of this non-linear current characteristics, we have to take into account energy conservation, the Pauli exclusion principle and, in addition, the interference between participating states. For the visualization of the interference effects, we introduce the transition probability (averaged over the z coordinate and the spin σ):

$$P(x,y;n,\,\tau) = \lim_{L\to\infty}\sum_\sigma \frac{1}{2L}\int_{-L/2}^{L/2}{\rm d}z|\langle 7_{\rm g}\,n\,\tau|\psi^\dagger_\sigma(\mathbf{r})|6_{\rm g}\rangle|^2 \qquad (4.22)$$

for the *physical* 7 particle basis, *i.e.*, the 7 particle basis that diagonalizes the stationary density matrix at a fixed bias. Here τ is the spin quantum number, $n=1,2$ labels the two states of the physical basis which are linear combinations of the orbitally degenerate states $|7_{\rm g}\ell\tau\rangle$ and can be interpreted as conduction channels. Each of the central panels of Figure 4.5 are surface plots of (4.22) at the different bias voltages *a-c*.

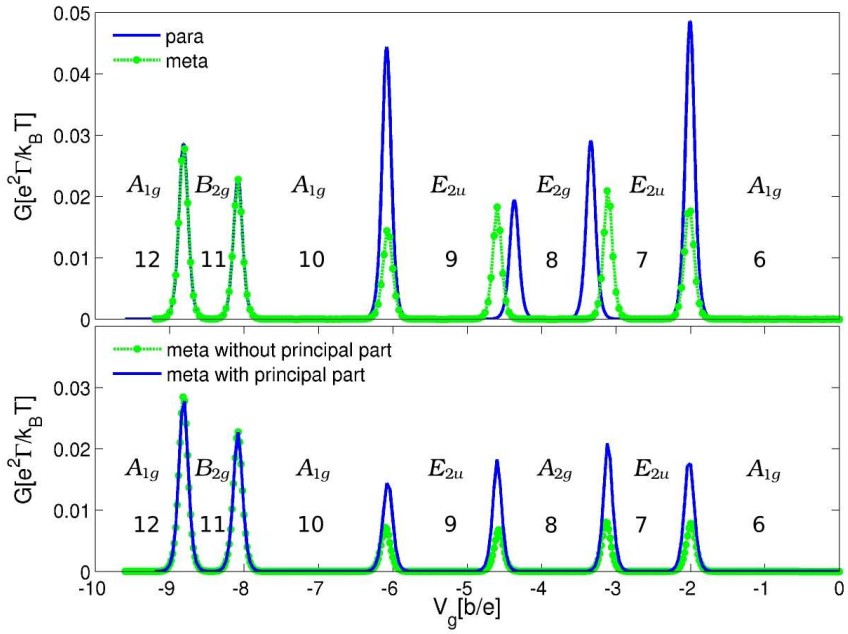

Figure 4.4: Conductance of the benzene ISET as a function of the gate voltage. Clearly visible are the peaks corresponding to the transitions between ground states with N and $N + 1$ particles. In the low conductance valleys the state of the system has a definite number of particles and symmetry as indicated in the upper panel for the para, in the lower for the meta configuration. Selective conductance suppression when changing from the meta to the para configuration is observed.

The 7 particle ground states can interfere and thus generate nodes in the transition probability at the contact atom close to one or the other lead, but, in the meta configuration, never at both contact atoms at the same time.

Energetic considerations are illustrated in the lower panels of Figure 4.5 for two key points of the current curve at positive biases. The left panel corresponds to the resonance peak of the current. Due to energy conservation, electrons can exit the molecule at both leads. On the contrary the entry is allowed only at the right leads. The current is suppressed when transitions occur to a state which cannot be depopulated (a blocking state). Since, energetically, transmissions to the 6 particle state are allowed at both leads, each 7 particle state can always be depopulated and no blocking occurs.

The current blocking scenario is depicted in the lower right panel of Figure 4.5. For large positive bias the transition from a 7 particle ground state to the 6 particle ground state is energetically forbidden at the left lead. Thus, for example, the *c* panel in Figure 4.5 visualizes the current blocking situation yielding NDC: while for both channels there is a non-vanishing transition probability from the source lead to the molecule, for the upper channel a node prevents an electron from exiting to the drain lead. In the long time limit the blocking state gets fully populated while the non-blocking state is empty. At large negative bias the blocking scenario is depicted in the panel *a* that shows the left-right symmetry obtained by a reflection through a plane perpendicular to the molecule and passing through the carbon atoms atoms 6 and 3. We remark that only a description that retains coherences between the degenerate 7 particle ground states correctly captures NDC at both positive and negative bias.

In contrast to the $6 \to 7$ transition, one does *not* observe NDC at the border of the 7 particle Coulomb diamond, but rather a strong suppression of the current. The upper panel of Figure 4.6 shows the current through the benzene ISET contacted in the meta configuration as a function of the bias voltage corresponding to the white dotted line of Figure 4.3. The middle panels show the transition probabilities between each of the 7 particle and the 6 particle ground state.

The lower panel of Figure 4.6 shows a sketch of the energetics at positive bias corresponding to the "expected" resonance peak. Here electrons can enter the molecular dot at both leads, while the exit is energetically forbidden at the left lead due to Paulis exclusion principle. Thus, if the system is in the 7 particle state which is blocking the right lead, this state cannot be depopulated, becoming the blocking state.

On the other hand, transitions from the 6 particle ground state to both 7 particle ground states are equally probable. Thus the blocking state will surely be populated at some time. The upper plot of the *b* panel in Figure 4.6 shows the transition probability to the blocking state that accepts electrons from the source lead but cannot release electrons to the drain.

As just proved, in this case the current blocking situation occurs already at the resonance bias voltage. For a higher positive bias, the transition probability from the blocking state at the drain lead increases and current can flow. This effect, though, can be captured only by taking into account also the energy non-conserving terms in (3.19). We study the influence of these terms in detail in chapter 5.

In the *para* configuration, the current as a function of the bias voltage is shown in

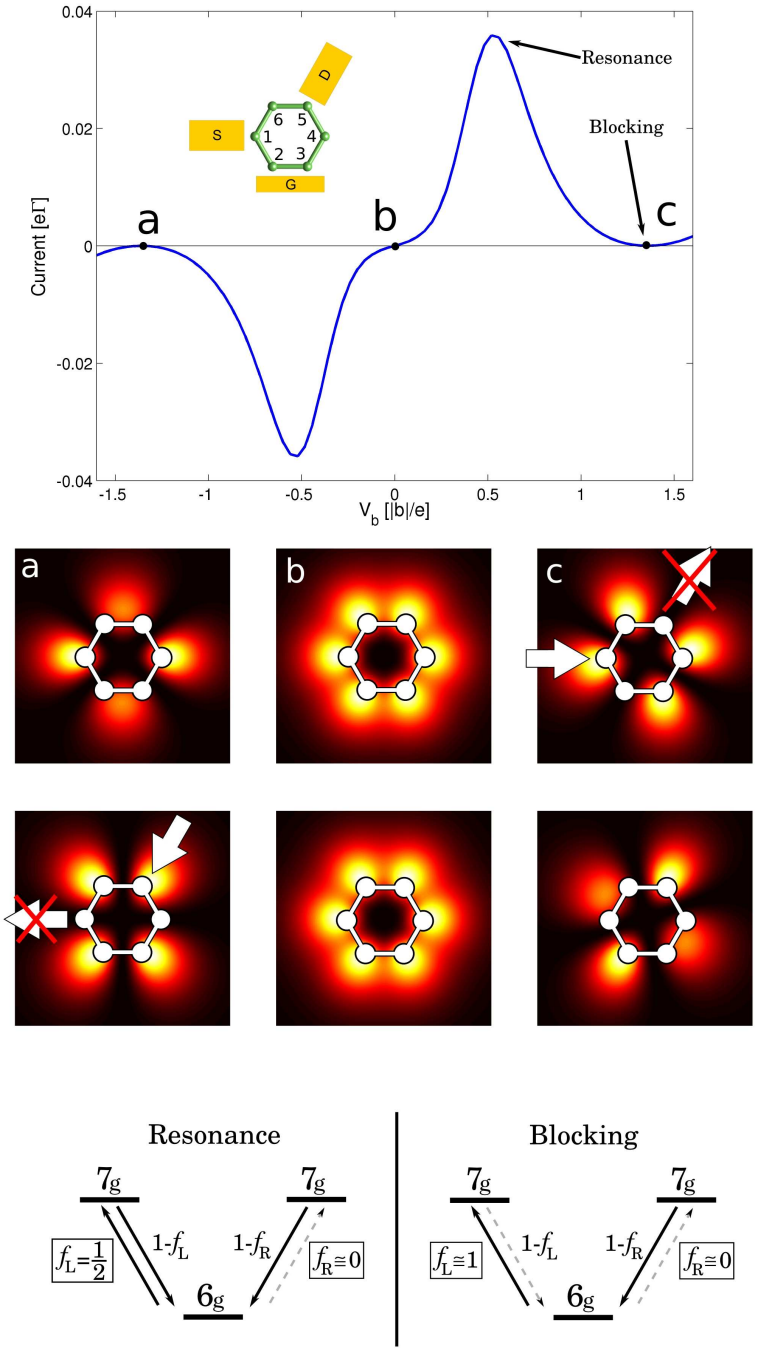

Figure 4.5: Upper panel - Current through the benzene ISET in the meta configuration calculated at bias and gate voltage conditions indicated by the dashed line of Figure 4.3. A pronounced NDC with current blocking is visible. Middle panels - Transition probabilities between the 6 particle and each of the two 7 particle ground states for bias voltage values labelled $a - c$ in the upper panel. The transition to a blocking state is visible in the upper (lower) part of the c (a) panels. Lower panels - Sketch of the energetics for the $6 \rightarrow 7$ transition in the meta configuration at bias voltages corresponding to the resonance current peak and current blocking as indicated in the upper panel of this figure.

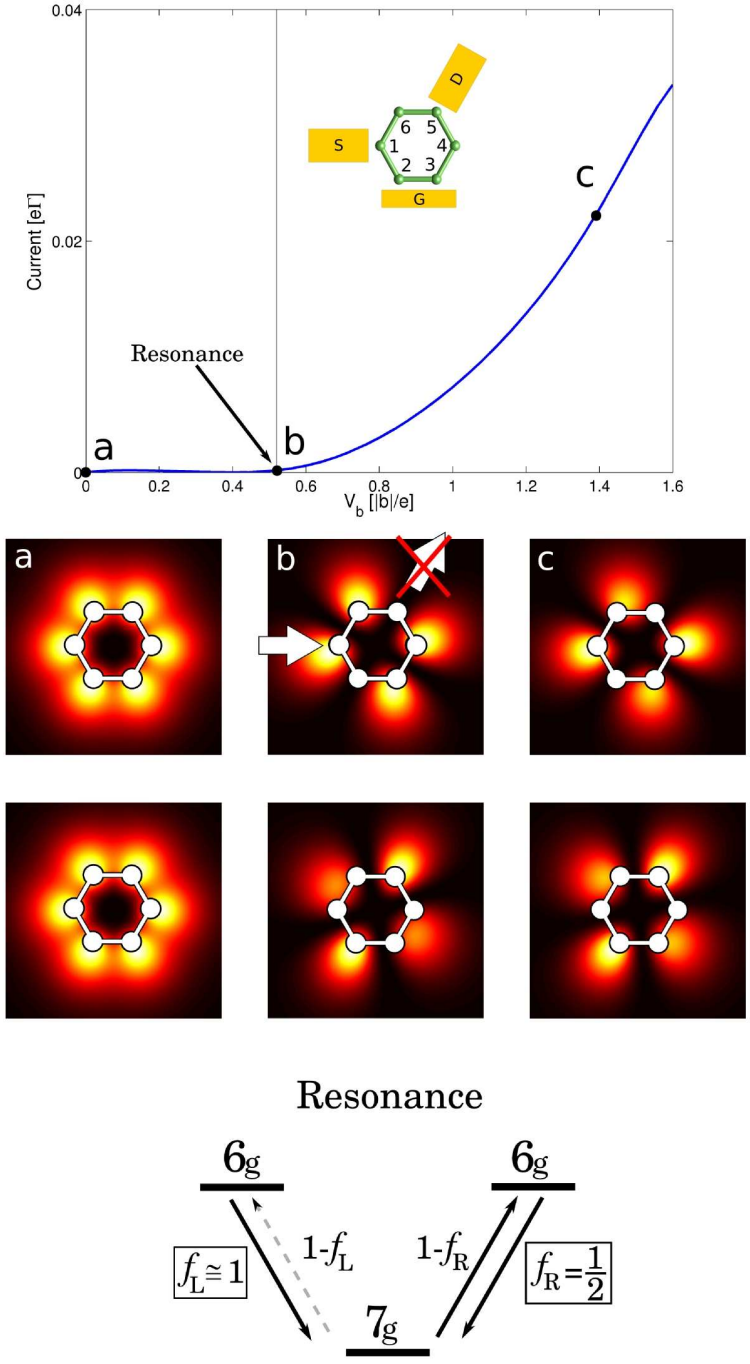

Figure 4.6: Upper panel - Current through the benzene ISET in the meta configuration calculated at bias and gate voltage conditions indicated by the dotted line of Figure 4.3. No NDC is visible. Middle panels - Transition probabilities between each of the 7 particle and the 6 particle ground state for bias voltage values labelled $a - c$ in the upper panel. Lower panel - Sketch of the energetics for the $7 \rightarrow 6$ transition in the meta configuration at bias voltage corresponding to the expected resonance peak. (compare to Figure 4.5).

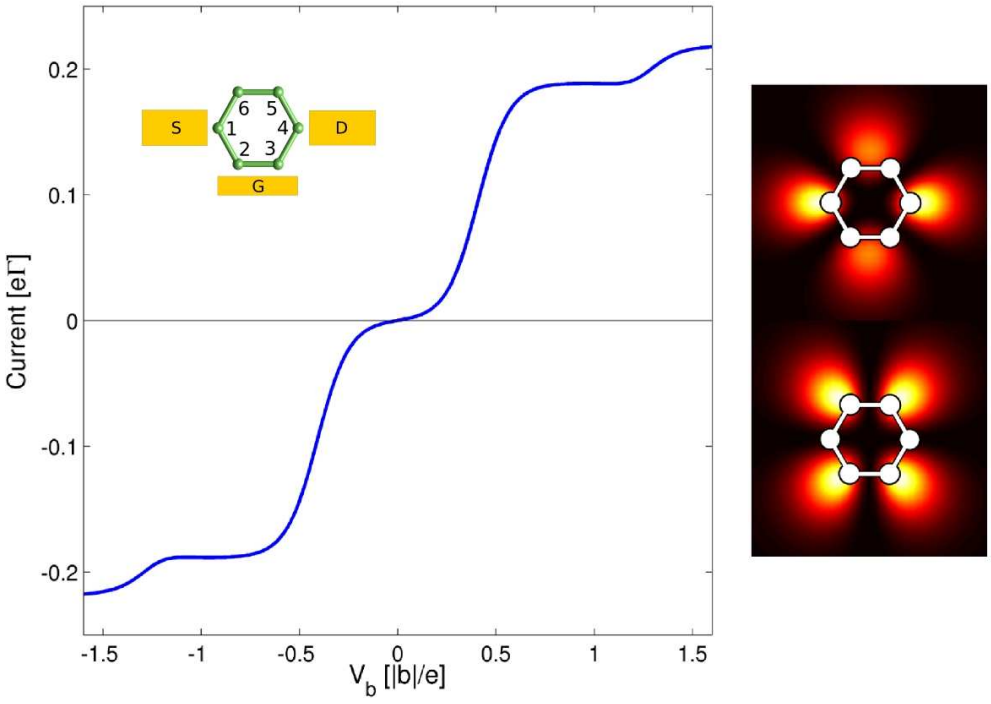

Figure 4.7: Left panel - Current through the benzene ISET in the para configuration calculated at bias and gate voltage conditions indicated by the dashed line of Figure 4.3. No interference effects are visible. Right panels - Transition probabilities between the 6 particle and the symmetric and antisymmetric 7 particle ground states.

Figure 4.7. The current is given for parameters corresponding to the white dashed line of Figure 4.3. In this case, no interference effects are visible. We see instead the typical step-like behavior of the current in the Coulomb blockade regime.
The panels on the right are the surface plots of

$$P(x,y;\tau) = \lim_{L\to\infty} \sum_{\sigma} \frac{1}{2L} \int_{-L/2}^{L/2} \mathrm{d}z |\langle 7_{\mathrm{g}}\, \tau; (\mathrm{a})\mathrm{sym}|\psi_{\sigma}^{\dagger}(\mathbf{r})|6_{\mathrm{g}}\rangle|^2. \tag{4.23}$$

The upper plot shows the transition probability to the symmetric 7 particle state, the lower to the antisymmetric. Remember that in the para configuration only the symmetric states contribute to transport, which means that orbital degeneracies or coherences between orbitally degenerate states do not play any role in the transport. Thus in the para configuration, no interference triggered current blocking or NDC can occur.

4.4 Reduced symmetry

In this section we study the effect of reduced symmetry on the results presented previously. To do so, we generalize the model Hamiltonian by taking into account the perturbations on the molecule due to the contacts and the bias voltage. The contact between molecule and leads is provided by different anchor groups. These linkers are coupled to the contact carbon atoms over a σ bond thus replacing the corresponding benzene hydrogen atoms. Due to the orthogonality of π and σ orbitals, the anchor groups affect in first approximation only the σ orbitals of benzene. In particular the different electron affinity of the atoms in the linkers imply a redistribution of the density of σ electrons. Assuming that transport is carried by π electrons only, we model the effect of this redistribution as a change in the on-site energy for the p_z orbitals of the contact carbon atoms:

$$H'_{\mathrm{PPP}} := H_{\mathrm{contact}} = \xi_{\mathrm{c}} \sum_{\alpha\sigma} d^{\dagger}_{\alpha\sigma} d_{\alpha\sigma}, \quad \alpha = L, R \tag{4.24}$$

where $R = 3, 4$, respectively, in the meta and para configuration, $L = 1$ in both setups. We also study the effect of an external bias on the benzene ISET. In particular we release the strict condition of potential drop all concentrated at the lead-molecule interface. Nevertheless, due to the weak coupling of the molecule to the leads, we assume that only a fraction of the bias potential drops across the molecule. For this residual potential we take the linear approximation $V_{\mathrm{b}}(\mathbf{r}) = -\frac{V_{\mathrm{b}}}{a}(\mathbf{r} \cdot \hat{\mathbf{r}}_{\mathrm{sd}}/a_0)$, where we choose the center of the molecule as the origin and $\hat{\mathbf{r}}_{\mathrm{sd}}$ is the unity vector directed along the source to drain direction. $a_0 = 1.43\,\mathring{A}$ is the bond length between two carbon atoms in benzene, a is the coefficient determining the intensity of the potential drop over the molecule. Since the p_z orbitals are strongly localized, we can assume that this potential will not affect the inter-site hopping, but only the on-site term of the Hamiltonian:

$$H'_{\mathrm{PPP}} := H_{\mathrm{bias}} = e \sum_{i\sigma} \xi_{\mathrm{b}_i} d^{\dagger}_{i\sigma} d_{i\sigma} \tag{4.25}$$

with $\xi_{\mathrm{b}_i} = \int d\mathbf{r}\; p_z(\mathbf{r} - \mathbf{R}_i) V_{\mathrm{b}}(\mathbf{r}) p_z(\mathbf{r} - \mathbf{R}_i)$.

Under the influence of the contacts or the bias potential, the symmetry of the molecule changes. Table 4.4 shows the point groups to which the molecule belongs in the perturbed setup. This point groups have only A- and B-type reducible representations. Thus the corresponding molecular orbitals do not exhibit orbital degeneracy.
No interference effects influence the transport in the para configuration. Thus we do not expect its transport characteristics to be qualitatively modified by the new set up with the corresponding loss of degeneracies.

In the meta configuration on the other hand, interferences between orbitally degenerate states play a crucial role in the explanation of the occurring transport features. Naïvely one would therefore expect that neither conductance suppression nor NDC and current

	PARA	META
Contact perturb.	D_{2h}	C_{2v}
Bias perturb.	C_{2v}	C_{2v}

Table 4.4: Point groups to which the molecule belongs under the influence of the contacts and the external bias potential.

blocking occur in a benzene ISET with reduced symmetry. Yet we find that, under certain conditions, the mentioned transport features are robust under the lowered symmetry.

The perturbations due to the contacts and the bias lead to an expected level splitting of the former orbitally degenerate states. Very different current-voltage characteristics are obtained depending on the relation between the energy splitting δE and other two important energy scales of the system: the tunnelling rate $\hbar\Gamma$ and the temperature $k_{\mathrm{B}}T$. In particular, when $\delta E \ll \hbar\Gamma \ll k_{\mathrm{B}}T$, interference phenomena persist. In contrast, when $\hbar\Gamma < \delta E \ll k_{\mathrm{B}}T$ interference phenomena disappear, despite the fact that, due to temperature broadening, the two states still can not be resolved. In this regime, due to the asymmetry in the tunnelling rates introduced by the perturbation, standard NDC phenomena, see Figure 4.9, occur.

In the absence of perfect degeneracy, we abandon the strict secular approximation scheme that would discard the coherences in the density matrix between states with different energies. We adopt instead a softer approximation by retaining also coherences between quasi-degenerate states. Since they have Bohr frequencies comparable to the tunnelling rate, they influence the stationary density matrix. Formulas for the GME and the current taking into account these coherence terms are presented in section 3.4.

Figure 4.8 shows from left to right closeup views of the stability diagram for the setup under the influence of increasing *contact perturbation* around the $6 \leftrightarrow 7$ resonance. The orbital degeneracy of the 7 particle states is lifted and the transport behavior for the $6 \leftrightarrow 7$ transition depends on the energy difference between the formerly degenerate 7 particle ground states. In panel *a* the energy difference is so small that the states are quasi-degenerate: $\delta E \ll \hbar\Gamma \ll k_{\mathrm{B}}T$. As expected, we recover NDC at the border of the 6 particle diamond and current suppression at the border of the 7 particle diamond, like in the unperturbed setup.

Higher on-site energy-shifts correspond to a larger level spacing. Panel *b* displays the situation in which the latter is of the order of the level broadening, but still smaller than the thermal energy ($\delta E \simeq \hbar\Gamma \ll k_{\mathrm{B}}T$): no interference causing NDC and current blocking can occur. Yet, due to thermal broadening, we cannot resolve the two 7 particle states.

Eventually, panel *c* presents the stability diagram for the case $\delta E > k_{\mathrm{B}}T > \hbar\Gamma$: the level spacing between the 7 particle ground and first excited state is now bigger than the thermal energy, thus the two transition lines corresponding to these states are clearly visible at the border of the 6 particle stability diamond.

Figure 4.9 shows closeup views of the stability diagram for the setup under the influ-

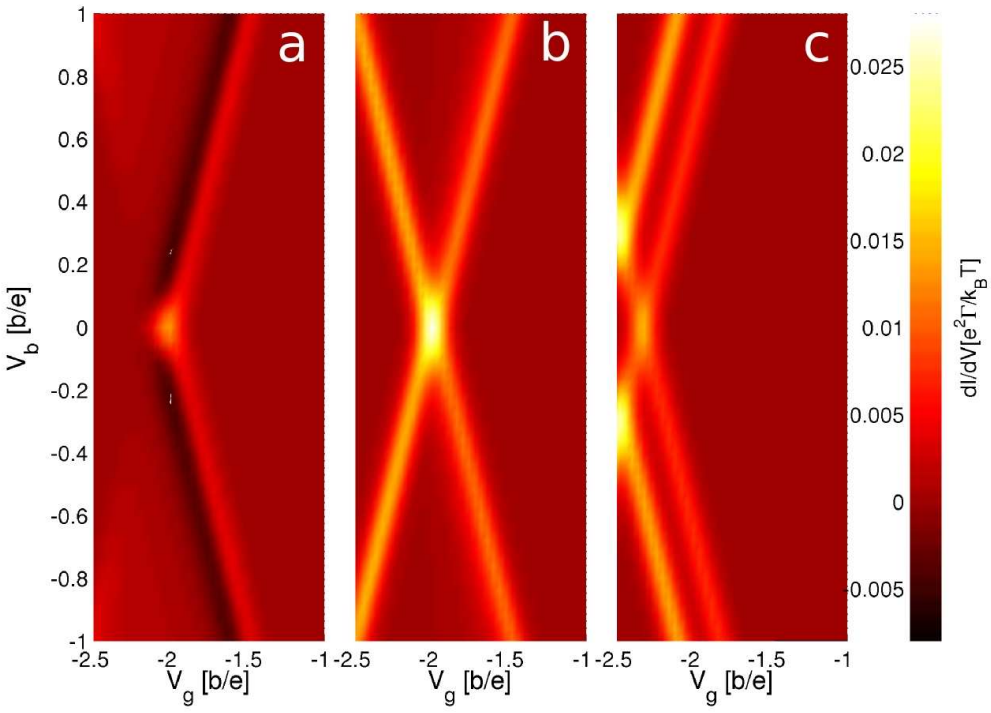

Figure 4.8: Closeup views of the stability diagram around the $6 \leftrightarrow 7$ resonance for the system under contact perturbation. The perturbation strength grows from left to right The parameter that describes the contact effect assumes the values $\xi_c = 0.15\hbar\Gamma$, $2\hbar\Gamma$, $15k_{\mathrm{B}}T$ from left to right respectively and $k_{\mathrm{B}}T = 10\hbar\Gamma$.

ence of the *bias perturbation* at the border of the 6 and 7 particle diamonds. The same region is plotted for different strengths of the external potential over the molecule. In contrast to the contact perturbation, the amount of level splitting of the former degenerate states is here bias dependent. This fact imposes a bias window of interference visibility. The bias must be small enough, for the 7 particle states to be quasi-degenerate and at the same time bigger than the thermal energy, so that the occurring NDC is not obscured by the thermally broadened conductance peak. A strong electrostatic potential perturbation closes the bias window and no interference effect can be detected.

Panel *a* of Figure 4.9 represents the weak perturbation regime with no qualitative differences with the unperturbed case. The typical fingerprints of interference (NDC at the border of the 6 particle diamond and current blocking for the $7 \rightarrow 6$ transition) are still visible for intermediate perturbation strength (panel *b*) but this time only in a limited bias window. Due to the perturbation strength, at some point in the bias, the level splitting is so big that the quasi-degeneracy is lifted and the interference effects destroyed. In panel *c* the quasi-degeneracy is lifted in the entire bias range. There is NDC at the border of the 6 particle diamond, but is not accompanied by current

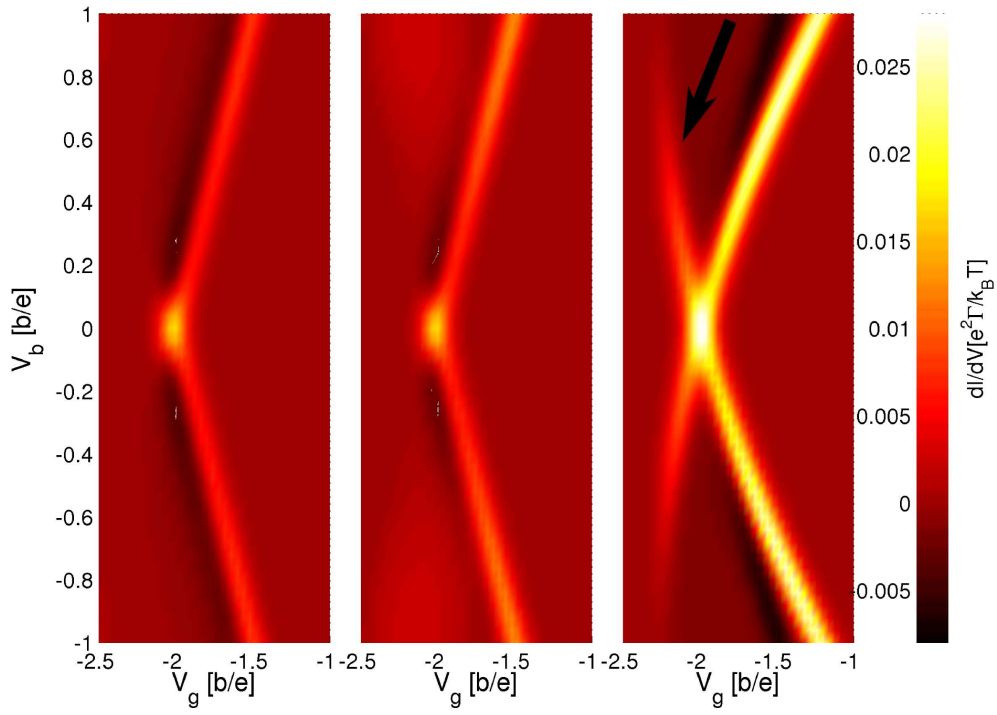

Figure 4.9: Closeup views of the stability diagram around the $6 \leftrightarrow 7$ resonance for the system under the effect of the bias potential, displayed for different strengths of the electrostatic potential drop over the molecule. The parameter that describe the strength of the electrostatic drop overthe molecule assumes the values $a = 25$, 12, 0.6 from left to right respectively.

blocking as proved by the excitation line at the border of the 7 particle diamond (see arrow): no interference occurs. The NDC is here associated to the sudden opening of a slow current channel, the one involving the 6 particle ground state and the 7 particle (non-degenerate) excited state (standard NDC).

Figure 4.10 refers to the setup under both the *bias and contact perturbations*. The left panel shows the energy of the lowest 7 particle states as a function of the bias. In the right panel we present the stability diagram around the $6 \leftrightarrow 7$ resonance. NDC and current blocking are clearly visible only in the bias region where, due to the combination of bias and contact perturbation, the two seven particle states return quasi-degenerate. Also the fine structure in the NDC region is understandable in terms of interference if we take into account the renormalization of the level splitting due to the energy non-conserving terms in the condition of quasi-degeneracy.

Interference effects predicted for the unperturbed benzene ISET are robust against various sources of symmetry breaking. Quasi-degeneracy, $\delta E \ll \hbar\Gamma \ll k_{\mathrm{B}}T$, is the necessary condition required for the detection of the interference in the stability diagram of the benzene ISET.

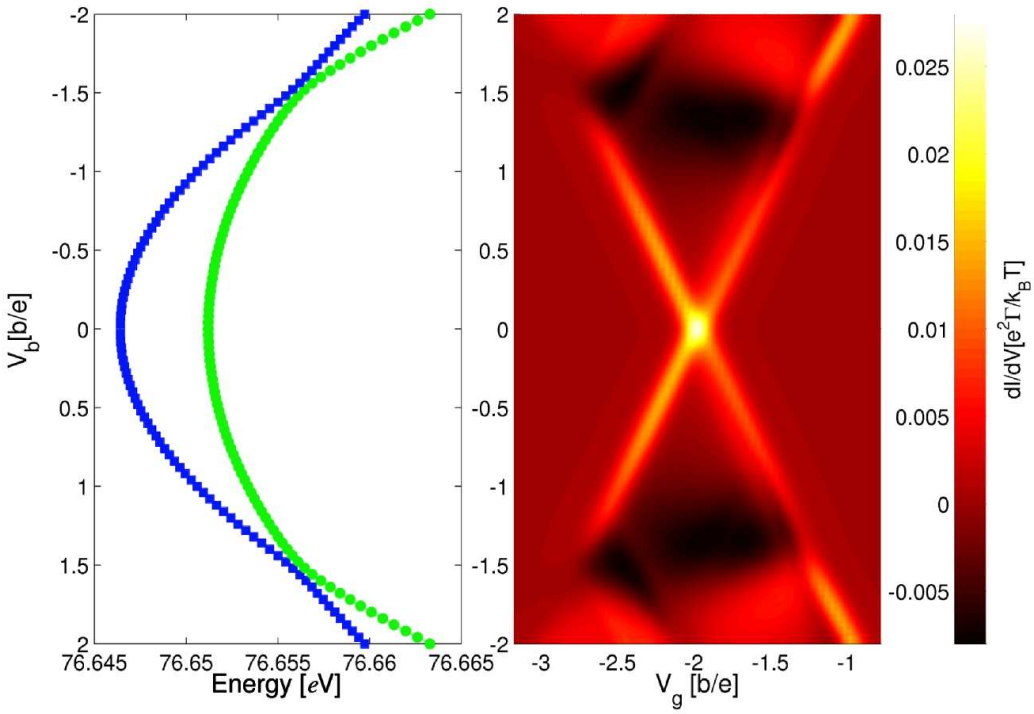

Figure 4.10: Combination of the bias and contact perturbations. Left panel - Energy levels of the 7 particle ground and first excited state as functions of the bias voltage. Right panel - Stability diagram around the $6 \leftrightarrow 7$ resonance. The perturbation parameters are in this case $\xi_c = 2\hbar\Gamma$ and $a = 12$.

The results presented in this chapter were obtained in collaboration with Dana Darau, Andrea Donarini and Milena Grifoni. They were published in

[17] G. Begemann, D. Darau, A. Donarini, and M. Grifoni, Phys. Rev. B **77**, 201406 (2008), Erratum: Phys. Rev. B **78**, 089901(E) (2008).

[18] D. Darau, G. Begemann, A. Donarini, and M. Grifoni, Phys. Rev. B **79**, 235404 (2009).

Chapter 5

All-electric spin control in interference single electron transistors

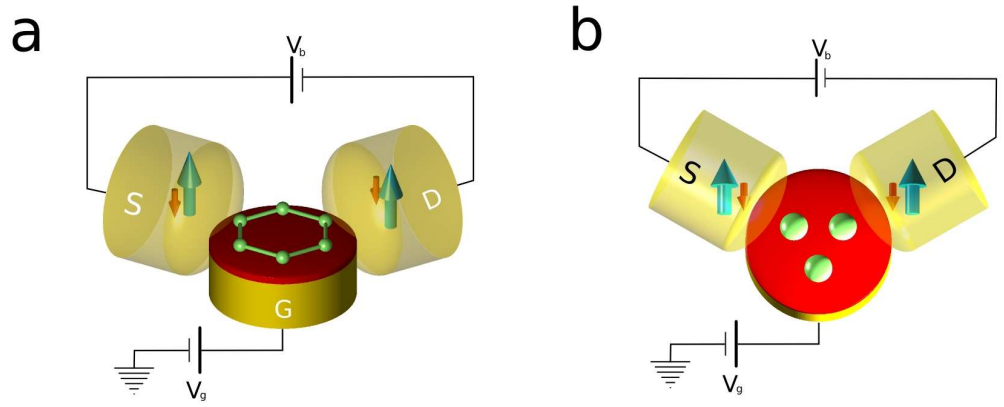

Figure 5.1: Two examples of interference single electron transistors (ISETs): a benzene molecular junction contacted in the meta configuration (a) and a triple quantum dot artificial molecule (b). The source and drain are parallel polarized ferromagnetic leads.

Interference blocking in SETs is expected whenever a non-degenerate N particle ground state and two degenerate $N+1$ particle ground states contribute simultaneously to transport and the ratio of the transition amplitudes between those N and $N+1$ particle states is different on the left and on the right, equation (4.1). This condition is rather general and can be fulfilled not only in benzene ISETs, but for example also in triangular quantum dots (TQD) (see Figure 5.1), or other systems that show orbital degeneracies.
In this chapter, we show that in ISETs in the presence of parallel polarized ferromagnetic leads the interplay between interference and the exchange interaction on the system generates an effective energy renormalization yielding different blocking biases for majority and minority spins. Hence, by tuning the bias voltage full control over

the spin of the trapped electron is achieved. We present here our results showing spin selective interference blockade, for both the benzene ISET and the TQD ISET. In the TQD ISET, we also demonstrate the possibility of switching between components of an excited triplet states by means of the bias voltage.
The system Hamiltonian for the TQD ISET is given by

$$\begin{aligned} H_{\mathrm{PPP}} &= \xi \sum_{i=1}^{3} \sum_{\sigma} d_{i\sigma}^{\dagger} d_{i\sigma} + b \sum_{i=1}^{3} \sum_{\sigma} \left(d_{i\sigma}^{\dagger} d_{i+1\sigma} + d_{i+1\sigma}^{\dagger} d_{i\sigma} \right) \\ &+ U \sum_{i=1}^{3} \left(n_{i\uparrow} - \frac{1}{2} \right) \left(n_{i\downarrow} - \frac{1}{2} \right) + \frac{1}{2} \sum_{i}^{3} V \left(n_{i\uparrow} + n_{i\downarrow} - 1 \right) \left(n_{i+1\uparrow} + n_{i+1\downarrow} - 1 \right), \end{aligned} \tag{5.1}$$

where cyclic boundary conditions are implied. Notice the formal similarity to the PPP Hamiltonian for benzene.
From what we learned in the previous chapter, we would conclude that the interference blocking is a threshold effect and the current remains blocked until a new excited state participates to the transport. However, as shown in Figure 5.2, panels a and b, the current is blocked only at specific values of the bias voltage. In presence of polarized leads, we observe current blocking at two specific bias values (panels c and d), and the analysis of the stationary solution of the GME reveals two blocking states with different spin projection. In the TQD ISET, we find analogous results.
The explanation for the blocking at specific biases only relies on the following observation: The blocking state (Figure 5.4) must be antisymmetric with respect to the plane perpendicular to the system and passing through its center and the atom closest to the drain; this state is thus also an eigenstate of the projection of the angular momentum in the direction of the drain lead. The corresponding eigenvalue depends on the symmetry of the atomic wave function with respect to the molecular plane: $\hbar$ or 0 for symmetric or antisymmetric wave functions respectively. At positive (negative) bias voltages we call this state the $R(L)$-antisymmetric state $|\psi_{R(L),a}\rangle$. But the coupling between the system and the leads not only generates the tunneling dynamics described so far, but also contributes to an internal dynamics of the system that distorts the antisymmetric state, but leaves the systems particle number unchanged.

5.1 Effective Hamiltonian for the internal dynamics

In fact the equation of motion for the reduced density matrix σ of the system (equation (3.19)) can be cast, to lowest non vanishing order in the coupling to the leads, in the form:

$$\dot{\sigma} = -\frac{i}{\hbar}[H_{\mathrm{sys}}, \sigma] - \frac{i}{\hbar}[H_{\mathrm{eff}}, \sigma] + \mathcal{L}_{\mathrm{tun}}\sigma. \tag{5.2}$$

The commutator with H_{sys} in equation (5.2) represents the coherent evolution of the system in absence of the leads. It vanishes in the secular approximation. The operator $\mathcal{L}_{\mathrm{tun}}$ describes the sequential tunnelling processes and it is defined as all the terms in

equation (3.19) that contain the Fermi function. Finally $H_{\rm eff}$ renormalizes the coherent dynamics associated to the system Hamiltonian. It includes all the terms containing the digamma function in equation (3.19). The transition amplitudes $\gamma_{\alpha i}$ between the N and $N+1$ particle states like the ones introduced in equation (4.1) are contained in both $H_{\rm eff}$ and $\mathcal{L}_{\rm tun}$. $H_{\rm eff}$ can be written as:

$$H_{\rm eff} = \sum_{\alpha\tau} \omega_{\alpha\tau} L_\alpha, \tag{5.3}$$

where L_α is the projection of the angular momentum in the direction of the lead α and, for paramagnetic systems, it does not depend on the spin degree of freedom τ. Moreover, $\omega_{\alpha\tau}$ is the renormalization frequency given to the states of spin τ by their coupling to the α lead. Similar effective dynamics has been mapped into the precession of a pseudo-spin around a pseudo-exchange field [69, 76]. In our case the presence of parallel polarized leads mixes the orbital and the spin degrees of freedom. Although $H_{\rm eff}$ is diagonal for what concerns the spin, and thus spin accumulation due to precession [68] of the spin degree of freedom is excluded, in the presence of polarized leads, the spin up and the spin down undergo different effective dynamics. In particular, we find that at the bias voltage where the blocking conditions for one spin species are exactly fulfilled, the other spin species still feels a renormalization and thus does not form a completely blocking state. This leads to a full population of one specific spin species at that bias voltage.

For sake of simplicity we give in the following the explicit form of the transition amplitudes $\gamma_{\alpha i}$, of the operator L_α and of the associated frequency $\omega_{\alpha\tau}$ only for the benzene ISET and for the ground state transition $6_g \rightarrow 7_g$ that is characterized by interference blocking. The argumentation is nevertheless very general and can be repeated for all the systems exhibiting rotational symmetry. The transition amplitudes read:

$$\gamma_{\alpha\ell} = \langle 6_g 00 | d_{M\tau} | 7_g \ell\tau \rangle \mathrm{e}^{-i\ell\phi_\alpha}, \tag{5.4}$$

where $|7_g\,\ell\,\tau\rangle$ are the orbitally degenerate 7 particle ground states, $\ell = \pm 2$ the z projection of the angular momentum in units of $\hbar$ and $d_{\mathrm{M}\tau}$ destroys an electron of spin τ in a reference carbon atom M placed in the middle between the two contact atoms. Moreover, ϕ_α is the angle of which we have to rotate the molecule to bring the reference atom M into the position of the contact atom α. The present choice of the reference atom implies that $\phi_L = -\phi_R = \frac{\pi}{3}$. In the Hilbert space generated by the two-fold orbitally degenerate $|7_g\,\ell\,\tau\rangle$ the operator L_α reads:

$$L_\alpha = \frac{\hbar}{2} \begin{pmatrix} 1 & e^{i2|\ell|\phi_\alpha} \\ e^{-i2|\ell|\phi_\alpha} & 1 \end{pmatrix}. \tag{5.5}$$

To derive the explicit form of this operator, it is convenient to choose the arbitrary phases of the states $|7_g \ell\tau\rangle$ in such a way that the rotation of π around the axis passing through the reference atom M and the center of the molecule transforms $|7_g \ell\tau\rangle$ into $-|7_g - \ell\tau\rangle$. In other terms

$$\exp(i\pi \tfrac{L_M}{\hbar}) = -\tau_x, \tag{5.6}$$

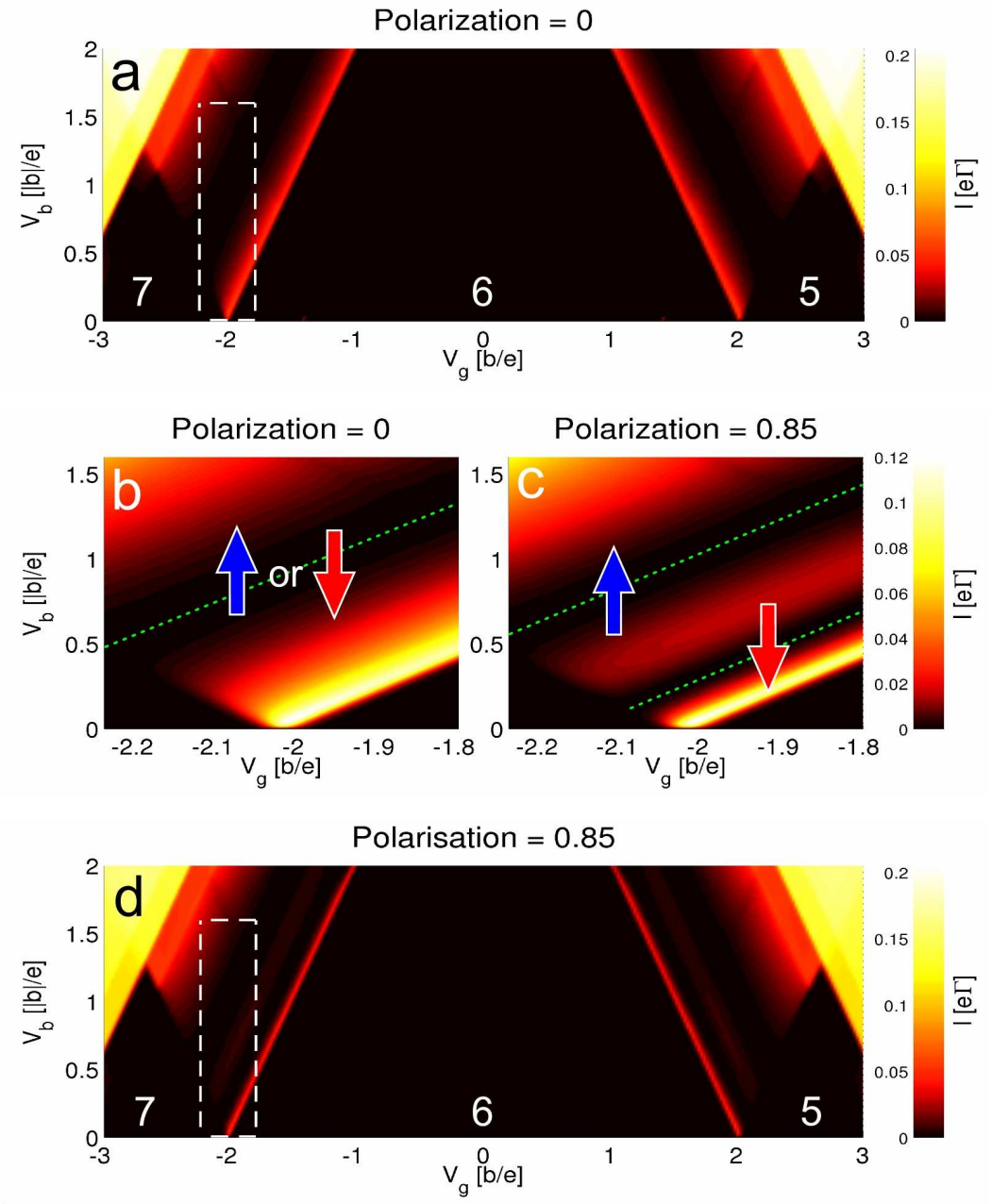

Figure 5.2: Benzene ISET: polarized vs. unpolarized configuration. Panel a - Current vs. bias and gate voltage for unpolarized leads. Panel d - Current vs. bias and gate voltage for polarized leads (polarization $P = 0.85$). Panels b and c - Blow up of the $6 \rightarrow 7$ particle transition for both configurations. The unpolarized case shows a single current blocking line and the trapped electron has either up or down polarization. The polarized case shows two current blocking lines, corresponding to the different spin of the trapped electron. The current is given in units of $e\Gamma$ where Γ is the bare average rate, and the temperature $k_B T = 0.01b$ where b is the hopping parameter

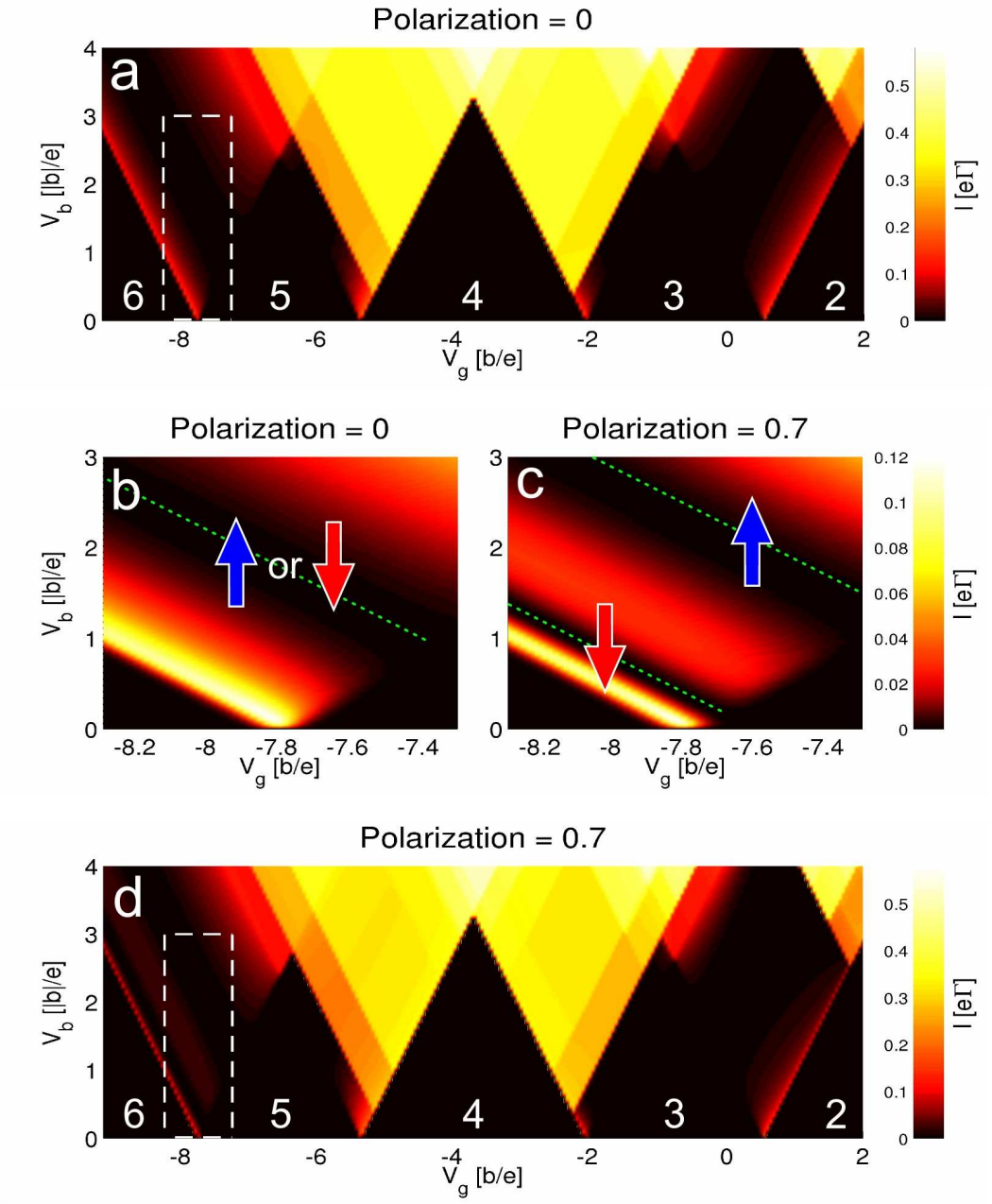

Figure 5.3: Triple dot ISET: polarized vs. unpolarized configuration. Panel a - Current vs. bias and gate voltage for unpolarized leads. Panel d - Current vs. bias and gate voltage for polarized leads (polarization $P = 0.7$). Panels b and c - Blow up of the $6 \rightarrow 5$ particle transition for both configurations. The selective spin blocking is analogous to the one of the benzene ISET (5.2).

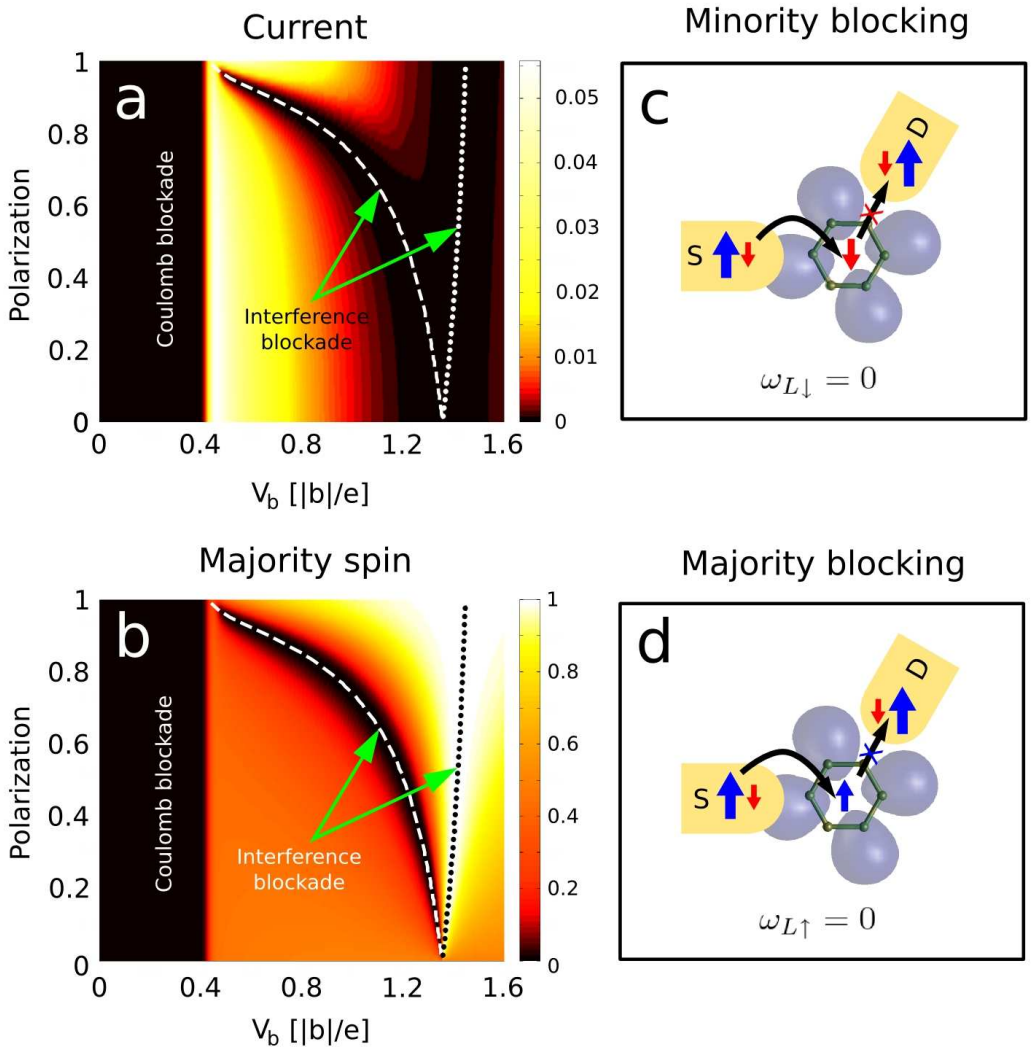

Figure 5.4: Spin control. Panel a - Current (in units of $e\Gamma$) through the benzene ISET vs bias and polarization at the $6 \rightarrow 7$ electrons transition. Panel b - Population of the majority spin 7 particle state. The two zero current lines at high bias correspond to the maximum or minimum population of the 7 particle majority spin state and thus identify the spin state of the trapped electron on the molecule. Panels c and d - Schematic representation of the spin selective blocking corresponding to the dashed (c) and dotted (d) lines of the panels a and b.

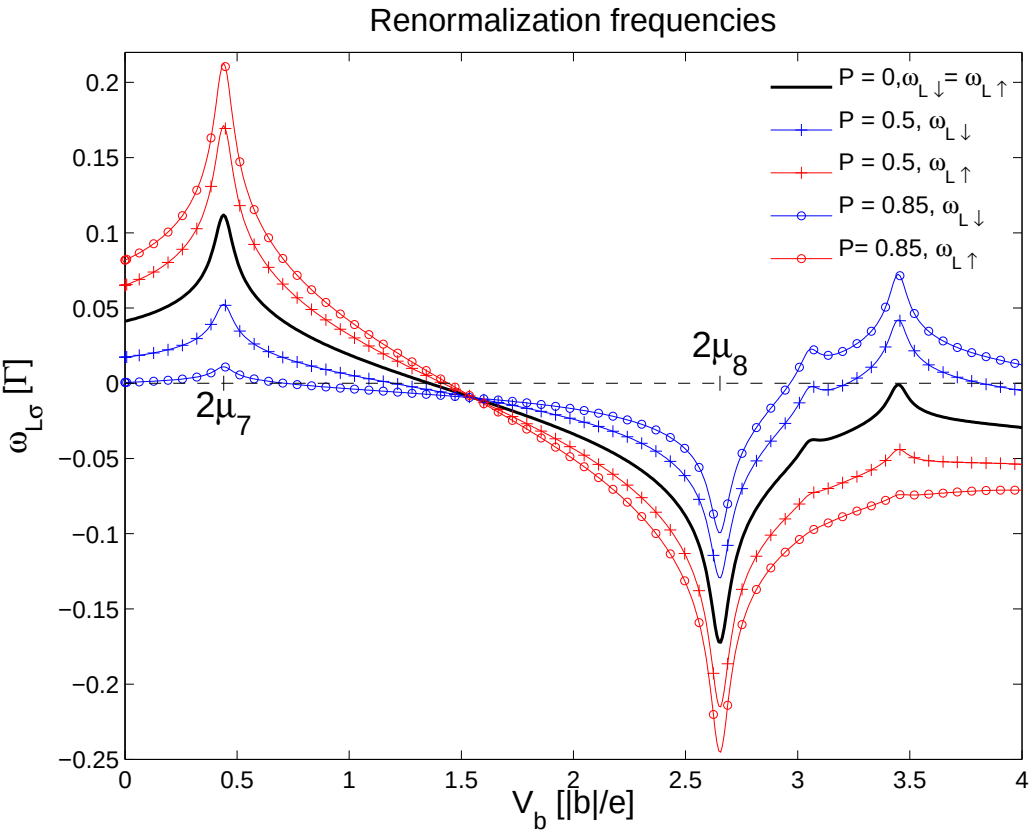

Figure 5.5: Blocking condition. Renormalization frequencies $\omega_{L\tau}$ of a benzene ISET as function of the bias and for different lead polarizations. The current blocking condition $\omega_{L\tau} = 0$ is fulfilled at different biases for the different spin states. $\mu_N = E_0^N - E_0^{N-1}$.

where τ_x is the first Pauli matrix. The relation is in fact an equation for L_M and the solution reads:

$$L_M = \frac{\hbar}{2}\begin{pmatrix} 1 & 1 \\ 1 & 1 \end{pmatrix}. \tag{5.7}$$

We obtain L_α by rotation of L_M in the molecular plane, namely:

$$L_\alpha = e^{-\frac{i}{\hbar}\phi_\alpha L_z} L_M e^{\frac{i}{\hbar}\phi_\alpha L_z} = \frac{\hbar}{2}\begin{pmatrix} 1 & e^{i2|\ell|\phi_\alpha} \\ e^{-i2|\ell|\phi_\alpha} & 1 \end{pmatrix}. \tag{5.8}$$

The frequency $\omega_{\alpha\tau}$ is defined in terms of transition amplitudes to all the states of neighbor particle numbers:

$$\begin{aligned} \omega_{\alpha\tau} \;=\; & \frac{1}{\pi}\sum_{\tau'\{E\}} \Gamma^0_{\alpha\tau'}\Big[\langle 7_g \ell\tau|d_{M\tau'}|8\{E\}\rangle\langle 8\{E\}|d^\dagger_{M\tau'}|7_g-\ell\tau\rangle p_\alpha(E-E_{7_g}) + \\ & \langle 7_g \ell\tau|d^\dagger_{M\tau'}|6\{E\}\rangle\langle 6\{E\}|d_{M\tau'}|7_g-\ell\tau\rangle p_\alpha(E_{7_g}-E)\Big], \end{aligned} \tag{5.9}$$

where the compact notation $|N\{E\}\rangle$ indicates all possible states with particle number N and energy E, $p_\alpha(x) = -\mathrm{Re}\psi\left[\frac{1}{2}+\frac{i\beta}{2\pi}(x-\mu_\alpha)\right]$ where $\beta = 1/k_{\mathrm{B}}T$, T is the temperature and ψ is the digamma function. Moreover $\Gamma^0_{\alpha\tau'} = \frac{2\pi}{\hbar}|t|^2 D_{\alpha\tau'}$ is the bare tunneling rate to the lead α of an electron of spin τ', where t is the tunnelling amplitude and $D_{\alpha\tau'}$ is density of states for electrons of spin τ' in the lead α at the corresponding chemical potential μ_α. We model the polarization in the leads by spin dependent densities of states:

$$D_{\alpha\sigma} = \begin{cases} D_\alpha(1+P), & \sigma = \uparrow, \\ D_\alpha(1-P), & \sigma = \downarrow. \end{cases} \tag{5.10}$$

Due to the particular choice of the arbitrary phase of the 7 particle ground states, $\omega_{\alpha\tau}$ is real and does not depend on the orbital quantum number ℓ. It depends instead on the bias and gate voltage through the energy of the 6, 7-ground and 8 particle states. In Figure 5.5 the black curve depicts $\omega_{L\tau}$ as a function of the bias in absence of polarization: the frequencies corresponding to the two spin species coincide and thus vanish at the same bias. The same condition,

$$\omega_{L\tau} = 0, \tag{5.11}$$

also determines the bias at which the current is completely blocked. In fact, at that bias the effective Hamiltonian contains only the projection of the angular momentum in the direction of the right lead (the drain) and the density matrix corresponding to the full occupation of the 7 particle R-antisymmetric state ($\sigma = |\psi_{R,a}\rangle\langle\psi_{R,a}|$) is the stationary solution of equation (5.2). As we leave the blocking bias the effective Hamiltonian contains also the projection of the angular momentum in the direction of the left lead and the R-antisymmetric state is no longer an eigenstate of H_{eff}. The corresponding density matrix is not a stationary solution of (5.2) and current flows through the system. The $L \leftrightarrow R$ symmetry of the system implies, for negative biases, the blocking condition $\omega_{R\tau} = 0$.

$\omega_{L/R}$ is also entering the formula for the linear conductance, equation (4.22). Also there, interference effects are less pronounced due to the renormalization of the involved states.

We concentrate here on the range of gate and bias voltages at which the dynamics is restricted to transitions involving the $|6_g 00\rangle$ and $|7_g \ell\tau\rangle$ many particle states of the benzene ISET.

The seven particle states are spin and orbital degenerate. The general theory of the GME would require a priori to keep a full 4x4 density matrix describing the 7 particle subspace. In the presence of parallel polarized leads, though, the coherences between different spin degrees of freedom can be neglected since spin is always conserved by the electrons while travelling through the device. The GME can thus be written in terms of the nine variables collected in the 1x1 matrix σ^{6_g} and the two 2x2 matrices $\sigma^{7_g\tau}$ with $\tau = \uparrow, \downarrow$. Due to the rotational symmetry of the system it is more convenient to refer to another set of variables, namely to describe the dynamics in terms of the occupation probabilities W_6, $\mathrm{W}_{7\tau}$ and the expectation values of the different projections of the angular momentum for the system. The new set of variables is:

$$\begin{aligned} \mathrm{W}_6 &= \sigma^{6_g}, \\ \mathrm{W}_{7\tau} &= \mathrm{Tr}\{\sigma^{7_g\tau}\}, \\ \mathrm{L}_{\alpha\tau} &= \mathrm{Tr}\{L_\alpha \sigma^{7_g\tau}\}, \\ \mathrm{L}_{z\tau} &= \mathrm{Tr}\{L_z \sigma^{7_g\tau}\}. \end{aligned} \tag{5.12}$$

The operator L_z is the generator of the set of discrete rotations around the axis perpendicular to the plane of the benzene molecule that bring the molecule into itself and can be written within the 7 particle Hilbert space spanned by the vectors $|7_g \ell\tau\rangle$ as $L_z = -\hbar|\ell|\tau_z$, where τ_z is the third Pauli matrix. The operator L_α generates, in the same space, the discrete rotations around the axis in the molecular plane and passing through the center and the atom closest to the contact α. Finally, the dynamics for the variables introduced in equation (5.12) is given by the equations:

$$\dot{\mathrm{W}}_6 = 2\sum_{\alpha\tau} \Gamma_{\alpha\tau} \left[-f_\alpha^+(\Delta E)\mathrm{W}_6 + f_\alpha^-(\Delta E)\mathrm{L}_{\alpha\tau} \right], \tag{5.13}$$

$$\dot{\mathrm{W}}_{7\tau} = 2\sum_{\alpha} \Gamma_{\alpha\tau} \left[f_\alpha^+(\Delta E)W_6 - f_\alpha^-(\Delta E)\mathrm{L}_{\alpha\tau} \right], \tag{5.14}$$

$$\begin{aligned} \dot{\mathrm{L}}_{\alpha\tau} = {} & -2\Gamma_{\alpha\tau} f_\alpha^-(\Delta E)\mathrm{L}_{\alpha\tau} + 2\left\{ \Gamma_{\alpha\tau} f_\alpha^+(\Delta E) + \Gamma_{\bar\alpha\tau} f_{\bar\alpha}^+(\Delta E)\cos^2[|\ell|(\phi_\alpha - \phi_{\bar\alpha})] \right\} \mathrm{W}_6 \\ & + \Gamma_{\bar\alpha\tau} f_{\bar\alpha}^-(\Delta E)\sin^2[|\ell|(\phi_\alpha - \phi_{\bar\alpha})]\mathrm{W}_{7\tau} - \Gamma_{\bar\alpha\tau} f_{\bar\alpha}^-(\Delta E)(\mathrm{L}_{\alpha\tau} + \mathrm{L}_{\bar\alpha\tau}) \\ & + \frac{\sin[2|\ell|(\phi_\alpha - \phi_{\bar\alpha})]}{4}\omega_{\bar\alpha\tau}\mathrm{L}_{z\tau}, \end{aligned} \tag{5.15}$$

$$\begin{aligned} \dot{\mathrm{L}}_{z\tau} = {} & -\sum_\alpha \Gamma_{\alpha\tau} f_\alpha^-(\Delta E)\mathrm{L}_{z\tau} - 2\tan[|\ell|(\phi_L - \phi_R)](\omega_{L\tau} - \omega_{R\tau})(\mathrm{W}_{7\tau} - \mathrm{L}_{L\tau} - \mathrm{L}_{R\tau}) \\ & - 2\cot[|\ell|(\phi_L - \phi_R)](\omega_{L\tau} + \omega_{R\tau})(\mathrm{L}_{L\tau} - \mathrm{L}_{R\tau}), \end{aligned} \tag{5.16}$$

where $\Gamma_{\alpha\tau} = \Gamma^0_{\alpha\tau}|\langle 6_g 00|d_{\alpha\tau}|7_g \ell\tau\rangle|^2$ is the tunnelling rate at the lead α involving the ground states with 6 and 7 particles. Terms describing sequential tunnelling from

and to the lead α are proportional to the Fermi functions $f_\alpha^+(x) := f(x-\mu_\alpha)$ and $f_\alpha^-(x) := 1 - f_\alpha^+(x)$, respectively, and $\Delta E = E_{7g} - E_{6g} - eV_g$ where E_{6g} and E_{7g} are the energies of the 6 and 7 particle ground states. Finally with $\bar{\alpha}$ we mean the lead opposite to the lead α. By using the expression $|\ell|$ (to be substituted with 2 for the $6 \rightarrow 7$ particle transition) we maintained the generality of the equations. The replacement $|\ell| = 2 \rightarrow 1$ and the appropriate redefinition of ΔE is enough to treat the $6 \rightarrow 5$ transition. Another important generalization concerns the position of the leads. The para ($\phi_L - \phi_R = \pi$) and ortho ($\phi_L - \phi_R = \pi/3$) configuration are also treated within the same equations. In particular one can see that all the terms containing the renormalization frequencies drop from the equations in the para configuration and that the equations for the ortho and meta configuration coincide.
The spin splitting of the renormalization frequencies is obtained from equation (5.9). By introducing the average bare rate $\Gamma = \frac{\Gamma^0_{\alpha\uparrow}+\Gamma^0_{\alpha\downarrow}}{2}$, for simplicity equal in both leads, and using the fact that benzene is paramagnetic we get:

$$\begin{aligned}\omega_{\alpha\uparrow} - \omega_{\alpha\downarrow} = 2\Gamma P_\alpha \frac{1}{\pi} \sum_{\{E\}} \\ \Big[&\langle 7_g \ell\uparrow | d_{M\uparrow} | 8\{E\}\rangle\langle 8\{E\} | d^\dagger_{M\uparrow} | 7_g - \ell\uparrow\rangle p_\alpha(E - E_{7_g}) \\ + &\langle 7_g \ell\uparrow | d^\dagger_{M\uparrow} | 6\{E\}\rangle\langle 6\{E\} | d_{M\uparrow} | 7_g - \ell\uparrow\rangle p_\alpha(E_{7_g} - E) \\ - &\langle 7_g \ell\uparrow | d_{M\downarrow} | 8\{E\}\rangle\langle 8\{E\} | d^\dagger_{M\downarrow} | 7_g - \ell\uparrow\rangle p_\alpha(E - E_{7_g}) \\ - &\langle 7_g \ell\uparrow | d^\dagger_{M\downarrow} | 6\{E\}\rangle\langle 6\{E\} | d_{M\downarrow} | 7_g - \ell\uparrow\rangle p_\alpha(E_{7_g} - E) \Big],\end{aligned} \tag{5.17}$$

where one appreciates the linear dependence of the spin splitting on the lead polarization P_α. The first and the third term of the sum would cancel each other if the energy of the singlet and triplet 8 particle states would coincide. An analogous condition, but this time on the 6 particle states, concerns the second and the fourth terms. For this reason the exchange interaction on the system is a necessary condition to obtain spin splitting of the renormalization frequencies and thus the full all-electric spin control.

5.2 Interference blocking for excited states

In Figure 5.3, we see the current stability diagram for a triangular quantum dot ISET. Interference is visible at the transitions $2 \leftrightarrow 3$, $3 \leftrightarrow 4$ (low bias only), $4 \leftrightarrow 5$ (low bias only) and $5 \leftrightarrow 6$. In Figure 5.6, we show the current stability diagram for the transitions involving 1 and 2 particle states. No interference is observed for low bias, since the groundstates for $N = 1, 2$ show no orbital degeneracies. The dominant feature in this plot is instead the region with strong current suppression at the border of the $N = 1$ diamond, starting a finite bias voltages. In the following, we will demonstrate that the blocking of the current is due to interference blockade triggered by the first excited 2-particle state, which is a (spin) triplet state with additional orbital degeneracies.

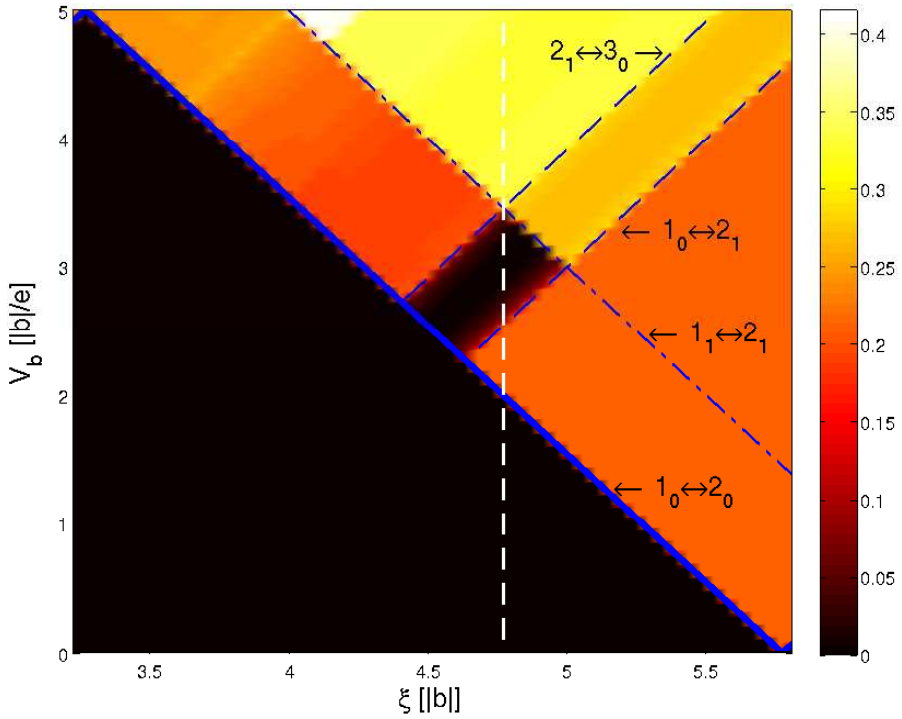

Figure 5.6: Part of the current stability diagram for the triple dot ISET. The current is color coded, the scale is in units of $e\Gamma$. Superimposed are blue lines that indicate the transport conditions, equation (3.2), for various channels. The $1_0 \leftrightarrow 2_0$ ground state transition is drawn as solid line, dashed and dot-dashed lines correspond to ground- to excited state or excited- to excited state transitions. The parameters used here in units of $|b|$: $U = 5$, $V = 2$, $k_{\mathrm{B}}T = 0.002$.

In Figure 5.7, we present a current-voltage curve for unpolarized leads for a gate voltage corresponding to the vertical dashed line in the stability diagram, Figure 5.6 (green line). For low bias, no current is flowing due to Coulomb blockade, and the $N = 2$ ground state is the only populated state. Once the bias is high enough so that $E_0^2 - E_0^1 = \mu^2 \geq \mu_{\mathrm{d}} = \mu_0 - \frac{V_{\mathrm{b}}}{2}$, electrons can tunnel out into the source, leaving the dot in the $N = 1$ ground state. The dots chemical potential μ^2 is indicated with the arrow a in Figure 5.9. In this situation, electrons can tunnel in from the source to populate again the $N = 2$ ground state, so that current can flow as a series of single electron tunneling processes, that change the configuration of the dot from the $N = 2$ to the $N = 1$ ground state and back. If the bias is increased further so that also the generalized chemical potential μ_{10}^2 (indicated by the arrow b in Figure 5.9) is in the bias window, $\mu_{\mathrm{s}} \geq \mu_{10}^2 = E_1^2 - E_0^1 \geq \mu_{\mathrm{d}}$, the current decreases and eventually vanishes at one particular point. Interference blockade occurs when the first excited two particle state can be populated via the transitions $2_0 \rightarrow 1_0, 1_0 \rightarrow 2_1$, namely when the conditions $-\frac{V_{\mathrm{b}}}{2} < \mu_{00}^2$ and $\frac{V_{\mathrm{b}}}{2} > \mu_{10}^2$ are fulfilled. The state 2_1 cannot be depopulated by tunneling out into 1_0 on the right lead due to interference. Only when $\mu_{01}^3 > \frac{V_{\mathrm{b}}}{2}$ or $-\frac{V_{\mathrm{b}}}{2} < \mu_{11}^2$,

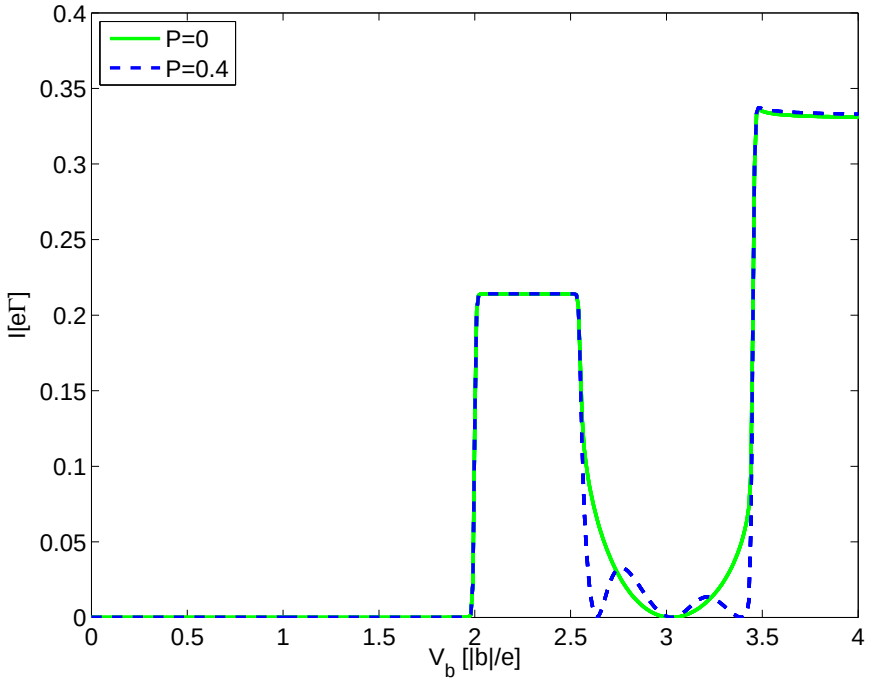

Figure 5.7: I-V-curve at $\xi = 4.7749|b|$ (corresponding to the white dashed line in Figure 5.6) for unpolarized leads (green line) or parallel polarized leads (blue line, polarization $P = 0.4$). The current is blocked at three different points.

other channels allow to depopulate the blocking state and current can flow. We see in Figure 5.6 that the lines indicating these conditions encircle the region where the current is blocked.

The mechanism for the blocking is the same as described earlier. Degenerate orbitals of the state E_1^2 interfere to form a state which is geometrically decoupled from the drain lead and therefore cannot be depopulated. This blocking is perfect only at one particular bias voltage, when the level renormalization induced by the internal dynamics is not affecting the decoupling mechanism. In Figure 5.7, we also show an I-V-curve for polarized leads (polarization = 0.4). In this case, the current is blocked at three different bias voltages, and at each blocking bias a different component of the triplet state (with $S_z = -1, 0, 1$) is trapped on the dot (see Figure 5.8). Also in this situation the components of the triplet with different S_z undergo a different effective renormalization.

We conclude that interference blockade in SETs can be used to prepare a quantum dot in a specific triplet state with all electrical means.

The results presented in this chapter were obtained in collaboration with Andrea Donarini and Milena Grifoni. They were published in

[19] A. Donarini, G. Begemann, and M. Grifoni, Nano Lett. **9**, 2897 (2009).

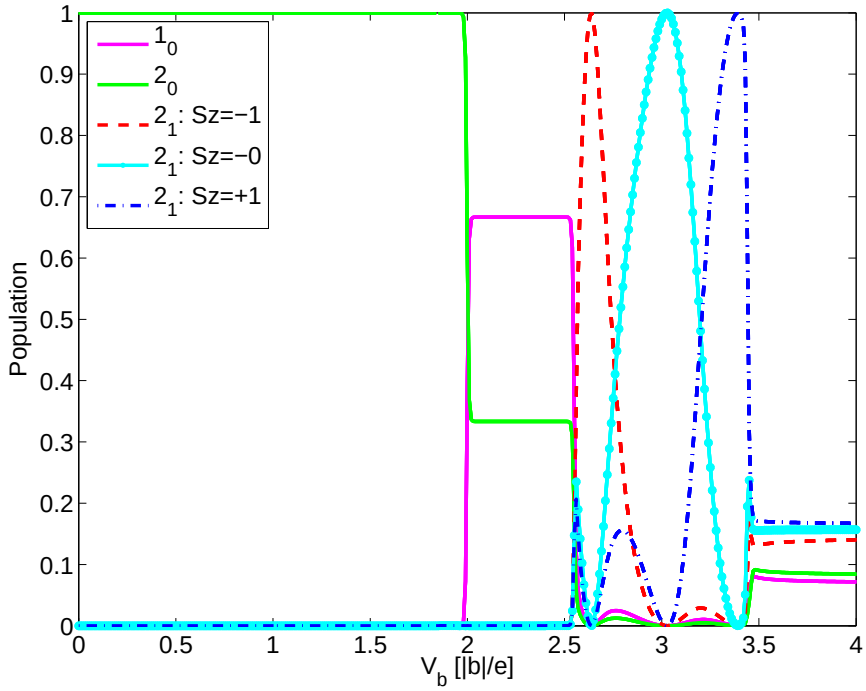

Figure 5.8: Populations of the relevant states for parallel polarized leads ($P = 0.4$) at $\xi = 4.7749|b|$. Notice that at each current blocking point in Figure 5.7, the dot is in a certain component of the triplet state.

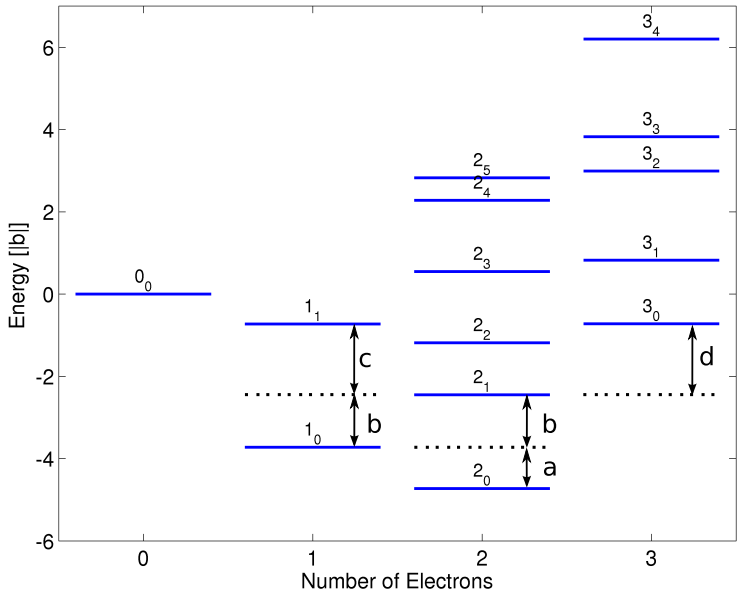

Figure 5.9: Spectrum of the triangular quantum dot for a specific gate voltage that corresponds to the dashed white line in the stability diagram in Figure 5.6 ($\xi = 4.7749$). Blue lines indicate the energies of the states, the black dashed auxiliary lines are used to visualize the (generalized) chemical potentials $\mu^2 = \mu^2_{00}$, μ^2_{10}, μ^2_{11}, μ^3_{01} corresponding to the arrows a, b, c, d, respectively.

Chapter 6

Nonequilibrium cotunneling: an effective Kondo Hamiltonian approach vs. exact results

In the Coulomb-blockade regime, sequential tunneling transport is exponentially suppressed and processes where two or more electrons tunnel simultaneously become the dominant transport mechanism [77]. These are called cotunneling processes and have received a lot of interest in recent years for several reasons. First, applications that rely on Coulomb blockade in quantum dots are limited by cotunneling. Second, cotunneling processes can act as an additional tool in transport spectroscopy to identify electronic and vibrational excitation energies in semiconducting [78, 79] or carbon nanotube [80] quantum dots. More recently, the interplay of sequential tunneling and cotunneling processes was in the focus of both experimental [78, 81] and theoretical works [34, 82]. This interplay comes about at high enough source-drain voltages, when inelastic cotunneling processes can lead to a nonequilibrium population of excited states and therefore enable sequential tunneling processes inside the Coulomb diamond (cotunneling assisted sequential tunneling).

To calculate the current and other observables in transport through quantum dots in the Coulomb blockade regime, there are a number of techniques, each of them having their advantages and (at least practical) limitations. A real-time transport approach was developed by Schoeller, König and Schön [70, 71, 72] to describe nonequilibrium transport properties of mesoscopic systems with strong Coulomb interaction. Following this theory, one can trace out the leads degrees of freedom and derive a formally exact equation of motion for the reduced density matrix (RDM) of the system. The theory allows for a systematic expansion in the tunneling Hamiltonian H_{T}, pinpointing the different tunneling processes. More specifically, sequential tunneling processes are attributed to contributions of second order in H_{T}, cotunneling to such of fourth order, and so on. The authors also established a diagrammatic representation of the various terms entering in the equation for the RDM. Alternatively, exactly the same equation can be derived within a Bloch-Redfield approach iterated to fourth order in H_{T}.

In systems with normal metal leads (where the spin projection S_z is conserved) and

without orbital degeneracies, a simple rate equation is sufficient to describe sequential tunneling processes [37]. Within this so-called master equation approach, one calculates transitions between states of the quantum dot system with Fermi's golden rule, again treating H_T as a perturbation. This approach can be generalized to higher order tunneling processes by making use of the so called T-matrix

$$T(E) = H_\mathrm{T} + H_\mathrm{T} \frac{1}{E - H_0 + i0^+} T(E), \tag{6.1}$$

where 0^+ is a symbolic notation for an infinitesimal positive number. The T-matrix, known from scattering theory, describes the propagation of particles from an initial to a final state, where the particle can propagate directly or experience an arbitrary number of scattering (in this case tunneling) events. In particular, transition rates from the initial to the final state can be calculated up to a given order in H_T. In the quantum transport context, the T-matrix based approach was e.g. applied to a double dot structure [34] or to molecular systems where electronic and vibronic degrees of freedom can be strongly coupled [36]. Compared to the GME, it is relatively simple and yields good agreement where additional effects due to level shifts and broadening are irrelevant, namely in the regime where the tunneling induced level width is much smaller than the temperature. It should be said that effects arising from interference between (quasi-)degenerate states cannot be taken into account by a rate equation approach based on the T-matrix. In systems where such effects are expected, the concept of the GME must be used, because the dynamics of off-diagonal elements of the RDM, responsible for coherence and interference, is not captured by simple rate equations.

If one aims at describing cotunneling processes only, implying that the quantum dot is in the deep Coulomb blockade regime, further simplifications are possible. In particular it was recently shown by Schmaus et al. [83] for a multilevel quantum dot with odd filling that a generalized Schrieffer-Wolff [84] transformation can be used to obtain an effective cotunneling Hamiltonian. Transport can then be calculated using e.g. rate equations or Green's function techniques.

In this chapter, we show that an effective Kondo Hamiltonian can be obtainend by eliminating linear contributions in H_T from H and projecting the leading second order contributions on a subspace with an odd number of electrons. This is equivalent to a Schrieffer-Wolff transformation. Renormalization group techniques for the Kondo model are available and give correct qualitative and quantitative predictions for the current and conductance that include higher order tunneling processes. These techniques can be applied when other excitations are well separated from the regime covered by the low energy Kondo Hamiltonian. In this thesis, we do not use these powerful but complex techniques, and restrict ourselves to fourth order rate equations to describe various cotunneling processes. In particular, a comparison between exact numerical results up to fourth order in H_T and approximation schemes is made to identify the validity and accuracy of the approximate methods.

We show here that sequential tunneling contributions can become relevant already inside the Coulomb diamond, when excited states become populated via inelastic cotunneling and enable sequential tunneling processes. At this point, the cotunneling

contributions to the rates can become negative, which would lead to an ill-defined set of rate equations if the sequential tunneling contributions were not large enough to assure positive definiteness of the rates. In section 6.5, we estimate the gate dependent renormalization of the energy levels that define the inelastic cotunneling threshold, as it was observed e.g. in [64].

6.1 Transport

In this chapter, we consider systems without orbital degeneracies and non-polarized leads, so that a rate equation approach to transport is sufficient. As we want to calculate cotunneling rates, we iterate the T-matrix to second order in H_{T}. We label the states of the quantum dot with their particle number N, the S_z-component of their spin η and an additional quantum number l. The rate for a transition between two states $|N'l'\eta'\rangle \to |Nl\eta\rangle$ of the quantum dot system is then given by

$$\Gamma_{|Nl\eta\rangle\langle N'l'\eta'|} = 2\pi \sum_{f,i} \left| \langle f_{Nl\eta}| H_{\mathrm{T}} + H_{\mathrm{T}} \frac{1}{E_{i_{N'l'\eta'}} - H_{\mathrm{QD}} - H_{\mathrm{leads}} + i0^+} \mathrm{H_T} |i_{N'l'\eta'}\rangle \right|^2 W_i \delta(E_{f_{Nl\eta}} - E_{i_{N'l'\eta'}}). \tag{6.2}$$

Here the sum goes over all possible initial and final states of the leads $|i_{Nl\eta}\rangle = |N\eta l\rangle|i_L\rangle|i_R\rangle$, $|f_{N'l'\eta'}\rangle = |N'\eta'l'\rangle|f_L\rangle|f_R\rangle$, the former weighted by a thermal distribution function W_i. The rate equation describing the dynamical population probabilities of the states is

$$\dot{P}^{Nl\eta} = \quad - \sum_{N'l'\eta'} \Gamma_{|N'l'\eta'\rangle\langle Nl\eta|}\ P^{Nl\eta} + \sum_{N'l'\eta'} \Gamma_{|Nl\eta\rangle\langle N'l'\eta'|}\ P^{N'l'\eta'}, \tag{6.3}$$

where $P^{Nl\eta}$ is the probability of finding the dot in the state $|Nl\eta\rangle$ and the stationary solution is given by

$$\sum_{N'l'\eta'} \Gamma_{|N'l'\eta'\rangle\langle Nl\eta|} P^{Nl\eta} = \sum_{N'l'\eta'} \Gamma_{|Nl\eta\rangle\langle N'l'\eta'|}\ P^{N'l'\eta'}, \tag{6.4}$$

with the additional normalization condition

$$\sum_{Nl\eta} P^{Nl\eta} = 1. \tag{6.5}$$

Equation (6.3) is very intuitive and sometimes just given heuristically. However, to lowest (second) order in H_{T} it follows directly from the GME, equation (3.19), by neglecting off-diagonal elements of the reduced density matrix (RDM) and identifying the occupation probabilities $P^{Nl\eta}$ with the diagonal elements of the RDM. With the help of the stationary solution, we calculate the current as

$$I = I_{\mathrm{sequential}} + I_{\mathrm{cotunneling}}, \tag{6.6}$$

with

$$I_{\text{sequential}} = \sum_{Nl\eta}\sum_{sm}\left(\Gamma^{L}_{|N+1sm\rangle\langle Nl\eta|} - \Gamma^{L}_{|N-1sm\rangle\langle Nl\eta|}\right) P^{Nl\eta}_{\text{stat}}, \tag{6.7}$$

$$I_{\text{cotunneling}} = \sum_{Nl\eta}\left[\sum_{l'\eta'}\left(\Gamma^{RL}_{|Nl'\eta'\rangle\langle Nl\eta|} - \Gamma^{LR}_{|Nl'\eta'\rangle\langle Nl\eta|}\right)\right] P^{Nl\eta}_{\text{stat}}. \tag{6.8}$$

Cotunneling rates that connect N- and $N \pm 2$-particle states are not taken into account. These processes can be neglected, because they are not seen inside the Coulomb diamonds and are of small magnitude outside. They were addressed in [85].
For the evaluation of equation (6.2), all possible configurations of the leads with different thermal weight have to be taken into account. We can write the possible initial states as

$$\sum_{i}|i_{Nl\eta}\rangle = |N\eta l\rangle\sum_{i_L}|i_L\rangle\sum_{i_R}|i_R\rangle, \tag{6.9}$$

and the final state follows from the initial state by summing over all possible tunneling processes that connect $|N\eta l\rangle$ with $|N'\eta' l'\rangle$. Specifically it means that for the sequential tunneling rates, we obtain

$$\sum_{f}|f_{N\pm1l'\eta'}\rangle = |N{+}1\ \eta' l'\rangle\sum_{k\alpha\sigma}c_{k\alpha\sigma}\sum_{i_L}|i_L\rangle\sum_{i_R}|i_R\rangle + |N{-}1\ \eta' l'\rangle\sum_{k\alpha\sigma}c^{\dagger}_{k\alpha\sigma}\sum_{i_L}|i_L\rangle\sum_{i_R}|i_R\rangle, \tag{6.10}$$

and for the cotunneling rates

$$\sum_{f}|f_{Nl'\eta'}\rangle = |N\eta' l'\rangle\sum_{kk'}\sum_{\alpha\alpha'}\sum_{\sigma\sigma'}c^{\dagger}_{k'\alpha'\sigma'}c_{k\alpha\sigma}\sum_{i_L}|i_L\rangle\sum_{i_R}|i_R\rangle. \tag{6.11}$$

The sum over k and k' are recast into integrals with the replacements $\sum_{k\alpha} \to \sum_{\alpha}\int d\epsilon_k\ \nu_\alpha$, where ν_α is the density of states in lead α. The expectation value of pairs of lead operators is by definition given by the Fermi function:

$$\sum_{i_L}\sum_{i_R}\langle i_L|\langle i_R|c^{\dagger}_{k\alpha\sigma}c_{k'\alpha'\sigma'}|i_R\rangle|i_L\rangle W_i = \delta_{\alpha\alpha'}\delta_{\sigma\sigma'}\delta_{kk'}\ f(\epsilon_k - \mu_\alpha). \tag{6.12}$$

6.2 The Kondo Hamiltonian

In the deep Coulomb blockade regime, each diamond in the stability diagram corresponds to an N-particle ground state. In such a situation, we can describe our system by an effective low energy Hamiltonian

$$H^N = \sum_{l\eta}E_{l\eta}|N\ l\eta\rangle\langle N\ l\eta| + H_{\text{leads}} + H^N_{\text{int}}, \tag{6.13}$$

that includes only N-electron states in the quantum dot and transitions between those via cotunneling events involving virtual excitations of $N \pm 1$ particle states. We can

derive this equation by lowest order perturbation theory [86]. If we write the state of the system as the sum of the terms $|N-1\rangle$, $|N\rangle$ and $|N+1\rangle$, where $|N\rangle$ represents all states with electron number N, then the Schrödinger equation can be written as

$$\begin{pmatrix} H_{N-1\ N-1} & H_{N-1\ N} & \\ H_{N\ N-1} & H_{N\ N} & H_{N\ N+1} \\ & H_{N+1\ N} & H_{N+1\ N+1} \end{pmatrix} \begin{pmatrix} |N-1\rangle \\ |N\rangle \\ |N+1\rangle \end{pmatrix} = E \begin{pmatrix} |N-1\rangle \\ |N\rangle \\ |N+1\rangle \end{pmatrix}, \tag{6.14}$$

where $H_{N\ N'} = P_N H P_{N'}$ and P_N is a projection operator onto the subspace with N particles. There is no term in the Hamiltonian that connects the $N-1$ and the $N+1$ spaces directly. The lead Hamiltonian is not written here, it gives contributions to the diagonal of the above matrix only. We can now eliminate $|N-1\rangle$ and $|N+1\rangle$ to obtain

$$\left(H_{NN} + H_{NN+1} \frac{1}{E - H_{N+1N+1}} H_{N+1N} + H_{NN-1} \frac{1}{E - H_{N-1N-1}} H_{N-1N} \right) |N\rangle = E|N\rangle. \tag{6.15}$$

Contributions from states with $N \pm 2$ are of higher order and are thus neglected in equations (6.14), (6.15). The last two terms in equation (6.15) can be recast into the form

$$H^N_{\rm int} = \sum_{\substack{kk' \\ \alpha\alpha'}} \sum_{\sigma\sigma'} \sum_{\substack{ll' \\ \eta\eta'}} \left[\frac{J^{ll'}_{\alpha\alpha'}}{2} \boldsymbol{\tau}_{\eta\eta'} \cdot \boldsymbol{\tau}_{\sigma'\sigma} |Nl\eta\rangle\langle Nl'\eta'| + \frac{P^{ll'}_{\alpha\alpha'}}{2} \delta_{\eta\eta'} \delta_{\sigma\sigma'} |Nl\eta\rangle\langle Nl'\eta'| \right] c^\dagger_{k\alpha\sigma} c_{k'\alpha'\sigma'}. \tag{6.16}$$

Details of the calculations are shown in section 6.5. The first term in equation (6.16) looks like the famous Kondo Hamiltonian with an anti-ferromagnetic spin-spin interaction, but generalized to two (or more) orbitals, while the second is a potential scattering term. The assumption that N is odd reflects itself in the possible values of $\eta = \pm\frac{1}{2}$ for $\uparrow, \downarrow$. The expressions for the coupling matrix elements read

$$\begin{aligned} J^{ll'}_{\alpha\alpha'} &= t^\alpha t^{\alpha'*} \sum_s \frac{\langle Nl\uparrow | d_{\alpha\downarrow} | N+1s\rangle\langle N+1s | d^\dagger_{\alpha'\uparrow} | Nl'\downarrow\rangle}{E_{Nl'} - E_{N+1s} + \epsilon_{k'\alpha'} + i0^+} + \\ &\quad t^\alpha t^{\alpha'*} \sum_s \frac{\langle Nl\downarrow | d^\dagger_{\alpha'\downarrow} | N-1s\rangle\langle N-1s | d_{\alpha\uparrow} | Nl'\uparrow\rangle}{E_{N-1s} - E_{Nl'} + \epsilon_{k\alpha} - i0^+}, \end{aligned} \tag{6.17}$$

$$\begin{aligned} P^{ll'}_{\alpha\alpha'} &= t^\alpha t^{\alpha'*} \sum_{s\sigma} \frac{\langle Nl\uparrow | d_{\alpha\sigma} | N+1s\rangle\langle N+1s | d^\dagger_{\alpha'\sigma} | Nl'\uparrow\rangle}{E_{Nl'} - E_{N+1s} + \epsilon_{k'\alpha'} + i0^+} + \\ &\quad t^\alpha t^{\alpha'*} \sum_{s\sigma} \frac{\langle Nl\uparrow | d^\dagger_{\alpha'\sigma} | N-1s\rangle\langle N-1s | d_{\alpha\sigma} | Nl'\uparrow\rangle}{E_{N-1s} - E_{Nl'} + \epsilon_{k\alpha} - i0^+}. \end{aligned} \tag{6.18}$$

The spin operator of the molecule can be expressed in terms of the vector of the Pauli matrices, $\boldsymbol{\tau} = \left\{ \begin{pmatrix} 0 & 1 \\ 1 & 0 \end{pmatrix}, \begin{pmatrix} 0 & -i \\ i & 0 \end{pmatrix}, \begin{pmatrix} 1 & 0 \\ 0 & -1 \end{pmatrix} \right\}$:

$$\mathbf{S}_{ll'} = \frac{1}{2} \sum_{\eta\eta'} |N\eta l\rangle \boldsymbol{\tau}_{\eta\eta'} \langle N\eta' l'|. \tag{6.19}$$

Schrieffer and Wolff [84] were the first to obtain a result similar to equation (6.13) starting from the single impurity Anderson model. They showed the relation between Anderson- and Kondo like models using a canonical transformation. The equations (6.17), (6.18) represent a generalization of their results to more complicated models with more orbitals and more charge states.

6.3 Different approximations/approaches

In the following, we calculate the current and conductance based on equations (6.2) and following. We use different approximation schemes of increasing complexity. The theory by Koller, Leijnse et al. [73, 87] based on the real-time diagrammatic approach [70] acts as a benchmark for our calculations. In this approach, kinetic equations for the reduced density matrix exact up to fourth order in H_T are developed. We refer to it as *KinEq*-approach.

6.3.1 First Approximation - cotunneling only

Well inside the Coulomb diamonds, the current is dominated by cotunneling processes. In a first approximation, we therefore neglect sequential tunneling contributions in equation (6.2). This is the regime where the system can be described by the low-energy Kondo Hamiltonian in equation (6.13). As a further simplification, we neglect the ϵ_k energy dependence in the denominators of the coupling constants J and P. This is justified for small (compared to the charging energy) bias voltages, so that the electrons that tunnel to and from the leads have energies around the equilibrium chemical potential and thus $\frac{1}{E_{N+1s}-E_{Nl}-\epsilon_k} \approx \frac{1}{E_{N+1s}-E_{Nl}}$ because of $E_{N+1s} - E_{Nl} \gg \epsilon_k, \epsilon_{k'}$. The sums over k and k' in the expression for the rates are recast into integrals, so that we obtain

$$\begin{aligned}\Gamma^{\alpha\alpha'}_{|N\eta l\rangle\langle N\eta' l'|} &= 2\pi \int d\epsilon_k \nu_\alpha \int d\epsilon_{k'} \nu_{\alpha'} f(\epsilon_k - \mu_\alpha)(1 - f(\epsilon_{k'} - \mu_{\alpha'})) \\ &\quad \delta\left(E_{Nl\eta} - E_{N\eta' l'} - \epsilon_k - \epsilon_{k'}\right) \left(\frac{\left|J^{ll'}_{RL}\right|^2}{2} \left(\mathbb{1} + \tau^x\right)_{\eta\eta'} + \delta_{\eta\eta'} \frac{\left|P^{ll'}_{RL}\right|^2}{2} \right),\end{aligned} \tag{6.20}$$

which can be solved easily to yield for example

$$\begin{aligned}\Gamma^{RL}_{|N\eta l\rangle\langle N\eta' l'|} &= 2\pi\ \nu_L \nu_R n_B\left(-(E_{N\eta' l'} - E_{N\eta l}) - eV_b\right)\left(-(E_{N\eta' l'} - E_{N\eta l}) - eV_b\right) \\ &\quad \left(\frac{\left|J^{ll'}_{RL}\right|^2}{2} \left(\mathbb{1} + \tau^x\right)_{\eta\eta'} + \delta_{\eta\eta'} \frac{\left|P^{ll'}_{RL}\right|^2}{2} \right),\end{aligned} \tag{6.21}$$

where $n_B(x) = \frac{1}{\exp(\beta x)-1}$ is the Bose Einstein distribution function. At low temperatures, $-n_B(-x)x \approx \theta(x)x$. As a result, the differential conductance is finite but constant as a function of V_b until inelastic cotunneling sets in. At this point, the dI/dV increases steplike, because a new transport channel is available. The resulting

nonequilibrium distribution of population probabilities generates typically a cusp in the dI/dV on top of the step.
This approximation is valid for gate voltages inside the N-electron Coulomb diamond, as long as the denominators of J and P are not vanishing, and for small bias voltages. We refer to this approximation as AppI.

6.3.2 Second Approximation - cotunneling only

To get a more precise description of the cotunneling conductance, we take into account in a second approximation the energy dependence of J and P. By shifting the integration variable $\epsilon_k \to \epsilon_k + \mu_L$ in equation (6.21), we see that J and P now explicitly depend on μ_L and therefore on the bias voltage. In the rates, one gets a summation over expressions of the general form

$$\Gamma \sim \int d\epsilon f(\epsilon)\left(1 - f(\epsilon + \mu_L - \mu_R + E_{Nl} - E_{Nl'})\right) \frac{1}{\epsilon - E1 \pm i0^+} \frac{1}{\epsilon - E2 \pm i0^+},$$

where $E1$ and $E2$ depend on l and l' and the summation indices in the expressions for J and P. If $E1 = E2$, these expressions cannot be evaluated directly, because of divergences stemming from second order poles. This problem was stated already in 1994 [88], and a regularization scheme has been developed and become standard within the T-matrix approach to transport [89, 36]. In this regularization scheme, a finite width $\gamma \sim \Gamma$ is attributed to the molecular levels which enters the denominators as imaginary parts. This level broadening physically stems from the tunneling coupling, but is not taken into account by the T-matrix approach. Thus the poles are shifted away from the real axis so that the integral can actually be performed. The resulting expression can be expanded in powers of γ and the leading term is found to be of order $1/\gamma$. Together with the prefactor of the rates, Γ^2, this term is identified to be a sequential tunneling term. It is excluded to avoid double counting of sequential tunneling processes. The next to leading order term is of order γ^0 and gives the regularized cotunneling rate. At this point, the actual value of the broadening does not matter and the limit $\gamma \to 0$ can safely be taken. The calculation of the current with regularized cotunneling processes and disregarding sequential tunneling rates is referred to as AppII.

6.3.3 T-matrix Approach

AppII fails when cotunneling assisted sequential tunneling processes become accessible. This can happen well inside the Coulomb diamond, when excited N particle states are populated via inelastic cotunneling. At the lines given by the resonance condition of the generalized chemical potential of the dot with the chemical potential of the leads (dashed lines inside the Coulomb diamond in Figure 6.1) the cotunneling rates become negative which leads to an ill-defined set of rate equations, unless we include also sequential tunneling terms and allow also states with $N \pm 1$ to be populated. For the calculation of the rates, we use equation (6.2). This is exactly the T-matrix approach mentioned in the introduction.

6.4 Results

We compare now the different approaches applied to a double quantum dot (DD) system, filled with one electron. The Hamiltonian is given by

$$\begin{aligned} H_{\mathrm{DD}} &= \sum_{\alpha=1}^{2}\sum_{\sigma}\xi_{\alpha\sigma}d^{\dagger}_{\alpha\sigma}d_{\alpha\sigma} + b\sum_{\sigma}\left(d^{\dagger}_{1\sigma}d_{2\sigma} + d^{\dagger}_{2\sigma}d_{1\sigma}\right) \\ &\quad + U\sum_{\alpha} n_{\alpha\uparrow}n_{\alpha\downarrow} + V(n_{1\uparrow}+n_{1\downarrow})(n_{2\uparrow}+n_{2\downarrow}). \end{aligned} \tag{6.22}$$

The parameters we use are (in units of $|b|, b<0$): $\xi = -V_g$, $U = 18.18$, $V = 9.32$, $\Gamma_L = \Gamma_R = 2\pi\nu_L|t^L|^2 = 0.0178$, $k_BT = 0.1136$. The energies of the $N=1$ states are $E_{Nl} = \pm b$ which leads to an inelastic cotunneling threshold of $\Delta = -2b$.
In Figure (6.2), the conductance through the DD calculated with the KinEq approach is plotted on a logarithmic color scale. We see the Coulomb diamond with $N=1$. Outside the diamond, there are additional lines that involve sequential tunneling between excited states and groundstates. Inside the diamond, at $V_{\mathrm{b}} = 1\Delta$ the threshold for inelastic cotunneling is clearly visible. Also the onset of the cotunneling assisted sequential tunneling (see dashed lines in Figure (6.1)) can be seen. In Figures (6.3) and (6.4), we plot the dI/dV versus bias voltage, calculated using the different approximation schemes at different values of the gate voltage.
We see that AppI yields good agreement with the KinEq approach only at small bias voltages. Inelastic cotunneling can be described correctly only if $\Delta \ll E_C$, which is not the case for the parameters here. This situation can be found e.g. in molecular quantum dots, where the perfect degeneracies in the spectrum of the isolated symmetric molecule are lifted by the asymmetric environment of the source-molecule-drain junction.
AppII and KinEq agree nicely as long as gate and bias voltages are such that one is in the innermost diamond defined by the dashed lines (see Figure (6.1)). At its borders, the cotunneling rates can become negative and the rate equations ill-defined. It is not valid outside of this region.
Inside the overall Coulomb diamond, the T-matrix approach and KinEq yield almost exactly the same result. Small relative deviations (few per cent) between the two approaches can be seen at the resonant lines, which can be attributed to the class of diagrams not taken into account by the T-Matrix. Larger deviations occur outside of the diamond (see Figure (6.5)).

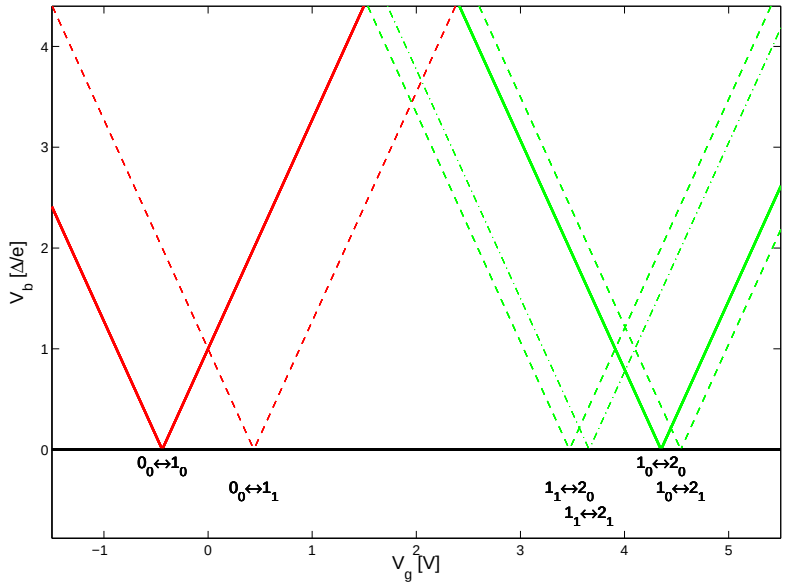

Figure 6.1: Sketch of the Coulomb diamond with one particle. Red lines indicate a transition between states with zero and one particles, green lines between states with one and two particles. Solid lines are for groundstate-groundstate transitions that define the Coulomb blockade region, dashed lines involve excited states.

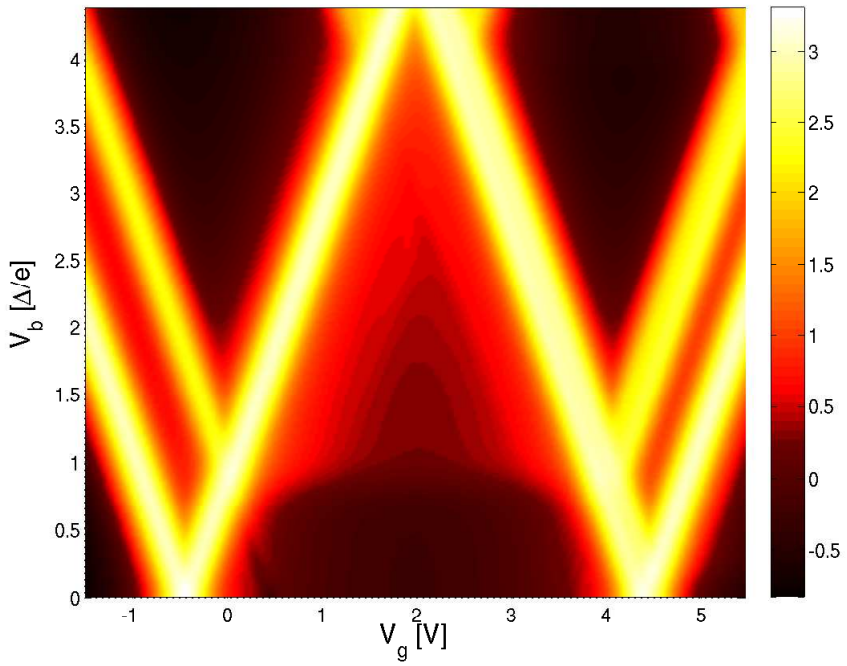

Figure 6.2: $log_{10}(dI/dV)$ calculated with KinEq. One nicely sees the general resemblance to Figure (6.1). The onset of inelastic cotunneling processes at $V_\mathrm{b} = \Delta$ is clearly visible.

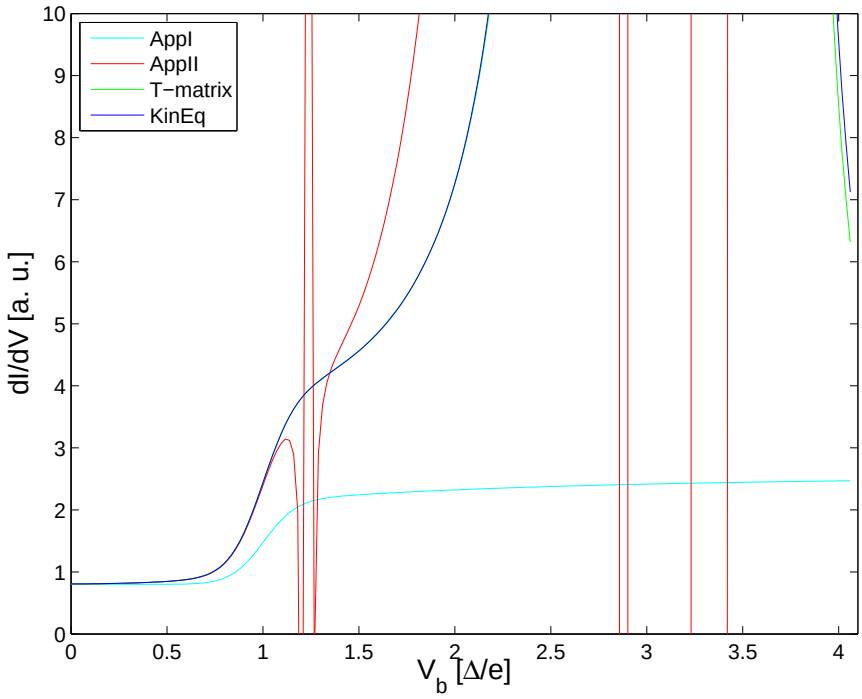

Figure 6.3: dI/dV as a function of bias voltage calculated with the different approaches at $V_g = 1V$. AppII yields divergences in the conductance at resonances. The T-matrix approach and KinEq are well behaved and include also sequential tunneling contributions which are of order $1/\Gamma$ larger than the cotunneling rates.

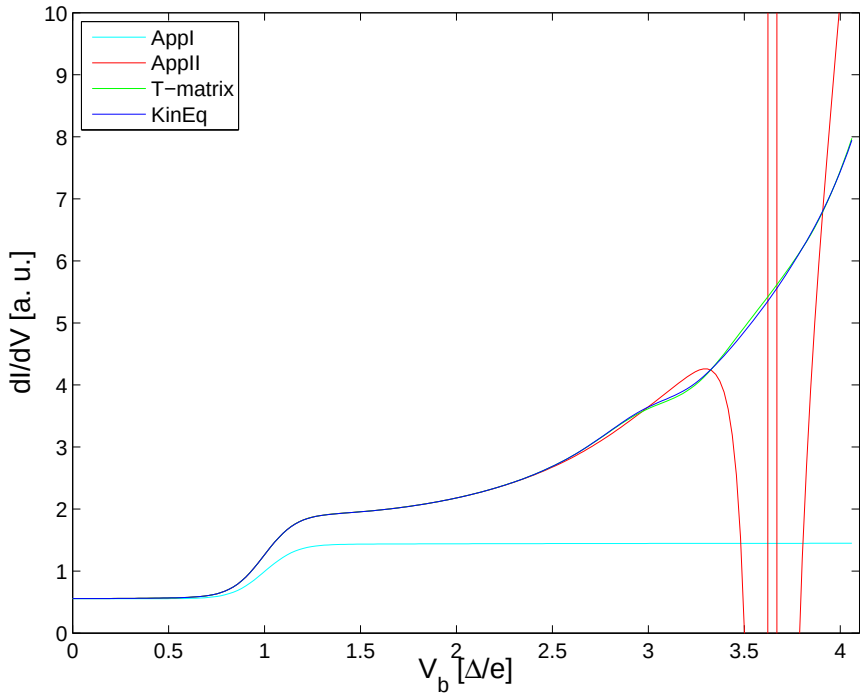

Figure 6.4: dI/dV as a function of bias voltage calculated with the different approaches at the center of the diamond ($V_g = 2V$). AppII and the T-matrix approach coincide for a large bias range. AppI underestimates the conductance.

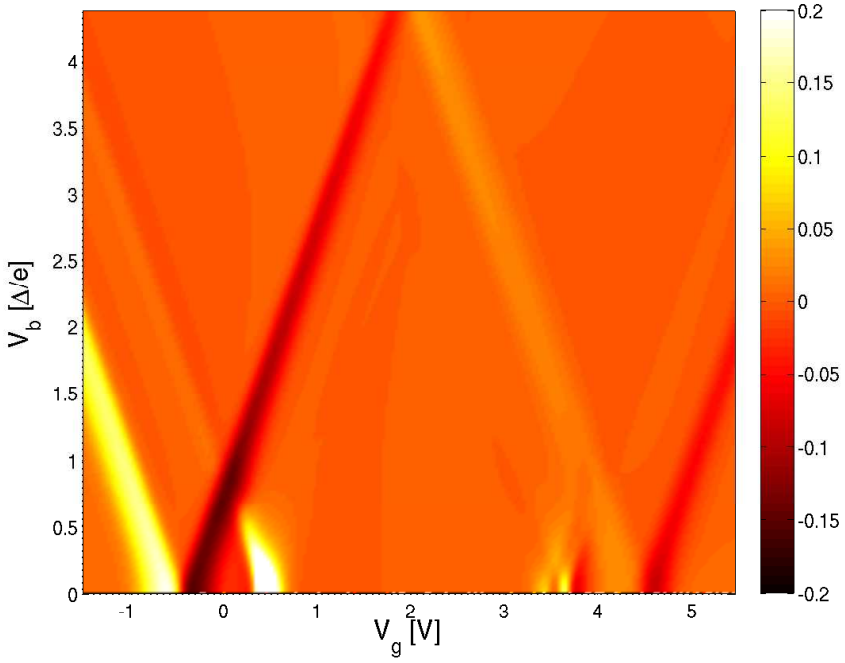

Figure 6.5: Relative difference in current between KinEq and the T-matrix approach. Deviations are seen at the position of the resonant lines (see Figure 6.1). Otherwise, the agreement is almost perfect.

6.5 Gate-dependent tunneling-induced level shifts

The coupling of the molecule to the leads has certain hybridization effects on the molecular states, such as broadening of the otherwise delta-like levels, and in addition a renormalization of the position of the energy levels. To see these effects within a perturbative approach, a summation to all orders in $H_{\rm T}$ over at least a certain class of contributions has to performed [90]. Instead, if we follow Haldane's scaling approach [91], the shift of the energy level $E_{l\eta}$ can be calculated by taking into account all possible fluctuations it can experience to lowest order in $H_{\rm T}$:

$$\delta E_{l\eta}=\sum_{\alpha\sigma s}\int_{-D}^{D}\frac{d\epsilon}{2\pi}Re\left[\Gamma_\alpha\frac{(1-f_\alpha(\epsilon))\left|\langle N{-}1s|d_{\alpha\sigma}|Nl\eta\rangle\right|^2}{E_{l\eta}-(E_{N{-}1s}+\epsilon)}+\Gamma_\alpha\frac{f_\alpha(\epsilon)\left|\langle N{+}1s|d^\dagger_{\alpha\sigma}|Nl\eta\rangle\right|^2}{E_{l\eta}-(E_{N{+}1s}-\epsilon)}\right], \tag{6.23}$$

where $\Gamma^\alpha=2\pi\nu_\alpha|t^\alpha|^2$ and D is the bandwidth of the lead conduction band. This shift does not depend on η. Evaluating the integrals at $T\approx 0$ yields

$$\begin{aligned}\delta E_{l\eta} &= \sum_{\alpha\sigma s}\frac{\Gamma^\alpha}{2\pi}\left[|\langle N{-}1s|d_{\alpha\sigma}|Nl\eta\rangle|^2\ln\frac{E_{l\eta}-E_{N{-}1s}-\mu_\alpha}{E_{l\eta}-E_{N{-}1s}-D}\right. \\ &\qquad\left.+\left|\langle N{+}1s|d^\dagger_{\alpha\sigma}|Nl\eta\rangle\right|^2\ln\frac{E_{l\eta}-E_{N{+}1s}+\mu_\alpha}{E_{l\eta}-E_{N{+}1s}-D}\right],\end{aligned} \tag{6.24}$$

and in the infinite band limit $D\to\infty$ we can approximate this as

$$\begin{aligned}\lim_{D\to\infty}\delta E_{l\eta} &= \sum_{\alpha\sigma s}\frac{\Gamma^\alpha}{2\pi}\left[|\langle N{-}1s|d_{\alpha\sigma}|Nl\eta\rangle|^2\ln\frac{(E_{N{-}1s}+\mu_\alpha-E_{l\eta})}{eV}\right. \\ &\qquad\left.+\left|\langle N{+}1s|d^\dagger_{\alpha\sigma}|Nl\eta\rangle\right|^2\ln\frac{(E_{N{+}1s}-\mu_\alpha-E_{l\eta})}{eV}\right] \\ &\quad-\sum_{\alpha\sigma s}\frac{\Gamma^\alpha}{2\pi}\ln\frac{D}{eV}\left[\langle Nl\eta|d^\dagger_{\alpha\sigma}|N{-}1s\rangle\langle N{-}1s|d_{\alpha\sigma}|Nl\eta\rangle\right. \\ &\qquad\left.+\langle Nl\eta|d_{\alpha\sigma}|N{+}1s\rangle\langle N{+}1s|d^\dagger_{\alpha\sigma}|Nl\eta\rangle\right] \\ &= \sum_{\alpha\sigma s}\frac{\Gamma^\alpha}{2\pi}\left[|\langle N{-}1s|d_{\alpha\sigma}|Nl\eta\rangle|^2\ln\frac{(E_{N{-}1s}+\mu_\alpha-E_{l\eta})}{eV}\right. \\ &\qquad\left.+\left|\langle N{+}1s|d^\dagger_{\alpha\sigma}|Nl\eta\rangle\right|^2\ln\frac{(E_{N{+}1s}-\mu_\alpha-E_{l\eta})}{eV}\right] \\ &\quad-\sum_{\alpha\sigma}\frac{\Gamma^\alpha}{2\pi}\ln\frac{D}{eV}\langle Nl\eta|d^\dagger_{\alpha\sigma}d_{\alpha\sigma}+d_{\alpha\sigma}d^\dagger_{\alpha\sigma}|Nl\eta\rangle \\ &= \sum_{\alpha\sigma s}\frac{\Gamma^\alpha}{2\pi}\left[|\langle N{-}1s|d_{\alpha\sigma}|Nl\eta\rangle|^2\ln\frac{(E_{N{-}1s}+\mu_\alpha-E_{l\eta})}{eV}\right. \\ &\qquad\left.+\left|\langle N{+}1s|d^\dagger_{\alpha\sigma}|Nl\eta\rangle\right|^2\ln\frac{(E_{N{+}1s}-\mu_\alpha-E_{l\eta})}{eV}\right]-\sum_{\alpha\sigma}\frac{\Gamma^\alpha}{2\pi}\ln\frac{D}{eV}.\end{aligned} \tag{6.25}$$

The difference between two N particle energies entering in the inelastic cotunneling rates is then gate dependent, but not depending on the exact value of D. The gate

dependence leads to a tilting of the otherwise horizontal cotunneling line in the stability diagram. This effect has been observed in a recent experiment by Holm [64].
It is very interesting to see the resemblance of this result with the result obtained by Sonja Koller [90]. She followed the real-time diagrammetic approach by König et al. [71], and obtained a renormalization by summing a given subclass of diagrams to all orders in H_{T}. Translated to our notation, her result for the renormalized energy difference of two levels $E_{l\eta} - E_{l'\eta'} + \delta E_{l\eta} - \delta E_{l'\eta'}$ reads

$$\begin{aligned}\delta E_{l\eta} - \delta E_{l'\eta'} \;=\; & \sum_{\alpha\sigma s} \frac{\Gamma^\alpha}{2\pi} \Bigg[|\langle N-1s|d_{\alpha\sigma}|Nl\eta\rangle|^2 \, \Psi\left(\frac{1}{2} + i\frac{\beta(E_{N-1s} + \mu_\alpha - E_{l\eta})}{2\pi}\right) \\ & + \left|\langle N+1s|d^\dagger_{\alpha\sigma}|Nl\eta\rangle\right|^2 \Psi\left(\frac{1}{2} + i\frac{\beta(E_{N+1s} - \mu_\alpha - E_{l\eta})}{2\pi}\right) \\ & - |\langle N-1s|d_{\alpha\sigma}|Nl'\eta'\rangle|^2 \, \Psi\left(\frac{1}{2} + i\frac{\beta(E_{N-1s} + \mu_\alpha - E_{l'\eta'})}{2\pi}\right) \\ & - \left|\langle N+1s|d^\dagger_{\alpha\sigma}|Nl'\eta'\rangle\right|^2 \Psi\left(\frac{1}{2} + i\frac{\beta(E_{N+1s} - \mu_\alpha - E_{l'\eta'})}{2\pi}\right)\Bigg], \end{aligned} \tag{6.26}$$

where Ψ is the digamma function and stems from the precise evaluation of integrals as in equation (6.23) at finite temperatures. In the limit $T \to 0$, her result agrees exactly with ours.

Derivation of equation (6.16)

This section can be regarded as an appendix to this chapter. We derive the expression for the effective Kondo Hamiltonian, equation (6.16). To evaluate equation (6.15), we use the projection operators P_N and P_{N+1} on the tunneling Hamiltonian:

$$H_{NN+1} = P_N H_{\mathrm{T}} P_{N+1} = \sum_{k\sigma\alpha} t^\alpha \sum_{Nl\eta} \sum_{sm} \langle Nl\eta|d_{\alpha\sigma}|N+1sm\rangle c^\dagger_{k\alpha\sigma}|Nl\eta\rangle\langle N+1sm|, \tag{6.27}$$

where $l\eta$ and sm run over all possible N and $N+1$ particle states, respectively. We show here the calculation for $H_{\mathrm{int}}^{N\to N+1\to N} := H_{NN+1}\frac{1}{E_i - H_{N+1N+1} - H_{\mathrm{leads}} + i0^+}H_{N+1N}$ in some detail, while for $H_{\mathrm{int}}^{N\to N-1\to N}$ we just added the result in equations (6.17) and (6.18). We find:

$$\begin{aligned} & H_{NN+1}\frac{1}{E_i - H_{N+1N+1} - H_{\mathrm{leads}} + i0^+}H_{N+1N} \qquad (6.28) \\ = \; & \sum_{k\alpha\sigma}\sum_{k'\alpha'\sigma'}\sum_{ll'}\sum_{\eta\eta'}\sum_{ss'}\sum_{mm'} t^\alpha t^{\alpha'*} c^\dagger_{k\alpha\sigma}|Nl\eta\rangle\langle Nl\eta|d_{\alpha\sigma}|N+1sm\rangle\langle N+1sm| \\ & \frac{1}{E_i - H_{N+1N+1} - H_{\mathrm{leads}} + i0^+}|N+1s'm'\rangle\langle N+1s'm'|d^\dagger_{\alpha'\sigma'}|Nl'\eta'\rangle\langle Nl'\eta'|c_{k'\alpha'\sigma'} \\ = \; & \sum_{k\alpha\sigma}\sum_{k'\alpha'\sigma'}\sum_{ll'}\sum_{\eta\eta'}\sum_{sm} \\ & t^\alpha t^{\alpha'*}\frac{\langle Nl\eta|d_{\alpha\sigma}|N+1sm\rangle\langle N+1sm|d^\dagger_{\alpha'\sigma'}|Nl'\eta'\rangle}{E_{Nl'\eta'} - E_{N+1sm} + \epsilon_{k'\alpha'\sigma'} + i0^+} c^\dagger_{k\alpha\sigma}c_{k'\alpha'\sigma'}|Nl\eta\rangle\langle Nl'\eta'|. \end{aligned}$$

To see the relation between equation (6.28) and equation (6.16), and to identify the exchange scattering $J^{ll'}_{\alpha\alpha'}$ and the potential scattering $P^{ll'}_{\alpha\alpha'}$, we perform the sum over σ and σ' in equation (6.28) term by term, for fixed $ll', \alpha\alpha', kk'$ and $E_{N+1sm} = E_{N+1s}$ for zero magnetic field. Still, we have to sum over m, in words over all the states with different S_z in the multiplet with Energy E_{N+1s}. Again, we show the calculation explicitly for $H_{\rm int}^{N\to N+1\to N}$. We obtain

$$\sum_{\sigma\sigma'}\sum_{\eta\eta'}\sum_{m} t^{\alpha}t^{\alpha'*}\frac{\langle N\eta l|d_{\alpha\sigma}|N+1sm\rangle\langle N+1sm|d^{\dagger}_{\alpha'\sigma'}|N\eta' l'\rangle}{E_{N\eta' l'}-E_{N+1s}+\epsilon_{k'\alpha'\sigma'}}c^{\dagger}_{k\alpha s}c_{k'\alpha'\sigma'}|Nl\eta\rangle\langle Nl'\eta'|$$

$$\begin{aligned}
&= t^{\alpha}t^{\alpha'*}\frac{\langle Nl\uparrow|d_{\alpha\downarrow}|N+1s\ 0\rangle\langle N+1s\ 0|d^{\dagger}_{\alpha'\uparrow}|Nl'\downarrow\rangle}{E_{Nl'\downarrow}-E_{N+1s}+\epsilon_{k'\alpha'\uparrow}+i0^{+}}c^{\dagger}_{k\alpha\downarrow}c_{k'\alpha'\uparrow}|N\uparrow l\rangle\langle N\downarrow l'|\\
&+t^{\alpha}t^{\alpha'*}\frac{\langle Nl\downarrow|d_{\alpha\uparrow}|N+1s\ 0\rangle\langle N+1s\ 0|d^{\dagger}_{\alpha'\downarrow}|Nl'\uparrow\rangle}{E_{Nl'\uparrow}-E_{N+1s}+\epsilon_{k'\alpha'\downarrow}+i0^{+}}c^{\dagger}_{k\alpha\uparrow}c_{k'\alpha'\downarrow}|Nl\downarrow\rangle\langle Nl'\uparrow|\\
&+\sum_{\eta} t^{\alpha}t^{\alpha'*}\frac{\langle N\eta l|d_{\alpha\uparrow}|N{+}1s\ \eta{+}\frac{1}{2}\rangle\langle N{+}1s\ \eta{+}\frac{1}{2}|d^{\dagger}_{\alpha'\uparrow}|N\eta l'\rangle}{E_{N\eta l'}-E_{N+1s}+\epsilon_{k'\alpha'\uparrow}+i0^{+}}c^{\dagger}_{k\alpha\uparrow}c_{k'\alpha'\uparrow}|N\eta l\rangle\langle N\eta l'|\\
&+\sum_{\eta} t^{\alpha}t^{\alpha'*}\frac{\langle N\eta l|d_{\alpha\downarrow}|N{+}1s\ \eta{-}\frac{1}{2}\rangle\langle N{+}1s\ \eta{-}\frac{1}{2}|d^{\dagger}_{\alpha'\downarrow}|N\eta l'\rangle}{E_{N\eta l'}-E_{N+1s}+\epsilon_{k'\alpha'\downarrow}+i0^{+}}c^{\dagger}_{k\alpha\downarrow}c_{k'\alpha'\downarrow}|N\eta l\rangle\langle N\eta l'|.
\end{aligned} \tag{6.29}$$

We want to write this in the form $\left[J^{-+}\tau^{-}_{\sigma'\sigma}\tau^{+}_{\eta\eta'}+J^{+-}\tau^{+}_{\sigma'\sigma}\tau^{-}_{\eta\eta'}+J^{zz}\tau^{z}_{\sigma'\sigma}\tau^{z}_{\eta\eta'}+P\delta_{\sigma'\sigma}\delta_{\eta\eta'}\right]$ $c^{\dagger}_{k\alpha\sigma}c_{k'\alpha'\sigma'}|Nl\eta\rangle\langle Nl'\eta'|$. Here, τ^{+} and τ^{-} are linear combinations of τ^{x} and τ^{y}, $\tau^{\pm} = \tau^{x}\pm i\tau^{y}$. In particular $\boldsymbol{\tau}\cdot\boldsymbol{\tau} = \tau^{x}\tau^{x}+\tau^{y}\tau^{y}+\tau^{z}\tau^{z} = \frac{1}{2}\left(\tau^{+}\tau^{-}+\tau^{-}\tau^{+}\right)+\tau^{z}\tau^{z}$. In the following, we identify J^{+-}, J^{-+}, J^{zz} and P (for simplicity, the indices $\alpha\alpha'$ and ll' are omitted at the moment), and show that $J^{+-} = J^{-+} = J^{zz} = J$. We do so by using angular momentum ladder operators $S^{+} = \sum_i d^{\dagger}_{i\uparrow}d_{i\downarrow}$ and $S^{-} = \sum_i d^{\dagger}_{i\downarrow}d_{i\uparrow}$, where i runs over all the atoms of the molecule, and their impact on the multiplet states with spin S and $S_z = m$ is

$$\begin{aligned}
S^{-}|S,m\rangle &= \hbar\sqrt{S(S+1)-m(m-1)}|S,m-1\rangle,\\
S^{+}|S,m\rangle &= \hbar\sqrt{S(S+1)-m(m+1)}|S,m+1\rangle,
\end{aligned} \tag{6.30}$$

together with the commutation relations

$$\begin{aligned}
\left[S^{+},d^{\dagger}_{\alpha\sigma}\right] &= \delta_{\sigma\downarrow}d^{\dagger}_{\alpha\uparrow},\\
\left[S^{+},d_{\alpha\sigma}\right] &= -\delta_{\sigma\uparrow}d_{\alpha\downarrow},\\
\left[S^{-},d^{\dagger}_{\alpha\sigma}\right] &= \delta_{\sigma\uparrow}d^{\dagger}_{\alpha\downarrow},\\
\left[S^{-},d_{\alpha\sigma}\right] &= -\delta_{\sigma\downarrow}d_{\alpha\uparrow}.
\end{aligned} \tag{6.31}$$

Using equations (6.30) and (6.31), we get

$$\begin{aligned}\langle Nl\downarrow|d_{\alpha\uparrow}|N+1s\ 0\rangle\langle N+1s\ 0|d^\dagger_{\alpha'\downarrow}|Nl'\uparrow\rangle \\ =\langle Nl\uparrow|S^+d_{\alpha\uparrow}|N+1s\ 0\rangle\langle N+1s\ 0|d^\dagger_{\alpha'\downarrow}S^+|Nl'\downarrow\rangle \\ =\langle Nl\uparrow|d_{\alpha\downarrow}|N+1s\ 0\rangle\langle N+1s\ 0|d^\dagger_{\alpha'\uparrow}|Nl'\downarrow\rangle,\end{aligned} \tag{6.32}$$

and with this we find that

$$J^{+-}=J^{-+}=t^\alpha t^{\alpha'*}\frac{\langle Nl\downarrow|d_{\alpha\uparrow}|N+1s\ 0\rangle\langle N+1s\ 0|d^\dagger_{\alpha'\downarrow}|Nl'\uparrow\rangle}{E_{Nl'}-E_{N+1s}+\epsilon_{k'\alpha'}+i0^+}. \tag{6.33}$$

To identify J^{zz} and P, we introduce the shorthand notation, $M_{\eta\sigma}=\langle N\eta l|d_{\alpha\sigma}|N+1sm\rangle\langle N+1sm|d^\dagger_{\alpha'\sigma}|N\eta l'\rangle$. Again with equations (6.30), (6.31), one can show that $M_{\uparrow\uparrow}=M_{\downarrow\downarrow}$ and $M_{\downarrow\uparrow}=M_{\uparrow\downarrow}$. With $|N\eta l\rangle\langle N\eta l'|=\frac{1}{2}\sum_\eta|N\eta l\rangle\langle N\eta l'|+\eta S^z_{ll'}$, the last two lines of equation (6.29) can be rewritten as

$$\begin{aligned}\frac{1}{E_{Nl'}-E_{N+1s}+\epsilon_{k'\alpha'}+i0^+}\Bigg[\sum_{\sigma\sigma'}\left[M_{\uparrow\uparrow}-M_{\downarrow\uparrow}\right]S^z_{ll'}\tau^z_{\sigma'\sigma}c^\dagger_{k\alpha\sigma}c_{k'\alpha'\sigma'}+ \\ \frac{1}{2}\sum_{\eta\sigma}\left[M_{\uparrow\uparrow}+M_{\downarrow\uparrow}\right]c^\dagger_{k\alpha\sigma}c_{k'\alpha'\sigma}|N\eta l\rangle\langle N\eta l'|\Bigg],\end{aligned} \tag{6.34}$$

from where we identify

$$\begin{aligned}J^{zz} &= t^\alpha t^{\alpha'*}\sum_m\Bigg[\frac{\langle Nl\uparrow|d_{\alpha\uparrow}|N+1sm\rangle\langle N+1sm|d^\dagger_{\alpha'\uparrow}|Nl'\uparrow\rangle}{E_{Nl'}-E_{N+1s}+\epsilon_{k'\alpha'}+i0^+} \\ &\quad-\frac{\langle Nl\uparrow|d_{\alpha\downarrow}|N+1sm\rangle\langle N+1sm|d^\dagger_{\alpha'\downarrow}|Nl'\uparrow\rangle}{E_{Nl'}-E_{N+1s}+\epsilon_{k'\alpha'}+i0^+}\Bigg],\end{aligned} \tag{6.35}$$

$$P=t^\alpha t^{\alpha'*}\sum_m\sum_\sigma\left[\frac{\langle Nl\uparrow|d_{\alpha\sigma}|N+1sm\rangle\langle N+1sm|d^\dagger_{\alpha'\sigma}|Nl'\uparrow\rangle}{E_{Nl'}-E_{N+1s}+\epsilon_{k'\alpha'}+i0^+}\right]. \tag{6.36}$$

The remaining task is to show that $J^{zz}=J^{+-}$ or in other terms that

$$\begin{aligned}\langle Nl\downarrow|d_{\alpha\uparrow}|N+1s\ 0\rangle\langle N+1s\ 0|d^\dagger_{\alpha'\downarrow}|Nl'\uparrow\rangle \\ =\Big[\langle Nl\uparrow|d_{\alpha\uparrow}|N+1s\ 1\rangle\langle N+1s\ 1|d^\dagger_{\alpha'\uparrow}|Nl'\uparrow\rangle \\ -\langle Nl\uparrow|d_{\alpha\downarrow}|N+1s\ 0\rangle\langle N+1s\ 0|d^\dagger_{\alpha'\downarrow}|Nl'\uparrow\rangle\Big],\end{aligned} \tag{6.37}$$

which can be done again by using equations (6.30), (6.31). We use in particular

$$\begin{aligned}\langle N\ S\ \eta|d_{\alpha\uparrow}|N{+}1\ S{+}\frac{1}{2}\ \eta{+}\frac{1}{2}\rangle = \\ \frac{\sqrt{(S+\frac{1}{2})(S+\frac{3}{2})-(\eta+\frac{1}{2})(\eta+\frac{3}{2})}}{\sqrt{S(S+1)-\eta(\eta-1)}}\langle N\ S\ \eta{-}1|d_{\alpha\uparrow}|N{+}1\ S{+}\frac{1}{2}\ \eta{-}\frac{1}{2}\rangle,\end{aligned} \tag{6.38}$$

from where it follows that equation (6.37) is fulfilled.

The results presented in this chapter were obtained in collaboration with Jens Paaske, Sonja Koller and Milena Grifoni. A publication is in preparation.

Chapter 7

Conclusions

We have investigated quantum transport through single molecule junctions with weak lead-molecule coupling. In chapter 2, the PPP-Hamiltonian for conjugated molecules was derived and specified for benzene. This model covers the excitations of benzene relevant for transport, and it is known to give good agreement with experiments on benzene in the gas phase. As the theoretical framework to describe transport through the molecule, we have derived the generalized master equation (GME) for the reduced density matrix (RDM) of the molecule to lowest non-vanishing order in the lead-molecule coupling in chapter 3.

In chapter 4, we have presented the results of our calculations on transport through a benzene interference single electron transistor (ISET), attached to the lead in para and meta configuration. In both cases, transport is characterized by Coulomb blockade. In meta configuration, we found that destructive interference of degenerate many-body eigenstates causes a reduction of the linear conductance with respect to the para configuration, and negative differential conductance (NDC) and current blocking at finite bias voltages. We tested the robustness of the interference effects against breaking of the exact symmetry of the benzene molecule, which is related to the presence of exact degeneracies. As the condition for the interference effects to survive, we have found the quasi degeneracy of two interfering states, meaning that the difference in energy must be smaller than the molecule-lead coupling strength, $\delta E \ll \hbar\Gamma \ll k_{\mathrm{B}}T$.

The energetic analysis of the sequential tunneling processes together with the Pauli exclusion principle in the leads and the interference-caused node in the transition probability of the blocking state would lead to the conclusion that current blocking is a threshold effect. We find instead that due to the internal dynamics of the molecular states induced by the coupling to the leads, the interference is perfectly destructive and the current is blocked completely only at one specific bias voltage. In chapter 5, we proposed to use the characteristic blocking behavior to obtain control over the molecules spin degree of freedom by means of the bias voltage. In the presence of parallel polarized leads, different components of spin multiplets experience different renormalizations, and thus the current is blocked at more than one specific bias voltage. Every time the current is blocked, the molecule is in a specific state of the multiplet, and the bias can be tuned to switch between different configurations. Spin control by

all-electrical means is highly desirable for spintronics and spin based quantum computing applications. In addition to benzene junctions, we propose other realizations of ISETs. As necessary conditions, we identified the presence of degenerate orbitals and the possibility to form superpositions of these orbitals that exhibit nodes at one electrode and not at the other. In particular, these conditions are fulfilled for systems with discrete rotational symmetry. We showed that qualitatively the same interference effects as in benzene can be expected in a triangular arrangement of quantum dots. Multiple quantum dots can be described by Hamiltonians formally equivalent to H_{PPP}, but with adjusted parameters.
In chapter 6, we left the sequential tunneling regime and investigated cotunneling processes. We showed that in the deep Coulomb blockade regime the system can be described by an effective Kondo Hamiltonian. We have derived different approximation schemes for the cotunneling rates, all based on the T-matrix formalism and a master equation approach, neglecting coherences. We compared these approximation schemes to the exact fourth order calculations by Koller et al. [73] and discussed their regimes of validity as well as their accuracy. The generalized master equation and the T-matrix approach show good agreement where additional effects due to level shifts and broadening are irrelevant, namely in the regime where the tunneling induced level width is much smaller than the temperature.

Perspectives

In the end of this thesis, we want to give some stimulus for a continuation of our work. Therefore, we list suggestions for future works and some of the problems that could not be resolved in the framework of this thesis.

- An estimate of the reduction of the addition energy due to screening effects of the electron electron interaction on the molecule in presence of polarizable environments is highly desirable. To calculate this quantity, we suggest to implement the approach of Kaasbjerg [56] for our model.

- Molecules are characterized by vibrations. The impact of these vibrational modes on the interference effects is an interesting question that should be addressed.

- A simple method that can deal with degeneracies, and therefore with interference effects in the cotunneling regime, is of great interest. Is it possible to generalize the T-matrix based rate equation approach to include coherences between degenerate states?

- In benzene, a multi-orbital Kondo effect is expected. To gain a quantitative understanding of the conductance in the Kondo regime, one can derive the parameters J and P in the Kondo model from the exact many-body eigenstates of benzene and use them as an input for renormalization group (RG) calculations.

Acknowledgements

Ich möchte mich ganz herzlich bei all jenen bedanken, die zum Gelingen der vorliegenden Arbeit beigetragen haben. Milena Grifoni hat mir die Möglichkeit gegeben, bei ihr diese Arbeit anzufertigen. Milena, es hat mir sehr viel Spaß gemacht, mit dir und in deiner Gruppe zu arbeiten. Deine ruhige, unaufgeregte, ganz besondere Art sorgen für eine sehr angenehme Atmosphäre und deine fachliche Führung ist eine große Hilfe.
Andrea Donarini verdient meinen besonderen Dank für seine endlose Geduld in zahllosen Diskussionen, für viele Ideen und Anregungen und für seine Bereitschaft, bei schwierigen, auch zeitaufwändigen Arbeiten immer zu helfen. Andrea, ohne dich hätte diese Arbeit nicht so viel Freude gemacht und wäre so auch nicht möglich gewesen.
I want to thank Jens Paaske for inviting me to spend 5 month with him in the theory group at the Nano-Science Center, University of Copenhagen. Jens, the time I spent in Denmark was a very important and most of all wonderful experience for me. I learned a lot from you, and I also enjoyed life with new friends in wonderful Copenhagen.
Financial Support from the Dansish Agency for Science, Technology and Innovation during my stay in Copenhagen is acknowledged.
Ich bedanke mich auch bei Dana Darau und Sonja Koller für die erfolgreiche Zusammenarbeit, die sich nicht zuletzt in den gemeinsamen Veröffentlichungen wiederspiegelt. Ihr zwei habt immer Zeit und Geduld, mir in Diskussionen neue Blickwinkel auf unsere Arbeit aufzuzeigen.
Bei Johannes Hausinger bedanke ich mich für das gute Auskommen, das wir in all den Jahren im gemeinsamen Büro hatten und für viele interessante Diskussionen und schöne Unternehmungen weit über die Physik hinaus.
Bei Lizy Lazar bedanke ich mich für ihre Unterstützung in vielen kleinen und großen Dingen des universitären Lebens und für ihre emotionale Unterstützung in schwierigen Phasen der Arbeit.
Katrin Will hat diese Arbeit Korrektur gelesen im Hinblick auf sprachliche Fehler. Auch dafür vielen Dank.
Besonderer Dank geht an meine Eltern, die mich immer unterstützt haben.

Diese Arbeit wurde von der Deutschen Forschungsgemeinschaft im Rahmen des Schwerpunktsprogramms 1243 *Quantentransport auf molekularer Ebene* finanziell gefördert.

Bibliography

[1] R. P. Feynman, R. B. Leighton, and M. Sands, *The Feynman Lectures on Physics*, Vol. III (Addison-Wesley, USA, 1965).

[2] R. P. Crease, Physics World **15** (2002).

[3] T. Young, Philos. Trans. R. Soc. London **94**, 1 (1804).

[4] C. Jönsson, Z. Phys. **161**, 454 (1961).

[5] P. G. Merli, G. F. Missiroli, and G. Pozzi, Am. J. Phys. **44**, 306 (1976).

[6] A. Tonomura, J. Endo, T. Matsuda, T. Kawasaki, and H. Ezawa, American Journal of Physics **57**, 117 (1989), and http://www.hitachi.com/rd/research/em/doubleslit.html.

[7] O. Carnal and J. Mlynek, Phys. Rev. Lett. **66**, 2689 (1991).

[8] D. W. Keith, C. R. Ekstrom, Q. A. Turchette, and D. Pritchard, Phys. Rev. Lett. **66**, 2693 (1991).

[9] M. Arndt, Nature **401**, 680 (1999).

[10] B. Brezger *et al.*, Phys. Rev. Lett. **88**, 100404 (2002).

[11] A. Yacoby, M. Heiblum, D. Mahalu, and H. Shtrikman, Phys. Rev. Lett. **74**, 4047 (1995).

[12] S. Gustavsson, R. Leturcq, M. Studer, T. Ihn, and K. Ensslin, Nano Lett. **8**, 2547 (2008).

[13] D. V. Cardamone, C. A. Stafford, and S. Mazumdar, Nano Lett. **6**, 2422 (2006).

[14] J. P. Bergfield and C. A. Stafford, Nano Letters **9**, 3072 (2009).

[15] S.-H. Ke, W. Yang, and H. U. Baranger, Nano Lett. **8**, 3257 (2008).

[16] Z. Quian, R. Li, X. Zhao, S. Hou, and S. Sanvito, Phys. Rev. B **78**, 113301 (2008).

[17] G. Begemann, D. Darau, A. Donarini, and M. Grifoni, Phys. Rev. B **77**, 201406 (2008), Erratum: Phys. Rev. B **78**, 089901(E) (2008).

[18] D. Darau, G. Begemann, A. Donarini, and M. Grifoni, Phys. Rev. B **79**, 235404 (2009).

[19] A. Donarini, G. Begemann, and M. Grifoni, Nano Lett. **9**, 2897 (2009).

[20] A. Nitzan and M. Ratner, Science **300**, 1384 (2003).

[21] A. Aviram and M. A. Ratner, Chem. Phys. Lett. **29**, 277 (1974).

[22] M. A. Reed, C. Zhou, C. J. Muller, T. P. Burgin, and J. M. Tour, Science **278**, 252 (1997).

[23] G. Binnig, H. Rohrer, C. Gerber, and E. Weibel, Phys. Rev. Lett. **49**, 57 (1982).

[24] F. Chen, J. Hihath, Z. Huang, X. Li, and N. J. Tao, Ann. Rev. Phys. Chem. **58**, 535 (2007).

[25] X. Xiao, B. Xu, and N. Tao, Angew. Chem. Int. Ed. **43**, 6148 (2004).

[26] F. Chen *et al.*, Nano Lett. **5**, 503 (2005).

[27] E. A. Osorio, T. Bjørnholm, J.-M. Lehn, M. Ruben, and H. S. J. van der Zant, J. Phys.: Condens. Matter **20**, 374121 (2008).

[28] S. Kubatkin *et al.*, Nature **425**, 698 (2003).

[29] A. Champagne, A. Pasupathy, and D. Ralph, Nano Lett. **5**, 305 (2005).

[30] T. Dadosh *et al.*, Nature **436**, 677 (2005).

[31] K. Stokbro, J. Taylor, M. Brandbyge, and G. Hong, p. 117, in Cuniberti *et al.* [92].

[32] A. Di Carlo, A. Pecchia, L. Latessa, T. Frauenheim, and G. Seifert, p. 153, in Cuniberti *et al.* [92].

[33] M. H. Hettler, W. Wenzel, M. R. Wegewijs, and H. Schoeller, Phys. Rev. Lett. **90**, 076805 (2003).

[34] V. N. Golovach and D. Loss, Phys. Rev. B **69**, 245327 (2004).

[35] M. R. Wegewijs, M. H. Hettler, C. Romeike, A. Thielmann, and J. König, p. 207, in Cuniberti *et al.* [92].

[36] J. Koch, F. von Oppen, and A. V. Andreev, Phys. Rev. B **74**, 205438 (2006).

[37] C. Timm, Phys. Rev. B **77**, 195416 (2008).

[38] S. A. Wolf, Science **294**, 1488 (2001).

[39] D. D. Awschalom and M. E. Flatte, Nat. Phys. **3**, 153 (2007).

[40] P. Shor, *Algorithms for Quantum Computation: Discrete Logarithms and Factoring*, in *Proceedings 35th Annual Symposium on Foundations of Computer Science*, p. 124, 1994.

[41] K. C. Nowack, F. H. L. Koppens, Y. V. Nazarov, and L. M. K. Vandersypen, Science **318**, 1430 (2007).

[42] V. N. Golovach, M. Borhani, and D. Loss, Phys. Rev. B **74**, 165319 (2006).

[43] L. Levitov and E. Rashba, Phys. Rev. B **67**, 115324 (2003).

[44] S. Debald and C. Emary, Phys. Rev. Lett. **94**, 226803 (2005).

[45] J. Walls, Phys. Rev. B **76**, 195307 (2007).

[46] J. R. Hauptmann, J. Paaske, and P. E. Lindelof, Nat. Phys. **4**, 373 (2008).

[47] R. Pariser and R. G. Parr, J. Chem. Phys. **21**, 466 (1953), J. Chem. Phys. **21**, 767 (1953).

[48] J. A. Pople, Farad. Trans. **49**, 1375 (1953).

[49] J. Linderberg and Y. Öhrn, J. Chem. Phys. **49**, 716 (1968).

[50] R. Bursill, C. Castleton, and W. Barford, Chem. Phys. Lett. **294**, 305 (1998).

[51] S. Ramasesha, I. D. L. Albert, and B. Sinha, Molecular Physics **72**, 537 (1991).

[52] G. L. Bendazzoli, S. Evangelisti, and L. Gagliardi, Int. J. Quant. Chem. **51**, 13 (1994).

[53] K. Ohno, Theoret. Chim. Acta **2**, 219 (1964).

[54] A. Danilov *et al.*, Nano Lett. **8**, 1 (2008).

[55] E. A. Osorio *et al.*, Adv. Mater. **19**, 281 (2007).

[56] K. Kaasbjerg and K. Flensberg, Nano Lett. **8**, 3809 (2008).

[57] H. Bruus and K. Flensberg, *Many-Body Quantum Theory in Condensed Matter Physics* (Oxford University Press, New York, 2004).

[58] J. Kondo, Prog. Theor. Phys. **32**, 37 (1964).

[59] D. Goldhaber-Gordon *et al.*, Nature **391**, 156 (1998).

[60] J. Nygård, D. Cobden, and P. Lindelof, Nature **408**, 342 (2000).

[61] W. Liang, M. Shores, M. Bockrath, J. Long, and H. Park, Nature **417**, 725 (2002).

[62] H. Grabert and M. H. Devoret, editors, *Single Charge Tunneling: Coulomb-Blockade Phenomena in Nanostructures* (Plenum Press and NATO Scientific Affairs Division, New York, 1992).

[63] J. M. Thijssen and H. S. J. Van der Zant, Phys. Stat. Sol. (B) **245**, 1455 (2008).

[64] J. V. Holm *et al.*, Phys. Rev. B **77**, 161406 (2008).

[65] L. Mayrhofer and M. Grifoni, Eur. Phys. J. B **56**, 107 (2007).

[66] R. Hornberger, S. Koller, G. Begemann, A. Donarini, and M. Grifoni, Phys. Rev. B **77**, 245313 (2008).

[67] K. Blum, *Density Matrix Theory and Applications* (Springer US, 1996).

[68] M. Braun, J. König, and J. Martinek, Phys. Rev. B **70**, 195345 (2004).

[69] M. G. Schultz and F. von Oppen, Phys. Rev. B **80**, 033302 (2009).

[70] H. Schoeller and G. Schön, Phys. Rev. B **50**, 18436 (1994).

[71] J. König, J. Schmid, H. Schoeller, and G. Schön, Phys. Rev. B **54**, 16820 (1996).

[72] J. König, H. Schoeller, and G. Schön, Phys. Rev. Lett. **76**, 1715 (1996).

[73] S. Koller, M. Grifoni, M. Leijnse, and M. R. Wegewijs, unpublished, 2009.

[74] J. Enderlein, 2009, package available under http://www.joerg-enderlein.de/research/resources.html.

[75] M. S. Dresselhaus, G. Dresselhaus, and A. Jorio, *Group Theory. Application to the Physics of Condensed Matter* (Springer, Berlin-Heidelberg, 2008).

[76] B. Wunsch, M. Braun, J. König, and D. Pfannkuche, Phys. Rev. B **72**, 205319 (2005).

[77] H. van Houten, C. W. J. Beenakker, and A. A. M. Staring, p. 167, in Grabert and Devoret [62].

[78] R. Schleser *et al.*, Phys. Rev. Lett. **94**, 206805 (2005).

[79] S. De Franceschi *et al.*, Phys. Rev. Lett. **86**, 878 (2001).

[80] S. Sapmaz *et al.*, Phys. Rev. B **71**, 153402 (2005).

[81] A. K. Hüttel, B. Witkamp, M. Leijnse, M. R. Wegewijs, and H. S. J. van der Zant, Phys. Rev. Lett. **102**, 225501 (2009).

[82] D. Becker and D. Pfannkuche, Phys. Rev. B **77**, 205307 (2008).

[83] S. Schmaus *et al.*, Phys. Rev. B **79**, 045105 (2009).

[84] J. R. Schrieffer and P. A. Wolff, Phys. Rev. **149**, 491 (1966).

[85] M. Leijnse, M. R. Wegewijs, and M. H. Hettler, arXiv:0903.3559, unpublished, 2009.

[86] A. C. Hewson, *The Kondo Problem to Heavy Fermions* (Cambridge University Press, UK, 1993).

[87] M. Leijnse and M. R. Wegewijs, Phys. Rev. B **78**, 235424 (2008).

[88] D. V. Averin, Physica B **194**, 979 (1994).

[89] M. Turek and K. Matveev, Phys. Rev. B **65**, 115332 (2002).

[90] S. Koller, *Spin phenomena and higher order effects in transport across interacting quantum-dots*, Dissertation, Universität Regensburg, 2009.

[91] F. D. M. Haldane, Phys. Rev. Lett. **40**, 416 (1978).

[92] G. Cuniberti, G. Fagas, and K. Richter, editors, *Introducing Molecular Electronics* (Springer, Berlin, 2005).

Transport through a double-quantum-dot system with noncollinearly polarized leads

R. Hornberger, S. Koller, G. Begemann, A. Donarini, and M. Grifoni
Institut für Theoretische Physik, Universität Regensburg, 93035 Regensburg, Germany
(Received 29 November 2007; revised manuscript received 21 February 2008; published 12 June 2008)

We investigate linear and nonlinear transport in a double quantum dot system weakly coupled to spin-polarized leads. In the linear regime, the conductance as well as the nonequilibrium spin accumulation are evaluated in analytic form. The conductance as a function of the gate voltage exhibits four peaks of different heights with mirror symmetry with respect to the charge neutrality point. As the polarization angle is varied, due to exchange effects, the position and shape of the peaks change in a characteristic way, which preserves the electron-hole symmetry of the problem. In the nonlinear regime, various spin-blockade effects are observed. Moreover, negative differential conductance features occur for noncollinear magnetizations of the leads. In the considered sequential tunneling limit, the tunneling magnetoresistance (TMR) is always positive with a characteristic gate voltage dependence for noncollinear magnetization. If a magnetic field is added to the system, the TMR can become negative.

DOI: 10.1103/PhysRevB.77.245313 PACS number(s): 73.63.Kv, 72.25.−b, 73.23.Hk, 85.75.−d

I. INTRODUCTION

Spin-polarized transport through nanostructures is attracting increasing interest due to its potential application in spintronics[1,2] as well as in quantum computing.[3] Downscaling magnetoelectronic devices to the nanoscale implies that Coulomb interaction effects become increasingly important.[4,5] In particular, the interplay between spin-polarization and Coulomb blockade can give rise to a complex transport behavior in which both the spin and the charge of the "information carrying" electron play a role. This has been widely demonstrated by many experimental studies on single-electron transistors (SETs) with ferromagnetic leads, with central element being either a ferromagnetic particle,[6–8] normal metal particles,[9,10] a two-level artificial molecule,[11] a C_{60} molecule,[12] or a carbon nanotube,[13] showing the increasing complexity and variety of the investigated systems. Initially, the theoretical work was mainly focused on the difference in the transport properties for parallel or antiparallel magnetizations in generic spin-valve SETs.[14–24] More recently, the interplay between spin and interaction effects for noncollinear magnetization configurations attracted quite some interest both in systems with a continuous energy spectrum,[25–28] as well as in single-level quantum dots,[29–36] many-level nanomagnets,[37] and in carbon nanotube quantum dots.[38] In the noncollinear case, a much richer physics is expected than in the collinear one. For example, two separate exchange effects have to be taken into account. On the one hand, there is the nonlocal interface exchange, in scattering theory for noninteracting systems described by the imaginary part of the spin-mixing conductance,[39] which in the context of current-induced magnetization dynamics acts as an effective field.[40] Such an effective field has been experimentally found to strongly affect the transport dynamics in spin valves with MgO tunnel junctions.[41] This effect has also been recently involved to explain negative tunneling magnetoresistance (TMR) effects in carbon nanotube spin valves[13] and called spin-dependent interface phase shifts.[22,42] The second exchange term is an interaction-dependent exchange effect due to virtual tunneling processes that is absent in noninteracting systems.[25,28,30,38] This latter exchange effect is potentially attractive for quantum information processing since it allows to switch on and off magnetic fields in arbitrary directions just by a gate electric potential.

Recently, there has been increasing interest in double-quantum-dot systems (that can be realized, e.g., in semiconducting structures[43] or carbon nanotubes[44]) as tunable systems attractive for studying fundamental spin correlations. In fact, the exchange Coulomb interaction induces a singlet-triplet splitting, which can be used to perform logic gates.[45] Moreover, Coulomb interaction together with the Pauli principle can be used to induce spin-blockade when the two electrons have triplet correlations.[46–49] The Pauli spin-blockade effect can be used to obtain a spin-polarized current even in the absence of spin-polarized leads; it requires a strong asymmetry between the two on-site energies of the left and right dots.

So far, transport through a double-dot (DD) system with spin-polarized leads has been addressed in few theoretical[23,24,50] and experimental[11] works, for the case of collinearly polarized leads only. While Ref. 23 addresses additional Pauli spin-blockade regimes when one lead is half-metallic and one is nonmagnetic, Ref. 24 focuses on the effects of higher order processes in symmetric DD systems, which can, e.g., yield a zero bias anomaly or a negative tunneling magnetoresistance. In Ref. 11, Coulomb blockade spectroscopy is used to measure the energy difference between symmetric and antisymmetric molecular states and to determine the spin of the transferred electron.

In this work, we investigate spin-dependent transport in the so-far unexplored case of a DD system connected to leads with arbitrary polarization direction. Specifically, we focus on the low transparency regime where a weak coupling between the DD and the leads is assumed. Our model takes into account interface reflections as well as exchange effects due to the interactions and relevant for noncollinear polarization. We focus on the case of a symmetric DD, so that rectification effects induced by Pauli spin-blockade are excluded. In the linear transport regime, the conductance is calculated in closed analytic form. This yields four distinct resonant tunneling regimes, but due to the electron-hole sym-

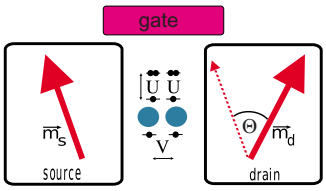

FIG. 1. (Color online) Schematic picture of the model: a double-quantum-dot system attached to polarized leads. The significance of the on-site and intersite interactions U and V, respectively, is depicted. The source and drain contacts are polarized and the direction of the magnetizations $\vec{m}_\alpha$ is indicated by the arrows.

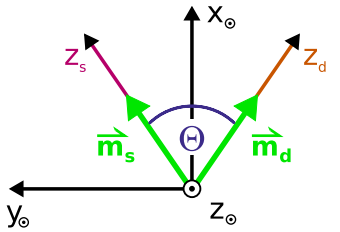

FIG. 2. (Color online) The spin quantization axis of the double-dot, $z_\odot$, is chosen to be perpendicular to the plane spanned by the magnetization directions $\vec{m}_s$, $\vec{m}_d$ in the leads. The latter enclose an angle Θ.

metry of the DD Hamiltonian, each possess a symmetric mirror with respect to the charge neutrality point. However, by applying an external magnetic field, this symmetry is broken, which can lead to negative tunneling magnetoresistance features. Finally, in the nonlinear regime, some excitation lines can be suppressed for specific polarization angles, and negative differential features also occur.

The method developed in this work to investigate charge and spin transport is based on the Liouville equation for the reduced density matrix (RDM) in lowest order in the reflection and tunneling Hamiltonians. The obtained equations of motion are fully equivalent to those that could be obtained by using the Green's function method[30,51] in the same weak-tunneling limit. The advantage of our approach is that it is, in our opinion, easier to understand and to apply for newcomers, as it is based on standard perturbation theory and does not require knowledge of the nonequilibrium Green's function formalism.

The paper is organized as follows. In Sec. II, we introduce the model system for the ferromagnetic DD single-electron transistor. In Sec. III, the coupled equations of motion for the elements of the DD reduced density matrix are derived. Readers not interested in the derivation of the dynamical equations can directly go to Secs. IV and V, where results for charge and spin transfer in the linear and nonlinear regimes, respectively, are discussed. Finally, we present results for the transport characteristics in the presence of an external magnetic field in Sec. VI. Conclusions are drawn in Sec. VII.

II. MODEL

We consider a two-level DD, or a single molecule with two localized atomic orbitals, attached to ferromagnetic source and drain contacts and with a capacitive coupling to a lateral gate electrode. The system is described by the total Hamiltonian,

$$\hat{H} = \hat{H}_\odot + \hat{H}_s + \hat{H}_d + \hat{H}_T + \hat{H}_R, \tag{1}$$

accounting for the DD Hamiltonian, the source (s) and drain (d) leads, and the tunneling (T) and reflection (R) Hamiltonians. The two contacts are considered to be magnetized along an arbitrary but fixed direction determined by the magnetization vectors $\vec{m}_\alpha$. The two magnetization axes enclose an angle $\Theta \in [0°, 180°]$ (see Fig. 1). The spin quantization axis $\vec{z}_\alpha$ in lead α is parallel to the magnetization $\vec{m}_\alpha$ of the lead. The majority of electrons in each contact will then be in the spin-up state. The Hamiltonians $\hat{H}_s, \hat{H}_d$ that model the source and drain contacts ($\alpha = s, d$) read as follows:

$$\hat{H}_\alpha = \sum_{k\sigma_\alpha} (\varepsilon_{k\sigma_\alpha} - \mu_\alpha) c^\dagger_{\alpha k\sigma_\alpha} c_{\alpha k\sigma_\alpha}, \tag{2}$$

where $c^\dagger_{\alpha k\sigma_\alpha}$ and $c_{\alpha k\sigma_\alpha}$ are electronic lead operators. They create, respectively annihilate, electrons with momentum k and spin σ_α in lead α. The electrochemical potentials $\mu_\alpha = \mu_{0\alpha} + eV_\alpha$ contain the bias voltages V_s and V_d at the left and right lead with $V_s - V_d = V_{\text{bias}}$. There is no voltage drop within the DD. We denote in the following $\varepsilon_{k\sigma_\alpha} - \mu_\alpha := \varepsilon_{\alpha k\sigma_\alpha}$.

Tunneling processes into and out of the DD are described by $\hat{H}_T$. We denote with $d^\dagger_{\alpha\sigma_\alpha}$, $d_{\alpha\sigma_\alpha}$ the creation and destruction operators in the DD. We assume that tunneling only can happen between a contact and the closest dot, so that we can use the convention that the lead indices $\alpha = s, d$ correspond to $\alpha = 1, 2$ for the DD. With t_α the tunneling amplitude, we find

$$\hat{H}_T = \sum_{\alpha k\sigma_\alpha} (t_\alpha d^\dagger_{\alpha\sigma_\alpha} c_{\alpha k\sigma_\alpha} + t^*_\alpha c^\dagger_{\alpha k\sigma_\alpha} d_{\alpha\sigma_\alpha}). \tag{3}$$

The so-called reflection Hamiltonian $\hat{H}_R$ includes reflection events at the lead-molecule interface.[28,38] For strongly shielded leads, the overall effect is the occurrence of a small energy shift Δ_R induced by the magnetic field in the contacts and built up during several cycles of reflections at the boundaries. It reads

$$\hat{H}_R = -\Delta_R \sum_{\alpha=s,d} (d^\dagger_{\alpha\uparrow_\alpha} d_{\alpha\uparrow_\alpha} - d^\dagger_{\alpha\downarrow_\alpha} d_{\alpha\downarrow_\alpha}). \tag{4}$$

Finally, the DD Hamiltonian needs to be specified. As the spin quantization axis of the DD, $\vec{z}_\odot$, we choose the direction perpendicular to the plane spanned by $\vec{z}_s$ and $\vec{z}_d$ (Ref. 30) (see Fig. 2). The two remaining basis vectors $\vec{x}_\odot$ and $\vec{y}_\odot$ are along $\vec{z}_s + \vec{z}_d$, respectively along $\vec{z}_s - \vec{z}_d$. The matrices that mathematically describe the above transformations read

$$M_{s\leftrightarrow\odot} = \frac{1}{\sqrt{2}} \begin{pmatrix} + e^{+i\Theta/4} & + e^{-i\Theta/4} \\ - e^{+i\Theta/4} & + e^{-i\Theta/4} \end{pmatrix} = M^*_{d\leftrightarrow\odot}. \tag{5}$$

We express the DD Hamiltonian in the localized basis such that, e.g., $|+,-\rangle$ describes a state with a spin-up electron on site 1 and a spin-down electron on site 2 (with spin directions expressed in the spin-coordinate system of the DD). Such state can be obtained by applying creation operators on the vacuum state, i.e., $|+,-\rangle = d^\dagger_{1\uparrow} d^\dagger_{2\downarrow} |0\rangle$. In general, the order-

TABLE I. Eigenstates of the double-dot system and corresponding eigenvalues and parity. In the limit $|b|\to\infty$ where the interdot hopping is unhindered, $R\to 0$ and $\alpha_0\to\beta_0$. For $|b|\to 0$, i.e., no interdot hopping takes place, we find that $R\to+\infty$ and $\alpha_0\to 1$, $\beta_0\to 0$ if $U>V$; state $|2\rangle$ then becomes degenerate to $|2'(0)\rangle$, forming a Heitler–London state. In turn, if $U<V$, then $R\to-\infty$ and $\alpha_0\to 0$, $\beta_0\to 1$.

Abbreviation	State	Eigenvalue	Spin
$\|0\rangle$	$\|0,0\rangle$	0	0
$\|1e\sigma\rangle$	$\frac{1}{\sqrt{2}}(\|\sigma,0\rangle+\|0,\sigma\rangle)$	$\xi'+b$	1/2
$\|1o\sigma\rangle$	$\frac{1}{\sqrt{2}}(\|\sigma,0\rangle-\|0,\sigma\rangle)$	$\xi'-b$	1/2
$\|2\rangle$	$\frac{\alpha_0}{\sqrt{2}}(\|+,-\rangle+\|-,+\rangle)$ $+\frac{\beta_0}{\sqrt{2}}(\|2,0\rangle+\|0,2\rangle)$	$2\xi'+\frac{1}{2}(U+V-\Delta)$	0
$\|2'(1)\rangle$	$\|+,+\rangle$		
$\|2'(0)\rangle$	$\frac{1}{\sqrt{2}}(\|+,-\rangle-\|-,+\rangle)$	$2\xi'+V$	1
$\|2'(-1)\rangle$	$\|-,-\rangle$		
$\|2''\rangle$	$\frac{1}{\sqrt{2}}(\|2,0\rangle-\|0,2\rangle)$	$2\xi'+U$	0
$\|2'''\rangle$	$\frac{\beta_0}{\sqrt{2}}(\|+,-\rangle+\|-,+\rangle)$ $-\frac{\alpha_0}{\sqrt{2}}(\|2,0\rangle+\|0,2\rangle)$	$2\xi'+\frac{1}{2}(U+V+\Delta)$	0
$\|3o\sigma\rangle$	$\frac{1}{\sqrt{2}}(\|2,\sigma\rangle+\|\sigma,2\rangle)$	$3\xi'+U+2V+b$	1/2
$\|3e\sigma\rangle$	$\frac{1}{\sqrt{2}}(\|2,\sigma\rangle-\|\sigma,2\rangle)$	$3\xi'+U+2V-b$	1/2
$\|4\rangle$	$\|2,2\rangle$	$4\xi'+2U+4V$	0
	in terms of $R=(U-V)/(4\|b\|)$: $\Delta=4\|b\|\sqrt{1+R^2}$, $\alpha_0=\frac{1}{\sqrt{2}}\frac{1}{\sqrt{1+R^2-R\sqrt{1+R^2}}}$		

ing of the creation operators is defined as $d^\dagger_{1\uparrow}d^\dagger_{2\uparrow}d^\dagger_{1\downarrow}d^\dagger_{2\downarrow}|0\rangle$. The DD Hamiltonian then reads

$$\hat{H}_\odot = \sum_{\alpha\sigma_\odot}\varepsilon_\alpha d^\dagger_{\alpha\sigma_\odot}d_{\alpha\sigma_\odot} + b\sum_{\sigma_\odot}(d^\dagger_{1\sigma_\odot}d_{2\sigma_\odot}+d^\dagger_{2\sigma_\odot}d_{1\sigma_\odot}) + \left(\xi-\frac{U}{2}-V\right)\sum_{\alpha=1}^{2}\sum_{\sigma_\odot}d^\dagger_{\alpha\sigma_\odot}d_{\alpha\sigma_\odot} + U\sum_{\alpha=1}^{2}n_{\alpha\uparrow_\odot}n_{\alpha\downarrow_\odot} + V(n_{1\uparrow_\odot}+n_{1\downarrow_\odot})(n_{2\uparrow_\odot}+n_{2\downarrow_\odot}), \quad (6)$$

where the spin index $\odot$ indicates that the operators are expressed in the spin-coordinate system of the DD. The tunneling coupling between the two sites is b, while U and V are on-site and intersite Coulomb interactions. In the following, we consider a *symmetric* DD with equal on-site energies $\varepsilon_1=\varepsilon_2$. Thus, we can incorporate the on-site energies in the parameter ξ proportional to the applied gate voltage V_{gate}.

To understand transport properties of the two-site system in the weak-tunneling regime, we have to analyze the eigenstates of the isolated interacting system. These states, which are expressed in terms of the localized states, and the corresponding eigenvalues are listed in Table I.[52] Table I also indicates the eigenvalues of the total spin operator. The ground states of the DD with odd particle number are spin degenerate. In contrast, the ground states with even particle number have total spin $S=0$ and are not degenerate. In the case of the two-particle ground state, the parameters α_0 and β_0 determine whether the electrons prefer to pair in the same dot or are delocalized over the DD structure. Since the eigenstates are normalized to one, the condition $\alpha_0^2+\beta_0^2=1$ holds. The energy difference between the $S=0$ ground state and the triplet is given by the exchange energy,

$$J=\frac{1}{2}(\Delta-U+V)=2|b|(R+\sqrt{1+R^2}),$$

where $\Delta=4|b|\sqrt{1+R^2}$ and $R=(V-U)/(4|b|)$.

Besides the triplet, one observes the presence of higher two-particle excited states with total spin $S=0$. Finally, we remark that $\hat{H}_T$ and $\hat{H}_R$ contain operators of the DD, $d^\dagger_{\alpha\sigma_\alpha}$ and $d_{\alpha\sigma_\alpha}$, in the spin-coordinate systems of the leads, while $\hat{H}_\odot$ is already expressed in terms of DD operators $d^\dagger_{\alpha\sigma_\odot}$ and $d_{\alpha\sigma_\odot}$ with spin expressed in the coordinate system of the DD.

III. DYNAMICAL EQUATIONS FOR THE REDUCED DENSITY MATRIX

In this section, we shortly outline how to derive the equation of motion for the RDM to lowest nonvanishing order in the tunneling and reflection Hamiltonians. The method is based on the well known Liouville equation for the total density matrix in lowest order in the tunneling and reflection Hamiltonians. Equations of motion for the reduced density matrix are obtained upon performing the trace over the lead degrees of freedom,[53] yielding, after standard approximations, Eqs. (13) and (14) below. In the case of spin-polarized leads, however, it is convenient to express the equations of motion for the RDM in the basis that diagonalizes the isolated system's Hamiltonian *and* in the system's spin quantization axis. After rotation from the leads' quantization axis to the DD one we obtain [Eq. (21)], which forms the basis of all the subsequent analysis.

Let us start from the Liouville equation for the total density matrix $\hat{\rho}^I(t)$ in the interaction picture,

$$i\hbar\frac{d\hat{\rho}^I(t)}{dt}=[\hat{H}^I_T(t)+\hat{H}^I_R(t),\hat{\rho}^I(t)], \quad (7)$$

with $\hat{H}_T$ and $\hat{H}_R$ transformed into the interaction picture by $\hat{H}^I_{T/R}(t)=e^{i/\hbar(\hat{H}_\odot+\hat{H}_s+\hat{H}_d)(t-t_0)}\hat{H}_{T/R}e^{-i/\hbar(\hat{H}_\odot+\hat{H}_s+\hat{H}_d)(t-t_0)}$, where t_0 indicates the time at which the perturbation is switched on. Integrating Eq. (7) over time and inserting the obtained expression in the right-hand side of Eq. (7) one equivalently finds

$$\hat{\rho}^I(t)=-\frac{i}{\hbar}[\hat{H}^I_R(t),\hat{\rho}^I(t_0)]-\frac{i}{\hbar}[\hat{H}^I_T(t),\hat{\rho}^I(t_0)]-\frac{1}{\hbar^2}\int_{t_0}^{t}dt'[\hat{H}^I_T(t)+\hat{H}^I_R(t),[\hat{H}^I_T(t')+\hat{H}^I_R(t'),\hat{\rho}^I(t')]]. \quad (8)$$

The time evolution of the RDM,

$$\hat{\rho}_{\odot}^{I}(t) := \mathrm{Tr}_{\mathrm{leads}}[\hat{\rho}^{I}(t)], \tag{9}$$

is now formally obtained from Eq. (8) by tracing out the lead degrees of freedom. To proceed, we make the following standard approximations.

(i) The leads are considered as reservoirs of noninteracting electrons that stay in thermal equilibrium at all times. In fact, we only consider weak tunneling and, therefore, the influence of the DD on the leads is marginal. Hence, we can approximatively factorize the density matrix of the total system as

$$\hat{\rho}^{I}(t) \approx \hat{\rho}_{\odot}^{I}(t)\hat{\rho}_{s}\hat{\rho}_{d}, \tag{10}$$

where $\hat{\rho}_s$ and $\hat{\rho}_d$ are time independent and given by the usual thermal equilibrium expression for the contacts $\hat{\rho}_{s/d}=\frac{e^{-\beta\hat{H}_{s/d}}}{Z_{s,d}}$, where β is the inverse temperature and $Z_{s/d}$ are the partition sums over all states of lead s/d.

(ii) We consider the lowest nonvanishing order in $\hat{H}_{T/R}$.

(iii) We apply the Markov approximation, i.e., in the integral in Eq. (8), we replace $\hat{\rho}_{\odot}^{I}(t')$ with $\hat{\rho}_{\odot}^{I}(t)$. In other words, it is assumed that the system loses all memory of its past due to the interaction with the lead electrons.

Furthermore, being interested in the long term behavior of the system only, we send $t_0 \to -\infty$. We finally obtain the generalized master equation (GME) for the reduced density matrix,

$$\dot{\hat{\rho}}_{\odot}^{I}(t) = -\frac{i}{\hbar}\mathrm{Tr}_{\mathrm{leads}}[\hat{H}_{R}^{I}(t), \hat{\rho}_{\odot}^{I}(t)\hat{\rho}_{s}\hat{\rho}_{d}] - \frac{1}{\hbar^2}\int_0^{\infty} dt''\ \mathrm{Tr}_{\mathrm{leads}}([\hat{H}_{T}^{I}(t),[\hat{H}_{T}^{I}(t-t''),\hat{\rho}_{\odot}^{I}(t)\hat{\rho}_{s}\hat{\rho}_{d}]]). \tag{11}$$

A. Contribution from the tunneling Hamiltonian

In the following, we derive the explicit expression for the GME in the basis of the isolated DD. For simplicity, we omit the contribution of the reflection Hamiltonian in a first instance. When we shall have obtained the final form of the GME due to the tunneling term, we will see that it is easy to insert the contribution from the reflection Hamiltonian. Let us then start from the tunneling Hamiltonian in the interaction picture,

$$\hat{H}_{T}^{I}(t) = \sum_{\alpha k\sigma_\alpha}\sum_{i,j} t_\alpha c_{\alpha k\sigma_\alpha}^{\dagger}(d_{\alpha\sigma_\alpha})_{ij}|i\rangle\langle j|\exp[i(\varepsilon_i-\varepsilon_j+\varepsilon_{\alpha k\sigma_\alpha})t/\hbar] + \mathrm{H.c.}, \tag{12}$$

where $(d_{\alpha\sigma_\alpha})_{ij}=\langle i|d_{\alpha\sigma_\alpha}|j\rangle$ and $(d_{\alpha\sigma_\alpha}^{\dagger})_{ij}=\langle i|d_{\alpha\sigma_\alpha}^{\dagger}|j\rangle$ are the electron annihilation and creation operators in the spin-quantization axis of lead α expressed in the basis of the energy eigenstates of the quantum dot system. To simplify Eq. (11), standard approximations are invoked. (i) The first one is the secular approximation: fast oscillations in time average out in the stationary limit we are interested in and thus can be neglected. Together with the relation $\mathrm{Tr}_{\mathrm{leads}}(\hat{\rho}_s\hat{\rho}_d c_{\alpha k\sigma_\alpha}^{\dagger}c_{\alpha' k'\sigma_\alpha})=\delta_{kk'}\delta_{\alpha\alpha'}\delta_{\sigma\sigma'}f_\alpha(\varepsilon_{\alpha k\sigma})$, where $f_\alpha(\varepsilon_{\alpha k\sigma})$ is the Fermi function, and the cyclic properties of the trace we get

$$\begin{aligned}
\dot{\hat{\rho}}_{\odot}^{I}(t) = -\frac{1}{\hbar^2}\int_0^{\infty} dt'' \sum_{\alpha k\sigma_\alpha}|t_\alpha|^2\Bigg\{ & \sum_{ilm} f_\alpha(\varepsilon_{\alpha k\sigma_\alpha})(d_{\alpha\sigma_\alpha})_{il}(d_{\alpha\sigma_\alpha}^{\dagger})_{lm}|i\rangle\langle m|\hat{\rho}_{\odot}^{I}(t)\exp[i(\varepsilon_m-\varepsilon_l+\varepsilon_{\alpha k\sigma_\alpha})t''/\hbar] \\
& + \sum_{ilm}(1-f_\alpha(\varepsilon_{\alpha k\sigma_\alpha}))(d_{\alpha\sigma_\alpha}^{\dagger})_{il}(d_{\alpha\sigma_\alpha})_{lm}|i\rangle\langle m|\hat{\rho}_{\odot}^{I}(t)\exp[-i(\varepsilon_l-\varepsilon_m+\varepsilon_{\alpha k\sigma_\alpha})t''/\hbar] \\
& + \sum_{ilm} f_\alpha(\varepsilon_{\alpha k\sigma_\alpha})\hat{\rho}_{\odot}^{I}(t)(d_{\alpha\sigma_\alpha})_{il}(d_{\alpha\sigma_\alpha}^{\dagger})_{lm}|i\rangle\langle m|\exp[-i(\varepsilon_i-\varepsilon_l+\varepsilon_{\alpha k\sigma_\alpha})t''/\hbar] \\
& + \sum_{ilm}(1-f_\alpha(\varepsilon_{\alpha k\sigma_\alpha}))\hat{\rho}_{\odot}^{I}(t)(d_{\alpha\sigma_\alpha}^{\dagger})_{il}(d_{\alpha\sigma_\alpha})_{lm}|i\rangle\langle m|\exp[+i(\varepsilon_l-\varepsilon_i+\varepsilon_{\alpha k\sigma_\alpha})t''/\hbar] \\
& - \sum_{iljm}(1-f_\alpha(\varepsilon_{\alpha k\sigma_\alpha}))(d_{\alpha\sigma_\alpha})_{ij}\hat{\rho}_{\odot}^{I}(t)_{jl}(d_{\alpha\sigma_\alpha}^{\dagger})_{lm}|i\rangle\langle m|\exp[+i(\varepsilon_m-\varepsilon_l+\varepsilon_{\alpha k\sigma_\alpha})t''/\hbar] \\
& - \sum_{iljm} f_\alpha(\varepsilon_{\alpha k\sigma_\alpha})(d_{\alpha\sigma_\alpha}^{\dagger})_{ij}\hat{\rho}_{\odot}^{I}(t)_{jl}(d_{\alpha\sigma_\alpha})_{lm}|i\rangle\langle m|\exp[-i(\varepsilon_l-\varepsilon_m+\varepsilon_{\alpha k\sigma_\alpha})t''/\hbar] \\
& - \sum_{iljm}(1-f_\alpha(\varepsilon_{\alpha k\sigma_\alpha}))(d_{\alpha\sigma_\alpha})_{ij}\hat{\rho}_{\odot}^{I}(t)_{jl}(d_{\alpha\sigma_\alpha}^{\dagger})_{lm}|i\rangle\langle m|\exp[-i(\varepsilon_i-\varepsilon_j+\varepsilon_{\alpha k\sigma_\alpha})t''/\hbar] \\
& - \sum_{iljm} f_\alpha(\varepsilon_{\alpha k\sigma_\alpha})(d_{\alpha\sigma_\alpha}^{\dagger})_{ij}\hat{\rho}_{\odot}^{I}(t)_{jl}(d_{\alpha\sigma_\alpha})_{lm}|i\rangle\langle m|\exp[+i(\varepsilon_j-\varepsilon_i+\varepsilon_{\alpha k\sigma_\alpha})t''/\hbar]\Bigg\}.
\end{aligned} \tag{13}$$

(ii) For the second approximation, we notice that we wish to evaluate single components $\langle n|\hat{\rho}^I_\odot|m\rangle$ of the RDM in the system's energy eigenbasis. Therefore, we assume that the DD is in a pure charge state with a certain number of electrons N and energy E_N. In fact, in the weak-tunneling limit, the time between two tunneling events is longer than the time where relaxation processes happen. That is, we can neglect matrix elements between states with different number of electrons and only regard elements of $\hat{\rho}^I_\odot$, which connect states with same electron number N and same energy E_N. So, we can divide $\hat{\rho}^I_\odot$ into submatrices labeled with N and E_N and find

$$\dot{\rho}^{E_N N}_{nm}(t) = -\frac{\pi}{\hbar}\sum_{\alpha\sigma_\alpha}\{\sum_{l,l'\in|N-1\rangle}, \sum_{j\in|E_N N\rangle}, \sum_{h,h'\in|N+1\rangle}\}|t_\alpha|^2\Bigg\{$$

$$\text{(a)} + \left[f_\alpha(\varepsilon_h-\varepsilon_j)D_{\alpha\sigma_\alpha}(\varepsilon_h-\varepsilon_j) + \frac{i}{\pi}\int d\varepsilon_k \frac{f_\alpha(\varepsilon_k)D_{\alpha\sigma_\alpha}(\varepsilon_k)}{\varepsilon_k-\varepsilon_h+\varepsilon_j}\right](d_{\alpha\sigma_\alpha})_{nh}(d^\dagger_{\alpha\sigma_\alpha})_{hj}\rho^{E_N N}_{jm}(t)$$

$$\text{(b)} + \left[(1-f_\alpha(\varepsilon_j-\varepsilon_l))D_{\alpha\sigma_\alpha}(\varepsilon_j-\varepsilon_l) - \frac{i}{\pi}\int d\varepsilon_k \frac{(1-f_\alpha(\varepsilon_k))D_{\alpha\sigma_\alpha}(\varepsilon_k)}{\varepsilon_k-\varepsilon_j+\varepsilon_l}\right](d^\dagger_{\alpha\sigma_\alpha})_{nl}(d_{\alpha\sigma_\alpha})_{lj}\rho^{E_N N}_{jm}(t)$$

$$\text{(c)} + \left[f_\alpha(\varepsilon_h-\varepsilon_j)D_{\alpha\sigma_\alpha}(\varepsilon_h-\varepsilon_j) - \frac{i}{\pi}\int d\varepsilon_k \frac{f_\alpha(\varepsilon_k)D_{\alpha\sigma_\alpha}(\varepsilon_k)}{\varepsilon_k-\varepsilon_h+\varepsilon_j}\right]\rho^{E_N N}_{nj}(t)(d_{\alpha\sigma_\alpha})_{jh}(d^\dagger_{\alpha\sigma_\alpha})_{hm}$$

$$\text{(d)} + \left[(1-f_\alpha(\varepsilon_j-\varepsilon_l))D_{\alpha\sigma_\alpha}(\varepsilon_j-\varepsilon_l) + \frac{i}{\pi}\int d\varepsilon_k \frac{(1-f_\alpha(\varepsilon_k))D_{\alpha\sigma_\alpha}(\varepsilon_k)}{\varepsilon_k-\varepsilon_j+\varepsilon_l}\right]\rho^{E_N N}_{nj}(t)(d^\dagger_{\alpha\sigma_\alpha})_{jl}(d_{\alpha\sigma_\alpha})_{lm}$$

$$\text{(e)} - 2(1-f_\alpha(\varepsilon_h-\varepsilon_j))D_{\alpha\sigma_\alpha}(\varepsilon_h-\varepsilon_j)(d_{\alpha\sigma_\alpha})_{nh'}(d^\dagger_{\alpha\sigma_\alpha})_{hm}\rho^{E_{h'}N+1}_{h'h}(t)$$

$$\text{(f)} - 2f_\alpha(\varepsilon_j-\varepsilon_l)D_{\alpha\sigma_\alpha}(\varepsilon_j-\varepsilon_l)(d^\dagger_{\alpha\sigma_\alpha})_{nl'}(d_{\alpha\sigma_\alpha})_{lm}\rho^{E_{l'}N-1}_{l'l}(t)\Bigg\}. \tag{14}$$

In Eq. (14), we used the notation $\rho^{E_N N}_{nm} := \langle n|\hat{\rho}^{I,E_N N}_\odot|m\rangle$.

By convention, $\{\Sigma_{l,l'}, \Sigma_j, \Sigma_{h,h'}\}$ means that in each line [(a)–(f)], we sum over the indices occurring in this line only. Notice that the sum over j is restricted to states of energy $E_j=E_N=E_n=E_m$. For the states with $N\pm1$ electrons, we have to sum over all energies; therefore, we indexed the density matrix with $E_h=E_{h'}$ in line (e) and $E_l=E_{l'}$ in line (f). Further, we replaced the sum over k by an integral, $\Sigma_k \to \int d\varepsilon_{\alpha k\sigma_\alpha} D_{\alpha\sigma_\alpha}(\varepsilon_{\alpha k\sigma_\alpha})$, where $D_{\alpha\sigma_\alpha}(\varepsilon_{\alpha k\sigma_\alpha})$ denotes the density of states in lead α for the spin direction σ_α, and applied the following useful formula:

$$\int d\varepsilon_{\alpha k\sigma_\alpha} G(\varepsilon_{\alpha k\sigma_\alpha})\int_0^t dt'' e^{\pm(i/\hbar)(\varepsilon_{\alpha k\sigma_\alpha}-E)t''}$$

$$= \pi\hbar G(E) \pm i\hbar \int' d\varepsilon_{\alpha k\sigma_\alpha}\frac{G(\varepsilon_{\alpha k\sigma_\alpha})}{(\varepsilon_{\alpha k\sigma_\alpha}-E)}, \tag{15}$$

where the prime at the integral denotes Cauchy's principal-part integration. In our case, $G(\varepsilon_{\alpha k\sigma_\alpha}) = D_{\alpha\sigma_\alpha}(\varepsilon_{\alpha k\sigma_\alpha}) f^\pm_\alpha(\varepsilon_{\alpha k\sigma_\alpha})$ with $f^+_\alpha = f_\alpha$ and $f^-_\alpha = 1-f_\alpha$. In order to simplify the notations, we replaced $\varepsilon_{\alpha k\sigma_\alpha}$ by ε_k in Eq. (14).

B. Transformation into the spin-coordinate system of the double dot

In Sec. II, we introduced the transformation rules for changing from the lead spin coordinates σ_α into the DD spin coordinates $\sigma_\odot$. These rules give

$$\begin{pmatrix} d^\dagger_{\alpha\uparrow_\alpha} \\ d^\dagger_{\alpha\downarrow_\alpha}\end{pmatrix} = \frac{1}{\sqrt{2}}\begin{pmatrix} +e^{-i\Theta_\alpha/2} & +e^{+i\Theta_\alpha/2} \\ -e^{-i\Theta_\alpha/2} & +e^{+i\Theta_\alpha/2}\end{pmatrix}\begin{pmatrix} d^\dagger_{\alpha\uparrow_\odot} \\ d^\dagger_{\alpha\downarrow_\odot}\end{pmatrix}, \tag{16}$$

with $\Theta_s := -\frac{\Theta}{2}$, $\Theta_d := +\frac{\Theta}{2}$.

Thus, Eq. (14) can be easily expressed in the DD spin quantization axis. For example, it holds

$$\sum_{\sigma_\alpha} D_{\alpha\sigma_\alpha} d^\dagger_{\sigma_\alpha} d_{\sigma_\alpha} = \frac{1}{2}(D_{\alpha\uparrow_\alpha}+D_{\alpha\downarrow_\alpha})\sum_{\sigma_\odot}\Phi_{\alpha\sigma_\odot\sigma_\odot} d^\dagger_{\alpha\sigma_\odot} d_{\alpha\sigma_\odot}$$

$$+\frac{1}{2}(D_{\alpha\uparrow_\alpha}-D_{\alpha\downarrow_\alpha})\sum_{\sigma_\odot}\Phi^*_{\alpha\sigma_\odot-\sigma_\odot} d^\dagger_{\alpha\sigma_\odot} d_{\alpha-\sigma_\odot}, \tag{17}$$

where we introduced

$$\Phi_{\alpha\sigma_\odot\sigma'_\odot} := \begin{cases} 1 & \sigma_\odot = \sigma'_\odot \\ e^{i\Theta_\alpha} & \sigma_\odot = \uparrow \quad \sigma'_\odot = \downarrow \\ e^{-i\Theta_\alpha} & \sigma_\odot = \downarrow \quad \sigma'_\odot = \uparrow . \end{cases}$$

For later convenience, we also define

$$F^{\pm}_{\alpha\sigma_\odot\sigma'_\odot} := \frac{1}{2}\begin{cases} D_{\alpha+_\alpha} f^{\pm}_\alpha(E) + D_{\alpha-_\alpha} f^{\pm}_\alpha(E) & \sigma_\odot = \sigma'_\odot \\ D_{\alpha+_\alpha} f^{\pm}_\alpha(E) - D_{\alpha-_\alpha} f^{\pm}_\alpha(E) & \sigma_\odot \neq \sigma'_\odot, \end{cases}$$

and its related principal-part integral,

$$P^{\pm}_{\alpha\sigma_\odot\sigma'_\odot}(E) := \int' d\varepsilon F^{\pm}_{\alpha\sigma_\odot\sigma'_\odot}(\varepsilon)(\varepsilon - E)^{-1}.$$

C. Contribution from the reflection Hamiltonian

In order to give the full expression for the GME in the system's eigenbasis, we need to compute the contribution from the reflection Hamiltonian in Eq. (11). In analogy to what we did to evaluate the contribution from the tunneling Hamiltonian, we must first transform $\hat{H}_R$ into the interaction picture and then perform the secular approximation to get rid of the time dependence. To start, we express $\hat{H}_R$ in the DD spin quantization basis,

$$\hat{H}^I_R = -\Delta_R \sum_\alpha \sum_{\substack{j\in|N\rangle \\ l\in|N-1\rangle}} \sum_{\sigma_\odot\neq\sigma'_\odot} \Phi^*_{\alpha\sigma_\odot\sigma'_\odot} d^\dagger_{\sigma_\odot jl} d_{\sigma'_\odot lj} |j\rangle\langle j|. \tag{18}$$

The commutator is easily evaluated to be

$$\begin{aligned} &-\frac{i}{\hbar}\mathrm{Tr}_{\mathrm{leads}}[\hat{H}^I_R, \hat{\rho}^I_\odot(t)\rho_s\rho_d] \\ &= -\frac{i}{\hbar}\sum_\alpha \Delta_R \sum_{j\in|N\rangle}\sum_{l\in|N-1\rangle}\sum_{\sigma_\odot\neq\sigma'_\odot} \Phi^*_{\alpha\sigma_\odot\sigma'_\odot}[d^\dagger_{\sigma_\odot jl} d_{\sigma'_\odot lj}|j\rangle \\ &\times\langle j|\hat{\rho}^I_\odot(t) - \hat{\rho}^I_\odot(t) d^\dagger_{\sigma_\odot jl} d_{\sigma'_\odot lj}|j\rangle\langle j|]. \end{aligned} \tag{19}$$

In order to include this commutator in the master equation [Eq. (14)], let us introduce the following abbreviation:

$$R_{\alpha\sigma_\odot\sigma'_\odot} = \frac{1}{|t^\alpha|^2}\Delta_R(\delta_{\sigma_\odot\uparrow}\delta_{\sigma'_\odot\downarrow} + \delta_{\sigma_\odot\downarrow}\delta_{\sigma'_\odot\uparrow}). \tag{20}$$

Now, we can add $R_{\alpha\sigma_\odot\sigma'_\odot}$ in Eq. (14) in lines (b) and (d) to find the final form of the complete master equation in the DD spin-coordinate system. It reads

$$\begin{aligned} \dot{\rho}^{E_N N}_{nm}(t) = &-\frac{\pi}{\hbar}\sum_{\alpha=s,d}|t^\alpha|^2 \sum_{\sigma_\odot,\sigma'_\odot}\Bigg\{\sum_{l,l'\in|N-1\rangle},\sum_{j\in|E_N N\rangle},\sum_{h,h'\in|N+1\rangle}\Bigg\}\Bigg\{ \\ &\text{(a)} + \Phi_{\alpha\sigma_\odot\sigma'_\odot}\left[F^+_{\alpha\sigma_\odot\sigma'_\odot}(\varepsilon_h-\varepsilon_j) + \frac{i}{\pi}P^+_{\alpha\sigma_\odot\sigma'_\odot}(\varepsilon_h-\varepsilon_j)\right](d_{\alpha\sigma_\odot})_{nh}(d^\dagger_{\alpha\sigma'_\odot})_{hj}\rho^{E_N N}_{jm}(t) \\ &\text{(b)} + \Phi^*_{\alpha\sigma_\odot\sigma'_\odot}\left[F^-_{\alpha\sigma_\odot\sigma'_\odot}(\varepsilon_j-\varepsilon_l) - \frac{i}{\pi}[P^-_{\alpha\sigma_\odot\sigma'_\odot}(\varepsilon_j-\varepsilon_l) + R_{\alpha\sigma_\odot\sigma'_\odot}]\right](d^\dagger_{\alpha\sigma_\odot})_{nl}(d_{\alpha\sigma'_\odot})_{lj}\rho^{E_N N}_{jm}(t) \\ &\text{(c)} + \Phi_{\alpha\sigma_\odot\sigma'_\odot}\left[F^+_{\alpha\sigma_\odot\sigma'_\odot}(\varepsilon_h-\varepsilon_j) - \frac{i}{\pi}P^+_{\alpha\sigma_\odot\sigma'_\odot}(\varepsilon_h-\varepsilon_j)\right]\rho^{E_N N}_{nj}(t)(d_{\alpha\sigma_\odot})_{jh}(d^\dagger_{\alpha\sigma'_\odot})_{hm} \\ &\text{(d)} + \Phi^*_{\alpha\sigma_\odot\sigma'_\odot}\left[F^-_{\alpha\sigma_\odot\sigma'_\odot}(\varepsilon_j-\varepsilon_l) + \frac{i}{\pi}[P^-_{\alpha\sigma_\odot\sigma'_\odot}(\varepsilon_j-\varepsilon_l) + R_{\alpha\sigma_\odot\sigma'_\odot}]\right]\rho^{E_N N}_{nj}(t)(d^\dagger_{\alpha\sigma_\odot})_{jl}(d_{\alpha\sigma'_\odot})_{lm} \\ &\text{(e)} - 2\Phi_{\alpha\sigma_\odot\sigma'_\odot}F^-_{\alpha\sigma_\odot\sigma'_\odot}(\varepsilon_h-\varepsilon_j)(d_{\alpha\sigma_\odot})_{nh'}\rho^{E_h N+1}_{h'h}(t)(d^\dagger_{\alpha\sigma'_\odot})_{hm} \\ &\text{(f)} - 2\Phi^*_{\alpha\sigma_\odot\sigma'_\odot}F^+_{\alpha\sigma_\odot\sigma'_\odot}(\varepsilon_j-\varepsilon_l)(d^\dagger_{\alpha\sigma_\odot})_{nl'}\rho^{E_l N-1}_{l'l}(t)(d_{\alpha\sigma'_\odot})_{lm}. \end{aligned} \tag{21}$$

D. Current formula

We now observe that Eq. (21) can be recast in the following Bloch–Redfield form:

$$\begin{aligned} \dot{\rho}^{E_N N}_{nm}(t) = &-\sum_{jj'} R^{NN}_{nmjj'}\rho^{E_N N}_{jj'}(t) + \sum_{hh'} R^{NN+1}_{nmhh'}\rho^{E_h N+1}_{hh'}(t) \\ &+ \sum_{ll'} R^{NN-1}_{nmll'}\rho^{E_l N-1}_{ll'}(t), \end{aligned} \tag{22}$$

where the sums in Eq. (22) run over states with fixed particle number: $j,j' \in \{|E_N N\rangle\}$, $h,h' \in \{|N+1\rangle\}$, $l,l' \in \{|N-1\rangle\}$. The Redfield tensors are given by ($\alpha=s,d$) (Ref. 38)

$$R^{NN}_{nmjj'} = \sum_{\alpha} \sum_{l(\text{or } h)} [\delta_{mj'}(\Gamma^{(+)NN+1}_{\alpha,nhhj} + \Gamma^{(+)NN-1}_{\alpha,nllj}) + \delta_{nj}(\Gamma^{(-)NN+1}_{\alpha,j'hhm} + \Gamma^{(-)NN-1}_{\alpha,j'llm})], \tag{23}$$

$$R^{NN\pm1}_{nmkk'} = \sum_{\alpha} (\Gamma^{(+)NN\mp1}_{\alpha,k'mnk} + \Gamma^{(-)NN\mp1}_{\alpha,k'mnk}), \tag{24}$$

where the quantities $\Gamma^{(\pm)NN\pm1}_{\alpha,njjk}$ can be easily read out from Eq. (21). They are

$$\Gamma^{(\pm)NN+1}_{\alpha,nhh'k} = \sum_{\sigma_\odot\sigma'_\odot} \left\{ \frac{\pi}{\hbar}\Phi_{\alpha\sigma_\odot\sigma'_\odot}|t_\alpha|^2 \left[F^{+}_{\alpha\sigma_\odot\sigma'_\odot}(\varepsilon_h - \varepsilon_k) \pm \frac{i}{\pi} P^{+}_{\alpha\sigma_\odot\sigma'_\odot}(\varepsilon_h - \varepsilon_k) \right] (d_{\alpha\sigma_\odot})_{nh} (d^{\dagger}_{\alpha\sigma'_\odot})_{h'k} \right\},$$

$$\Gamma^{(\pm)NN-1}_{\alpha,nll'k} = \sum_{\sigma_\odot\sigma'_\odot} \left\{ \frac{\pi}{\hbar}\Phi^{*}_{\alpha\sigma_\odot\sigma'_\odot}|t_\alpha|^2 \left[F^{-}_{\alpha\sigma_\odot\sigma'_\odot}(\varepsilon_k - \varepsilon_l) \mp \frac{i}{\pi}(P^{-}_{\alpha\sigma_\odot\sigma'_\odot}(\varepsilon_k - \varepsilon_l) + R_{\alpha\sigma_\odot\sigma'_\odot}) \right] \times (d^{\dagger}_{\alpha\sigma_\odot})_{nl} (d_{\alpha\sigma'_\odot})_{l'k} \right\}.$$

With the stationary density matrix $\hat{\rho}^{I}_{\odot st}$ being known, the current (through lead $\alpha=s/d=\pm$) follows from

$$I = 2\alpha e\, \mathrm{Re} \sum_{N} \sum_{n,n',j} (\Gamma^{(+)NN+1}_{\alpha,njjn'} - \Gamma^{(+)NN-1}_{\alpha,njjn'}) \rho^{E_n N}_{n'n,st}. \tag{25}$$

We numerically solve Eq. (22) and use the result to evaluate the current flowing through the DD, as will be Secs. V–VII. At low-bias voltages, however, we can make some further approximations to arrive at an analytical formula for the static dc.

IV. LOW-BIAS REGIME

A. General considerations

A low-bias voltage ensures that merely one channel is involved with respect to transport properties. Here, we focus on gate voltages that align charge states N and $N+1$. Moreover, we can focus on density matrix elements that involve the energy ground states $E^{(0)}_N$ and $E^{(0)}_{N+1}$ only. In the following, we shall use the following compact notations:

$$\hat{\rho}^{I,E^{(0)}_N N}_{\odot} := \hat{\rho}^{(N)}_{\odot}, \quad \langle n|\hat{\rho}^{(N)}_{\odot}|m\rangle = \rho^{(N)}_{nm}. \tag{26}$$

Evaluation of the current requires the knowledge of $\hat{\rho}^{(N)}_{\odot}$ and $\hat{\rho}^{(N+1)}_{\odot}$, i.e., a solution of the set of coupled equations that are obtained from Eq. (21) or, equivalently, from Eq. (22). In the low-bias regime, this task is simplified since (i) terms which try to couple states with particle numbers unlike N and $N+1$ can be neglected; (ii) we can reduce the sums over h,h' in the equation for $\dot{\hat{\rho}}^{(N)}_{\odot}$ and over l,l' in the equation for $\dot{\hat{\rho}}^{(N+1)}_{\odot}$ to energy-ground states $E^{(0)}_N$ and $E^{(0)}_{N+1}$ because all the other transitions are exponentially suppressed by the Fermi function. Notice, however, that these two approximations are not appropriate for the principal-part terms since they are not energy conserving. The resulting equations for $\hat{\rho}^{(N)}_{\odot}$ and $\hat{\rho}^{(N+1)}_{\odot}$ [Eqs. (B1) and (B2), respectively] can be found in Appendix B. In the following, we shall apply those equations to derive an analytical expression for the conductance in the four different resonant charge state regimes possible in a DD system, i.e.,

$$N=0 \leftrightarrow N=1, \quad N=1 \leftrightarrow N=2,$$

$$N=2 \leftrightarrow N=3, \quad N=3 \leftrightarrow N=4. \tag{27}$$

In all of the four cases, we get a system of five coupled equations involving diagonal and off-diagonal elements of the RDM. The matrix elements of the dot operators between the involved states entering these equations are given in Appendix A. Before going into the details of these equations, it is instructive to analyze the structure and the physical significance of the involved RDM elements.

B. Elements of the reduced density matrix

N=0. In the case of an empty system, we have only one density matrix element in the corresponding block with fixed particle number $N=0$, i.e.,

$$\rho^{(0)}_{00}(t) = :W_0, \tag{28}$$

describing the probability to find an empty double-dot system.

N=1. In this case, we have four eigenstates for the system, where the two *even* ones build the degenerate ground state and the two *odd* ones are excited states (see Table I). In the low-bias regime, we only need to take into account transitions between ground states. Therefore, we have to deal with the 2×2 matrix,

$$\begin{pmatrix} \rho^{(1)}_{1e\uparrow 1e\uparrow} & \rho^{(1)}_{1e\uparrow 1e\downarrow} \\ \rho^{(1)}_{1e\downarrow 1e\uparrow} & \rho^{(1)}_{1e\downarrow 1e\downarrow} \end{pmatrix} = : \begin{pmatrix} W_{1\uparrow} & w_1 e^{i\alpha_1} \\ w_1 e^{-i\alpha_1} & W_{1\downarrow} \end{pmatrix}. \tag{29}$$

The total occupation probability for one electron is

$$W_1 := W_{1\uparrow} + W_{1\downarrow}. \tag{30}$$

The meaning of the off-diagonal elements, the so-called coherences, becomes clear if we regard the average spin in the system,

$$S^{(1)}_i = \frac{1}{2}\mathrm{Tr}[\sigma^{Pauli}_i \hat{\rho}^{(1)}_{\odot}(t)], \tag{31}$$

where $i=x,y,z$ and $\sigma^{\mathrm{Pauli}}_i$ are the Pauli spin matrices. This yields

$$S^{(1)}_x = w_1 \cos\alpha_1, \quad S^{(1)}_y = -w_1 \sin\alpha_1, \tag{32}$$

$$S^{(1)}_z = \frac{1}{2}(W_{1\uparrow} - W_{1\downarrow}). \tag{33}$$

N=2. For the case $N=2$, we actually have six different eigenstates, but only one of them, $|2\rangle$, is a ground state (with spin $S=0$), see Table I. Only this ground state must be considered in the low-bias regime, yielding

$$\rho_{22}^{(2)}(t) =: W_2. \tag{34}$$

This element describes the probability to find a dot with two electrons.

N=3. In this case, we have again four eigenstates for the system, whereas the two *odd* ones build the degenerate ground state and the two *even* ones are excited. In the low-bias regime, we only need to deal with the 2×2 matrix involving the three-particle ground states,

$$\begin{pmatrix} \rho_{3o\uparrow 3o\uparrow}^{(3)} & \rho_{3o\uparrow 3o\downarrow}^{(3)} \\ \rho_{3o\downarrow 3o\uparrow}^{(3)} & \rho_{3o\downarrow 3o\downarrow}^{(3)} \end{pmatrix} =: \begin{pmatrix} W_{3\uparrow} & w_3 e^{i\alpha_3} \\ w_3 e^{-i\alpha_3} & W_{3\downarrow} \end{pmatrix}. \tag{35}$$

The total occupation probability for three electrons is

$$W_3 := W_{3\uparrow} + W_{3\downarrow}.$$

As for the case $N=1$, the off-diagonal elements yield information on the average spin $S_i^{(3)} = \frac{1}{2}\mathrm{Tr}[\sigma_i^{\mathrm{Pauli}} \hat{\rho}_{\odot}^{(3)}(t)]$ in the system through the following relations:

$$S_x^{(3)} = w_3 \cos\alpha_3, \quad S_y^{(3)} = -w_3 \sin\alpha_3, \tag{36}$$

$$S_z^{(3)} = \frac{1}{2}(W_{3\uparrow} - W_{3\downarrow}). \tag{37}$$

N=4. Finally, if the double quantum dot is completely filled with four electrons, we only have one nondegenerate state. Correspondingly, there is only one relevant RDM matrix element,

$$\rho_{44}^{(4)}(t) =: W_4, \tag{38}$$

describing the probability to find four electrons in the system. The total spin is $S=0$.

Hence, we see that in all of the four cases [Eq. (27)], we get a system of five equations with the five independent physical quantities W_N, W_{N+1} and $S_x^{(i)}, S_y^{(i)}, S_z^{(i)}$ with $i=1$ or 3.

C. Conductance formula

We shall exemplarily present results for the resonant transition $N=1 \leftrightarrow N=2$. For the other transitions, similar considerations apply. The quantities of interest are $W_1, W_2, S_x^{(1)}, S_y^{(1)}, S_z^{(1)}$, which are related through Eqs. (32) and (36) to the density matrix elements of $\hat{\rho}_{\odot}^{(1)}$. From Eqs. (B1) and (B2) and Table III, and with $W_1 = 1 - W_2$ we finally obtain the following:

$$\dot{W}_1 = -\frac{\pi}{\hbar}\sum_{\alpha=s,d} |t_\alpha|^2 k_+^2 [2F_{\alpha\downarrow\downarrow}^{+}(\mu_2) W_1 - 4F_{\alpha\downarrow\downarrow}^{-}(\mu_2) W_2 - 4F_{\alpha\uparrow\downarrow}^{+}(\mu_2) \vec{S}^{(1)} \cdot \vec{m}_\alpha], \tag{39}$$

$$\dot{\vec{S}}^{(1)} = -\frac{\pi}{\hbar}\sum_{\alpha=s,d} |t_\alpha|^2 k_+^2 \Bigg\{ 2F_{\alpha\uparrow\uparrow}^{+}(\mu_2)\vec{S}^{(1)} - [F_{\alpha\uparrow\downarrow}^{+}(\mu_2) W_1 - 2F_{\alpha\uparrow\downarrow}^{-}(\mu_2) W_2]\vec{m}_\alpha + \frac{2}{\pi k_+^2}\mathcal{P}_\alpha(\mu_1, \{E_2\} - E_1^{(0)})\vec{m}_\alpha \times \vec{S}^{(1)} \Bigg\}. \tag{40}$$

We have introduced the notation $4k_\pm^2 := (\alpha_0 \pm \beta_0)^2$. All of the nonvanishing principle-value factors $P_{\alpha\uparrow\downarrow}^{\pm}$ and the reflection parameter $R_{\alpha\uparrow\downarrow}$ have been merged to the following compact form:

$$\mathcal{P}_\alpha(\mu_1, \{E_2\} - E_1^{(0)}) := -\frac{1}{2}[P_{\alpha\downarrow\uparrow}^{-}(\mu_1) + R_{\alpha\downarrow\uparrow}] - k_+^2 P_{\alpha\uparrow\downarrow}^{+}(\mu_2) + \frac{1}{4}P_{\alpha\uparrow\downarrow}^{+}(\varepsilon_{2'} - \varepsilon_{1e}) - \frac{1}{4}P_{\alpha\uparrow\downarrow}^{+}(\varepsilon_{2''} - \varepsilon_{1e}) - k_-^2 P_{\alpha\uparrow\downarrow}^{+}(\varepsilon_{2'''} - \varepsilon_{1e}), \tag{41}$$

where we introduced the chemical potential $\mu_{N+1} = E_{N+1}^{(0)} - E_N^{(0)}$ and $\{E_2\}$ denotes the four different two-particle energies. We notice that the set of coupled equation [Eq. (39) and (40)] for the evolution of the populations and of the spin accumulation has a similar structure to that reported in Refs. 28, 30, and 38 for a single-level quantum dot, a metallic island, and a single-walled carbon nanotube, respectively. Some prefactors and the argument of the principal-part terms, however, are DD specific. In particular, as in Refs. 28 and 30, we clearly identify a spin precession term originating from the combined action of the reflection at the interface and the interaction. The associated effective exchange splitting is γB_1, where $\gamma = -g\mu_B$ is the gyromagnetic ratio and

$$\vec{B}_1 := \frac{2}{\gamma}\sum_\alpha |t_\alpha|^2 \mathcal{P}_\alpha \vec{m}_\alpha \tag{42}$$

is the corresponding effective exchange field. We now focus on the stationary limit. In the absence of the precession term, the spin accumulation has only a $S_y^{(1)}$ component since, due to our particular choice of the spin quantization axis, $S_x^{(1)} = 0$ holds. The exchange field tilts the accumulated spin out of the magnetizations' plane and gives rise to a nonzero $S_z^{(1)}$ component *proportional* to B_1 and $S_y^{(1)}$.

To get further insight in the spin dynamics, we observe that since we are looking at the low-bias regime, we can linearize the Fermi function f_α in the bias voltage, i.e.,

TABLE II. Matrix elements for the $N=0 \leftrightarrow N=1$ transition induced by operators $d_{\alpha\uparrow}$ and $d_{\alpha\downarrow}$, $\alpha = 1, 2$.

	$0 \leftrightarrow 1$			
	$\|1e\uparrow\rangle$	$\|1e\downarrow\rangle$	$\|1o\uparrow\rangle$	$\|1o\downarrow\rangle$
$d_{1\uparrow}:\langle 0\|$	$\frac{1}{\sqrt{2}}$	0	$\frac{1}{\sqrt{2}}$	0
$d_{1\downarrow}:\langle 0\|$	0	$\frac{1}{\sqrt{2}}$	0	$\frac{1}{\sqrt{2}}$
$d_{2\uparrow}:\langle 0\|$	$\frac{1}{\sqrt{2}}$	0	$-\frac{1}{\sqrt{2}}$	0
$d_{2\downarrow}:\langle 0\|$	0	$\frac{1}{\sqrt{2}}$	0	$-\frac{1}{\sqrt{2}}$

$$f_\alpha(\xi) = (1 + e^{\beta(\xi + eV_\alpha)})^{-1} \approx f(\xi)(1 - f(-\xi)e\beta V_\alpha). \quad (43)$$

By introducing the polarization of the contacts,

$$p_\alpha(\xi) := \frac{D_{\alpha\uparrow_\alpha}(\xi) - D_{\alpha\downarrow_\alpha}(\xi)}{D_{\alpha\uparrow_\alpha}(\xi) + D_{\alpha\downarrow_\alpha}(\xi)},$$

we can express the $F^{\pm}_{\alpha\sigma_\odot\sigma'_\odot}$ factors as

$$F^{\pm}_{\alpha\uparrow\uparrow}(\xi) \approx \frac{1}{2} D_\alpha(\xi) f(\pm\xi)(1 \mp f(\mp\xi)e\beta V_\alpha),$$

$$F^{\pm}_{\alpha\uparrow\downarrow}(\xi) = p_\alpha(\xi) F^{\pm}_{\alpha\uparrow\uparrow}(\xi),$$

where $D_\alpha = D_{\alpha\uparrow_\alpha} + D_{\alpha\downarrow_\alpha}$. It is also sufficient for our calculations to regard the density of states as a constant quantity, $D_\alpha(\xi) = D_\alpha$. Consequently, the polarization is also constant, $p_\alpha(\xi) = p_\alpha$. Finally, we focus in the following on the symmetric case where both leads have the same properties, which, in particular, means that tunneling elements, polarizations, density of states, and reflection amplitude are equal,

$$t_1 = t_2 =: t, \quad p_1 = p_2 =: p,$$

$$D_1 = D_2 =: D, \quad R_{1\sigma_\odot - \sigma_\odot} = R_{2\sigma_\odot - \sigma_\odot} =: R. \quad (44)$$

Upon introducing the linewidth $\Gamma = \frac{2\pi}{\hbar} D|t|^2$, the conductance $G_{12} = I_{12}/V_{\text{bias}}$ for the resonant regime $N=1 \leftrightarrow N=2$ reads

$$G_{12}(\Theta) = \frac{\Gamma}{2} e^2 \beta k_+^2 \frac{f(\mu_2) f(-\mu_2)}{f(-\mu_2) + 1} \times \left\{ 1 - \frac{p^2 \sin^2\left(\frac{\Theta}{2}\right)}{1 + [B_1/f(\mu_2) 2\Gamma k_+^2]^2 \cos^2\left(\frac{\Theta}{2}\right)} \right\}. \quad (45)$$

Similarly, we find for an arbitrary resonance ($i=0,1,2,3$),

$$G_{ii+1}(\Theta) = \frac{\Gamma}{2} e^2 \beta |\langle i+1|d^\dagger|i\rangle|^2 \frac{f(\mu_{i+1}) f(-\mu_{i+1})}{1 + f((-1)^i \mu_{i+1})} \left\{ 1 - \frac{p^2 \sin^2\left(\frac{\Theta}{2}\right)}{1 + [B_{i+1}/f((-1)^{i+1}\mu_{i+1}) 2\Gamma |\langle i+1|d^\dagger|i\rangle|^2]^2 \cos^2\left(\frac{\Theta}{2}\right)} \right\}, \quad (46)$$

where $|\langle i+1|d^\dagger|i\rangle|$ is a shortcut notation for the nonvanishing matrix elements $|\langle E^{(0)}_{i+1} i+1|d^\dagger_{\alpha\odot}|E^{(0)}_i i\rangle|$ calculated in Tables II–V. It holds $|\langle 1|d^\dagger_{\alpha\odot}|0\rangle| = |\langle 4|d^\dagger_{\alpha\odot}|3\rangle| = 1/\sqrt{2}$ and $|\langle 2|d^\dagger_{\alpha\odot}|1\rangle| = |\langle 3|d^\dagger_{\alpha\odot}|2\rangle| = k_+$. Moreover, we gathered together the principal-part contributions and the ones coming from the reflection Hamiltonian in the effective magnetic fields,

$$\vec{B}_2 = \vec{B}_1,$$

$$\vec{B}_3 = \vec{B}_4 := \frac{2}{\gamma} \sum_\alpha |t_\alpha|^2 \mathcal{P}'_\alpha(\mu_4, E^{(0)}_3 - \{E_2\}) \vec{m}_\alpha.$$

The latter are defined in terms of the following function:

$$\mathcal{P}'_\alpha(\mu_4, E^{(0)}_3 - \{E_2\}) := -\frac{1}{2}[P^+_{\alpha\downarrow\uparrow}(\mu_4) + R_{\alpha\downarrow\uparrow}] - k_+^2 P^-_{\alpha\uparrow\downarrow}(\mu_3) + \frac{1}{4} P^-_{\alpha\uparrow\downarrow}(\varepsilon_{3o} - \varepsilon_{2'}) - \frac{1}{4} P^-_{\alpha\uparrow\downarrow}(\varepsilon_{3o} - \varepsilon_{2''}) - k_-^2 P^-_{\alpha\uparrow\downarrow}(\varepsilon_{3o} - \varepsilon_{2'''}).$$

Moreover, a closer look to Eq. (46) shows that its angular dependence is strongly coupled to the square of the ratio $(\gamma B_i)/\{\hbar\Gamma f[(-1)^i \mu_i]\}$, which is the effective exchange splitting rescaled by the coupling and the Fermi function. The ratio occurs in the denominators, and its value depends on the gate voltage. As the change of B_i under the variation in the gate voltage is comparatively small, the factor dominating the gate voltage evolution is the Fermi function. This accounts for the population of the dot: only if a nonzero spin is present (i.e., odd filling: one or three electrons) the effective magnetic field can have an influence. That is why correspondingly the renormalized effective exchange splitting vanishes for even fillings, namely, below $0 \leftrightarrow 1$ and $2 \leftrightarrow 3$, respectively, above the $1 \leftrightarrow 2$ and $3 \leftrightarrow 4$ resonances. This can nicely be seen from Fig. 3 (remember that $V_{\text{gate}} \propto -\xi$, so "below" means larger, "above" means smaller ξ), where the four different factors $(\gamma B_i)^2/\{f((-1)^i \mu_i)\Gamma\}^2$ are plotted. The curves belonging to the resonances involving the half-filling do not immediately go to zero but show a more complex behavior with some small intermediate peaks due to the influence of the various excited states present for a two-electron population of the dot. As we expect, $G_{01}(\xi)$ and $G_{34}(\xi)$ [$G_{12}(\xi)$ and $G_{23}(\xi)$, respectively] are mirror symmetric with respect to each other when the gate voltage is varied. This in turn reflects the electron-hole symmetry of the DD Hamiltonian. The parameters of the figures are chosen to be as follows ($b<0$):

$$k_B T = 4 \times 10^{-2}|b|, \quad \hbar\Gamma = 4 \times 10^{-3}|b|,$$

$$U = 6|b|, \quad V = 1.6|b|, \quad (47)$$

and $p=0.8$, $R=0.05D$. As expected, the peaks are mirror symmetric with respect to the half-filling gate voltage. Notice also the occurrence of different peak heights, both in the parallel and in the antiparallel case. For both polarizations, the principal-part terms entering Eq. (46) vanish, the spin accumulation is entirely in the magnetization plane, and the peak ratio is solely determined by the ratio of the ground state overlaps $2/k_+^2$. For polarization angles $\Theta \neq 0, \pi$, the ra-

TABLE III. Matrix elements for the $N=1\leftrightarrow N=2$ transition induced by $d^{\dagger}_{\alpha\uparrow}$ and $d^{\dagger}_{\alpha\downarrow}$, $\alpha=1,2$. The notation $|2'(s_z)\rangle$, with $s_z=0,\pm 1$, specifies which one of the triplet elements is addressed.

		$1\leftrightarrow 2$			
		$\lvert 1e\uparrow\rangle$	$\lvert 1e\downarrow\rangle$	$\lvert 1o\uparrow\rangle$	$\lvert 1o\downarrow\rangle$
$d^{\dagger}_{1\uparrow}$:	$\langle 2g\rvert$	0	$\frac{\alpha_0+\beta_0}{2}$	0	$\frac{-\alpha_0+\beta_0}{2}$
	$\langle 2'(+1)\rvert$	$\frac{1}{\sqrt{2}}$	0	$-\frac{1}{\sqrt{2}}$	0
	$\langle 2'(0)\rvert$	0	$\frac{1}{2}$	0	$-\frac{1}{2}$
	$\langle 2'(-1)\rvert$	0	0	0	0
	$\langle 2''\rvert$	0	$\frac{1}{2}$	0	$\frac{1}{2}$
	$\langle 2'''\rvert$	0	$\frac{-\alpha_0+\beta_0}{2}$	0	$\frac{-\alpha_0-\beta_0}{2}$
$d^{\dagger}_{1\downarrow}$:	$\langle 2g\rvert$	$\frac{-\alpha_0-\beta_0}{2}$	0	$\frac{\alpha_0-\beta_0}{2}$	0
	$\langle 2'(+1)\rvert$	0	0	0	0
	$\langle 2'(0)\rvert$	$\frac{1}{2}$	0	$-\frac{1}{2}$	0
	$\langle 2'(-1)\rvert$	0	$\frac{1}{\sqrt{2}}$	0	$-\frac{1}{\sqrt{2}}$
	$\langle 2''\rvert$	$-\frac{1}{2}$	0	$-\frac{1}{2}$	0
	$\langle 2'''\rvert$	$\frac{\alpha_0-\beta_0}{2}$	0	$\frac{\alpha_0+\beta_0}{2}$	0
$d^{\dagger}_{2\uparrow}$:	$\langle 2g\rvert$	0	$\frac{\alpha_0+\beta_0}{2}$	0	$\frac{\alpha_0-\beta_0}{2}$
	$\langle 2'(+1)\rvert$	$-\frac{1}{\sqrt{2}}$	0	$-\frac{1}{\sqrt{2}}$	0
	$\langle 2'(0)\rvert$	0	$-\frac{1}{2}$	0	$-\frac{1}{2}$
	$\langle 2'(-1)\rvert$	0	0	0	0
	$\langle 2''\rvert$	0	$-\frac{1}{2}$	0	$\frac{1}{2}$
	$\langle 2'''\rvert$	0	$\frac{-\alpha_0+\beta_0}{2}$	0	$\frac{\alpha_0+\beta_0}{2}$
$d^{\dagger}_{2\downarrow}$:	$\langle 2g\rvert$	$\frac{-\alpha_0-\beta_0}{2}$	0	$\frac{-\alpha_0+\beta_0}{2}$	0
	$\langle 2'(+1)\rvert$	0	0	0	0
	$\langle 2'(0)\rvert$	$-\frac{1}{2}$	0	$-\frac{1}{2}$	0
	$\langle 2'(-1)\rvert$	0	$-\frac{1}{\sqrt{2}}$	0	$-\frac{1}{\sqrt{2}}$
	$\langle 2''\rvert$	$\frac{1}{2}$	0	$-\frac{1}{2}$	0
	$\langle 2'''\rvert$	$\frac{\alpha_0-\beta_0}{2}$	0	$\frac{-\alpha_0-\beta_0}{2}$	0

tio is also determined by the nontrivial angular and voltage dependence of the effective exchange fields. Finally, as expected from the conductance formula Eq. (46), the conductance is suppressed in the antiparallel compared to the parallel case. The four conductance peaks are plotted as a function of the gate voltage in Fig. 4 for the polarization angles $\Theta=0$ and $\Theta=\pi$, top and bottom figures, respectively. These features of the conductance are nicely captured by the color plot of Fig. 5, where numerical results for the conductance plotted as a function of gate voltage and polarization angle are shown. The conductance suppression nearby $\Theta=\pi$ is clearly seen.

In the following, we analyze in detail the single resonance transitions. Due to the mirror symmetry, it is convenient to investigate together the $N=0\leftrightarrow N=1$, $N=3\leftrightarrow N=4$ and $N=1\leftrightarrow N=2$, $N=2\leftrightarrow N=3$ resonances. We use the convention that for a fixed resonance, the parameter $\xi=0$ when $\mu_{N+1}=0$.

1. Resonant regimes $N=0\leftrightarrow N=1$ and $N=3\leftrightarrow N=4$

The expected mirror symmetry of G_{01} and G_{34} is shown in Fig. 6, where the conductance peaks are plotted for different polarization angles Θ of the contacts. Notice that the analytical expressions [Eq. (46)] (continuous lines) perfectly match the results obtained from a numerical integration of the master equation [Eq. (21)] with the current formula [Eq. (25)]. We also can see that the maxima of the conductance decrease with Θ growing up to π. It can be shown that the peaks for $\Theta=0$ and $\Theta=\pi$ lie at the same value of ξ because the effective fields B_i exactly vanish due to trigonometrical prefactors. In other words, virtual processes captured in the effective fields B_i do not play a role in the collinear cases. For noncollinear configurations, however, the peak maxima are shifted toward the gate voltages where an odd population of the dot dominates because there the effective exchange field can act on the accumulating spin and make it precess, which eases tunneling out. These findings are in agreement with results obtained for a single-level quantum dot,[30] a metallic island,[28] and carbon nanotubes.[38] To quantify the relative magnitude of the current for a given polarization angle Θ with respect to the case $\Theta=0$, we introduce the angle-dependent TMR as

$$\mathrm{TMR}_{NN+1}(\Theta,\xi)=1-\frac{G_{N,N+1}(\Theta,\xi)}{G_{N,N+1}(0,\xi)}.$$

For the $0\leftrightarrow 1$ transition, it reads

TABLE IV. Matrix elements for the $N=2\leftrightarrow N=3$ transition governed by $d_{\alpha\uparrow}$ and $d_{\alpha\downarrow}$, $\alpha=1,2$.

		$2\leftrightarrow 3$			
		$\|3o\uparrow\rangle$	$\|3o\downarrow\rangle$	$\|3e\uparrow\rangle$	$\|3e\downarrow\rangle$
	$\langle 2g\|$	$\frac{\alpha_0+\beta_0}{2}$	0	$\frac{\alpha_0-\beta_0}{2}$	0
$d_{1\uparrow}$:	$\langle 2'(+1)\|$	0	0	0	0
	$\langle 2'(0)\|$	$-\frac{1}{2}$	0	$-\frac{1}{2}$	0
	$\langle 2'(-1)\|$	0	$\frac{1}{\sqrt{2}}$	0	$\frac{1}{\sqrt{2}}$
	$\langle 2''\|$	$-\frac{1}{2}$	0	$\frac{1}{2}$	0
	$\langle 2'''\|$	$\frac{-\alpha_0+\beta_0}{2}$	0	$\frac{\alpha_0+\beta_0}{2}$	0
$d_{1\downarrow}$:	$\langle 2g\|$	0	$\frac{-\alpha_0-\beta_0}{2}$	0	$\frac{-\alpha_0+\beta_0}{2}$
	$\langle 2'(+1)\|$	$\frac{1}{\sqrt{2}}$	0	$\frac{1}{\sqrt{2}}$	0
	$\langle 2'(0)\|$	0	$-\frac{1}{2}$	0	$-\frac{1}{2}$
	$\langle 2'(-1)\|$	0	0	0	0
	$\langle 2''\|$	0	$\frac{1}{2}$	0	$-\frac{1}{2}$
	$\langle 2'''\|$	0	$\frac{\alpha_0-\beta_0}{2}$	0	$\frac{-\alpha_0-\beta_0}{2}$
$d_{2\uparrow}$:	$\langle 2g\|$	$\frac{-\alpha_0-\beta_0}{2}$	0	$\frac{\alpha_0-\beta_0}{2}$	0
	$\langle 2'(+1)\|$	0	0	0	0
	$\langle 2'(0)\|$	$-\frac{1}{2}$	0	$\frac{1}{2}$	0
	$\langle 2'(-1)\|$	0	$\frac{1}{\sqrt{2}}$	0	$-\frac{1}{\sqrt{2}}$
	$\langle 2''\|$	$-\frac{1}{2}$	0	$-\frac{1}{2}$	0
	$\langle 2'''\|$	$\frac{\alpha_0-\beta_0}{2}$	0	$\frac{\alpha_0+\beta_0}{2}$	0
$d_{2\downarrow}$:	$\langle 2g\|$	0	$\frac{\alpha_0+\beta_0}{2}$	0	$\frac{-\alpha_0+\beta_0}{2}$
	$\langle 2'(+1)\|$	$\frac{1}{\sqrt{2}}$	0	$-\frac{1}{\sqrt{2}}$	0
	$\langle 2'(0)\|$	0	$-\frac{1}{2}$	0	$\frac{1}{2}$
	$\langle 2'(-1)\|$	0	0	0	0
	$\langle 2''\|$	0	$\frac{1}{2}$	0	$\frac{1}{2}$
	$\langle 2'''\|$	0	$\frac{-\alpha_0+\beta_0}{2}$	0	$\frac{-\alpha_0-\beta_0}{2}$

$$\mathrm{TMR}_{01}=\frac{p^2\sin^2\left(\frac{\Theta}{2}\right)}{1+[B_1^2/f^2(-\mu_1)\Gamma^2]\cos^2\left(\frac{\Theta}{2}\right)}. \tag{48}$$

Hence, the TMR vanishes for $\Theta=0$ and takes the constant value,

$$\mathrm{TMR}_{01}(\pi,\xi)=p^2,$$

at $\Theta=\pi$. For the remaining polarization angles, $\Theta\neq 0$ and $\Theta\neq\pi$, the TMR is gate voltage dependent and positive. The behavior of the TMR as a function of the gate voltage is shown in Fig. 7. To understand the gate voltage dependence of the TMR at noncollinear angles, we have to remember that the dot is depleted with increasing ξ. For the $0\leftrightarrow 1$ transition, this means that at positive ξ, the dot is predominantly empty, so that an electron that enters the dot also leaves it fast. In this situation, the TMR is finite and its value depends in a complicated way on the amplitude of the exchange field. At negative ξ, the DD is predominantly occupied with an

TABLE V. Matrix elements for the $N=3\leftrightarrow N=4$ transition induced by the operators $d^\dagger_{\alpha\uparrow}$ and $d^\dagger_{\alpha\downarrow}$, $\alpha=1,2$.

	$3\leftrightarrow 4$			
	$\|3o\uparrow\rangle$	$\|3o\downarrow\rangle$	$\|3e\uparrow\rangle$	$\|3e\downarrow\rangle$
$d^\dagger_{1\uparrow}:\langle 2,2\|$	0	$\frac{1}{\sqrt{2}}$	0	$-\frac{1}{\sqrt{2}}$
$d^\dagger_{1\downarrow}:\langle 2,2\|$	$\frac{1}{\sqrt{2}}$	0	$-\frac{1}{\sqrt{2}}$	0
$d^\dagger_{2\uparrow}:\langle 2,2\|$	0	$-\frac{1}{\sqrt{2}}$	0	$-\frac{1}{\sqrt{2}}$
$d^\dagger_{2\downarrow}:\langle 2,2\|$	$-\frac{1}{\sqrt{2}}$	0	$-\frac{1}{\sqrt{2}}$	0

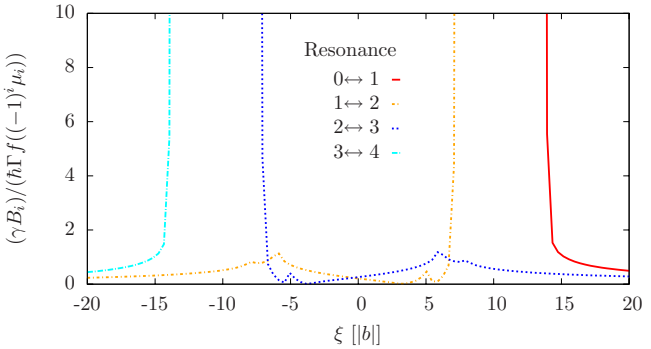

FIG. 3. (Color online) Gate voltage dependence of the renormalized effective exchange splitting entering the conductance formula [Eq. (46)]. Notice the mirror symmetry of the $0\leftrightarrow 1$ with the $3\leftrightarrow 4$ curve and of the $1\leftrightarrow 2$ with the $2\leftrightarrow 3$ one.

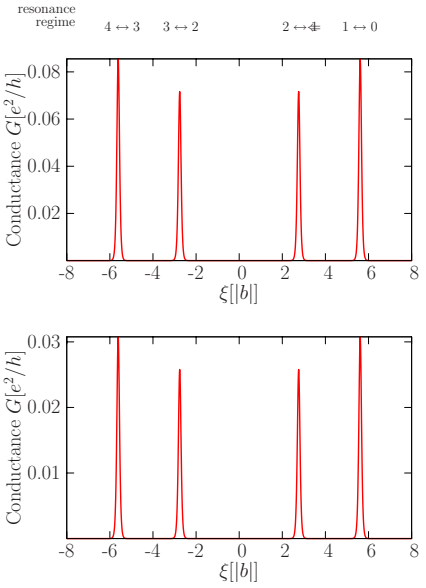

FIG. 4. (Color online) Conductance at low bias for the parallel case $\Theta=0$ (top) and antiparallel case $\Theta=\pi$ (bottom). Notice the different peak heights and the mirror symmetry with respect to the half-filling value $\xi=0$. The conductance in the antiparallel configuration is always smaller than that in the parallel one.

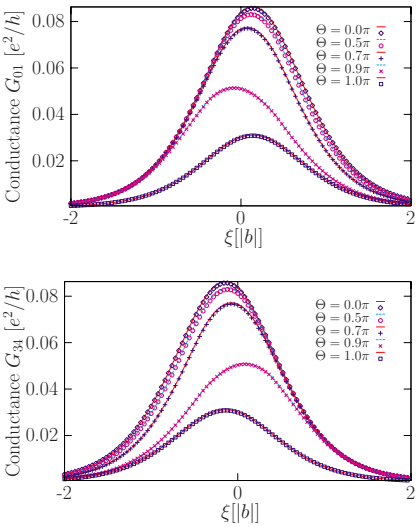

FIG. 6. (Color online) The conductance $G_{01}(\xi)$ (upper figure) [$G_{34}(\xi)$ (lower figure)] vs gate voltage for different polarization angles. The mirror symmetry of the conductance peaks for the $0\leftrightarrow1$ and $3\leftrightarrow4$ transitions is clearly observed. Notice the excellent agreement between the prediction of the analytical formula [Eq. (46)] (continuous lines) and the results of a numerical integration of Eq. (21) with Eq. (25) (symbols).

electron that can now interact with the exchange field, which makes the spin precess and thus eases tunneling out of the dot. Consequently, $G_{NN+1}(\Theta,\xi)\approx G_{NN+1}(0,\xi)$ and the TMR vanishes. Finally, Fig. 8 illustrates the angular dependence of the normalized conductance for three different values of the gate voltage. We detect a common absolute minimum for the conductance at $\Theta=\pi$, i.e., transport is weakened in the antiparallel case. The width of the curves is dependent on the renormalized effective exchange $(\gamma B_i)/(\Gamma f)$. The larger its value, the narrower the curves because the spin precession can equilibrate the accumulated spin for all angles but $\Theta=\pi$. Notice again the equivalence of the curves belonging to $\xi=\pm2|b|$ for the $1\leftrightarrow2$ resonance to the curves with $\xi=\mp2|b|$ for the $3\leftrightarrow4$ resonance.

2. Resonant regimes $N=1\leftrightarrow N=2$ and $N=2\leftrightarrow N=3$

For the resonant $1\leftrightarrow2$ and $2\leftrightarrow3$ transitions, qualitatively analogous results as for the $0\leftrightarrow1$ and $3\leftrightarrow4$ transitions are found. Thus, exemplarily, we only show the angular dependence of the normalized conductance in Fig. 9, showing the expected absolute conductance minimum at $\Theta=0$.

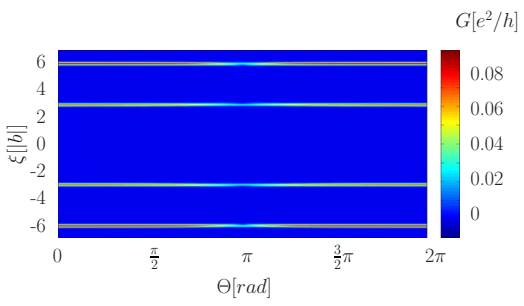

FIG. 5. (Color online) Conductance as a function of the polarization angle and of the gate voltage. The minimal conductance peaks occur as expected at $\Theta=\pi$.

V. NONLINEAR TRANSPORT

In this section, we present the numerical results deduced from the general master equation [Eq. (21)] combined with the current formula [Eq. (25)]. We show the differential conductance $\frac{dI}{dV}(\xi,V_{\text{bias}})$ for the three distinct angles $\Theta=0$, Θ

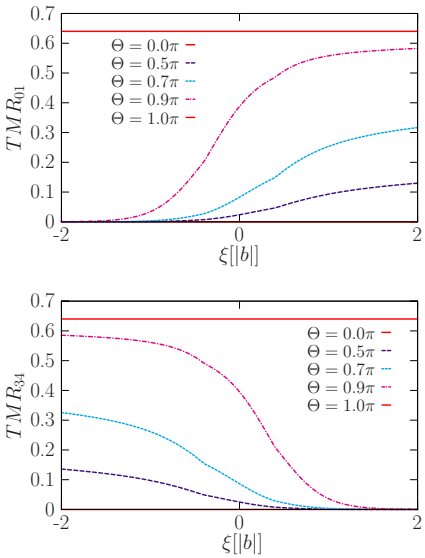

FIG. 7. (Color online) TMR for the $0\leftrightarrow1$ (upper figure) and $3\leftrightarrow4$ (lower figure) transitions vs gate voltage. The TMR is always positive and for collinear lead magnetizations, $\Theta=0$ and $\Theta=\pi$, independent of gate voltage.

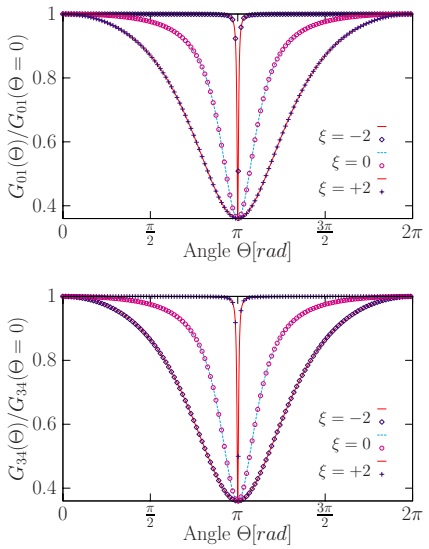

FIG. 8. (Color online) $G_{01}(\Theta)/G_{01}(0)$ (upper figure) $[G_{34}(\Theta)/G_{34}(0)$ (lower figure)] vs polarization angle. For all the three chosen values of the gate voltage, the curve displays an absolute minimum at $\Theta=\pi$. Notice the overall agreement of the analytical predictions [Eq. (46)] given by the continuous curves with outcomes of a numerical solution of the master equation [Eq. (21)] together with Eq. (25) (symbols).

$=\frac{\pi}{2}$, and $\Theta=\pi$, see Fig. 10, top, middle, and bottom, respectively. The results confirm the electron-hole symmetry and the symmetry upon bias voltage inversion $I(\xi,V_{\text{bias}})=-I(\xi,-V_{\text{bias}})$. In all of the three cases, we can nicely see the expected three closed and the two half-open diamonds, where the current is blocked and the electronic number of the double-dot system stays constant. At higher bias voltages, the contribution of excited states is manifested in the appearance of several excitation lines. One clearly sees that transition lines present in the parallel case are *absent* in the antiparallel case. Moreover, in the case of noncollinear polarization, $\Theta=\pi/2$, negative differential conductance (NDC) is observed.

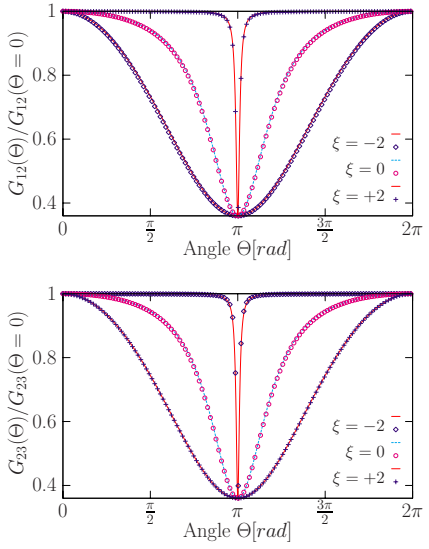

FIG. 9. (Color online) $G_{12}(\Theta)/G_{12}(0)$ (upper figure) $[G_{23}(\Theta)/G_{23}(0)$ (lower figure)] vs polarization angle. Notice the overall agreement of the analytical predictions [Eqs. (45) and (46)] (continuous lines) with the data (symbols) coming from numerical solutions of the equations for the reduced density matrix.

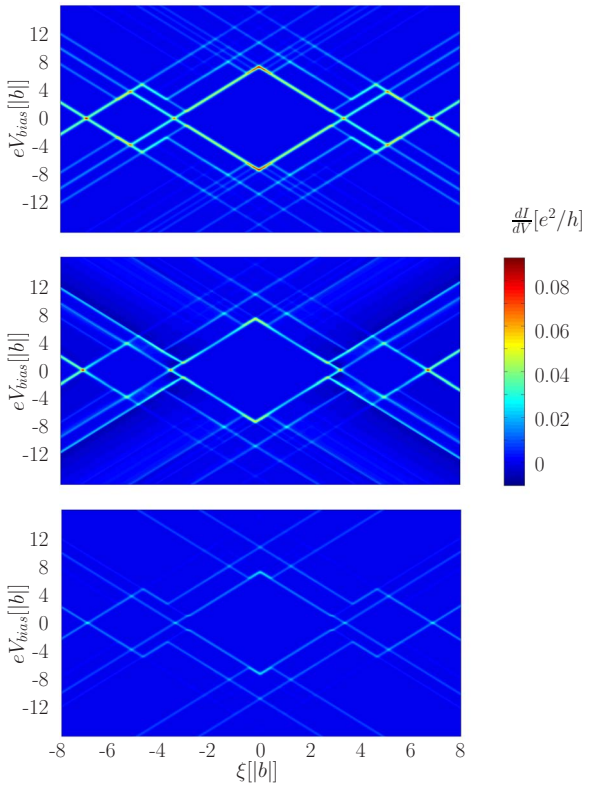

FIG. 10. (Color online) Differential conductance $\frac{dI}{dV}$ for the parallel $\Theta=0$ (top), perpendicular $\Theta=\pi/2$ (middle), and antiparallel $\Theta=\pi$ (bottom) configurations. The two half diamond and three diamond regions correspond to bias and gate voltage values where transport is Coulomb blocked. The excitation lines, where excited states start to contribute to resonant transport, are clearly visible in all of the three cases. However, a negative differential conductance is observed in the perpendicular case, while some excitation lines are absent in the antiparallel configuration.

In the following, we want not only to explain the origin of these two features, but alongside also give another example for spin-blockade effects, which play a decisive role in the DD physics. As a starting point, we plot in Fig. 11 (top) the current through the system for the three different angles $\Theta=\{0,\frac{\pi}{2},\pi\}$ at a fixed gate voltage $\xi=4|b|$ and positive bias voltages. We recognize that for $eV_{\text{Bias}}<2.4|b|$, the current is Coulomb blocked in all of the three cases. In this configuration, exactly one electron stays in the double-dot. From about $eV_{\text{bias}}\geq 2.4|b|$, the channel where the ground state energies μ_1 and μ_2 are degenerate opens ($|1e\sigma\rangle\leftrightarrow|2\rangle$ transition) and the current begins to flow. With increasing bias, more and more transport channels become energetically favorable. In particular, for all the polarization angles Θ, we observe two consecutive steps corresponding to $|0\rangle\leftrightarrow|1e\sigma\rangle$ and $|1e\sigma\rangle\leftrightarrow|2'\rangle$ transitions. The latter, occurring at about $eV_{\text{bias}}=4|b|$, involves the excited two-particle triplet states $|2'(S_z)\rangle$.

The next excitation step, indicated with a circle in Fig. 11 (top), belongs to the $|1o\sigma\rangle\leftrightarrow|2''\rangle$ transition. The associated

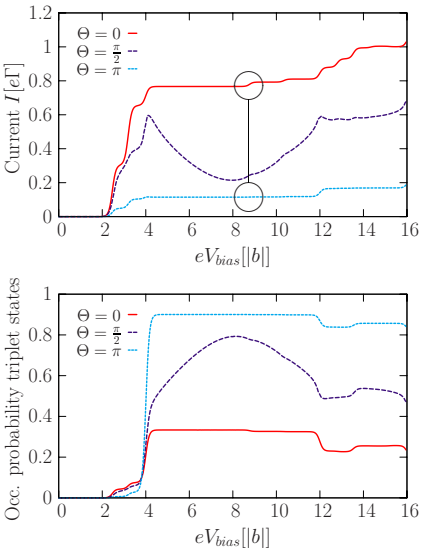

FIG. 11. (Color online) Current (top) and triplet occupation (bottom) for the two collinear ($\Theta=0,\Theta=\pi$) cases and the perpendicular case ($\Theta=\frac{\pi}{2}$) at a fixed gate voltage $\xi=4|b|$. Notice the occurrence of a pronounced negative differential conductance feature for perpendicular polarization $\Theta=\pi/2$.

line is missing for the antiparallel configuration, as well as the lines corresponding to $|1o\sigma\rangle \leftrightarrow |2'''\rangle$, $|1e\sigma\rangle \leftrightarrow |2''\rangle$, $|2\rangle \leftrightarrow |3o\sigma\rangle$, and $|1e\sigma\rangle \leftrightarrow |2'''\rangle$. Crucially, in all of these transitions, a two-particle state with *total spin zero* is involved. In order to explain the absence of these lines, let us, e.g., focus on the first missing step corresponding to the $|1o\sigma\rangle \leftrightarrow |2''\rangle$ resonance. In the parallel case (say, both contacts polarized spin-up), there is always an open channel corresponding to the situation in which the spin in the DD is antiparallel to that in the leads (i.e., $|1o-\rangle$). In the antiparallel case (say, source polarized spin-up and drain polarized spin-down), originally a spin-down might be present in the dot. An electron that enters the DD from the source must then be spin-up (in order to form the $|2''\rangle$ state), but as the drain is down-polarized, it will be the spin-down electron that leaves the DD, which corresponds to a spin flip. Now, the presence of a spin-up electron in the DD prevents a majority (another spin-up) electron from the source to enter the DD, such that we end up in a blocking state. The transition is hence forbidden.

A similar yet different spin-blockade effect determines the occupation probabilities for the triplet state (Fig. 11, bottom). Naturally, for all angles, the probability to be in the triplet state increases above the resonance at $eV_{\mathrm{bias}}=4|b|$, but interestingly, such probability is *largest* in the antiparallel case. This is due to the fact that a majority spin in the parallel configuration (spin-up) can be easily transmitted through the DD via the triplet states $|2'(1)\rangle$ or $|2'(0)\rangle$. In the antiparallel case, however, a blocking state establishes (say, again source polarized spin-up and drain polarized spin-down). Let initially a spin-down electron be present on the DD. From the source electrode, most likely a majority electron (polarized spin-up) will enter the dot. Now, just as in the previous case, the consecutive tunneling event will cause a spin flip in the DD because the spin-down electron (majority electron of the drain) will leave the dot. So, the DD is finally in a spin-up state, and once the next majority spin-up electron from the source enters, the DD ends up in the triplet state $|2'(+1)\rangle$ and will remain there for a long time due to the fact that the majority spins in the drain are down polarized. Hence, the triplet state $|2'(+1)\rangle$ acts as a trapping state.

Notice that the two distinct spin-blockade effects are different from the Pauli spin-blockade discussed in the DD literature.[46–49] Moreover, the second effect, relying on the existence of degenerate triplet states, is also different from the spin-blockade found in Ref. 30 for a single-level quantum dot.

Finally, let us turn to the negative differential conductance, which occurs for noncollinearly polarized leads (see the dashed blue lines in Fig. 11) and which we find to become more evident for higher polarizations (not shown). By neglecting the exchange field, we would just expect the magnitude of the current for the noncollinear polarizations to lie somewhere in between the values for the parallel and the antiparallel current because the noncollinear polarization could, in principle, be rewritten as a linear combination of the parallel and the antiparallel configuration. Now, the effect of the exchange is to cause precession and therewith equilibration of the accumulating spin, which corresponds to shifting the balance in favor of the parallel configuration, i.e., enhancing the current. The decisive point is that the exchange field is not only gate dependent but also bias voltage dependent and reaches a minimum around $eV_{\mathrm{bias}}\approx 8|b|$. This explains the decrease of the current up to this point. Afterward, the influence of the spin precession regains weight. The same consideration applies for the other NDC regions observed in Fig. 10, e.g., in the gate voltage region $\xi\approx 2|b|$ involving the $N=0\leftrightarrow N=1$ transition, as described in Ref. 30.

VI. EFFECTS OF AN EXTERNAL MAGNETIC FIELD

In this section, we wish to discuss the qualitative changes brought by an external magnetic field applied to the DD. Specifically, the magnetic field is assumed to be parallel to the magnetization direction of the drain. For simplicity, we focus on the experimental standard case of parallel and antiparallel lead polarizations and of low-bias voltages. Then, the magnetic field causes an energy shift $\mp E_{\mathrm{Zeeman}}$ depending on whether the electron spin is parallel or antiparallel, respectively, to it. For collinear polarization angles, the principal-part contributions vanish, and the equations for the RDM are easily obtained. We exemplarily report results for $0\leftrightarrow 1$ and $1\leftrightarrow 2$ transitions. Let us then consider the parameter regime nearby the $0\leftrightarrow 1$ resonance and setup a system of three equations with three unknown variables, W_0, $W_{1\uparrow}$, and $W_{1\downarrow}$. The first equation corresponds to the normalization condition $W_{1\uparrow}+W_{1\downarrow}+W_0=1$. The remaining equations are the equations of motion for $W_{1\uparrow/\downarrow}$, which can be written as

$$\dot{W}_{1\uparrow} = -\frac{\pi}{\hbar}\sum_{\alpha=s,d}|t_\alpha|^2[F^-_{\alpha\uparrow}(\mu_{1\uparrow})W_{1\uparrow} - F^+_{\alpha\uparrow}(\mu_{1\uparrow})W_0], \quad (49)$$

$$\dot{W}_{1\downarrow} = -\frac{\pi}{\hbar}\sum_{\alpha=s,d}|t^{\alpha}|^2[F^{-}_{\alpha\downarrow}(\mu_{1\downarrow})W_{1\downarrow} - F^{+}_{\alpha\downarrow}(\mu_{1\downarrow})W_0], \quad (50)$$

where

$$\mu_{1\uparrow/\downarrow} = \mu_1 \mp E_{\text{Zeeman}}, \quad (51)$$

and $F^{\pm}_{\alpha\sigma_\odot}(E)=D_{\alpha\sigma_\odot}f^{\pm}(E)$. $D_{\alpha\uparrow/\downarrow}=D_{\alpha\pm_\alpha}$. On the other hand, $D_{s\uparrow/\downarrow}=D_{s\mp_s}$ and $D_{d\uparrow/\downarrow}=D_{d\pm_d}$ in the antiparallel case.

Upon considering symmetric contacts ($t_1=t_2=t$, $D_1=D_2=D$), we find the following in the parallel case:

$$G_{01}(\Theta=0) = \frac{\Gamma e^2}{8\beta}f(-\mu_{1\uparrow})f(-\mu_{1\downarrow}) \times \frac{p[f(\mu_{1\uparrow})-f(\mu_{1\downarrow})]+f(\mu_{1\uparrow})+f(\mu_{1\downarrow})}{f(-\mu_{1\uparrow})f(\mu_{1\downarrow})+f(-\mu_{1\uparrow})f(-\mu_{1\downarrow})+f(\mu_{1\uparrow})f(-\mu_{1\downarrow})}. \quad (52)$$

For the antiparallel case, we obtain

$$G_{01}(\Theta=\pi) = G_{01}(\Theta=0)\frac{1-p^2[f(\mu_{1\uparrow})+f(\mu_{1\downarrow})]}{p[f(\mu_{1\uparrow})-f(\mu_{1\downarrow})]+f(\mu_{1\uparrow})+f(\mu_{1\downarrow})}. \quad (53)$$

Analogously, we find the following for the $1\leftrightarrow 2$ transition:

$$G_{12}(\Theta=0) = \frac{\Gamma e^2 k_+^2}{2\beta}f(\mu_{2\uparrow})f(\mu_{2\downarrow}) \times \frac{p[f(-\mu_{2\downarrow})-f(-\mu_{2\uparrow})]+f(-\mu_{2\uparrow})+f(-\mu_{2\downarrow})}{f(-\mu_{2\uparrow})f(\mu_{2\downarrow})+f(-\mu_{2\uparrow})f(-\mu_{2\downarrow})+f(\mu_{2\uparrow})f(-\mu_{2\downarrow})}, \quad (54)$$

$$G_{12}(\Theta=\pi) = G_{12}(\Theta=0) \times \frac{1-p^2[f(-\mu_{2\uparrow})+f(-\mu_{2\downarrow})]}{p[f(-\mu_{2\downarrow})-f(-\mu_{2\uparrow})]+f(-\mu_{2\uparrow})+f(-\mu_{2\downarrow})}. \quad (55)$$

The remaining resonances are analogously calculated. Figure 12 shows the four conductance resonances for the parallel and antiparallel configurations. Strikingly, the applied magnetic field breaks the symmetry between tunneling regimes $0\leftrightarrow 1$ and $3\leftrightarrow 4$, as well as between $1\leftrightarrow 2$ and $2\leftrightarrow 3$ resonances in case of *parallel* contact polarizations. The reason for this behavior is the following: in the low-bias regime, transitions between ground states dominate transport. In particular, the magnetic field removes the spin degeneracy of $|1e\sigma\rangle$ and $|3o\sigma\rangle$ states, such that states with spin aligned to the external magnetic field are energetically favored. Therefore, the transport electron in tunneling regime $0\leftrightarrow 1$ is a majority spin carrier. For the case $3\leftrightarrow 4$, however, two of the three electrons of the ground state $|3o\uparrow\rangle$ have spin-up, such that the fourth electron that can be added to the DD has to be a minority spin carrier. Therefore, the conductance gets diminished with respect to the $0\leftrightarrow 1$ transition, and the mirror symmetry present in the zero field case is broken. Analogously, the broken symmetry in the case of the $1\leftrightarrow 2$ and $2\leftrightarrow 3$ transitions can be understood. Correspondingly, the TMR can become negative for values of the gate voltages around the $2\leftrightarrow 3$ and $3\leftrightarrow 4$ resonances. We observe that a negative TMR has recently been predicted in Ref. 42 for the case of a single impurity Anderson model with orbital and spin degeneracies (see Fig. 13). In that work, a negative TMR arises due to the assumption that multiple reflections at the interface cause spin-dependent energy shifts. In our approach, however, where the contribution from the reflection Hamiltonian is treated to the lowest order, see Eq. (19), such spin-dependent energies originate from the magnetic-field-induced Zeeman splitting.

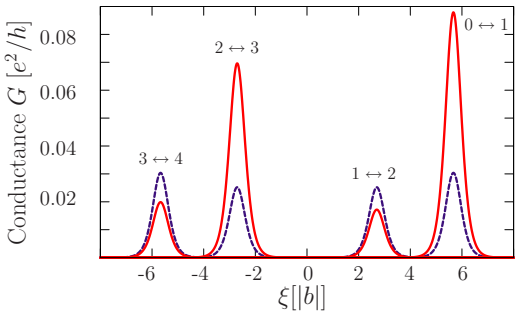

FIG. 12. (Color online) Conductance vs gate voltage for parallel (continuous line) and antiparallel (dashed lines) contact configurations and Zeeman splitting $E_{\text{Zeeman}}=0.05|b|$. The magnetic field breaks the mirror symmetry with respect to the gate voltage in the *parallel* configuration.

VII. CONCLUSIONS

In summary, we have evaluated linear and nonlinear transport through a double-quantum-dot (DD) coupled to polarized leads with arbitrary polarization directions. Due to strong Coulomb interactions, the DD operates as a single-electron transistor, a F-SET, at low enough temperatures. A detailed analysis of the current-voltage characteristics of the DD and comparison with results of previous studies on other

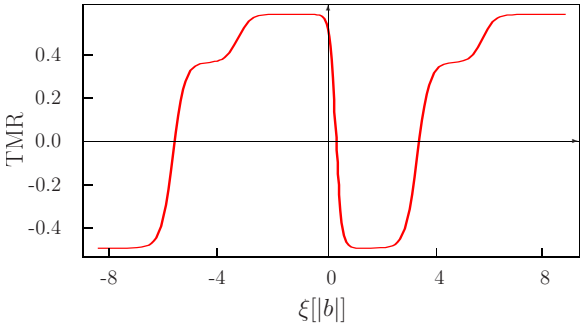

FIG. 13. (Color online) TMR vs gate voltage in the presence of an external magnetic field. In contrast to the zero field case, the TMR can become negative in the vicinity of the $2\leftrightarrow 3$ and $3\leftrightarrow 4$ resonances.

F-SET systems with noncollinear polarization (a single-level quantum dot,[30] a metallic island,[28] and a carbon nanotube[38]) brings us to the identification of *universal* behaviors of a F-SET, i.e., a behavior shared by *any* of those F-SETs, independent of the specific kind of conductor that is considered as the central system, as well as system-specific features.

The presence of an interfacial exchange field together with an interaction-induced one is universal. These exchange fields can act only for noncollinear polarizations and cause a precession of the accumulated spin on the dot and therewith ease the tunneling. This effect has various implications. It determines, e.g., the gate and angular dependences, as well as the height of single conductance peaks and can yield negative differential conductance features. Another universal feature is the occurrence of a negative tunneling magnetoresistance—even in the weak-tunneling limit—if a Zeeman-splitting exists.

The following features are specific to the DD system: in the low-bias regime, the problem can be analytically solved, and for tunneling regimes $0 \leftrightarrow 1$ and $1 \leftrightarrow 2$ ($2 \leftrightarrow 3$ and $3 \leftrightarrow 4$, respectively), the system behaves equivalent to a single-level quantum dot, where the Coulomb blockade peaks are found to be mirror symmetric with respect to the charge neutrality point. This mirror symmetry reflects the electron-hole symmetries of a system and is therefore typical for the DD, as well as the ratio of the peak heights. An external magnetic field lifts this symmetry and can cause a negative tunneling magnetoresistance. In the nonlinear bias regime, the presence of various excited states gives rise to interesting DD specific features. For example, a suppression of several excitation lines for an antiparallel lead configuration originates from a spin-blockade effect. It occurs because a trapping state is formed whenever a transition involves a two-electron state with total spin zero. A second spin-blockade effect we described involves the two-electron triplet state. The common mechanism of these two spin-blockades is the following: in both cases, a tunneling event can only occur if initially the dot is populated with an unpaired electron possessing the majority spin of the drain. The second step is that a majority electron of the source will enter, forming a spin-zero state. Then, the first electron can leave the dot, causing a spin flip. If the triplet state is involved, the dot will be left in a trapping state once a second majority electron from the source enters. Otherwise, we are directly in a blocking state. Finally, for noncollinear lead polarizations, negative differential conductance can be observed. All in all, due to their universality and the multiplicity of their properties, F-SETs based on DD systems seem good candidates for future magnetoelectronic devices.

ACKNOWLEDGMENTS

Financial support under the DFG Program Nos. SFB689 and SPP1243 is acknowledged.

APPENDIX A: MATRIX ELEMENTS OF THE DOT OPERATORS

Tables II–V show all the possible matrix elements $\langle N-1|d_{\alpha\sigma_\odot}|N\rangle$ and $\langle N|d^\dagger_{\alpha\sigma_\odot}|N-1\rangle$ with $\alpha=\{1,2\}$ and $\sigma_\odot=\{\uparrow,\downarrow\}$, which occur in the master equations [Eqs. (B1) and (B2)]. Notice that we only need to illustrate either the matrix elements $\langle N-1|d_{\alpha\sigma_\odot}|N\rangle$ or $\langle N|d^\dagger_{\alpha\sigma_\odot}|N-1\rangle$ because they are complex conjugated to each other.

APPENDIX B: MASTER EQUATION FOR THE REDUCED DENSITY MATRIX IN THE LINEAR REGIME

We explicitly report here the coupled equations of motion for elements $\dot{\rho}^{(N)}_{nm}(t)$ and $\dot{\rho}^{(N+1)}_{nm}(t)$ of the RDM to be solved in the low-bias regime. They are obtained from the generalized master equation [Eq. (21)] upon observing that (i) in the linear regime, terms that couple states with particle numbers unlike N and $N+1$ can be neglected; (ii) we can reduce the sum over h and h' and over l,l' only to energy ground states. In the remaining energy nonconserving terms, the sum has to go also over excited states. With $\mu_{N+1} := E^{(0)}_{N+1} - E^{(0)}_N$ being the chemical potential, we finally arrive at the following two master equations:

$$\begin{aligned}
\dot{\rho}^{(N)}_{nm}(t) = -\frac{\pi}{\hbar}\sum_{\alpha=s,d}|t^\alpha|^2 \sum_{\sigma_\odot,\sigma'_\odot}\Bigg\{ \sum_{l\in|N-1\rangle}, \sum_{j\in|E^{(0)}_N,N\rangle}, \sum_{h,h'\in|E^{(0)}_{N+1},N+1\rangle}, \sum_{\hat{h}\in|N+1\rangle}\Bigg\}\Bigg\{ & \Phi_{\alpha\sigma_\odot\sigma'_\odot}F^+_{\alpha\sigma_\odot\sigma'_\odot}(\mu_{N+1})(d_{\alpha\sigma_\odot})_{nh}(d^\dagger_{\alpha\sigma'_\odot})_{hj}\rho^{(N)}_{jm}(t) \\
& + \Phi_{\alpha\sigma_\odot\sigma'_\odot}\frac{i}{\pi}P^+_{\alpha\sigma_\odot\sigma'_\odot}(\varepsilon_{\hat{h}}-\varepsilon_j)(d_{\alpha\sigma_\odot})_{n\hat{h}}(d^\dagger_{\alpha\sigma'_\odot})_{\hat{h}j}\rho^{(N)}_{jm}(t) - \Phi^*_{\alpha\sigma_\odot\sigma'_\odot}\frac{i}{\pi}[P^-_{\alpha\sigma_\odot\sigma'_\odot}(\varepsilon_j-\varepsilon_l)+R_{\alpha\sigma_\odot\sigma'_\odot}](d^\dagger_{\alpha\sigma_\odot})_{nl}(d_{\alpha\sigma'_\odot})_{lj}\rho^{(N)}_{jm}(t) \\
& + \Phi_{\alpha\sigma_\odot\sigma'_\odot}F^+_{\alpha\sigma_\odot\sigma'_\odot}(\mu_{N+1})\rho^{(N)}_{nj}(t)(d_{\alpha\sigma_\odot})_{jh}(d^\dagger_{\alpha\sigma'_\odot})_{hm} - \Phi_{\alpha\sigma_\odot\sigma'_\odot}\frac{i}{\pi}P^+_{\alpha\sigma_\odot\sigma'_\odot}(\varepsilon_{\hat{h}}-\varepsilon_j)\rho^{(N)}_{nj}(t)(d_{\alpha\sigma_\odot})_{j\hat{h}}(d^\dagger_{\alpha\sigma'_\odot})_{\hat{h}m} \\
& + \Phi^*_{\alpha\sigma_\odot\sigma'_\odot}\frac{i}{\pi}[P^-_{\alpha\sigma_\odot\sigma'_\odot}(\varepsilon_j-\varepsilon_l)+R_{\alpha\sigma_\odot\sigma'_\odot}]\rho^{(N)}_{nj}(t)(d^\dagger_{\alpha\sigma_\odot})_{jl}(d_{\alpha\sigma'_\odot})_{lm} - 2\Phi_{\alpha\sigma_\odot\sigma'_\odot}F^-_{\alpha\sigma_\odot\sigma'_\odot}(\mu_{N+1})(d_{\alpha\sigma_\odot})_{nh'}\rho^{(N+1)}_{h'h}(t)(d^\dagger_{\alpha\sigma'_\odot})_{hm}\Bigg\},
\end{aligned} \tag{B1}$$

$$\dot{\rho}^{(N+1)}_{nm}(t) = -\frac{\pi}{\hbar}\sum_{\alpha=s,d}|t^{\alpha}|^2\sum_{\sigma_{\odot},\sigma'_{\odot}}\left\{\sum_{\hat{l}\in|E_N,N\rangle},\sum_{l,l'\in|E^{(0)}_N,N\rangle},\sum_{j\in|E^{(0)}_{N+1},N+1\rangle},\sum_{h\in|E_{N+2},N+2\rangle}\right\}\Bigg\{\Phi_{\alpha\sigma_{\odot}\sigma'_{\odot}}\frac{i}{\pi}P^{+}_{\alpha\sigma_{\odot}\sigma'_{\odot}}(\varepsilon_h-\varepsilon_j)$$

$$\times(d_{\alpha\sigma_{\odot}})_{nh}(d^{\dagger}_{\alpha\sigma'_{\odot}})_{hj}\rho^{(N+1)}_{jm}(t)+\Phi^{*}_{\alpha\sigma_{\odot}\sigma'_{\odot}}F^{-}_{\alpha\sigma_{\odot}\sigma'_{\odot}}(\mu_{N+1})(d^{\dagger}_{\alpha\sigma_{\odot}})_{nl}(d_{\alpha\sigma'_{\odot}})_{lj}\rho^{(N+1)}_{jm}(t)-\Phi^{*}_{\alpha\sigma_{\odot}\sigma'_{\odot}}\frac{i}{\pi}[P^{-}_{\alpha\sigma_{\odot}\sigma'_{\odot}}(\varepsilon_j-\varepsilon_{\hat{l}})+R_{\alpha\sigma_{\odot}\sigma'_{\odot}}]$$

$$\times(d^{\dagger}_{\alpha\sigma_{\odot}})_{nl}(d_{\alpha\sigma'_{\odot}})_{\hat{l}j}\rho^{(N+1)}_{jm}(t)-\Phi_{\alpha\sigma_{\odot}\sigma'_{\odot}}\frac{i}{\pi}P^{+}_{\alpha\sigma_{\odot}\sigma'_{\odot}}(\varepsilon_h-\varepsilon_j)\rho^{(N+1)}_{nj}(t)(d_{\alpha\sigma_{\odot}})_{jh}(d^{\dagger}_{\alpha\sigma'_{\odot}})_{hm}+\Phi^{*}_{\alpha\sigma_{\odot}\sigma'_{\odot}}[F^{-}_{\alpha\sigma_{\odot}\sigma'_{\odot}}(\mu_{N+1})]\rho^{(N+1)}_{nj}(t)$$

$$\times(d^{\dagger}_{\alpha\sigma_{\odot}})_{j\hat{l}}(d_{\alpha\sigma'_{\odot}})_{\hat{l}m}+\Phi^{*}_{\alpha\sigma_{\odot}\sigma'_{\odot}}\frac{i}{\pi}[P^{-}_{\alpha\sigma_{\odot}\sigma'_{\odot}}(\varepsilon_j-\varepsilon_{\hat{l}})+R_{\alpha\sigma_{\odot}\sigma'_{\odot}}]\rho^{(N+1)}_{nj}(t)(d^{\dagger}_{\alpha\sigma_{\odot}})_{j\hat{l}}(d_{\alpha\sigma'_{\odot}})_{\hat{l}m}-2\Phi^{*}_{\alpha\sigma_{\odot}\sigma'_{\odot}}F^{+}_{\alpha\sigma_{\odot}\sigma'_{\odot}}(\mu_{N+1})$$

$$\times(d^{\dagger}_{\alpha\sigma_{\odot}})_{nl'}\rho^{(N)}_{l'l}(t)(d_{\alpha\sigma'_{\odot}})_{lm}\Bigg\}. \tag{B2}$$

Notice that we kept the sums over excited states $l,\hat{h}$ in Eq. (B1) and $\hat{l},h$ in Eq. (B2), which are responsible for the virtual transitions.

[1] S. Maekawa and T. Shinjo, *Spin Dependent Transport in Magnetic Nanostrucures* (Taylor & Francis, New York, 2002).
[2] G. E. W. Bauer and L. W. Molenkamp, New J. Phys. **9** (2007).
[3] D. D. Awscahalom, D. Loss, and N. Samarth (Springer, Berlin, 2002).
[4] *Single Charge Tunneling: Coulomb Blockade Phenomena in Nanostructures*, NATO Advanced Studies Institute, Series B: Physics, edited by H. Grabert and M. Devoret (Plenum, New York, 1992), Vol. 294.
[5] *Mesoscopic Electron Transport*, edited by L. L. Sohn, L. P. Kouwenhoven, and G. Schön (Kluwer, Dordrecht, 1997).
[6] K. Ono, H. Shimada, and Y. Ootuka, J. Phys. Soc. Jpn. **66**, 1261 (1997).
[7] L. F. Schelp, A. Fert, F. Fettar, P. Holody, S. F. Lee, J. L. Maurice, F. Petroff, and A. Vaurès, Phys. Rev. B **56**, R5747 (1997).
[8] K. Yakushiji, F. Ernult, H. Imamura, K. Yamane, S. Mitani, K. Takanashi, S. Takahashi, S. Maekawa, and H. Fujimori, Nat. Mater. **4**, 57 (2005).
[9] L. Y. Zhang, C. Y. Wang, Y. G. Wei, X. Y. Liu, and D. Davidović, Phys. Rev. B **72**, 155445 (2005).
[10] A. Bernand-Mantel, P. Seneor, N. Lidgi, M. Muñoz, V. Cros, S. Fusil, K. Bouzehouane, C. Deranlot, A. Vaures, F. Petroff, and A. Fert, Appl. Phys. Lett. **89**, 062502 (2006).
[11] M. Pioro-Ladrière, M. Ciorga, J. Lapointe, P. Zawadzki, M. Korkusinski, P. Hawrylak, and A. S. Sachrajda, Phys. Rev. Lett. **91**, 026803 (2003).
[12] A. N. Pasupathy, R. C. Bialczak, J. Martinek, J. E. Grose, L. A. K. Donev, P. L. McEuen, and D. C. Ralph, Science **306**, 86 (2004).
[13] S. Sahoo, T. Kontos, J. Furer, C. Hoffmann, M. Gräber, A. Cottet, and C. Schönenberger, Nat. Phys. **1**, 99 (2005).
[14] J. Barnaś and A. Fert, Phys. Rev. Lett. **80**, 1058 (1998).
[15] S. Takahashi and S. Maekawa, Phys. Rev. Lett. **80**, 1758 (1998).
[16] K. Majumdar and S. Hershfield, Phys. Rev. B **57**, 11521 (1998).
[17] A. N. Korotkov and V. I. Safarov, Phys. Rev. B **59**, 89 (1999).
[18] A. Brataas, Yu. V. Nazarov, J. Inoue, and G. E. W. Bauer, Eur. Phys. J. B **9**, 421 (1999).
[19] A. Brataas and X. H. Wang, Phys. Rev. B **64**, 104434 (2001).
[20] I. Weymann, J. König, J. Martinek, J. Barnaś, and G. Schön, Phys. Rev. B **72**, 115334 (2005).
[21] L. Y. Gorelik, S. I. Kulinich, R. I. Shekhter, M. Jonson, and V. M. Vinokur, Phys. Rev. Lett. **95**, 116806 (2005).
[22] A. Cottet and M.-S. Choi, Phys. Rev. B **74**, 235316 (2006).
[23] J. Fransson, Nanotechnology **17**, 5344 (2006).
[24] I. Weymann, Phys. Rev. B **75**, 195339 (2007).
[25] L. Balents and R. Egger, Phys. Rev. B **64**, 035310 (2001).
[26] C. Bena and L. Balents, Phys. Rev. B **65**, 115108 (2002).
[27] J. N. Pedersen, J. Q. Thomassen, and K. Flensberg, Phys. Rev. B **72**, 045341 (2005).
[28] W. Wetzels, G. E. W. Bauer, and M. Grifoni, Phys. Rev. B **72**, 020407(R) (2005); **74**, 224406 (2006).
[29] N. Sergueev, Qing-Feng Sun, Hong Guo, B. G. Wang, and Jian Wang, Phys. Rev. B **65**, 165303 (2002).
[30] J. König and J. Martinek, Phys. Rev. Lett. **90**, 166602 (2003); M. Braun, J. König, and J. Martinek, Phys. Rev. B **70**, 195345 (2004); J. König, J. Martinek, J. Barnaś, and G. Schön, in *CFN Lectures on Functional Nanostructures*, Lecture Notes in Physics Vol. 658, edited by K. Busch, A. Powell, C. Röthig, G. Schön, and J. Weissmüller (Springer, New York, 2005), pp. 145–164.
[31] W. Rudziński, J. Barnaś, R. Świrkowicz, and M. Wilczyński, Phys. Rev. B **71**, 205307 (2005).
[32] J. Fransson, Europhys. Lett. **70**, 796 (2005).
[33] S. Braig and P. W. Brouwer, Phys. Rev. B **71**, 195324 (2005).
[34] I. Weymann and J. Barnaś, Eur. Phys. J. B **46**, 289 (2005).
[35] H.-F. Mu, G. Su, and Q.-R. Zheng, Phys. Rev. B **73**, 054414 (2006).
[36] I. Weymann and J. Barnaś, Phys. Rev. B **75**, 155308 (2007).
[37] O. Parcollet and X. Waintal, Phys. Rev. B **73**, 144420 (2006).
[38] S. Koller, L. Mayrhofer, and M. Grifoni, New J. Phys. **9**, 348 (2007).
[39] A. Brataas, Yu. V. Nazarov, and G. E. W. Bauer, Phys. Rev. Lett. **84**, 2481 (2000); A. Brataas, Y. V. Nazarov, and G. E. W. Bauer, Eur. Phys. J. B **22**, 99 (2001); A. Brataas, G. E. W. Bauer, and P. J. Kelly, Phys. Rep. **427**, 157 (2006).
[40] M. D. Stiles and A. Zangwill, Phys. Rev. B **66**, 014407 (2002).

[41] A. A. Tulapurkar, Y. Suzuki, A. Fukushima, H. Kubota, H. Maehara, K. Tsunekawa, D. D. Djayaprawira, N. Watanabe, and S. Yuasa, Nature (London) **438**, 339 (2005).
[42] A. Cottet, T. Kontos, W. Belzig, C. Schönenberger, and C. Bruder, Europhys. Lett. **74**, 320 (2006).
[43] W. G. van der Wiel, S. De Franceschi, J. M. Elzerman, T. Fujisawa, S. Tarucha, and L. P. Kouwenhoven, Rev. Mod. Phys. **75**, 1 (2002).
[44] M. R. Gräber, W. A. Coish, C. Hoffmann, M. Weiss, J. Furer, S. Oberholzer, D. Loss, and C. Schönenberger, Phys. Rev. B **74**, 075427 (2006).
[45] D. Loss and D. P. DiVincenzo, Phys. Rev. A **57**, 120 (1998).
[46] K. Ono, D. G. Austing, Y. Tokura, and S. Tarucha, Science **297**, 1313 (2002).
[47] H. W. Liu, T. Fujisawa, T. Hayashi, and Y. Hirayama, Phys. Rev. B **72**, 161305(R) (2005).
[48] A. C. Johnson, J. R. Petta, C. M. Marcus, M. P. Hanson, and A. C. Gossard, Phys. Rev. B **72**, 165308 (2005).
[49] J. Fransson and M. Råsander, Phys. Rev. B **73**, 205333 (2006).
[50] Y. Tanaka and N. Kawakami, J. Phys. Soc. Jpn. **73**, 2795 (2004).
[51] J. König, H. Schoeller, and G. Schön, Phys. Rev. Lett. **76**, 1715 (1996).
[52] B. R. Bułka and T. Kostyrko, Phys. Rev. B **70**, 205333 (2004).
[53] K. Blum, *Density Matrix Theory and Its Applications*, 2nd ed. (Plenum, New York, 1996).

PHYSICAL REVIEW B **77**, 201406(R) (2008)

Symmetry fingerprints of a benzene single-electron transistor: Interplay between Coulomb interaction and orbital symmetry

Georg Begemann, Dana Darau, Andrea Donarini, and Milena Grifoni
Theoretische Physik, Universität Regensburg, 93040 Regensburg, Germany
(Received 18 April 2008; published 29 May 2008)

The interplay between Coulomb interaction and orbital symmetry produces specific transport characteristics in molecular single electron transistors (SETs) that can be considered as the fingerprints of the contacted molecule. Specifically we predict, for a benzene SET, selective conductance suppression and the appearance of negative differential conductance when changing the contacts from para to meta configuration. Both effects originate from destructive interference in transport involving states with *orbital degeneracy*.

DOI: 10.1103/PhysRevB.77.201406 PACS number(s): 85.65.+h, 73.63.−b

Understanding the conduction characteristics through single molecules is one of the crucial issues in molecular electronics.[1] The dynamics of the electron transfer to and from the molecule depends on the intrinsic electronic spectrum of the molecule as well as on the electronic coupling of the molecule to its surroundings.

In recent years, the measurement of stability diagrams of single electron transistor (SET) devices has become a very powerful tool to do spectroscopy of small conducting systems via transport experiments. Thus the capability to perform three terminal measurements on single molecules[2–10] has been a fundamental achievement for molecular electronics. Such molecular transistors might display transport properties that are very different from those of conventional SETs. In fact, vibrational or torsional modes[7,10] and intrinsic symmetries of the molecule can hinder or favor transport through the SET, visible, e.g., in the absence or presence of specific excitation lines in the stability diagram of the molecular SET, or in negative differential conductance features. Many-body phenomena such as, e.g., the Kondo effect, have been observed as well.[2,3,5,10]

Despite the experimental progress, the theoretical understanding of the properties of single organic molecules coupled to electrodes is far from being satisfactory. On the one hand, numerical approaches to transport based, e.g., on the combination of Green's function methods with density-functional theory have become a standard approach to study transport at the nanoscale.[1] However, this technique is not appropriate for the description of transport through a molecule weakly coupled to leads, due to the crucial role played by the Coulomb interaction in these systems. Hence, in Ref. 11, an electronic structure calculation for a benzene molecule was performed in order to arrive at an effective interacting Hamiltonian for the π orbitals, to be solved to determine the I-V characteristics of a benzene junction.

In this paper, we consider the electronic transport through a benzene SET. Similar to Ref. 11, in order to devise a semiquantitative description, we start from an interacting Hamiltonian of isolated benzene where only the localized p_z orbitals are considered and the ions are assumed to have the same spatial symmetry as the relevant electrons. The Hamiltonian for the isolated molecule possesses $4^6=4096$ eigenstates, to be calculated numerically, and whose symmetries can be established with the help of group theory. Large degeneracies of the electronic states occur. For example, while the six-particle ground state (A_{1g} symmetry) is nondegenerate, there exist four seven-particle ground states due to spin and orbital (E_{2u} symmetry) degeneracy. When coupling the benzene SET to leads in the meta and para configurations (see Fig. 1), these orbital symmetries lead to very different stability diagrams for the two configurations (see Fig. 2). Striking are the selective reduction of conductance (Fig. 3) and the occurrence of negative differential conductance (NDC) features when changing from para to meta configuration. As shown in Fig. 4, the NDC effect occurs due to the formation of a blocking state at certain values of the bias voltage. The blocking is clearly visible by monitoring the position-dependent many-body transition probabilities, which, at given values of the bias voltage, can exhibit nodes at the same position as one of the contacts. NDC for benzene junctions has been predicted also in Ref. 11, but in the para configuration and *only* in the presence of a dissipative electromagnetic bath. In our work, NDC occurs despite the absence of the bath. Both of the effects we predict originate from bias-dependent interference of orbitally degenerate states: coherences, neglected in Ref. 11, are essential to capture interference effects when solving the equations for the benzene's occupation probabilities. Interference phenomena in transport through benzene have been recently discussed also in Refs. 12 and 13. The parameter regime is, however, very different, as both discuss the strong tunneling limit, where Coulomb blockade effects are not relevant.

We start from the total Hamiltonian $H=H_{\text{ben}}+H_{\text{leads}}+H_T$, where the Hamiltonian for benzene reads

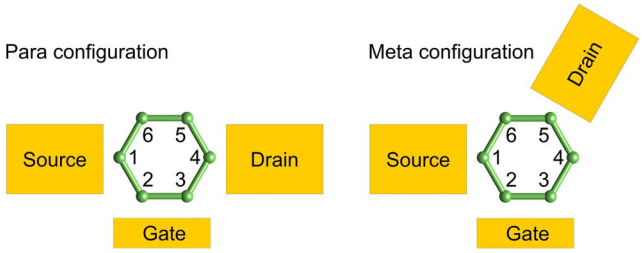

FIG. 1. (Color online) The two different setups for the benzene SET considered in this paper.

$$H_{\text{ben}} = \xi_0 \sum_{i\sigma} d_{i\sigma}^{\dagger} d_{i\sigma} + b \sum_{i\sigma} (d_{i\sigma}^{\dagger} d_{i+1\sigma} + d_{i+1\sigma}^{\dagger} d_{i\sigma}) + U \sum_{i} \left(n_{i\uparrow} - \frac{1}{2} \right) \left(n_{i\downarrow} - \frac{1}{2} \right) + V \sum_{i} (n_{i\uparrow} + n_{i\downarrow} - 1)(n_{i+1\uparrow} + n_{i+1\downarrow} - 1). \quad (1)$$

Here $d_{i\sigma}^{\dagger}$ creates an electron of spin σ in the p_z orbital of carbon i, $i=1,\ldots,6$ runs over the six carbon atoms of benzene and $n_{i\sigma}=d_{i\sigma}^{\dagger}d_{i\sigma}$. This Hamiltonian respects the D_{6h} symmetry of benzene and also the particle-hole symmetry. Mechanical oscillations at this level are neglected and all the atoms are considered in their equilibrium position. The parameters b, U, and V for isolated benzene are given in the literature[14] and are chosen to fit excitation spectra. Even if the presence of metallic electrodes is expected to cause a substantial renormalization of U and V, we do not expect the main results of this work to be affected by this change. The weak coupling suggests that the symmetry of the molecule will remain unchanged and with it the structure of the Hamiltonian (1). The gate voltage V_g is introduced by a renormalized on-site energy $\xi=\xi_0-eV_g$ and we conventionally set $V_g=0$ at the charge-neutrality point. We represent source and drain leads as two resevoirs of noninteracting electrons: $H_{\text{leads}}=\Sigma_{\alpha k\sigma}(\epsilon_k-\mu_\alpha)c_{\alpha k\sigma}^{\dagger}c_{\alpha k\sigma}$, where $\alpha=L,R$ and the chemical potentials μ_α of the leads depend on the applied bias voltage $\mu_{L,R}=\mu_0\pm\frac{V_b}{2}$. In the following, we will measure the energy starting from the equilibrium chemical potential $\mu_0=0$. The coupling to source and drain leads is described by

$$H_T = t \sum_{\alpha k\sigma} (d_{\alpha\sigma}^{\dagger} c_{\alpha k\sigma} + c_{\alpha k\sigma}^{\dagger} d_{\alpha\sigma}), \quad (2)$$

where we define $d_{\alpha\sigma}^{\dagger}$ as the creator of the electron in the benzene carbon atom that is closest to the lead α. In particular, $d_{R\sigma}^{\dagger}:=d_{4\sigma}^{\dagger},d_{5\sigma}^{\dagger}$ in the para and meta configurations, respectively, while $d_{L\sigma}^{\dagger}:=d_{1\sigma}^{\dagger}$ in both setups. Due to the weak coupling to the leads, we can assume that the potential drop is all concentrated at the lead-molecule interface and is not affecting the molecule itself. Given the high degeneracy of the spectrum, the method of choice to treat the dynamics in the weak coupling is the Liouville equation method already used, e.g., in Refs. 15 and 16. The starting point is the Liouville equation for the reduced density operator $\dot{\sigma}=\text{Tr}_{\text{leads}}\{\dot{\rho}\}=-\frac{i}{\hbar}\text{Tr}_{\text{leads}}\{[H,\rho]\}$, where ρ is the density operator.[17] Due to the weak coupling to the leads, we treat the effects of H_T to the lowest nonvanishing order. The reduced density operator σ is defined on the Fock space of benzene, but coherences between states with different particle number and different energy can be neglected, the former because they are decoupled from the dynamics of the populations, the latter being irrelevant due to their fast fluctuation (secular approximation). As a result, we arrive at a generalized master equation (GME) where coherences between degenerate states are retained. This approach is robust against the small asymmetries introduced in the molecule by the coupling to the leads or by deformation as far as the energy splitting that lifts the orbital degeneracy is comparable to the thermal energy. In particular, the results presented in this paper are robust against the residual potential drop that even in weak coupling could affect the molecule itself. The GME is conveniently expressed in terms of the reduced density operator $\sigma^{NE}=\mathcal{P}_{NE}\sigma\mathcal{P}_{NE}$, where $\mathcal{P}_{NE}:=\Sigma_{\ell\tau}|NE\ell\tau\rangle\langle NE\ell\tau|$ is the projection operator on the subspace of N particles and energy E. The sum runs over the orbital and spin quantum numbers ℓ and τ, respectively. Eventually the GME reads

$$\dot{\sigma}^{NE} = -\sum_{\alpha\tau} \frac{\Gamma_\alpha}{2} \Big\{ d_{\alpha\tau} \Big[f_\alpha^{+}(H_{\text{ben}}-E) + \frac{i}{\pi} p_\alpha(H_{\text{ben}}-E) \Big] d_{\alpha\tau}^{\dagger} \sigma^{NE} + d_{\alpha\tau}^{\dagger} \Big[f_\alpha^{-}(E-H_{\text{ben}}) - \frac{i}{\pi} p_\alpha(E-H_{\text{ben}}) \Big] d_{\alpha\tau} \sigma^{NE} + \text{H.c.} \Big\} + \sum_{\alpha\tau E'} \Gamma_\alpha \mathcal{P}_{NE} \{ d_{\alpha\tau}^{\dagger} f_\alpha^{+}(E-E') \sigma^{N-1E'} d_{\alpha\tau} + d_{\alpha\tau} f_\alpha^{-}(E'-E) \sigma^{N+1E'} d_{\alpha\tau}^{\dagger} \} \mathcal{P}_{NE}, \quad (3)$$

where $\Gamma_{L,R}=\frac{2\pi}{\hbar}|t_{L,R}|^2\mathcal{D}_{L,R}$ is the bare transfer rates with the constant densities of states of the leads $\mathcal{D}_{L,R}$.

Terms describing sequential tunneling from and to the lead α are proportional to the Fermi function $f(x-\mu_\alpha):=f_\alpha^{+}(x)$ and $f_\alpha^{-}(x)=1-f_\alpha^{+}(x)$, respectively. Still in the sequential tunneling limit, but due to the presence of coherences, also energy nonconserving terms appear in the generalized master equation; they are proportional to the function $p_\alpha(x)=-\text{Re}\psi[\frac{1}{2}+\frac{i\beta}{2\pi}(x-\mu_\alpha)]$, where ψ is the digamma function.[16,17] Finally, we write the GME on the basis of the energy eigenstates for isolated benzene and find numerically the stationary solution.

A closer analysis of the master equation allows us also to define a current operator (one per molecule-lead contact)

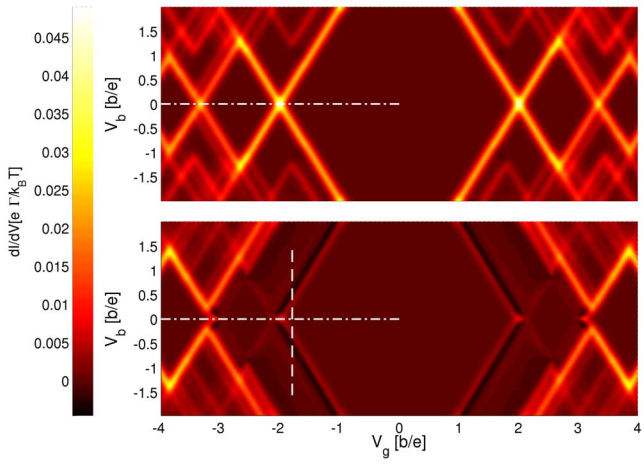

FIG. 2. (Color online) Stability diagram for the benzene SET connected in the para (above) and meta (below) configuration. White dot-dashed lines highlight the conductance cuts presented in Fig. 3; the white dashed line shows the region corresponding to the current trace presented in Fig. 4. The parameters used are $U=4|b|$, $V=2.4|b|$, $T=0.04|b|$, and $\Gamma=10^{-3}|b|$.

$$\hat{I}_\alpha = \sum_{NE\tau} \mathcal{P}_{NE}[d_{\alpha\tau} f_\alpha^+(H_{\text{ben}} - E) d^\dagger_{\alpha\tau} - d^\dagger_{\alpha\tau} f_\alpha^-(E - H_{\text{ben}}) d_{\alpha\tau}]\mathcal{P}_{NE} \tag{4}$$

and calculate the stationary current as the average $I_L = \text{Tr}\{\sigma_{\text{stat}} \hat{I}_L\} = -I_R$, with σ_{stat} the stationary density operator. In Fig. 2, we present the stability diagram for the benzene SET contacted in the para (upper panel) and meta position (lower panel). Bright ground-state transition lines delimit diamonds of zero differential conductance typical of the Coulomb blockade regime while a rich pattern of satellite lines represents the transitions between excited states. Though several differences can be noticed, most striking are the suppression of conductance and the appearance of NDC when passing from para to meta configuration.

A zero bias cut of the stability diagrams as a function of the gate voltage V_g is plotted in Fig. 3. Only transitions between lowest energy states are relevant for the conductance. The number of p_z electrons on the molecule and the symmetry of the many-body state corresponding to the conductance valleys are reported. The conductance in the meta and para configuration is the same for the $N=11 \leftrightarrow 12$ and $N=10 \leftrightarrow 11$ transitions, while it is systematically suppressed in all other cases. In other terms, transitions between states with A or B symmetry, which do not have orbital degeneracy, are invariant under configuration change; transitions that involve *both* of the orbitally degenerate E symmetry states are suppressed. *Destructive interference* between orbitally degenerate states explains the systematic conductance suppression. The eight-particle ground state is antisymmetric[11] (with respect to the plane through the contact atoms and perpendicular to the molecular plane), thus excluded from transport in the para configuration and replaced by the first excited symmetric E_{2g} state. This explains the peculiar position of the 7-8 and 8-9 resonances. By neglecting the energy nonconserving terms in Eq. (3), we derived an analytical formula for the conductance close to the resonance between N and $N+1$ particle states,

$$G_{N,N+1}(\Delta E) = 2e^2 \frac{\Gamma_L \Gamma_R}{\Gamma_L + \Gamma_R} \frac{\left|\sum_{nm\tau} \langle N,n|d_{L\tau}|N+1,m\rangle\langle N+1,m|d^\dagger_{R\tau}|N,n\rangle\right|^2}{\sum_{nm\alpha\tau} |\langle N,n|d_{\alpha\tau}|N+1,m\rangle|^2} \times \left[-\frac{f'(\Delta E)}{(S_{N+1} - S_N) f(\Delta E) + S_N}\right], \tag{5}$$

where $\Delta E = E_{g,N} - E_{g,N+1} + eV_g$ is the energy difference between the benzene ground states with N and $N+1$ electrons diminished by a term linear in the side gate; n and m label the S_N-fold and S_{N+1}-fold degenerate ground states with N and $N+1$ particles, respectively. Interference effects are contained in the numerator of the third factor (overlap factor Λ). In order to make these more visible, we remind the reader that $d^\dagger_{R\tau} = \mathcal{R}^\dagger_\phi d^\dagger_{L\tau} \mathcal{R}_\phi$, where $\mathcal{R}_\phi$ is the rotation operator of an angle ϕ and $\phi = \pi$ for the para while $\phi = 2\pi/3$ forthe meta configuration. All eigenstates of H_{ben} are eigenstates of the discrete rotation operators with angles multiples of $\pi/3$ and the eigenvalues are phase factors. The overlap factor now reads

$$\Lambda = \left|\sum_{nm\tau} |\langle N,n|d_{L\tau}|N+1,m\rangle|^2 e^{i\phi_{nm}}\right|^2, \tag{6}$$

where ϕ_{nm} encloses the phase factors coming from the rotation of the states $|N,n\rangle$ and $|N+1,m\rangle$. Interference is possible only when S_N or $S_{N+1} > 1$, that is, in the presence of degenerate states. It generates a considerable reduction by passing

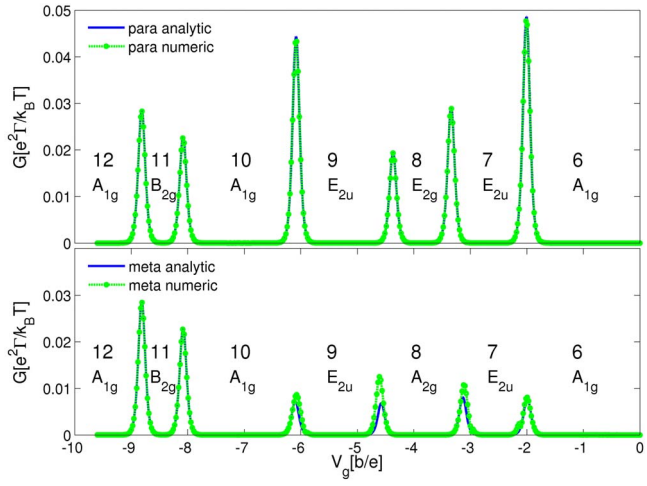

FIG. 3. (Color online) Conductance of the benzene SET as a function of the gate voltage in the para (above) and meta (below) configurations. In the low conductance valleys, the state of the system has a definite number of particles and symmetry as indicated. Selective conductance suppression when changing from the meta to the para configuration is observed.

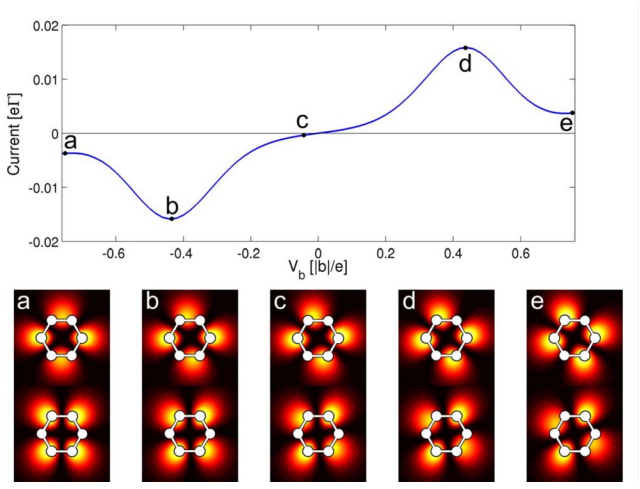

FIG. 4. (Color online) Upper panel: Current through the benzene SET in the meta configuration calculated at bias and gate voltage conditions indicated by the dashed line of Fig. 2. A pronounced NDC is visible. Lower panels: Transition probabilities between the six-particle and each of the two seven-particle ground states for bias voltage values labeled $a-e$ in the upper panel. The transitions to a blocking state are visible in the upper (lower) part of the e (a) panels.

from the para to the meta configuration, as seen in Fig. 3.

Interference also affects nonlinear transport and produces in the meta configuration NDC at the border of the six-particle state diamond (Fig. 2). The upper panel of Fig. 4 shows the current through the benzene SET contacted in the meta configuration as a function of the bias voltage. The current is given for parameters corresponding to the white dashed line of Fig. 2. In this region, only the six- and seven-particle ground states are populated. The six-particle ground state is not degenerate. The seven-particle ground state is fourfold degenerate, although the twofold spin degeneracy is not important since spin coherences vanish in the stationary limit and the $S_z=\frac{1}{2}$ and $-\frac{1}{2}$ density matrices are equal for symmetry. At low bias, the six-particle state is mainly occupied. As the bias is raised, transitions $6\leftrightarrow 7$ occur and current flows. Above a certain bias threshold, a blocking state is populated and the current is reduced. To visualize this, we introduce the probability (averaged over the z coordinate and the spin σ)

$$P(x,y;\ell\ \tau)=\lim_{L\to\infty}\sum_{\sigma}\frac{1}{2L}\int_{-L/2}^{L/2}\mathrm{d}z\left|\langle 7g\ \ell\ \tau|\psi_{\sigma}^{\dagger}(\vec{r})|6g\rangle\right|^2 \quad (7)$$

for benzene to make a transition between the state $|6g\rangle$ and one of the states $|7g\,\ell\,\tau\rangle$ by adding or removing an electron in position $\vec{r}$ and spin σ. Each of the lower panels of Fig. 4 is a surface plot of $P(x,y;\ell\,\tau)$ for the seven-particle basis that diagonalizes the stationary density matrix at a fixed bias. The upper plot of the e panel describes the transitions to the blocking seven-particle state that accepts electrons from the source lead (close to carbon 1) but cannot release electrons to the drain (close to carbon 5). The energy nonconserving rates prevent the complete efficiency of the blocking by ensuring a slow depopulation of the blocking state. At large negative bias, the blocking scenario is depicted in panel a. We remark that only a description that retains coherences between the degenerate seven-particle ground states correctly captures NDC at both positive and negative bias.

To summarize, we analyzed the transport characteristics of a benzene-based SET. The interplay between Coulomb interaction and orbital symmetry is manifested in a destructive interference involving orbitally degenerate states, leading to selective conductance suppression and negative differential conductance when changing the contacts from para to meta configuration.

We acknowledge financial support from the DFG within the research programs SPP 1243 and SFB 689.

[1] *Introducing Molecular Electronics*, edited by G. Cuniberti, G. Fagas, and K. Richter (Springer, Berlin, 2005).
[2] J. Park, A. N. Pasupathy, J. I. Goldsmith, C. Chang, Yu. Yaish, J. R. Petta, M. Rinkoski, J. P. Sethna, H. D. Abruna, P. L. McEuen, and D. C. Ralph, Nature **417**, 722 (2002).
[3] W. Liang, M. P. Shores, M. Bockrath, J. R. Long, and H. Park, Nature **417**, 725 (2002).
[4] S. Kubatkin, A. Danilov, M. Hjort, J. Cornil, J.-L. Brédas, N. Stuhr-Hansen, P. Hedegård, and T. Bjørnholm, Nature **425**, 698 (2003).
[5] L. H. Yu, Z. K. Keane, J. W. Ciszek, L. Cheng, J. M. Tour, T. Baruah, M. R. Pederson, and D. Natelson, Phys. Rev. Lett. **95**, 256803 (2005).
[6] A. V. Danilov, S. Kubatkin, S. Kafanov, P. Hedegård, N. Stuhr-Hansen, K. Moth-Poulsen, and T. Bjørnholm, Nano Lett. **8**, 1 (2008).
[7] D.-H. Chae, J. F. Berry, S. Jung, F. A. Cotton, C. A. Murillo, and Z. Yao, Nano Lett. **6**, 165 (2006).
[8] M. Poot, E. Osorio, K. O'Neill, J. M. Thijssen, D. Vanmaekelbergh, C. A. van Walree, L. W. Jenneskens, and H. S. J. van der Zant, Nano Lett. **6**, 1031 (2006).
[9] H. B. Heersche, Z. de Groot, J. A. Folk, H. S. J. van der Zant, C. Romeike, M. R. Wegewijs, L. Zobbi, D. Barreca, E. Tondello, and A. Cornia, Phys. Rev. Lett. **96**, 206801 (2006).
[10] E. A. Osorio, K. O'Neill, N. Stuhr-Hansen, O. F. Nielsen, T. Bjørnholm, and H. S. J. van der Zant, Adv. Mater. (Weinheim, Ger.) **19**, 281 (2007).
[11] M. H. Hettler, W. Wenzel, M. R. Wegewijs, and H. Schoeller, Phys. Rev. Lett. **90**, 076805 (2003).
[12] D. V. Cardamone, C. A. Stafford, and S. Mazumdar, Nano Lett. **6**, 2422 (2006).
[13] A. Gagliardi, G. C. Solomon, A. Pecchia, T. Frauenheim, A. Di Carlo, N. S. Hush, and J. R. Reimers, Phys. Rev. B **75**, 174306 (2007).
[14] W. Barford, *Electronic and Optical Properties of Conjugated Polymers* (Clarendon Press, Oxford, 2005).
[15] A. Donarini, M. Grifoni, and K. Richter, Phys. Rev. Lett. **97**, 166801 (2006).
[16] L. Mayrhofer and M. Grifoni, Eur. Phys. J. B **56**, 107 (2007).
[17] K. Blum, *Density Matrix Theory and Applications* (Plenum, New York, 1996).

Interference effects on the transport characteristics of a benzene single-electron transistor

D. Darau, G. Begemann, A. Donarini, and M. Grifoni
Institut für Theoretische Physik, Universität Regensburg, 93035 Regensburg, Germany
(Received 14 October 2008; revised manuscript received 18 February 2009; published 9 June 2009)

Interference effects strongly affect the transport characteristics of a benzene single-electron transistor, and for this reason we call it interference single-electron transistor (I-SET). We focus on the effects of degeneracies between many-body states of the isolated benzene. We show that the particular current blocking and selective conductance suppression occurring in the benzene I-SET are due to *interference* effects between the orbitally degenerate states. Further we study the impact of reduced symmetry due to anchor groups or potential drop over the molecule. We identify in the *quasidegeneracy* of the involved molecular states the necessary condition for the robustness of the results.

DOI: 10.1103/PhysRevB.79.235404 PACS number(s): 85.65.+h, 85.85.+j

I. INTRODUCTION

Molecular electronics, due to perfect reproducibility and versatile chemical tailoring of its basic components, represents one of the most promising answers to the increasing miniaturization demand of information technology. A crucial issue in molecular electronics is thus the understanding of the conduction characteristics through single molecules.[1]

Single-molecule-transport measurements rely on the fabrication of a nanogap between source and drain electrodes and the formation of a stable molecule-electrode contact. Nanogaps are nowadays routinely obtained using different techniques including electromigration,[2–10] mechanical break-junction,[11–14] and scanning tunneling microscopy.[15–17] Also the challenging goal of effectively gating a nanometer-sized molecule in the presence of macroscopic metallic leads has been achieved.[6,14,18]

A stable contact between molecule and leads is commonly realized with the mediation of anchor groups attached to the molecule during its chemical synthesis. Also direct coupling of the molecule to the electric leads, though, has been very recently reported.[13] One of the advantages of the first connecting method is some control over the contact configuration of the molecule[19] and the possibility of designing the strength of the tunneling coupling by choosing specific anchor groups.[6,17,20,21] All previous achievements combined with the experience accumulated with semiconducting and carbon-based single-electron transistors (SETs) allowed in recent years to measure stability diagrams of single-molecule transistor devices thus realizing molecular spectroscopy via transport experiments.[2–10]

Single-molecule transistors display transport properties which are very different from those of conventional single-electron transistors. In fact, vibrational or torsional modes[7,10] and intrinsic symmetries of the molecule can hinder or favor transport through the molecular SET, visible, e.g., in the absence or presence of specific excitation lines in the stability diagram or in negative differential conductance features. Many-body phenomena as, e.g., the Kondo effect, have been observed as well.[2,3,5,10,22]

Despite the experimental progress, the theoretical understanding of the properties of single organic molecules coupled to electrodes is far from being satisfactory. On one hand, numerical approaches to transport based on the combination of Green's-function methods with tight-binding model or density functional theory have become standard in the study of transport at the nanoscale.[1] These methods are appropriate to investigate quantum transport through molecular bridges strongly coupled to leads. In this regime various groups have recently discussed the possibility of observing interference effects,[23–26] e.g., in conjugated monocyclic molecules as benzene or annulene.[23,25] However, for the description of transport through a molecule weakly coupled to leads, other methods are required. In the Coulomb blockade regime, for example, due to the crucial role played by the Coulomb interaction in these systems it is common to resort to a Pauli rate equation[27] or to a generalized master equation for the reduced density matrix (RDM). For example, in the work of Hettler *et al.*,[28] an electronic structure calculation has been performed in order to construct an effective interacting Hamiltonian for the π orbitals of benzene, and the I-V characteristics of the corresponding molecular junction have been calculated within the rate equation approach.

In the presence of degenerate states, however, coherences of the density matrix influence the dynamics and a master equation approach is appropriate.[29–38] Such coherences can give rise to precession effects in spin transport[30,35] or cause interference in a molecular single-electron transistor.[32,35,37] In the present work we wish to generalize the discussion on interference phenomena in a benzene interference SET presented in Ref. 37 to the case in which the perfect degeneracy is broken due, e.g., to contact effects or to the applied external bias. To this extent the master equation used in Ref. 37 will be generalized to treat the case of quasidegenerate states. Conditions for the persistence of interference phenomena are identified. We observe that the effects of quasidegenerate states on transport have been very recently addressed also in Ref. 38. We treat the transport through the benzene I-SET in two different setups, the para and the metaconfiguration, depending on the position of the leads with respect to the benzene molecule (see Fig. 1). Similar to Ref. 28, we start from an interacting Hamiltonian of isolated benzene where only the localized p_z orbitals are considered and the ions are assumed to have the same spatial symmetry as the relevant electrons. We calculate the $4^6=4096$ energy eigenstates of the benzene Hamiltonian numerically.

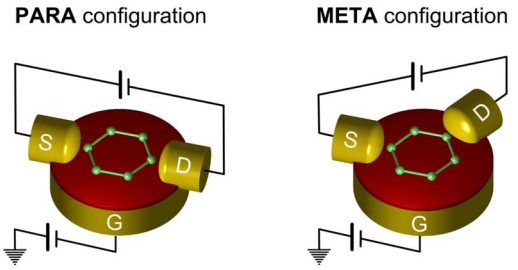

FIG. 1. (Color online) Schematic representation of the two different setups for the benzene I-SET considered in this paper. The molecule, lying on a dielectric substrate, is weakly contacted to source and drain leads as well as capacitively gated.

Subsequently, with the help of group theory, we classify the eigenstates according to their different symmetries and thus give a group-theoretical explanation to the large degeneracies occurring between the electronic states. For example, while the six-particle ground state (A_{1g} symmetry) is nondegenerate, there exist four seven-particle ground states due to spin and orbital (E_{2u} symmetry) degeneracies. Fingerprints of these orbital symmetries are clearly visible in the strong differences in the stability diagrams obtained by coupling the benzene I-SET to the leads in the meta and paraconfiguration. Striking are the selective reduction conductance and the appearance of regions of interference-driven current blocking with associated negative differential conductance (NDC) when changing from the para to the metaconfiguration.

NDC and current blocking for benzene junctions have been predicted in Ref. 28 but also in the paraconfiguration *and* in the presence of an external electromagnetic field. In our work NDC occurs despite the absence of an external field in the unperturbed setup and with no asymmetry in the tunneling rates. In fact, NDC and current blocking triggered by interference take place any time a SET presents an N-particle nondegenerate state and two degenerate $N+1$-particle states such that the ratio between the transition *amplitudes* $\gamma_{i\alpha}$ ($i=1,2$, $\alpha=L,R$) between those N- and $N+1$-particle states is different for tunneling at the left (L) and at the right (R) lead,

$$\frac{\gamma_{1\mathrm{L}}}{\gamma_{2\mathrm{L}}} \neq \frac{\gamma_{1\mathrm{R}}}{\gamma_{2\mathrm{R}}}. \tag{1}$$

Notice that no asymmetry in the tunneling *rates*, which are proportional to $|\gamma_{i\alpha}|^2$, is implied by Eq. (1). This fact excludes the interpretation of the physics of the interference-SET in terms of standard NDC with asymmetric couplings. Due to condition (1) there exist linear combinations of the degenerate $N+1$-particle states which are coupled to one of the leads but *not* to the other. The state that is decoupled from the right lead represents a blocking state for the current flowing $L\rightarrow R$ since electrons can populate this state by tunneling from the left lead but cannot tunnel out toward the right lead. Vice versa the state decoupled from the left lead is a blocking state for the current $R\rightarrow L$. Typically these two blocking states are not orthogonal and thus cannot form together a valid basis set. The basis set that diagonalizes the stationary density matrix (what we call in the manuscript as the "physical basis") contains at large positive biases the $L\rightarrow R$ blocking state and is thus different from the physical basis at large negative biases which necessarily contains the $R\rightarrow L$ blocking state. More generally the "physical basis" *depends continuously* on the bias. Thus only a treatment that includes coherences in the density matrix can capture the full picture at all biases. By neglecting for simplicity the spin degree of freedom, the seven-particle ground state of benzene is two times degenerate while the six-particle one is nondegenerate. If we choose for the seven-particle states the eigenstates of the z projection of the angular momentum we obtain the relation

$$\frac{\gamma_{1\mathrm{L}}}{\gamma_{2\mathrm{L}}} = \frac{\gamma_{1\mathrm{R}}}{\gamma_{2\mathrm{R}}} e^{4i\phi}, \tag{2}$$

where ϕ is the angle between the left and the right leads. Thus in the metaconfiguration ($\phi=2\pi/3$) condition (1) is fulfilled, while in the paraconfiguration ($\phi=\pi$) the amplitude ratios are equal. This condition implies that in the paraconfiguration one of the seven-particle states is decoupled from *both* leads at the same time and can thus (in first approximation) be excluded from the dynamics. In contrast, in the metaconfiguration, the linear combination of uniformly distributed eigenstates of the angular momentum creates states with a peculiar interference pattern. The position of their nodes allows to characterize them as different blocking states.

This paper is outlined as follows: in Sec. II we introduce the model Hamiltonian of the system and present a density matrix approach setting up a generalized master equation describing the electron dynamics. We give the expression for the current in the fully symmetric setup [the generalized master equation (GME) and the current formula for the setup under perturbation are given in Appendix A]. Further we provide a detailed analysis of the symmetry characteristics of the molecular eigenstates.

In Sec. III we present numerical and analytical results of transport calculations for the unperturbed setup. We study the occurring interference effects and provide an explanation of the phenomena based on symmetry considerations.

In Sec. IV we present the results for the perturbed setup including a detailed discussion of the transport in this case. We identify in the *quasidegeneracy* of the contributing molecular states the necessary condition for the robustness of the interference effects. Conclusions and remarks are presented in Sec. V.

II. MODEL HAMILTONIAN AND DENSITY MATRIX APPROACH

A. Model Hamiltonian

For the description of the benzene molecule weakly coupled to source and drain leads, we adopt the total Hamiltonian $H=H^0_{\mathrm{ben}}+H_{\mathrm{leads}}+H_{\mathrm{T}}+H'_{\mathrm{ben}}$. The first term is the interacting Hamiltonian for isolated benzene,[39–41]

$$H_{\text{ben}}^0 = \xi_0 \sum_{i\sigma} d_{i\sigma}^\dagger d_{i\sigma} + b \sum_{i\sigma} (d_{i\sigma}^\dagger d_{i+1\sigma} + d_{i+1\sigma}^\dagger d_{i\sigma}) + U \sum_i \left(n_{i\uparrow} - \tfrac{1}{2}\right)\left(n_{i\downarrow} - \tfrac{1}{2}\right) + V \sum_i (n_{i\uparrow} + n_{i\downarrow} - 1)(n_{i+1\uparrow} + n_{i+1\downarrow} - 1), \quad (3)$$

where $d_{i\sigma}^\dagger$ creates an electron of spin σ in the p_z orbital of carbon i; $i=1,\ldots,6$ runs over the six carbon atoms of benzene and $n_{i\sigma}=d_{i\sigma}^\dagger d_{i\sigma}$.

Only the p_z orbitals (one per carbon atom) are explicitly taken into account, while the core electrons and the nuclei are combined into frozen ions, with the same spatial symmetry as the relevant electrons. They contribute only to the constant terms of the Hamiltonian and enforce particle-hole symmetry. Mechanical oscillations are neglected, and all atoms are considered at their equilibrium position.

This Hamiltonian for isolated benzene is respecting the D_{6h} symmetry of the molecule. Since for every site there are four different possible configurations $(|0\rangle, |\uparrow\rangle, |\downarrow\rangle, |\uparrow\downarrow\rangle)$, the Fock space has the dimension $4^6=4096$, which requires a numerical treatment. Although the diagonalization of the Hamiltonian is not a numerical challenge, it turns out to be of benefit for the physical understanding of the transport processes to divide H_{ben} into blocks, according to the number N of p_z electrons (from 0 to 12), the z projection S_z of the total spin, and the orbital symmetries of benzene (see Table I).

The parameters b, U, and V for isolated benzene are given in the literature[42] and are chosen to fit optical excitation spectra. The presence of metallic electrodes and the dielectric in the molecular I-SET, is expected to cause a substantial renormalization of U and V.[4,43] Nevertheless, we do not expect the main results of this work to be affected by this change. We consider the benzene molecule weakly coupled to the leads. Thus, to first approximation, we assume the symmetry of the isolated molecule not to be changed by the screening. Perturbations due to the lead-molecule contacts reduce the symmetry in the molecular junction. They are included in H'_{ben} [see Eqs. (24) and (25)] and will be treated in Sec. IV.

The effect of the gate is included as a renormalization of the on-site energy $\xi=\xi_0-eV_g$ (V_g is the gate voltage), and we conventionally set $V_g=0$ at the charge neutrality point. Source and drain leads are two reservoirs of noninteracting electrons: $H_{\text{leads}}=\Sigma_{\alpha k\sigma}(\epsilon_k-\mu_\alpha)c_{\alpha k\sigma}^\dagger c_{\alpha k\sigma}$, where $\alpha=L,R$ stands for the left or right lead and the chemical potentials μ_α of the leads depend on the applied bias voltage $\mu_{L,R}=\mu_0 \pm \frac{V_b}{2}$. In the following we will measure the energy starting from the equilibrium chemical potential $\mu_0=0$. The coupling to source and drain leads is described by the tunneling Hamiltonian

$$H_T = t \sum_{\alpha k\sigma} (d_{\alpha\sigma}^\dagger c_{\alpha k\sigma} + c_{\alpha k\sigma}^\dagger d_{\alpha\sigma}), \quad (4)$$

where we define $d_{\alpha\sigma}^\dagger$ as the creator of an electron in the benzene carbon atom which is closest to the lead α. In particular $d_{R\sigma}^\dagger := d_{4\sigma}^\dagger, d_{5\sigma}^\dagger$, respectively, in the para and metaconfiguration, while $d_{L\sigma}^\dagger := d_{1\sigma}^\dagger$ in both setups.

TABLE I. Overview of the six-particle states of benzene, sorted by S_z and symmetry. Orbitals with A- and B-types of symmetry show no degeneracy, while E-type orbitals are doubly degenerate.

N	No. of ↑	No. of ↓	No. of states	No. of states with a certain symmetry
6	6	0	1	$1\ B_{1u}$
	5	1	36	$4\ A_{1g}$ $2\ A_{2g}$ $2\times 6\ E_{2g}$ $4\ B_{1u}$ $2\ B_{2u}$ $2\times 6\ E_{1u}$
	4	2	225	$16\ A_{1g}$ $20\ A_{2g}$ $2\times 36\ E_{2g}$ $22\ B_{1u}$ $17\ B_{2u}$ $2\times 39\ E_{1u}$
	3	3	400	$38\ A_{1g}$ $30\ A_{2g}$ $2\times 66\ E_{2g}$ $38\ B_{1u}$ $30\ B_{2u}$ $2\times 66\ E_{1u}$
	2	4	225	⋮
	1	5	36	
	0	6	1	

B. Dynamics of the reduced density matrix

Given the high degeneracy of the spectrum, the method of choice to treat the dynamics in the weak coupling is the Liouville equation method already used, e.g., in Refs. 32 and 34. In this section we shortly outline how to derive the equation of motion for the RDM to lowest nonvanishing order in the tunneling Hamiltonian. For more details we refer to Refs. 34 and 35.

Starting point is the Liouville equation for the total density operator of molecule and leads ρ in the interaction picture, treating H_T as a perturbation: $i\hbar\frac{d\rho^I(t)}{dt}=[H_T^I,\rho^I(t)]$. This equation integrated over time and iterated to the second order reads as

$$\dot{\rho}^I(t) = -\frac{i}{\hbar}[H_T^I(t),\rho^I(t_0)] - \frac{1}{\hbar^2}\int_{t_0}^t dt'[H_T^I(t),[H_T^I(t'),\rho^I(t')]]. \quad (5)$$

Since we are only interested in the transport through the molecule, we treat from now on the time evolution of the RDM $\sigma=\text{Tr}_{\text{leads}}\{\rho^I(t)\}$,[44] which is formally obtained from Eq. (5) by tracing out the lead degrees of freedom: $\dot{\sigma}=\text{Tr}_{\text{leads}}\{\dot{\rho}^I\}$.

In order to proceed, we make the following standard approximations:

(i) the leads are considered as reservoirs of noninteracting electrons in thermal equilibrium. Hence we can factorize the density matrix as $\rho^{\mathrm{I}}(t)=\sigma(t)\rho_{\mathrm{s}}\rho_{\mathrm{d}}=\sigma(t)\rho_{\mathrm{leads}}$.

(ii) Since the molecule is weakly coupled to the leads we treat the effects of H_{T} to the lowest nonvanishing order.

(iii) Due to the continuous interaction of the system with the leads and at high enough temperature, it is legitimate to apply the Markov approximation and obtain an equation for $\dot{\sigma}$ which is local in time [$\sigma(t)$ instead of $\sigma(t')$ inside the integral]. In particular the Markov approximation becomes exact in the stationary limit ($t\to\infty$) we will focus on. Since we are interested in the long-term behavior of the system, we set $t_0\to-\infty$ in Eq. (5) and finally obtain the GME,

$$\dot{\sigma}(t)=\frac{-1}{\hbar^2}\int_0^\infty dt''\ \mathrm{Tr}_{\mathrm{leads}}\{[H_{\mathrm{T}}^{\mathrm{I}}(t),[H_{\mathrm{T}}^{\mathrm{I}}(t-t''),\sigma(t)\rho_{\mathrm{leads}}]]\}. \tag{6}$$

The reduced density operator σ is defined on the Fock space of benzene, yet we can neglect coherences between states with different particle number since they are decoupled from the dynamics of the populations. For simplicity, we continue here the derivation of the GME only for the symmetric case with exact orbital degeneracy, i.e., neglecting H'_{ben} (the perturbed case is presented in Appendix A).

(iv) Further we also neglect coherences between states with different energy (secular approximation). They are irrelevant due to their fast fluctuation compared to the dynamics of the system triggered by the tunneling coupling.

Under these considerations, it is convenient to express the GME in terms of the reduced density operator $\sigma^{\mathrm{NE}}=\mathcal{P}_{\mathrm{NE}}\sigma\mathcal{P}_{\mathrm{NE}}$, where $\mathcal{P}_{\mathrm{NE}}:=\Sigma_{\ell\tau}|NE\ell\tau\rangle\langle NE\ell\tau|$ is the projection operator on the subspace of N particles and energy E. The sum runs over the orbital and spin quantum numbers ℓ and τ, respectively. The orbital quantum number ℓ distinguishes between orbitally degenerate states. The exact meaning of ℓ will be illustrated in the next section. In Appendix A we derive a GME that retains coherences also between quasidegenerate states. That approach treats with special care the small asymmetries introduced in the molecule by the coupling to the leads. In fact it interpolates between the degenerate case treated here and the fully nondegenerate case in which the GME reduces to a master equation for populations only. Equation (6) can be further manipulated by projection into the subspace of N particle and energy E. Since we assume the density matrix to be factorized and the leads to be in thermal equilibrium, also the traces over the leads degree of freedom can be easily performed. Eventually, the GME for the degenerate case reads as

$$\begin{aligned}\dot{\sigma}^{\mathrm{NE}}=&-\sum_{\alpha\tau}\frac{\Gamma_\alpha}{2}\Bigg\{\mathcal{P}_{\mathrm{NE}}d_{\alpha\tau}\left[f_\alpha^+(H_{\mathrm{ben}}^0-E)-\frac{i}{\pi}p_\alpha(H_{\mathrm{ben}}^0-E)\right]d_{\alpha\tau}^\dagger\sigma^{\mathrm{NE}}\\&+\mathcal{P}_{\mathrm{NE}}d_{\alpha\tau}^\dagger\left[f_\alpha^-(E-H_{\mathrm{ben}}^0)-\frac{i}{\pi}p_\alpha(E-H_{\mathrm{ben}}^0)\right]d_{\alpha\tau}\sigma^{\mathrm{NE}}+\mathrm{H.c.}\Bigg\}\\&+\sum_{\alpha\tau\mathrm{E}'}\Gamma_\alpha\mathcal{P}_{\mathrm{NE}}\{d_{\alpha\tau}^\dagger f_\alpha^+(E-E')\sigma^{\mathrm{N-1E}'}d_{\alpha\tau}+d_{\alpha\tau}f_\alpha^-(E'-E)\sigma^{\mathrm{N+1E}'}d_{\alpha\tau}^\dagger\}\mathcal{P}_{\mathrm{NE}},\end{aligned} \tag{7}$$

where $\Gamma_{\mathrm{L,R}}=\frac{2\pi}{\hbar}|t_{\mathrm{L,R}}|^2\mathcal{D}_{\mathrm{L,R}}$ are the bare transfer rates with the constant densities of states of the leads $\mathcal{D}_{\mathrm{L,R}}$. Terms describing sequential tunneling from and to the lead α are proportional to the Fermi functions $f_\alpha^+(x):=f(x-\mu_\alpha)$ and $f_\alpha^-(x):=1-f_\alpha^+(x)$, respectively. Still in the sequential tunneling limit, but only in the equations for the coherences, one finds also the energy nonconserving terms, proportional to the function $p_\alpha(x)=-\mathrm{Re}\ \psi[\frac{1}{2}+\frac{i\beta}{2\pi}(x-\mu_\alpha)]$, where ψ is the digamma function. Both the Fermi functions and the digamma function result from the trace over the lead degrees of freedom.[30,34,44]

A closer analysis of the master equation allows also the formulation of an expression for the current operator. We start from the definition of the time derivative of the charge on benzene,

$$\frac{d}{dt}\langle Q\rangle=\mathrm{Tr}\{\hat{N}\dot{\sigma}\}=\langle I_{\mathrm{L}}+I_{\mathrm{R}}\rangle, \tag{8}$$

where $Q=\Sigma_{i\tau}(d_{i\tau}^\dagger d_{i\tau}-6)$ is the operator of the charge on benzene, $\hat{N}$ is the particle number operator, and $I_{\mathrm{L,R}}$ are the current operators at the left (right) contact. Conventionally, in the definition of $I_{\mathrm{L,R}}$ we assume the current to be positive when it is increasing the charge on the molecule. Thus, in the stationary limit, $\langle I_{\mathrm{L}}+I_{\mathrm{R}}\rangle$ is zero. We write this expression in the basis of the subspaces of N particles and energy E,

$$\langle I_{\mathrm{L}}+I_{\mathrm{R}}\rangle=\sum_{\mathrm{NE}}\mathrm{Tr}\{\hat{N}\mathcal{P}_{\mathrm{NE}}\dot{\sigma}\mathcal{P}_{\mathrm{NE}}\}=\sum_{\mathrm{NE}}\mathrm{Tr}\{N\dot{\sigma}^{\mathrm{NE}}\}. \tag{9}$$

Further we insert Eq. (7) in Eq. (9) and take advantage of the cyclic properties of the trace to find

$$\langle I_L + I_R \rangle = \sum_{NE} \sum_{\alpha\tau} N\Gamma_\alpha \, \mathrm{Tr}\Big\{ -[f_\alpha^+(H_{ben}^0 - E) d_{\alpha\tau}^\dagger \sigma^{NE} d_{\alpha\tau} + f_\alpha^-(E - H_{ben}^0) d_{\alpha\tau} \sigma^{NE} d_{\alpha\tau}^\dagger] + \sum_{E'} \mathcal{P}_{NE}[f_\alpha^+(E - E') \times d_{\alpha\tau}^\dagger \sigma^{N-1E'} d_{\alpha\tau} + f_\alpha^-(E' - E) d_{\alpha\tau} \sigma^{N+1E'} d_{\alpha\tau}^\dagger] \Big\}. \tag{10}$$

Notice that the energy nonconserving contributions drop from the expression of the current. Still they contribute to the average current via the density matrix. Since E and E' are dummy variables, we can switch them in the summands containing E'. Applying the relation

$$\sum_{NE'} \mathrm{Tr}\{\mathcal{P}_{NE'} g(E')\} = \mathrm{Tr}\{g(H_{ben}^0)\},$$

where $g(E')$ is a generic function, we substitute E' with H_{ben}^0 in Eq. (10). Further we can conveniently rearrange the sum over N, arriving at the expression for the current,

$$\langle I_L + I_R \rangle = \sum_{NE} \sum_{\alpha\tau} \Gamma_\alpha \, \mathrm{Tr} \{ d_{\alpha\tau}^\dagger \sigma^{NE} d_{\alpha\tau} [-N f_\alpha^+(H_{ben}^0 - E) + (N+1) f_\alpha^+(H_{ben}^0 - E)] + d_{\alpha\tau} \sigma^{NE} d_{\alpha\tau}^\dagger [-N f_\alpha^-(E - H_{ben}^0) + (N-1) f_\alpha^-(E - H_{ben}^0)] \}. \tag{11}$$

This relation can be further simplified in order to identify the current operators. The one corresponding to the left contact is, e.g.,

$$I_L = \Gamma_L \sum_{NE\tau} \mathcal{P}_{NE}[d_{L\tau} f_L^+(H_{ben}^0 - E) d_{L\tau}^\dagger + - d_{L\tau}^\dagger f_L^-(E - H_{ben}^0) d_{L\tau}] \mathcal{P}_{NE}. \tag{12}$$

With this relation we can calculate the stationary current as the average $\langle I_L \rangle = \mathrm{Tr}\{\sigma_{stat} I_L\} = -\langle I_R \rangle$, with σ_{stat} as the stationary density operator. The expression of the current operator for the perturbed system is given in Appendix A.

C. Symmetry of the benzene eigenstates

In this section, we will review the symmetry characteristics of the eigenstates of the interacting Hamiltonian of benzene, focusing on the symmetry operations σ_v and C_n which have a major impact on the electronic transport through the molecular I-SET. Benzene belongs to the D_{6h} point group. Depending on their behavior under symmetry operations, one can classify the molecular orbitals by their belonging to a certain irreducible representation of the point group.

Table I shows an overview of the states of the neutral molecule (the six-particle states) sorted by S_z and symmetries. The eigenstates of the interacting benzene molecule have either A-, B-, or E-type symmetries. While orbitals having A or B symmetries can only be spin degenerate, states with an E symmetry show an additional twofold orbital degeneracy, essential for the explanation of the transport features occurring in the metaconfiguration.

TABLE II. Degeneracy, energy, and symmetry of the ground states of the isolated benzene molecule for different particle numbers. We choose the on-site and intersite Coulomb interactions to be $U=10$ eV and $V=6$ eV, and the hopping to be $b=-2.5$ eV. Notice, however, that screening effects from the leads and the dielectric are expected to renormalize the energy of the benzene many-body states.

N	Degeneracy	Energy(at $\xi=0$) [eV]	Symmetry	Symmetry behavior under σ_v
0	1	0	A_{1g}	sym
1	2	−22	A_{2u}	sym
2	1	−42.25	A_{1g}	sym
3	4	−57.42	E_{1g}	2 sym, [2 antisym]
4	[3]	[−68.87]	$[A_{2g}]$	[antisym]
	2	−68.37	E_{2g}	1 sym, [1 antisym]
5	4	−76.675	E_{1g}	2 sym, [2 antisym]
6	1	−81.725	A_{1g}	sym
7	4	−76.675	E_{2u}	2 sym, [2 antisym]
8	[3]	[−68.87]	$[A_{2g}]$	[antisym]
	2	−68.37	E_{2g}	1 sym, [1 antisym]
9	4	−57.42	E_{2u}	2 sym, [2 antisym]
10	1	−42.25	A_{1g}	sym
11	2	−22	B_{2g}	sym
12	1	0	A_{1g}	sym

Transport at low bias is described in terms of transitions between ground states with different particle number. Table II shows the symmetries of the ground states (and of some first excited states) of interacting benzene for all possible particle numbers. Ground-state transitions occur both between orbitally nondegenerate states (with A and B symmetries), as well as between orbitally degenerate and nondegenerate states (E- to A-type states).

The interacting benzene Hamiltonian commutes with all the symmetry operations of the D_{6h} point group; thus, it has a set of common eigenvectors with each operation. The element of D_{6h} of special interest for the *para*configuration is σ_v, i.e., the reflection about the plane through the contact atoms and perpendicular to the molecular plane. The molecular orbitals with A and B symmetries are eigenstates of σ_v with eigenvalue of ± 1; i.e., they are either symmetric or antisymmetric with respect to the σ_v operation. The behavior of the E-type orbitals under σ_v is basis dependent, yet one can always choose a basis in which one orbital is symmetric and the other one antisymmetric.

Let us now consider the generic transition amplitude $\langle N | d_{\alpha\tau} | N+1 \rangle$, where $d_{\alpha\tau}$ destroys an electron of spin τ on the contact atom closest to the α lead. It is useful to rewrite this amplitude in the form

$$\langle N | d_{\alpha\tau} | N+1 \rangle = \langle N | \sigma_v^\dagger \sigma_v d_{\alpha\tau} \sigma_v^\dagger \sigma_v | N+1 \rangle, \tag{13}$$

where we have used the property $\sigma_v^\dagger \sigma_v = 1$. Since in the para-configuration both contact atoms lie in the mirror plane σ_v, it

follows that $\sigma_v d_\alpha \sigma_v^\dagger = d_\alpha$. If the participating states are both symmetric or both antisymmetric under σ_v, Eq. (13) is trivial. For states with different symmetry it is

$$\langle N, \mathrm{sym}|d_{\alpha\tau}|N+1, \mathrm{antisym}\rangle = -\langle N, \mathrm{sym}|d_{\alpha\tau}|N+1, \mathrm{antisym}\rangle, \tag{14}$$

implying that the matrix element vanishes. In other terms, there is a selection rule that forbids transitions between symmetric and antisymmetric states. Further, since the ground state of the neutral molecule is symmetric, for the transport calculations in the paraconfiguration we select the effective Hilbert space containing only states symmetric with respect to σ_v. Correspondingly, when referring to the N-particle ground state we mean the energetically lowest *symmetric* state. For example, in the case of four- and eight-particle states it is the first excited state to be the *effective* ground state. In the paraconfiguration also the orbital degeneracy of the E-type states is effectively cancelled due to the selection of the symmetric orbital (see Table II).

Small violations of this selection rule, due, e.g., to molecular vibrations or coupling to an electromagnetic bath, result in the weak connection of different metastable electronic subspaces. We suggest this mechanism as a possible explanation for the switching and hysteretic behavior reported in various molecular junctions. This effect is not addressed in this work.

For a simpler analysis of the different transport characteristics it is useful to introduce a unified geometrical description of the two configurations. In both cases, one lead is rotated by an angle ϕ with respect to the position of the other lead. Hence we can write the creator of an electron in the right contact atom $d_{R\tau}^\dagger$ in terms of the creation operator of the left contact atom and the rotation operator,

$$d_{R\tau}^\dagger = \mathcal{R}_\phi^\dagger d_{L\tau}^\dagger \mathcal{R}_\phi, \tag{15}$$

where $\mathcal{R}_\phi$ is the rotation operator for the anticlockwise rotation of an angle ϕ around the axis perpendicular to the molecular plane and piercing the center of the benzene ring; $\phi = \pi$ for the paraconfiguration and $\phi = (2\pi/3)$ for the metaconfiguration.

The energy eigenstates of the interacting Hamiltonian of benzene can be classified also in terms of their quasiangular momentum. In particular, the eigenstates of the z projection of the quasiangular momentum are the ones that diagonalize all operators $\mathcal{R}_\phi$ with angle multiples of $\pi/3$. The corresponding eigenvalues are phase factors $e^{-i\ell\phi}$ where $\hbar\ell$, the quasiangular momentum of the state, is an integer multiple of $\hbar$. The discrete rotation operator of an angle $\phi = \pi$ (C_2 symmetry operation) is the one relevant for the paraconfiguration. All orbitals are eigenstates of the C_2 rotation with the eigenvalue of ± 1.

The relevant rotation operator for the metaconfiguration corresponds to an angle $\phi = 2\pi/3$ (C_3 symmetry operation). Orbitals with an A or B symmetry are eigenstates of this operator with the eigenvalue of +1 (angular momentum $\ell = 0$ or $\ell = 3$). Hence we can already predict that there will be no difference based on rotational symmetry between the paraconfiguration and the metaconfiguration for transitions between states involving A- and B-type symmetries. Orbitals with E symmetry however behave quite differently under the C_3 operation. They are the pairs of states of angular momenta $\ell = \pm 1$ or $\ell = \pm 2$. The diagonal form of the rotation operator on the twofold degenerate subspace of E symmetry reads as

$$C_3 = \begin{pmatrix} e^{-i|\ell|2\pi/3} & 0 \\ 0 & e^{i|\ell|2\pi/3} \end{pmatrix}. \tag{16}$$

For the twofold orbitally degenerate seven-particle ground states $|\ell| = 2$. This analysis in terms of the quasiangular momentum makes the calculation of the fundamental interference condition [Eq. (2)] given in Sec. I easier. In fact the following relation holds between the transition amplitudes of the six- and seven-particle ground states:

$$\gamma_{\ell R} \equiv \langle 7_g \ell\tau|d_{R\tau}^\dagger|6_g\rangle = \langle 7_g \ell\tau|\mathcal{R}_\phi^\dagger d_{L\tau}^\dagger \mathcal{R}_\phi|6_g\rangle = e^{-i\ell\phi}\gamma_{\ell L}, \tag{17}$$

and Eq. (2) follows directly.

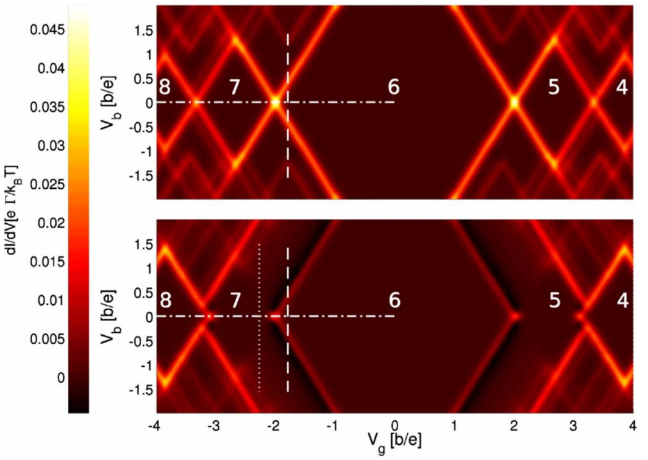

FIG. 2. (Color online) Stability diagram for the benzene I-SET contacted in the para (above) and metaconfiguration (below). Dot-dashed lines highlight the conductance cuts presented in Fig. 3, the dashed lines mark the regions corresponding to the current traces presented in Figs. 4 and 6, and the dotted line is the region corresponding to the current trace presented in Fig. 5. The parameters used are $U = 4|b|$, $V = 2.4|b|$, $k_B T = 0.04|b|$, $\hbar\Gamma_L = \hbar\Gamma_R = 10^{-3}|b|$.

III. TRANSPORT CALCULATIONS: FULLY SYMMETRIC SETUP

With the knowledge of the eigenstates and eigenvalues of the Hamiltonian for the isolated molecule, we implement Eq. (7) and look for a stationary solution. The symmetries of the eigenstates are reflected in the transition amplitudes contained in the GME. We find numerically its stationary solution and calculate the current and the differential conductance of the device. In Fig. 2 we present the stability diagram for the benzene I-SET contacted in the paraconfiguration (upper panel) and metaconfiguration (lower panel). Bright ground-state transition lines delimit diamonds of zero differential conductance typical for the Coulomb blockade regime,

while a rich pattern of satellite lines represents the transitions between excited states. Though several differences can be noticed, most striking are the suppression of the linear conductance, the appearance of negative differential conductance (NDC), and the strong suppression of the current at the right (left) border of the seven- (five-) particle diamond when passing from the para to the metaconfiguration. All these features are different manifestations of the interference between orbitally degenerate states and ultimately reveal the specific symmetry of benzene.

A. Linear conductance

We study the linear transport regime both numerically and analytically. For the analytical calculation of the conductance we consider the low-temperature limit where only ground states with N and $N+1$ particles have considerable occupation probabilities, with N fixed by the gate voltage. Therefore only transitions between these states are relevant and we can treat just the terms of Eq. (7) with N and $N+1$ particles and the ground-state energies $E_{\mathrm{g,N}}$ and $E_{\mathrm{g,N+1}}$, respectively. A closer look at Eq. (7) reveals that the spin coherences are decoupled from the other elements of the density matrix. Thus we can set them to zero, and write Eq. (7) in a block diagonal form on the basis of the ground states of N and $N+1$ particles. Additionally, since the total Hamiltonian H is symmetric in spin, the blocks of the GME with the same particle but different spin quantum number τ must be identical. Finally, since around the resonance the only populated states are the N- and $N+1$-particle states, the conservation of probability implies that

$$1 = \sum_n \sigma_{nn}^{\mathrm{N}} + \sum_m \sigma_{mm}^{\mathrm{N+1}}, \tag{18}$$

where σ_{nn}^{N} is the population of the N-particle ground state and n contains the orbital and spin quantum numbers. With all these observations we can reduce Eq. (7) to a much smaller set of coupled differential equations, which can be treated analytically. The stationary solution of this set of equations can be derived more easily by neglecting the energy nonconserving terms in Eq. (7). These are contained in the elements of the GME describing the dynamics of the coherences between orbitally degenerate states. With this simplification we derive an analytical formula for the conductance close to the resonance between N- and $N+1$-particle states as the first order coefficient of the Taylor series of the current in the bias,

$$G_{\mathrm{N,N+1}}(\Delta E) = 2e^2 \frac{\Gamma_{\mathrm{L}}\Gamma_{\mathrm{R}}}{\Gamma_{\mathrm{L}}+\Gamma_{\mathrm{R}}} \Lambda_{\mathrm{N,N+1}} \times \left[-\frac{S_{\mathrm{N}} S_{\mathrm{N+1}} f'(\Delta E)}{(S_{\mathrm{N+1}} - S_{\mathrm{N}}) f(\Delta E) + S_{\mathrm{N}}} \right], \tag{19}$$

where $\Delta E = E_{\mathrm{g,N}} - E_{\mathrm{g,N+1}} + eV_{\mathrm{g}}$ is the energy difference between the benzene ground states with N and $N+1$ electrons diminished by a term linear in the gate voltage. Interference effects are contained in the overlap factor $\Lambda_{\mathrm{N,N+1}}$,

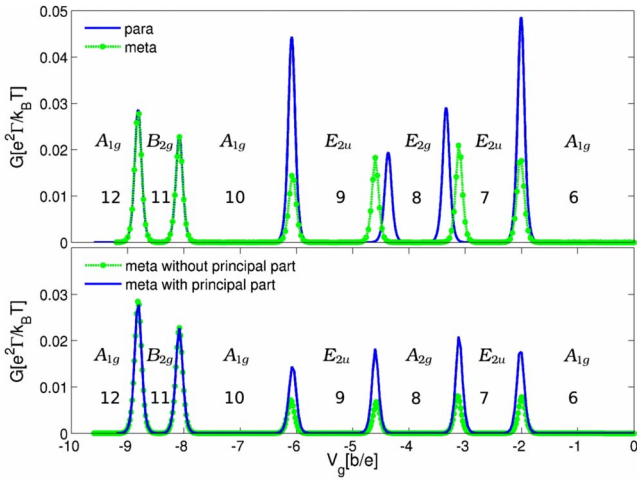

FIG. 3. (Color online) Conductance of the benzene I-SET as a function of the gate voltage. Clearly visible are the peaks corresponding to the transitions between ground states with N and $N+1$ particles. In the low conductance valleys the state of the system has a definite number of particles and symmetry as indicated in the upper panel for the para; in the lower for the metaconfiguration. Selective conductance suppression when changing from the meta to the paraconfiguration is observed.

$$\Lambda_{\mathrm{N,N+1}} = \frac{\left| \sum_{nm\tau} \langle N,n|d_{\mathrm{L}\tau}|N+1,m\rangle\langle N+1,m|d_{\mathrm{R}\tau}^{\dagger}|N,n\rangle \right|^2}{S_{\mathrm{N}} S_{\mathrm{N+1}} \sum_{nm\alpha\tau} |\langle N,n|d_{\alpha\tau}|N+1,m\rangle|^2},$$

where n and m label the S_{N}-fold and $S_{\mathrm{N+1}}$-fold degenerate ground states with N and $N+1$ particles, respectively. In order to make the interference effects more visible we remind that $d_{\mathrm{R}\tau}^{\dagger} = \mathcal{R}_{\phi}^{\dagger} d_{\mathrm{L}\tau}^{\dagger} \mathcal{R}_{\phi}$, with $\phi = \pi$ for the paraconfiguration while $\phi = 2\pi/3$ for the metaconfiguration. Due to the behavior of all eigenstates of H_{ben}^{0} under discrete rotation operators with angles multiples of $\pi/3$, we can rewrite the overlap factor as

$$\Lambda_{\mathrm{N,N+1}} = \frac{\left| \sum_{nm\tau} |\langle N,n|d_{\mathrm{L}\tau}|N+1,m\rangle|^2 e^{i\phi_{nm}} \right|^2}{S_{\mathrm{N}} S_{\mathrm{N+1}} 2 \sum_{nm\tau} |\langle N,n|d_{\mathrm{L}\tau}|N+1,m\rangle|^2}, \tag{20}$$

where ϕ_{nm} encloses the phase factors coming from the rotation of the states $|N,n\rangle$ and $|N+1,m\rangle$.

The energy nonconserving terms neglected in Eq. (19) influence only the dynamics of the coherences between orbitally degenerate states. Thus, Eq. (19) provides an exact description of transport for the paraconfiguration, where orbital degeneracy is cancelled. Even if Eq. (19) captures the essential mechanism responsible for the conductance suppression, we have derived an exact analytical formula also for the metaconfiguration, and we present it in Appendix B.

In Fig. 3 we present an overview of the results of both the para and the metaconfiguration. A direct comparison of the conductance (including energy nonconserving terms) in the two configurations is displayed in the upper panel. The lower panel illustrates the effect of the energy nonconserving terms

on the conductance in the metaconfiguration. The number of p_z electrons on the molecule and the symmetry of the lowest energy states corresponding to the conductance valleys are reported. The symmetries displayed in the upper panel belong to the (effective) ground states in the paraconfiguration; the corresponding symmetries for the metaconfiguration are shown in the lower panel.

Figure 3 shows that the results for the para and the metaconfiguration coincide for the $10 \leftrightarrow 11$ and $11 \leftrightarrow 12$ transitions. The ground states with $N=10,11,12$ particles have A- or B-type symmetries. They are therefore orbitally nondegenerate, no interference can occur, and thus the transitions are invariant under configuration change. For every other transition we see a noticeable difference between the results of the two configurations (Fig. 3). In all these transitions one of the participating states is orbitally degenerate. First we notice that the linear conductance peaks for the $7 \leftrightarrow 8$ and $8 \leftrightarrow 9$ transitions in the paraconfiguration are *shifted* with respect to the corresponding peaks in the metaconfiguration. The selection of an effective symmetric Hilbert space associated to the paraconfiguration reduces the total degeneracy by canceling the orbital degeneracy. In addition, the ground-state energy of the four- and eight-particle states is different in the two configurations since in the paraconfiguration the *effective* ground state is in reality the first excited state. The degeneracies S_N, S_{N+1} of the participating states as well as the ground-state energy are both entering the degeneracy term of Eq. (19),

$$\Delta = -\frac{f'(\Delta E)}{(S_{N+1} - S_N) f(\Delta E) + S_N}, \tag{21}$$

and determine the shift of the conductance peaks.

Yet, the most striking effect regarding transitions with orbitally degenerate states participating is the *systematic suppression* of the linear conductance when changing from the para to the metaconfiguration. The suppression is appreciable despite the conductance enhancement due to the energy nonconserving terms (see Fig. 3, lower panel). Thus, we will for simplicity discard them in the following discussion.

The conductance is determined by the combination of two effects: the reduction to the symmetric Hilbert space in the paraconfiguration and the interference effects between degenerate orbitals in the metaconfiguration. The reduction to the symmetric Hilbert space implies also a lower number of conducting channels (see Table III). One would expect a suppression of transport in the paraconfiguration. The actual opposite behavior is partially explained by Δ_{max} (see Table III) which is higher in the paraconfiguration.

The second effect determining transport is the interference between the E-type states, which is accounted for in the overlap factor Λ. The overlap factor is basis independent; thus, we can write the transition probabilities for the $6 \leftrightarrow 7$ transition as $|\langle 6_g | d_{L\tau} | 7_g \ell \tau \rangle|^2 = C$, where τ and ℓ are the spin and the quasiangular momentum quantum number, respectively. The transition probabilities have the same value since all four seven-particle states are in this basis equivalent (see Appendix C). Under the C_2 rotation the symmetric seven-particle ground state does not acquire any phase factor. Under the C_3 rotation, however, the two orbitally degenerate states acquire different phase factors, namely, $e^{i4\pi/3}$ and $e^{-i4\pi/3}$, respectively. Thus the overlap factors Λ for the $6 \leftrightarrow 7$ transition are

TABLE III. Number of channels participating to transport, overlap factor, and resonance value of the degeneracy term in the para and the metaconfiguration for the $6 \leftrightarrow 7$ transition peak. It is $C = |\langle 6_g | d_{L\tau} | 7_g \ell \tau \rangle|^2$, where τ and ℓ are the spin and the quasiangular momentum quantum numbers, respectively. The values of Δ_{max} are given for $k_B T = 0.04|b|$.

	No. of channels $S_N S_{N+1}$	Overlap factor Λ	Degeneracy term Δ_{max} $[1/k_B T]$
PARA	2	C	0,17
META	4	$\frac{1}{8}C$	0,11

$$\Lambda_{para} = \frac{1}{2 \cdot 8C} |4C|^2 = C,$$

$$\Lambda_{meta} = \frac{1}{4 \cdot 8C} |2Ce^{+i4\pi/3} + 2Ce^{-i4\pi/3}|^2 = \frac{1}{8}C.$$

The linear conductance is determined by the product among the number of conducting channels, the overlap factor, and the degeneracy term. Yet, it is the *destructive interference* between degenerate E-type orbitals, accounted for in the overlap factor Λ, that gives the major contribution to the strong suppression of the conductance in the metaconfiguration.

B. NDC and current blocking

Interference effects between orbitally degenerate states are also affecting nonlinear transport, producing in the *meta*-configuration current blocking and thus NDC at the border of the six-particle state diamond (Fig. 2). The upper panel of Fig. 4 shows the current through the benzene I-SET contacted in the metaconfiguration as a function of the bias voltage. The current is given for parameters corresponding to the white dashed line of Fig. 2. In this region only the six- and seven-particle ground states are populated.

At low bias the six-particle state is mainly occupied. As the bias is raised, transitions $6 \leftrightarrow 7$ occur and current flows. Above a certain bias threshold a blocking state is populated and the current drops. For the understanding of this nonlinear current characteristics, we have to take into account energy conservation, the Pauli exclusion principle, and the interference between participating states. For the visualization of the interference effects, we introduce the transition probability (averaged over the z coordinate and the spin σ),

$$P(x,y;n,\tau) = \lim_{L\to\infty} \sum_{\sigma} \frac{1}{2L} \int_{-L/2}^{L/2} dz |\langle 7_g n \tau | \psi_\sigma^\dagger(\mathbf{r}) | 6_g \rangle|^2, \tag{22}$$

for the *physical* seven-particle basis, i.e., the seven-particle basis that diagonalizes the stationary density matrix at a fixed

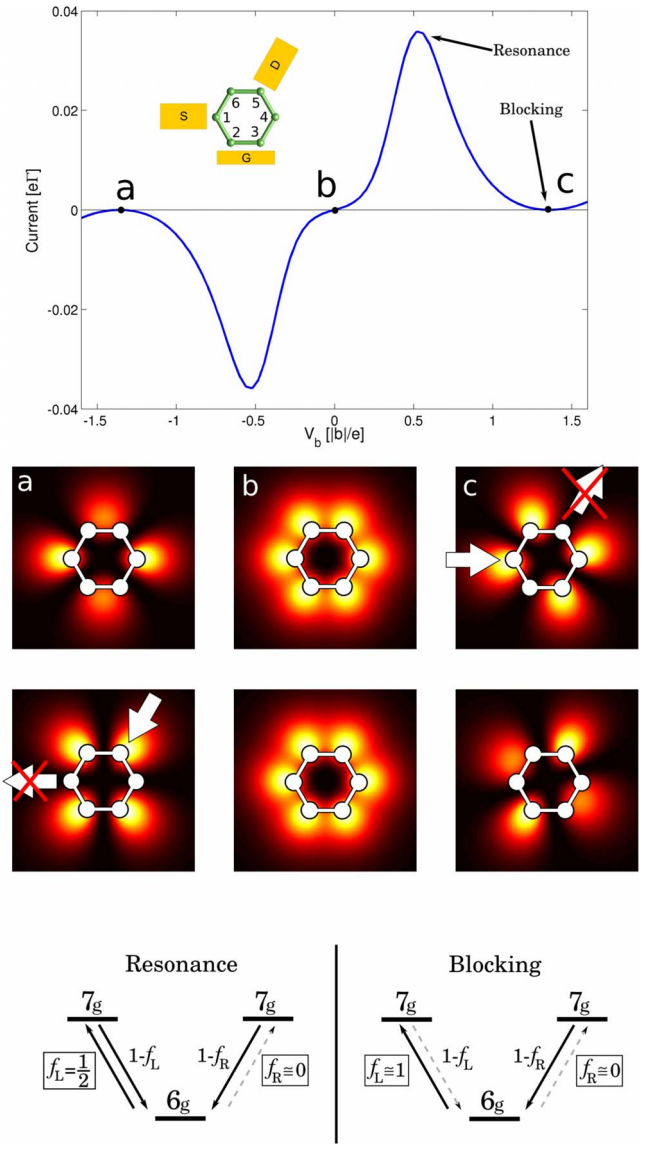

FIG. 4. (Color online) Upper panel—current through the benzene I-SET in the metaconfiguration calculated at bias and gate voltage conditions indicated by the dashed line of Fig. 2. A pronounced NDC with current blocking is visible. Middle panels—transition probabilities between the six-particle and each of the two seven-particle ground states for bias voltage values labeled *a*-*c* in the upper panel. The transition to a blocking state is visible in the upper (lower) part of the *c* (*a*) panels. Lower panels—sketch of the energetics for the $6\rightarrow 7$ transition in the metaconfiguration at bias voltages corresponding to the resonance current peak and current blocking as indicated in the upper panel of this figure.

bias. Here τ is the spin quantum number; $n=1,2$ labels the two states of the physical basis which are linear combinations of the orbitally degenerate states $|7_g \ell \tau\rangle$ and can be interpreted as conduction channels. Each of the central panels of Fig. 4 are surface plots of Eq. (22) at the different bias voltages *a*-*c*. The seven-particle ground states can interfere and thus generate nodes in the transition probability at the contact atom close to one or the other lead but, in the metaconfiguration, never at both contact atoms at the same time.

Energetic considerations are illustrated in the lower panels of Fig. 4 for two key points of the current curve at positive biases. The left panel corresponds to the resonance peak of the current. Due to energy conservation, electrons can enter the molecule only from the left lead. On the contrary the exit is allowed at both leads. The current is suppressed when transitions occur to a state which cannot be depopulated (a blocking state). Since, energetically, transmissions to the six-particle state are allowed at both leads, each seven-particle state can always be depopulated and no blocking occurs.

The current blocking scenario is depicted in the lower right panel of Fig. 4. For large positive bias the transition from a seven-particle ground state to the six-particle ground state is energetically forbidden at the left lead. Thus, for example, the *c* panel in Fig. 4 visualizes the current blocking situation yielding NDC: while for both channels there is a nonvanishing transition probability from the source lead to the molecule, for the upper channel a node prevents an electron from exiting to the drain lead. In the long time limit the blocking state gets fully populated while the nonblocking state is empty. At large negative bias the blocking scenario is depicted in panel *a* that shows the left-right symmetry obtained by a reflection through a plane perpendicular to the molecule and passing through the carbon atoms 6 and 3.

The temperature sets the scale of the large bias condition, and, correspondingly, the width of the current peak presented in Fig. 4 grows with it. The peak is not symmetric though. Its shape depends also on the energy renormalization introduced by the coupling to the leads[45] [principal part contribution in the GME Eq. (7)]. The result is a nonlinear dependence of the peak width with the temperature. We remark that only a description that retains coherences between the degenerate seven-particle ground states correctly captures NDC at both positive and negative biases.

In contrast to the $6\rightarrow 7$ transition, one does *not* observe NDC at the border of the seven-particle Coulomb diamond but rather a strong suppression of the current. The upper panel of Fig. 5 shows the current through the benzene I-SET contacted in the metaconfiguration as a function of the bias voltage corresponding to the white dotted line of Fig. 2. The middle panels show the transition probabilities between each of the seven-particle and the six-particle ground states.

The lower panel of Fig. 5 shows a sketch of the energetics at positive bias corresponding to the "expected" resonance peak. Here electrons can enter the molecular dot at both leads, while the exit is energetically forbidden at the left lead. Thus, if the system is in the seven-particle state which is blocking the right lead, this state cannot be depopulated, becoming the blocking state.

On the other hand, transitions from the six-particle ground state to both seven-particle ground states are equally probable. Thus the blocking state will surely be populated at some time. The upper plot of the *b* panel in Fig. 5 shows the transition probability to the blocking state that accepts electrons from the source lead but cannot release electrons to the drain.

We just proved that in this case the current blocking situation occurs already at the resonance bias voltage. For a higher positive bias, the transition probability from the blocking state at the drain lead increases and current can

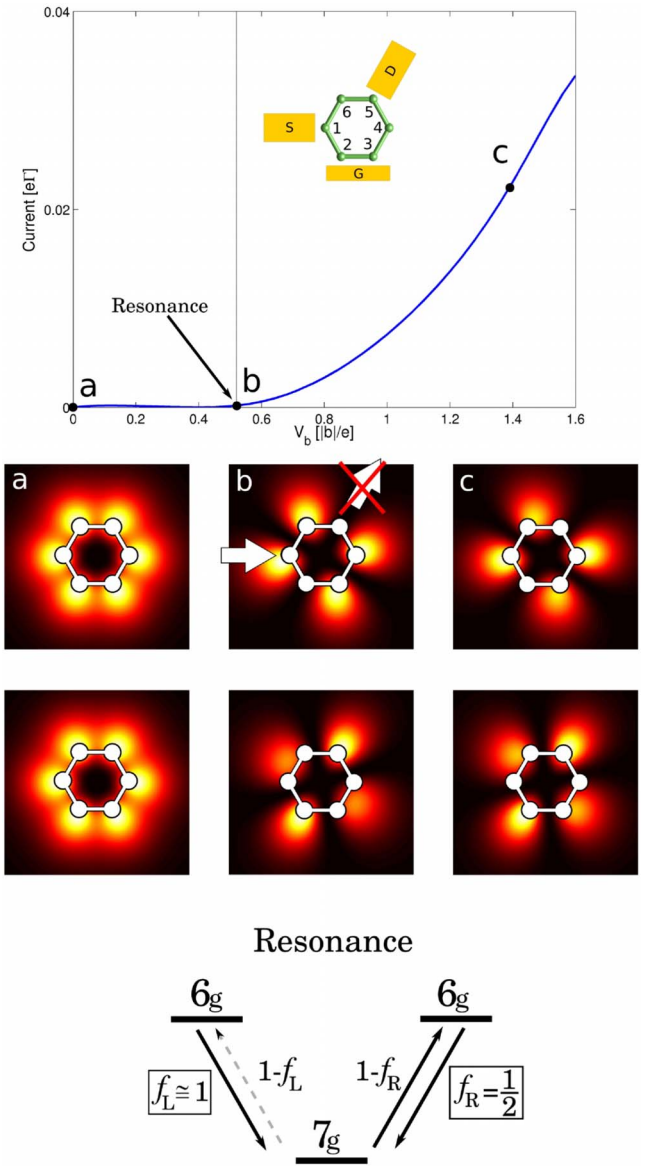

FIG. 5. (Color online) Upper panel—current through the benzene I-SET in the metaconfiguration calculated at bias and gate voltage conditions indicated by the dotted line of Fig. 2. No NDC is visible. Middle panels—transition probabilities between each of the seven-particle and the six-particle ground state for bias voltage values labeled as *a*-*c* in the upper panel. Lower panel—sketch of the energetics for the $7\rightarrow 6$ transition in the metaconfiguration at bias voltage corresponding to the expected resonance peak. (compare to Fig. 4).

flow. This effect, though, can be captured only by taking into account also the energy nonconserving terms in Eq. (7).

In the *para*configuration, the current as a function of the bias voltage is shown in Fig. 6. The current is given for parameters corresponding to the white dashed line of Fig. 2. In this case, no interference effects are visible. We see instead the typical steplike behavior of the current in the Coulomb blockade regime.

The panels on the right are the surface plots of

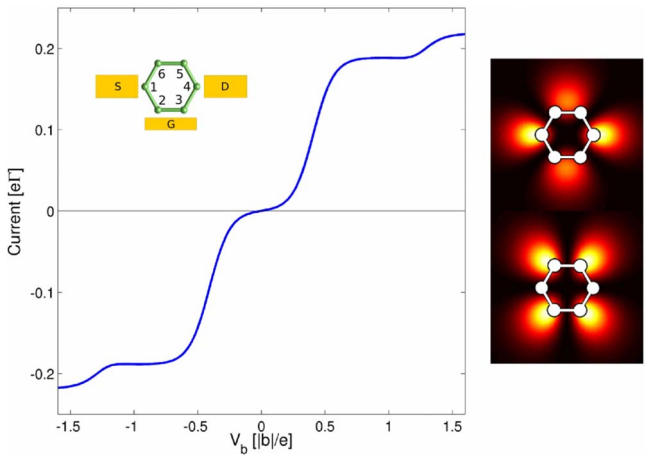

FIG. 6. (Color online) Left panel—current through the benzene I-SET in the paraconfiguration calculated at bias and gate voltage conditions indicated by the dashed line of Fig. 2. No interference effects are visible. Right panels—transition probabilities between the six-particle and the symmetric and antisymmetric seven-particle ground states.

$$P(x,y;\tau) = \lim_{L\to\infty} \sum_{\sigma} \frac{1}{2L} \int_{-L/2}^{L/2} dz |\langle 7_g \tau; (a)sym | \psi_\sigma^\dagger(\mathbf{r}) | 6_g \rangle|^2. \tag{23}$$

The upper plot shows the transition probability to the symmetric seven-particle state and the lower to the antisymmetric. Remember that in the paraconfiguration only the symmetric states contribute to transport. Evidently the symmetric state is in the paraconfiguration nonblocking. Additionally, since the coherences between orbitally degenerate states and therefore the energy nonconserving terms do not play any role in the transport, the physical basis states are not bias dependent. Thus in the paraconfiguration there are always nonblocking states populated and no NDC can occur.

IV. REDUCED SYMMETRY

In this section we study the effect of reduced symmetry on the results presented previously. We generalize the model Hamiltonian by taking into account the perturbations on the molecule due to the contacts and the bias voltage. The contact between molecule and leads is provided by different anchor groups. These linkers are coupled to the contact carbon atoms over a σ bond thus replacing the corresponding benzene hydrogen atoms. Due to the orthogonality of π and σ orbitals, the anchor groups affect in first approximation only the σ orbitals of benzene. In particular the different electron affinities of the atoms in the linkers imply a redistribution of the density of σ electrons. Assuming that transport is carried by π electrons only, we model the effect of this redistribution as a change in the on-site energy for the p_z orbitals of the contact carbon atoms,

$$H'_{\text{ben}} := H_{\text{contact}} = \xi_c \sum_{\alpha\sigma} d^\dagger_{\alpha\sigma} d_{\alpha\sigma}, \quad \alpha = L,R, \tag{24}$$

where $R=4,5$, respectively, in the para and metaconfiguration and $L=1$ in both setups.

TABLE IV. Point groups to which the molecule belongs under the influence of the contacts and the external bias potential.

	PARA	META
Contact perturb.	D_{2h}	C_{2v}
Bias perturb.	C_{2v}	C_{2v}

We also study the effect of an external bias on the benzene I-SET. In particular we release the strict condition of potential drop all concentrated at the lead-molecule interface. Nevertheless, due to the weak coupling of the molecule to the leads, we assume that only a fraction of the bias potential drops across the molecule, similar to Hettler *et al.*[28] For this residual potential we take the linear approximation $V_b(\mathbf{r}) = -\frac{V_b}{a}(\mathbf{r}\cdot\hat{\mathbf{r}}_{sd}/a_0)$, where we choose the center of the molecule as the origin and $\hat{\mathbf{r}}_{sd}$ is the unity vector directed along the source to drain direction. $a_0 = 1.43$ Å is the bond length between two carbon atoms in benzene; a is the coefficient determining the intensity of the potential drop over the molecule. Since the p_z orbitals are strongly localized, we can assume that this potential will not affect the intersite hopping but only the on-site term of the Hamiltonian,

$$H'_{ben} := H_{bias} = e\sum_{i\sigma} \xi_{b_i} d^\dagger_{i\sigma} d_{i\sigma} \tag{25}$$

with $\xi_{b_i} = \int d\mathbf{r} p_z(\mathbf{r}-\mathbf{R}_i) V_b(\mathbf{r}) p_z(\mathbf{r}-\mathbf{R}_i)$.

Under the influence of the contacts or the bias potential, the symmetry of the molecule changes. Table IV shows the point groups to which the molecule belongs in the perturbed setup. This point groups have only A- and B-type irreducible representations. Thus the corresponding molecular orbitals do not exhibit orbital degeneracy.

No interference effects influence the transport in the para-configuration. Thus we do not expect its transport characteristics to be qualitatively modified by the new setup with the corresponding loss of degeneracies.

In the metaconfiguration, on the other hand, interferences between orbitally degenerate states play a crucial role in the explanation of the occurring transport features. Naïvely one would therefore expect that neither conductance suppression nor NDC and current blocking occur in a benzene I-SET with reduced symmetry. Yet we find that, under certain conditions, the mentioned transport features are robust under the lowered symmetry.

The perturbations due to the contacts and the bias lead to an expected level splitting of the former orbitally degenerate states. Very different current-voltage characteristics are obtained depending on the relation between the energy splitting δE and other two important energy scales of the system: the tunneling rate Γ and the temperature T. In particular, when $\delta E \ll \Gamma \ll T$, interference phenomena persist. In contrast, when $\Gamma < \delta E \ll T$, interference phenomena disappear despite the fact that, due to temperature broadening, the two states still cannot be resolved. In this regime, due to the asymmetry in the tunneling rates introduced by the perturbation, standard NDC phenomena (see Fig. 8) occur.

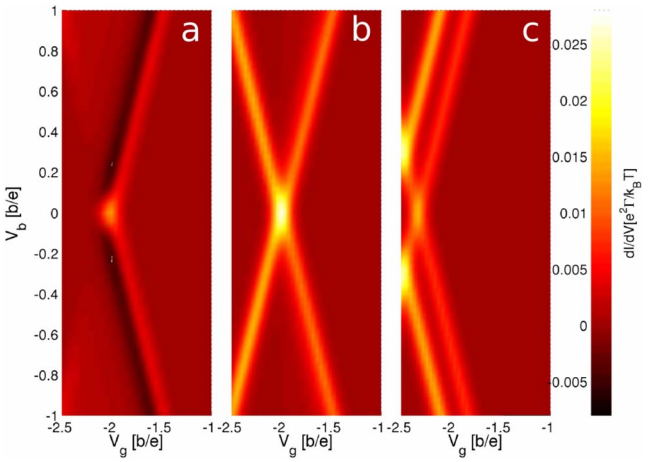

FIG. 7. (Color online) Close-up views of the stability diagram around the $6 \leftrightarrow 7$ resonance for the system under contact perturbation. The perturbation strength grows from left to right The parameter that describes the contact effect assumes the values $\xi_c = 0.15\Gamma, 2\Gamma, 15T$ from left to right, respectively, and $T = 10\Gamma$.

In the absence of perfect degeneracy, we abandon the strict secular approximation scheme that would discard the coherences in the density matrix between states with different energies. We adopt instead a softer approximation by retaining also coherences between quasidegenerate states. Since they have Bohr frequencies comparable to the tunneling rate, they influence the stationary density matrix. Formulas for the GME and the current taking into account these coherence terms are presented in Appendix A.

Figure 7 shows from left to right close-up views of the stability diagram for the setup under the influence of increasing *contact perturbation* around the $6 \leftrightarrow 7$ resonance. The orbital degeneracy of the seven-particle states is lifted, and the transport behavior for the $6 \leftrightarrow 7$ transition depends on the energy difference between the formerly degenerate seven-particle ground states. In panel a the energy difference is so small that the states are quasidegenerate: $\delta E \ll \hbar\Gamma \ll k_B T$. As expected, we recover NDC at the border of the six-particle diamond and current suppression at the border of the seven-particle diamond, such as in the unperturbed setup.

Higher on-site energy shifts correspond to a larger level spacing. Panel b displays the situation in which the latter is of the order of the level broadening but still smaller than the thermal energy ($\delta E \simeq \hbar\Gamma \ll k_B T$): no interference causing NDC and current blocking can occur. Yet, due to thermal broadening, we cannot resolve the two seven-particle states.

Eventually, panel c presents the stability diagram for the case $\delta E > k_B T > \hbar\Gamma$: the level spacing between the seven-particle ground and first excited state is now bigger than the thermal energy; thus, the two transition lines corresponding to these states are clearly visible at the border of the six-particle stability diamond.

Figure 8 shows close-up views of the stability diagram for the setup under the influence of the *bias perturbation* at the border of the six- and seven-particle diamonds. The same region is plotted for different strengths of the external potential over the molecule. In contrast to the contact perturbation, the amount of level splitting of the former degenerate states

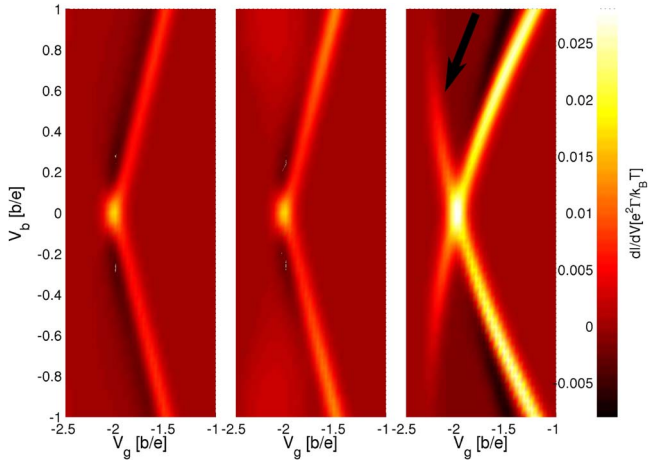

FIG. 8. (Color online) Close-up views of the stability diagram around the $6 \leftrightarrow 7$ resonance for the system under the effect of the bias potential, displayed for different strengths of the electrostatic potential drop over the molecule. The parameter that describe the strength of the electrostatic drop over the molecule assumes the values $a=25, 12, 0.6$ from left to right, respectively.

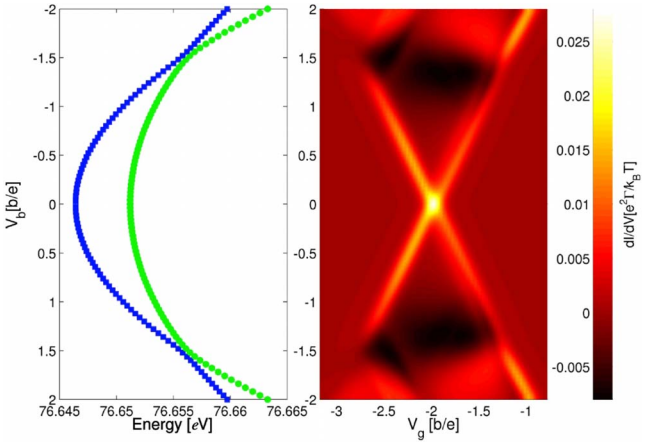

FIG. 9. (Color online) Combination of the bias and contact perturbations. Left panel—energy levels of the seven-particle ground and first excited state as functions of the bias voltage. Right panel—stability diagram around the $6 \leftrightarrow 7$ resonance. The perturbation parameters are in this case $\xi_c = 2\Gamma$ and $a=12$.

is here bias dependent. This fact imposes a bias window of interference visibility. The bias must be small enough for the seven-particle states to be quasidegenerate and at the same time bigger than the thermal energy so that the occurring NDC is not obscured by the thermally broadened conductance peak. A strong electrostatic potential perturbation closes the bias window and no interference effect can be detected.

Panel *a* of Fig. 8 represents the weak perturbation regime with no qualitative differences with the unperturbed case. The typical fingerprints of interference (NDC at the border of the six-particle diamond and current blocking for the $7 \rightarrow 6$ transition) are still visible for intermediate perturbation strength (panel *b*) but this time only in a limited bias window. Due to the perturbation strength, at some point in the bias, the level splitting is so big that the quasidegeneracy is lifted and the interference effects are destroyed. In panel *c* the quasidegeneracy is lifted in the entire bias range. There is NDC at the border of the six-particle diamond, but it is not accompanied by current blocking as proven by the excitation line at the border of the seven-particle diamond (see arrow): no interference occurs. The NDC is here associated to the sudden opening of a slow current channel, the one involving the six-particle ground state and the seven-particle (nondegenerate) excited state (standard NDC).

Figure 9 refers to the setup under both the *bias and contact perturbations*. The left panel shows the energy of the lowest seven-particle states as a function of the bias. In the right panel we present the stability diagram around the $6 \leftrightarrow 7$ resonance. NDC and current blocking are clearly visible only in the bias region where, due to the combination of bias and contact perturbation, the quasidegeneracy of the two seven-particle states is reestablished. Also the fine structure in the NDC region is understandable in terms of interference if in the condition of quasidegeneracy we take into account the renormalization of the level splitting due to the energy nonconserving terms.

Interference effects predicted for the unperturbed benzene I-SET are robust against various sources of symmetry breaking. Quasidegeneracy, $\delta E \ll \hbar\Gamma \ll k_B T$, is the necessary condition required for the detection of the interference in the stability diagram of the benzene I-SET.

V. CONCLUSIONS

In this paper we analyze the transport characteristics of a benzene I-SET. Two different setups are considered, the para and the metaconfiguration, depending on the position of the leads with respect to the molecule.

Within an effective p_z orbital model, we diagonalize exactly the Hamiltonian for the molecule. We further apply a group-theoretical method to classify the many-body molecular eigenstates according to their symmetry and quasiangular momentum. With the help of this knowledge we detect the orbital degeneracy and, in the paraconfiguration, we select the states relevant for transport.

We introduce a generic interference condition [Eq. (1)] for I-SETs in terms of the tunneling transitions *amplitudes* of degenerate states with respect to the source and drain leads. By applying it to the benzene I-SET we predict the existence of interference effects in the metaconfiguration In order to study the dynamics of the molecular I-SET, we use a density matrix approach which starts from the Liouville equation for the total density operator and which enables the treatment of quasidegenerate states.

The stability diagrams for the two configurations show striking differences. In the linear regime a selective conductance suppression is visible when changing from the para to the metaconfiguration. Only transitions between ground states with well-defined particle number are affected by the change in the lead configuration. With the help of the group-theoretical classification of the states we recognize in this effect a fingerprint of the *destructive interference* between orbitally degenerate states. We derive an analytical formula for the conductance that reproduces exactly the numerical

result and supports their interpretation in terms of interference. Other interference effects are also visible in the nonlinear regime where they give rise to NDC and current blocking at the border of the six-particle Coulomb diamond as well as to current suppression for transitions between seven- and six-particle states.

We provide a detailed discussion of the impact of the reduced symmetry due to linking groups between the molecule and the leads or to an electrostatic potential drop over the molecule. We classify different transport regimes and set up the limits within which the discussed transport features are robust against perturbations. We identify in the *quasidegeneracy* of the molecular states the necessary condition for interference effects.

ACKNOWLEDGMENT

We acknowledge financial support by the Deutsche Forschungsgemeinschaft within the research programs Schwerpunktprogramm 1243 and Sonderforschungsbereich 689.

APPENDIX A: GME AND CURRENT IN THE NONSECULAR APPROXIMATION

The bias and the contact perturbations in our model for a benzene I-SET lower the symmetry of the active part of the junction and consequently lift the degeneracy that appeared so crucial for the interference effects. The robustness of the latter relies on the fact that the necessary condition is rather quasidegeneracy, expressed by the relation $\delta E \ll \hbar\Gamma$.

Nevertheless, if the perfect degeneracy is violated, the secular approximation applied to obtain Eq. (7) does not capture this softer condition. We report here the general expression for the generalized master equation and the associated current operator in the Born-Markov approximation and under the only further condition (exact in absence of superconductors) that coherences between states with different particle number are decoupled from the populations and vanish exactly in the stationary limit,

$$\begin{aligned}
\dot{\sigma}^{\mathrm{N}}_{\mathrm{EE}'} = & -\frac{i}{\hbar}(E-E')\sigma^{\mathrm{N}}_{\mathrm{EE}'} - \sum_{\alpha\tau\mathrm{F}} \frac{\Gamma_\alpha}{2} \mathcal{P}_{\mathrm{NE}} \Bigg\{ d^\dagger_{\alpha\tau}\Bigg[-\frac{i}{\pi} p_\alpha (F - H^0_{\mathrm{ben}}) + f^-_\alpha (F - H^0_{\mathrm{ben}}) \Bigg] d_{\alpha\tau} \\
& + d_{\alpha\tau}\Bigg[-\frac{i}{\pi} p_\alpha (H^0_{\mathrm{ben}} - F) + f^+_\alpha (H^0_{\mathrm{ben}} - F) \Bigg] d^\dagger_{\alpha\tau} \Bigg\} \sigma^{\mathrm{N}}_{\mathrm{FE}'} \\
& - \sum_{\alpha\tau\mathrm{F}} \frac{\Gamma_\alpha}{2} \sigma^{\mathrm{N}}_{\mathrm{EF}} \Bigg\{ d^\dagger_{\alpha\tau}\Bigg[+\frac{i}{\pi} p_\alpha (F - H^0_{\mathrm{ben}}) + f^-_\alpha (F - H^0_{\mathrm{ben}}) \Bigg] d_{\alpha\tau} \\
& + d_{\alpha\tau}\Bigg[+\frac{i}{\pi} p_\alpha (H^0_{\mathrm{ben}} - F) + f^+_\alpha (H^0_{\mathrm{ben}} - F) \Bigg] d^\dagger_{\alpha\tau} \Bigg\} \mathcal{P}_{\mathrm{NE}'} \\
& + \sum_{\alpha\tau\mathrm{FF}'} \frac{\Gamma_\alpha}{2} \mathcal{P}_{\mathrm{NE}} \Bigg\{ d^\dagger_{\alpha\tau} \sigma^{\mathrm{N-1}}_{\mathrm{FF}'} d_{\alpha\tau}\Bigg[+\frac{i}{\pi} p_\alpha (E' - F') + f^+_\alpha (E' - F') - \frac{i}{\pi} p_\alpha (E - F) + f^+_\alpha (E - F) \Bigg] \\
& + d_{\alpha\tau} \sigma^{\mathrm{N+1}}_{\mathrm{FF}'} d^\dagger_{\alpha\tau}\Bigg[+\frac{i}{\pi} p_\alpha (F' - E') + f^-_\alpha (F' - E') - \frac{i}{\pi} p_\alpha (F - E) + f^-_\alpha (F - E) \Bigg] \Bigg\} \mathcal{P}_{\mathrm{NE}'}, \qquad \text{(A1)}
\end{aligned}$$

where $\sigma^{\mathrm{N}}_{\mathrm{EE}'}$ is, different from Eq. (7), in the Schrödinger picture. Equation (7) represents a special case of Eq. (A1) in which all energy spacings between states with the same particle number are either zero or much larger than the level broadening $\hbar\Gamma$. The problem of a master equation in the presence of quasidegenerate states in order to study transport through molecules has been recently addressed in the work of Schultz and von Oppen.[38] The authors claimed in their work that the singular coupling limit should be used in order to derive an equation for the density matrix in the presence of quasidegenerate states. Equation (A1) is derived in the weak coupling limit and bridges all the regimes as illustrated by Figs. 7–9.

The current operators associated to the master equation just presented read as:

$$\begin{aligned}
I_\alpha = & \frac{\Gamma_\alpha}{2} \sum_{\mathrm{NEF}\tau} \mathcal{P}_{\mathrm{NE}} \Bigg\{ d^\dagger_{\alpha\tau}\Bigg[+\frac{i}{\pi} p_\alpha (E - H^0_{\mathrm{ben}}) + f^-_\alpha (E - H^0_{\mathrm{ben}}) \Bigg] d_{\alpha\tau} \\
& + d^\dagger_{\alpha\tau}\Bigg[-\frac{i}{\pi} p_\alpha (F - H^0_{\mathrm{ben}}) + f^-_\alpha (F - H^0_{\mathrm{ben}}) \Bigg] d_{\alpha\tau} \\
& - d_{\alpha\tau}\Bigg[+\frac{i}{\pi} p_\alpha (H^0_{\mathrm{ben}} - E) + f^+_\alpha (H^0_{\mathrm{ben}} - E) \Bigg] d^\dagger_{\alpha\tau} \\
& - d_{\alpha\tau}\Bigg[-\frac{i}{\pi} p_\alpha (H^0_{\mathrm{ben}} - F) + f^+_\alpha (H^0_{\mathrm{ben}} - F) \Bigg] d^\dagger_{\alpha\tau} \Bigg\} \mathcal{P}_{\mathrm{NF}}, \qquad \text{(A2)}
\end{aligned}$$

where $\alpha = L, R$ indicates the left or right contact. Nevertheless, within the limits of derivation of the master equation,

this formula can be simplified. Actually, if $E-F \leq \hbar\Gamma$, then F can be safely substituted with E in the argument of the principal values and of the Fermi functions, with an error of order $\frac{E-F}{k_B T} < \frac{\hbar\Gamma}{k_B T}$ which is negligible (the generalized master equation that we are considering is valid for $\hbar\Gamma \ll k_B T$). The approximation $E \sim F$ breaks down only if $E-F \sim k_B T$, but this implies that $E-F \gg \hbar\Gamma$ which is the regime of validity of the secular approximation. Consequently, in this regime, terms with $E \neq F$ do not contribute to the average current because they vanish in the stationary density matrix. Ultimately we can thus reduce the current operators to the simpler form,

$$I_\alpha = \Gamma_\alpha \sum_{\mathrm{NE}\tau} \mathcal{P}_{\mathrm{NE}} \{ + d^\dagger_{\alpha\tau} [f^-_\alpha (E - H^0_{\mathrm{ben}})] d_{\alpha\tau},$$

$$- d_{\alpha\tau} [f^+_\alpha (H^0_{\mathrm{ben}} - E)] d^\dagger_{\alpha\tau}, \qquad \text{(A3)}$$

which is almost equal to the current operator corresponding to the secular approximation. The only difference is here the absence of the second projector operator that allows contributions to the current coming from coherences between different energy eigenstates.

APPENDIX B: ANALYTICAL FORMULA FOR THE LINEAR CONDUCTANCE INCLUDING THE ENERGY NONCONSERVING TERMS

In the derivation of the conductance formula (20) we neglected the energy nonconserving terms in Eq. (7). Since in the GME they appear only in the dynamics of the coherences between orbitally degenerate states, Eq. (20) is exact for the paraconfiguration, where the orbital degeneracy is cancelled. This is not the case in the metaconfiguration where the orbital (quasi-)degeneracy is essential for the description of interference. Thus we derived a generic analytical formula for the conductance, taking into account the energy nonconserving terms. It reads as

$$G_{\mathrm{N,N+1}}(\Delta E) = e^2 \Gamma \Lambda_{\mathrm{N,N+1}} \left[- \frac{S_{\mathrm{N}} S_{\mathrm{N+1}} f'(\Delta E)}{(S_{\mathrm{N+1}} - S_{\mathrm{N}}) f(\Delta E) + S_{\mathrm{N}}} \right] \left\{ 1 + \frac{\mathrm{aux}(S_{\mathrm{N}}, S_{\mathrm{N+1}}) 3\mathcal{P}^2}{16 \Lambda^2_{\mathrm{N,N+1}} (S_{\mathrm{N}} S_{\mathrm{N+1}})^2 [f^{\pm}(\Delta E)]^2 + \mathcal{P}^2} \right\}. \qquad \text{(B1)}$$

Here, it is $\Gamma = \Gamma_{\mathrm{L}} = \Gamma_{\mathrm{R}}$. $\Lambda_{\mathrm{N,N+1}}$ is the overlap factor introduced in Sec. III A, Eq. (21). The auxiliary function $\mathrm{aux}(S_{\mathrm{N}}, S_{\mathrm{N+1}})$ in the correction term is zero if there are *no* orbitally degenerate ground states involved in the transition. If one of the participating states is orbitally degenerate it is $\mathrm{aux}(S_{\mathrm{N}}, S_{\mathrm{N+1}}) = 1$. The sign in $f^{\pm}(\Delta E)$ is defined as follows: $f^+(\Delta E)$ has to be used if the N-particle ground state is orbitally degenerate. If instead the $N+1$-particle ground state exhibits orbital degeneracy, $f^-(\Delta E)$ has to be inserted. The energy nonconserving terms are included in the factor $\mathcal{P} = \mathcal{P}_{\mathrm{L}}|_{V_{\mathrm{bias}}=0} = \mathcal{P}_{\mathrm{R}}|_{V_{\mathrm{bias}}=0}$. It is defined only if a degenerate state is participating transport. In case that, e.g., the N-particle ground state is orbitally degenerate, $\mathcal{P}_\alpha$ with $\alpha = L, R$ read as

$$\mathcal{P}_\alpha = \sum_{\mathrm{E}',l} \sum_{nm} \left[\frac{i}{\pi} p_\alpha (E_{\mathrm{g,N}} - E') \right] \langle N-1, E' l | d_{\alpha\tau} | N_{\mathrm{g}}, n \rangle \langle N_{\mathrm{g}}, m | d^\dagger_{\alpha\tau} | N-1, E' l \rangle$$

$$+ \sum_{\mathrm{E}',l} \sum_{nm} \left[\frac{i}{\pi} p_\alpha (E' - E_{\mathrm{g,N}}) \right] \langle N+1, E' l | d^\dagger_{\alpha\tau} | N_{\mathrm{g}}, n \rangle \langle N_{\mathrm{g}}, m | d_{\alpha\tau} | N+1, E' l \rangle, \qquad \text{(B2)}$$

where $p_\alpha(x) = -\mathrm{Re}\, \psi[\frac{1}{2} + \frac{i\beta}{2\pi}(x - \mu_\alpha)]$ and ψ is the digamma function, as defined in Sec. II B.

APPENDIX C: TRANSITION PROBABILITIES FOR THE 6↔7 TRANSITION

In the calculation of the overlap factor Λ in Sec. III A we used the relation

$$|\langle 6_{\mathrm{g}} | d_{\mathrm{L}} | 7_{\mathrm{g}}, \ell = 2 \rangle|^2 = |\langle 6_{\mathrm{g}} | d_{\mathrm{L}} | 7_{\mathrm{g}}, \ell = -2 \rangle|^2 \qquad \text{(C1)}$$

for the transition probabilities between the six-particle ground state and the seven-particle ground states $|7_{\mathrm{g}}, \ell\rangle$, where ℓ is the eigenvalue of the quasiangular momentum. This relation is now to be proven.

Again, we take advantage of the symmetry properties of the molecular states with respect to the σ_{v} operation and to the rotation operator R_ϕ for rotations about a discrete angle $\phi = \frac{n\pi}{3}$, as introduced in Sec. II C. The starting point is the

generic relation between these two operators,

$$\mathcal{R}_\phi \sigma_v = \sigma_v \mathcal{R}_{-\phi}. \quad \text{(C2)}$$

We can now apply both sides of this relation to the seven-particle ground states $|7_g, \ell = \pm 2\rangle$,

$$\mathcal{R}_\phi \sigma_v |7_g, \ell = \pm 2\rangle = \sigma_v \mathcal{R}_{-\phi} |7_g, \ell = \pm 2\rangle. \quad \text{(C3)}$$

The seven-particle ground states $|7_g, \ell = \pm 2\rangle$ are eigenstates of each $\mathcal{R}_\phi$, and the corresponding eigenvalues are phase factors,

$$\mathcal{R}_\phi |7_g, \ell = \pm 2\rangle = e^{\mp 2i\phi} |7_g, \ell = \pm 2\rangle. \quad \text{(C4)}$$

Thus, Eq. (C3) becomes

$$\mathcal{R}_\phi (\sigma_v |7_g, \ell = \pm 2\rangle) = e^{\pm 2i\phi} (\sigma_v |7_g, \ell = \pm 2\rangle). \quad \text{(C5)}$$

Yet, according to Eq. (C4), this equation can only be valid if

$$\sigma_v |7_g, \ell = \pm 2\rangle = \lambda |7_g, \ell = \mp 2\rangle \quad \text{(C6)}$$

and, since $\sigma_v^2 = 1$, λ can only be a phase factor. For the calculation of the transition probabilities we use further the property $\sigma_v^\dagger \sigma_v = 1$. Since the left contact atom (atom 1) lies in the reflection plane σ_v, it is $\sigma_v d_L \sigma_v^\dagger = d_L$. Also, since the symmetry of the six-particle ground state is A_{1g}, it is $\sigma_v |6_g\rangle = |6_g\rangle$. Under these considerations, we can write for the transition probability to the state $|7_g, \ell = 2\rangle$

$$\begin{aligned} |\langle 6_g | d_L | 7_g, \ell = 2\rangle|^2 &= |\langle 6_g | \sigma_v^\dagger \sigma_v d_L \sigma_v^\dagger \sigma_v | 7_g, \ell = 2\rangle|^2 \\ &= |\langle 6_g | d_L \sigma_v | 7_g, \ell = 2\rangle|^2 \\ &= |\langle 6_g | d_L | 7_g, \ell = -2\rangle|^2. \end{aligned} \quad \text{(C7)}$$

[1] *Introducing Molecular Electronics*, edited by G. Cuniberti, G. Fagas, and K. Richter (Springer, Berlin, 2005).
[2] J. Park, A. N. Pasupathy, J. I. Goldsmith, C. Chang, Yu. Yaish, J. R. Petta, M. Rinkoski, J. P. Sethna, H. D. Abruna, P. L. McEuen, and D. C. Ralph, Nature (London) **417**, 722 (2002).
[3] W. Liang, M. P. Shores, M. Bockrath, J. R. Long, and H. Park, Nature (London) **417**, 725 (2002).
[4] S. Kubatkin, A. Danilov, M. Hjort, J. Cornil, J.-L. Brédas, N. Stuhr-Hansen, P. Hedegård, and T. Bjørnholm, Nature (London) **425**, 698 (2003).
[5] L. H. Yu, Z. K. Keane, J. W. Ciszek, L. Cheng, J. M. Tour, T. Baruah, M. R. Pederson, and D. Natelson, Phys. Rev. Lett. **95**, 256803 (2005).
[6] A. V. Danilov, S. Kubatkin, S. Kafanov, P. Hedegård, N. Stuhr-Hansen, K. Moth-Poulsen, and T. Bjørnholm, Nano Lett. **8**, 1 (2008).
[7] D.-H. Chae, J. F. Berry, S. Jung, F. A. Cotton, C. A. Murillo, and Z. Yao, Nano Lett. **6**, 165 (2006).
[8] M. Poot, E. Osorio, K. O'Neill, J. M. Thijssen, D. Vanmaekelbergh, C. A. van Walree, L. W. Jenneskens, and H. S. J. van der Zant, Nano Lett. **6**, 1031 (2006).
[9] H. B. Heersche, Z. de Groot, J. A. Folk, H. S. J. van der Zant, C. Romeike, M. R. Wegewijs, L. Zobbi, D. Barreca, E. Tondello, and A. Cornia, Phys. Rev. Lett. **96**, 206801 (2006).
[10] E. A. Osorio, K. O'Neill, N. Stuhr-Hansen, O. F. Nielsen, T. Bjørnholm, and H. S. J. van der Zant, Adv. Mater. **19**, 281 (2007).
[11] E. Lörtscher, H. B. Weber, and H. Riel, Phys. Rev. Lett. **98**, 176807 (2007).
[12] R. H. M. Smit, Y. Noat, C. Untiedt, N. D. Lang, M. C. van Hemert, and J. M. van Ruitenbeek, Nature (London) **419**, 906 (2002).
[13] M. Kiguchi, O. Tal, S. Wohlthat, F. Pauly, M. Krieger, D. Djukic, J. C. Cuevas, and J. M. van Ruitenbeek, Phys. Rev. Lett. **101**, 046801 (2008).
[14] A. R. Champagne, A. N. Pasupathy, and D. C. Ralph, Nano Lett. **5**, 305 (2005).
[15] L. Venkataraman, J. E. Klare, C. Nuckolls, M. S. Hybertsen, and M. L. Steigerwald, Nature (London) **442**, 904 (2006).
[16] J. Repp, G. Meyer, S. M. Stojkovic, A. Gourdon, and C. Joachim, Phys. Rev. Lett. **94**, 026803 (2005).
[17] X. Xiao, B. Xu, and N. J. Tao, Nano Lett. **4**, 267 (2004).
[18] D. I. Gittins, D. Bethell, D. J. Schiffrin, and R. J. Nichols, Nature (London) **408**, 67 (2000).
[19] M. Mayor, H. B. Weber, J. Reichert, M. Elbing, C. von Hänisch, D. Beckmann, and M. Fischer, Angew. Chem., Int. Ed. **42**, 5834 (2003).
[20] F. Chen, X. Li, J. Hihath, Z. Huang, and N. J. Tao, J. Am. Chem. Soc. **128**, 15874 (2006).
[21] L. Venkataraman, J. E. Klare, I. W. Tam, C. Nuckolls, M. S. Hybertsen, and M. L. Steigerwald, Nano Lett. **6**, 458 (2006).
[22] N. Roch, S. Florens, V. Bouchiat, W. Wernsdorfer, and F. Balestro, Nature (London) **453**, 633 (2008).
[23] D. V. Cardamone, C. A. Stafford, and S. Mazumdar, Nano Lett. **6**, 2422 (2006).
[24] A. Gagliardi, G. C. Solomon, A. Pecchia, T. Frauenheim, A. Di Carlo, N. S. Hush, and J. R. Reimers, Phys. Rev. B **75**, 174306 (2007).
[25] S.-H. Ke, W. Yang, and U. Baranger, Nano Lett. **8**, 3257 (2008).
[26] Z. Qian, R. Li, X. Zhao, S. Hou, and S. Sanvito, Phys. Rev. B **78**, 113301 (2008).
[27] H. Bruus and K. Flensberg, *Many-Body Quantum Theory in Condensed Matter Physics* (Oxford University Press, Oxford, 2004).
[28] M. H. Hettler, W. Wenzel, M. R. Wegewijs, and H. Schoeller, Phys. Rev. Lett. **90**, 076805 (2003).
[29] S. A. Gurvitz and Ya. S. Prager, Phys. Rev. B **53**, 15932 (1996).
[30] M. Braun, J. König, and J. Martinek, Phys. Rev. B **70**, 195345 (2004).
[31] B. Wunsch, M. Braun, J. König, and D. Pfannkuche, Phys. Rev. B **72**, 205319 (2005).
[32] A. Donarini, M. Grifoni, and K. Richter, Phys. Rev. Lett. **97**, 166801 (2006).
[33] U. Harbola, M. Esposito, and S. Mukamel, Phys. Rev. B **74**, 235309 (2006).
[34] L. Mayrhofer and M. Grifoni, Eur. Phys. J. B **56**, 107 (2007).
[35] S. Koller, L. Mayrhofer, and M. Grifoni, New J. Phys. **9**, 348 (2007).

[36] J. N. Pedersen, B. Lassen, A. Wacker, and M. H. Hettler, Phys. Rev. B **75**, 235314 (2007).
[37] G. Begemann, D. Darau, A. Donarini, and M. Grifoni, Phys. Rev. B **77**, 201406(R) (2008); **78**, 089901(E) (2008).
[38] M. G. Schultz and F. von Oppen, arXiv:0812.1491 (unpublished).
[39] J. Linderberg and Y. Öhrn, J. Chem. Phys. **49**, 716 (1968).
[40] R. Pariser and R. G. Parr, J. Chem. Phys. **21**, 466 (1953).
[41] J. A. Pople, Trans. Faraday Soc. **49**, 1375 (1953).
[42] W. Barford, *Electronic and Optical Properties of Conjugated Polymers* (Clarendon Press, Oxford, 2005).
[43] K. Kaasbjerg and K. Flensberg, Nano Lett. **8**, 3809 (2008).
[44] K. Blum, *Density Matrix Theory and Applications* (Plenum Press, New York, 1996).
[45] A. Donarini, G. Begemann, and M. Grifoni, arXiv:0904.0167 (unpublished).

NANO LETTERS

2009
Vol. 9, No. 8
2897-2902

All-Electric Spin Control in Interference Single Electron Transistors

Andrea Donarini,* Georg Begemann, and Milena Grifoni

Theoretische Physik, Universität Regensburg, 93040 Regensburg, Germany

Received April 15, 2009; Revised Manuscript Received June 17, 2009

ABSTRACT

Single particle interference lies at the heart of quantum mechanics. The archetypal double-slit experiment[1] has been repeated with electrons in vacuum[2,3] up to the more massive C_{60} molecules.[4] Mesoscopic rings threaded by a magnetic flux provide the solid-state analogues.[5,6] Intramolecular interference has been recently discussed in molecular junctions.[7−11] Here we propose to exploit interference to achieve all-electrical control of a single electron spin in quantum dots, a highly desirable property for spintronics[12−14] and spin−qubit applications.[15−19] The device consists of an interference single electron transistor,[10,11] where destructive interference between orbitally degenerate electronic states produces current blocking at specific bias voltages. We show that in the presence of parallel polarized ferromagnetic leads the interplay between interference and the exchange interaction on the system generates an effective energy renormalization yielding different blocking biases for majority and minority spins. Hence, by tuning the bias voltage full control over the spin of the trapped electron is achieved.

The all-electrical solutions to the challenge of single spin control that have been proposed[15−18] and realized[19,20] are based either on spin−orbit coupling[15−19] or on tunneling-induced spin splitting in the Kondo regime.[20] Our proposal relies on the current blocking occurring in an interference single electron transistor (ISET) due to interference between degenerate states. The conditions for interference blocking are very generic[11] and admit several different realizations. We consider here for clarity a benzene and a triple-dot ISET, Figure 1. Both are described by the Hamiltonian

$$H = H_{\mathrm{sys}} + H_{\mathrm{leads}} + H_{\mathrm{T}} \qquad (1)$$

where H_{sys} represents the central system and also contains the energy shift operated by a capacitively coupled gate electrode at the potential V_g. The Hamiltonian H_{sys} is in both cases invariant with respect to a discrete set of rotations around the vertical axis passing through the center of the system. This fact allows a classification of its eigenstates in terms of the z component of the angular momentum l and also ensures the existence of *degenerate* states with different l. Then, a generic eigenstate is represented by the ket $|Nl\sigma E\rangle$ where N is the number of electrons on the system, σ is the spin, and E the energy of the state. When degenerate states participate to transport, they interfere since, like the two paths of the double-slit experiment, they are occupied simultaneously by the traveling electron, but in different superpositions under diverse transport conditions. H_{lead} describes the ferromagnetic leads with equal (for simplicity) parallel polarization P and with a difference eV_b between their electrochemical potentials. Finally, H_T accounts for the weak tunneling coupling between the system and the leads,

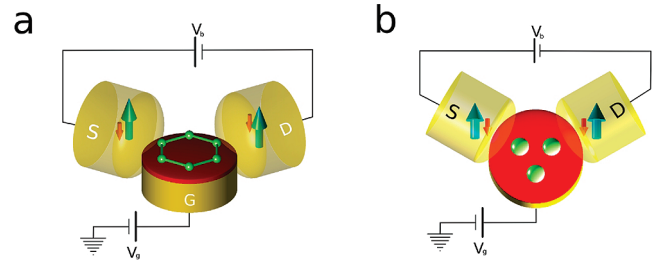

Figure 1. Two examples of interference single electron transistors (ISETs): a benzene molecular junction contacted in the meta configuration (a) and a triple quantum dot artificial molecule (b). The source and drain are parallel polarized ferromagnetic leads.

characteristic of SETs, and we consider the tunneling events restricted to the atoms or to the dots closest to the corresponding lead (Figure 1). We explicitly consider the Coulomb interaction only in the central part of the device (see the Supporting Information) due to the strong confinement experienced there by the electrons while, apart from the polarization assumption, we assume a noninteracting approximation for the leads. In the weak coupling regime the current through the ISET essentially consists of sequential tunneling events at the source and drain lead that increase or decrease by 1 the number of electrons on the system. The different panels of Figure 2 and Figure 3 show the current through the benzene and triple dot ISET, respectively, as a function of bias and gate voltage. As in all SETs at low bias, so-called Coulomb diamonds, where transport is energetically forbidden, occur. Within the diamonds the particle number is fixed as indicated in the figures. The only exceptions are the charge degenerate points where two diamonds meet. Here the energy difference of two ground states with consecutive

10.1021/nl901199p CCC: $40.75
Published on Web 07/28/2009

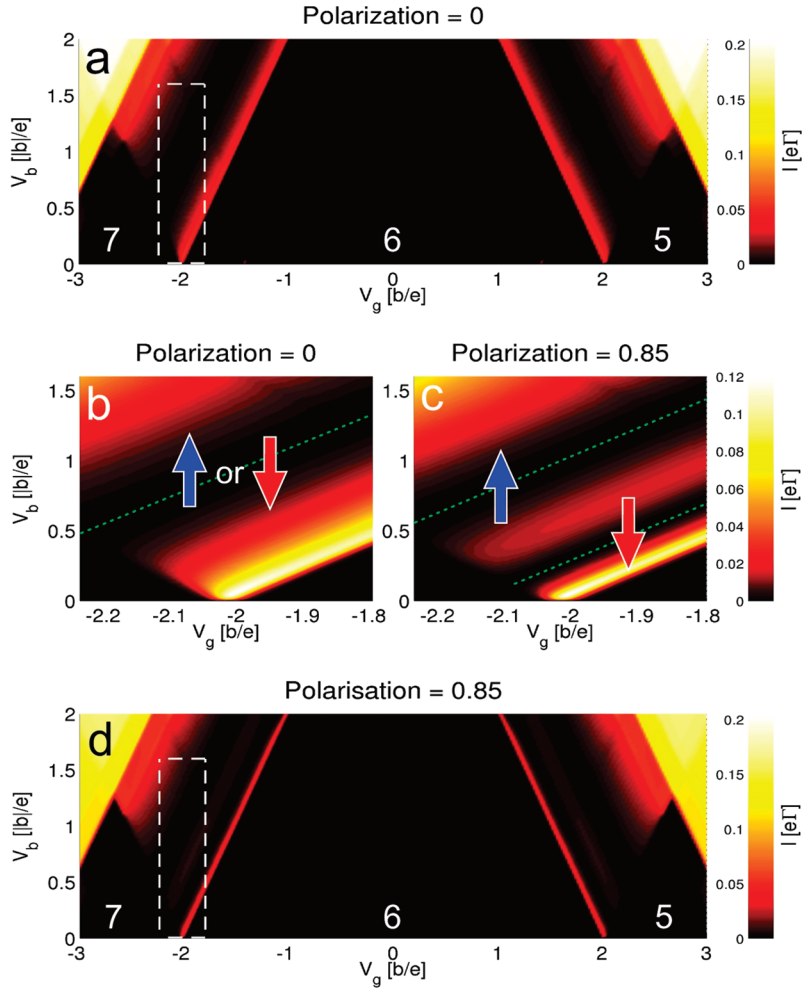

Figure 2. Benzene ISET: polarized vs unpolarized configuration. Panel a. Current vs bias and gate voltage for unpolarized leads. Panel d. Current vs bias and gate voltage for polarized leads (polarization $P = 0.85$). Panels b and c. Blow up of the $6 \rightarrow 7$ particle transition for both configurations. The unpolarized case shows a single current blocking line and the trapped electron has either up or down polarization. The polarized case shows two current blocking lines, corresponding to the different spin of the trapped electron. The current is given in units of $e\Gamma$ where Γ is the bare average rate (Supporting Information), and the temperature $k_B T = 0.01b$ where b is the hopping parameter (Supporting Information).

particle numbers is equal to the equilibrium chemical potential of the leads. At finite bias the incoming electrons have enough energy to overcome the level spacing and the Coulomb repulsion and the current flows. As a signature of the new states that enter the bias window, by increase of the voltage the current typically increases steplike.

In ISETs an exception to this picture is represented by the *interference blockade* where the current decreases for increasing bias generating negative differential conductance (NDC) and eventually vanishes (see green lines in the panels b and c of Figure 2 and Figure 3). Panels b in the same figures indicate moreover that, for a given gate voltage and in absence of polarization in the leads, the current is blocked only at one specific bias voltage. For parallel polarized leads, however, at a given gate voltage, the current is blocked at *two specific* bias voltages, one for each spin configuration (panels c). As demonstrated below, the blocking of the minority electrons occurs for the smaller bias voltages. As such full control of the spin configuration in the ISET can be electrically achieved. The interference blockade and its spin selectivity are also demonstrated in panels a and b of Figure 4. Along the dotted (dashed) line a majority (minority) spin electron is trapped into the molecule. The molecular spin state can thus be manipulated simply by adjusting the bias across the ISET. In the following we discuss the physics of the spin-selective interference blocking and present the necessary ingredients for its occurrence.

This novel blocking is explained by the presence of an N-particle nondegenerate state and two degenerate $N + 1$ particle states that simultaneously contribute to transport. It also requires that the ratio between the transition *amplitudes* $\gamma_{\alpha i}$ ($i = 1, 2$, $\alpha = \mathrm{L,R}$) between those N and $N + 1$ particle states is different for tunneling at the left (L) and at the right (R) lead[11]

$$\frac{\gamma_{L1}}{\gamma_{L2}} \neq \frac{\gamma_{R1}}{\gamma_{R2}} \tag{2}$$

This condition is fulfilled in both cases presented in Figure 1 due to the geometrical configuration of the left and right lead. Due to condition (2), the degenerate states interfere among

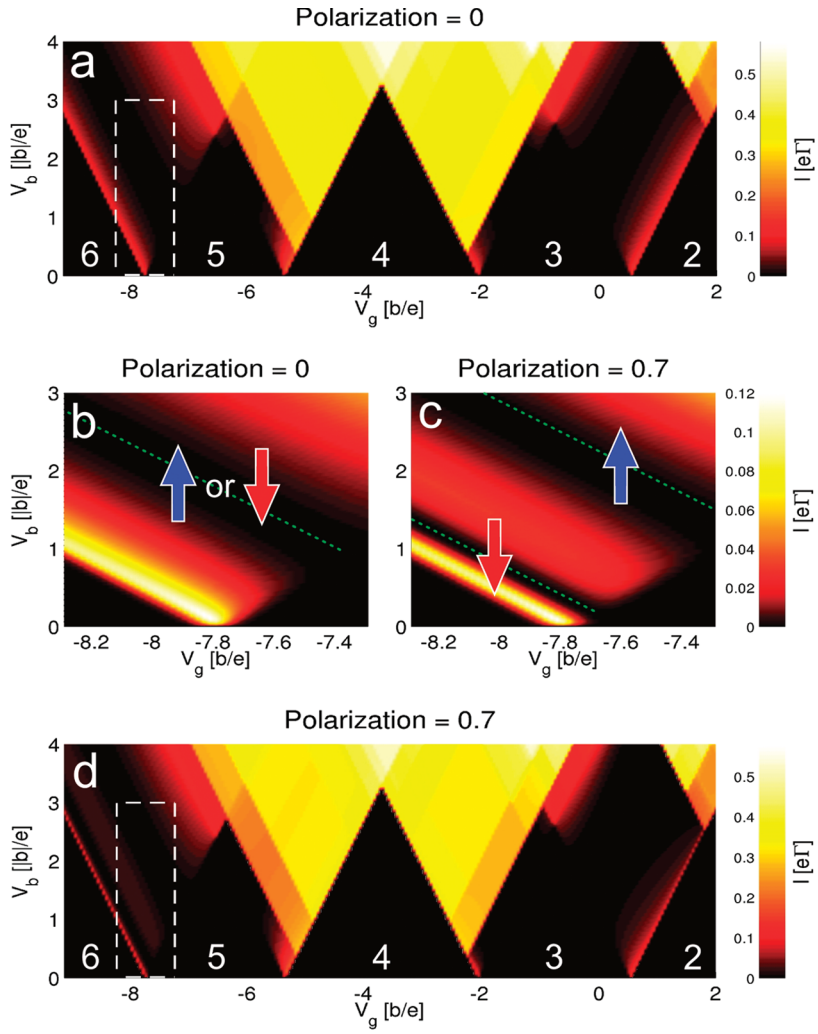

Figure 3. Triple dot ISET: polarized vs unpolarized configuration. Panel a. Current vs bias and gate voltage for unpolarized leads. Panel d. Current vs bias and gate voltage for polarized leads (polarization $P = 0.7$). Panels b and c. Blow up of the $6 \rightarrow 5$ particle transition for both configurations. The selective spin blocking is analogous to the one of the benzene ISET (Figure 2).

themselves such to form pairs of blocking and nonblocking states. The blocking state is only coupled to the source lead (panels c and d of Figure 4) while the nonblocking one to both source and drain. An electron that populates the blocking state can neither leave toward the drain nor, at high enough bias, return to the source since all energetically available states are there filled. The nonblocking state is thus excluded from the dynamics and the current vanishes.

As such we would conclude that the interference blocking is a threshold effect and the current remains blocked until a new excited state participates to the transport. However, as shown in Figure 2 and Figure 3, the current is blocked only at specific values of the bias voltage. The explanation of this phenomenon relies on two observations: (i) The blocking state (Figure 4) must be antisymmetric with respect to the plane perpendicular to the system and passing through its center and the atom (quantum dot) closest to the drain; this state is thus also an eigenstate of the projection of the angular momentum in the direction of the drain lead.[21] At positive (negative) bias voltages we call this state the $R(L)$-antisymmetric state $|\psi_{R(L),a}\rangle$. (ii) The coupling between the system and the leads not only generates the tunneling dynamics described so far but also contributes to an internal dynamics of the system that leaves unchanged its particle number. In fact the equation of motion for the reduced density matrix ρ of the system can be cast, to lowest nonvanishing order in the coupling to the leads, in the form

$$\dot{\rho} = -\frac{i}{\hbar}[H_{\mathrm{sys}}, \rho] - \frac{i}{\hbar}[H_{\mathrm{eff}}, \rho] + \mathscr{L}_{\mathrm{tun}}\rho \qquad (3)$$

The commutator with H_{sys} in eq 3 represents the coherent evolution of the system in absence of the leads. The operator $\mathscr{L}_{\mathrm{tun}}$ describes instead the sequential tunneling processes and is defined in terms of the transition amplitudes $\gamma_{\alpha i}$ between the N and $N + 1$ particle states like the ones introduced in eq 2. Finally H_{eff} renormalizes the coherent dynamics associated to the system Hamiltonian. It reads

$$H_{\mathrm{eff}} = \sum_{\alpha\sigma} \omega_{\alpha\sigma} L_{\alpha} \qquad (4)$$

where L_α is the projection of the angular momentum in the direction of the lead α and, for paramagnetic systems, it does not depend on the spin degree of freedom σ. Moreover, $\omega_{\alpha\sigma}$ is the frequency renormalization given to the states of spin σ by their coupling to the α lead. Similar effective dynamics has been mapped into the precession of a pseudospin around a pseudoexchange field.[22,23] In our case the presence of parallel polarized leads mixes the orbital and the spin degrees of freedom. Nevertheless, for what concerns the spin, H_{eff} is diagonal and thus spin accumulation due to precession[24] of the spin degree of freedom is excluded. Yet, in the presence of polarized leads, the spin up and the spin down undergo different effective dynamics. Equation 3 is an example of Bloch−Redfield equation describing the dynamics of a system coupled to thermal baths. A more detailed version of (3) is presented in the Supporting Information.

For sake of simplicity we give in the following the explicit form of the transition amplitudes $\gamma_{\alpha l}$, of the operator L_α and of the associated frequency $\omega_{\alpha\sigma}$ only for the benzene ISET and for the ground state transition $6_g \rightarrow 7_g$ that is characterized by interference blocking. The argumentation is nevertheless very general and can be repeated for all the systems exhibiting rotational symmetry. The transition amplitudes read

$$\gamma_{\alpha l} = \langle 6_g 00 | d_{M\sigma} | 7_g l\sigma \rangle e^{-il\phi_\alpha} \tag{5}$$

where $|7_g l\sigma\rangle$ are the orbitally degenerate 7 particle ground states, $l = \pm 2$ the z projection of the angular momentum in units of $\hbar$, and $d_{M\sigma}$ destroys an electron of spin σ in a reference carbon atom M placed in the middle between the two contact atoms. Moreover, ϕ_α is the angle of which we have to rotate the molecule to bring the reference atom M into the position of the contact atom α. The present choice of the reference atom implies that $\phi_L = -\phi_R = \pi/3$. In the Hilbert space generated by the 2-fold orbitally degenerate $|7_g l\sigma\rangle$ the operator L_α reads

$$L_\alpha = \frac{\hbar}{2}\begin{pmatrix} 1 & e^{i2l|l|\phi_\alpha} \\ e^{-i2l|l|\phi_\alpha} & 1 \end{pmatrix} \tag{6}$$

For a derivation of (6) see Supporting Information. The frequency $\omega_{\alpha\sigma}$ is defined in terms of transition amplitudes to all the states of neighbor particle numbers

$$\omega_{\alpha\sigma} = \frac{1}{\pi}\sum_{\sigma'\{E\}} \Gamma^0_{\alpha\sigma'}[\langle 7_g l\sigma | d_{M\sigma'} | 8\{E\}\rangle\langle 8\{E\}| d^\dagger_{M\sigma'} | 7_g -l\sigma\rangle p_\alpha(E - E_{7g}) + \langle 7_g l\sigma | d^\dagger_{M\sigma'} | 6\{E\}\rangle\langle 6\{E\}| d_{M\sigma'} | 7_g -l\sigma\rangle p_\alpha(E_{7g} - E)] \tag{7}$$

where the compact notation $|N\{E\}\rangle$ indicates all possible states with particle number N and energy E, $p_\alpha(x) = -\text{Re}\psi[(1/2) + (i\beta/2\pi)(x - \mu_\alpha)]$ where $\beta = 1/k_B T$, T is the temperature and ψ is the digamma function. Moreover $\Gamma^0_{\alpha\sigma'} = (2\pi/\hbar)|t|^2 D_{\alpha\sigma'}$ is the bare tunneling rate to the lead α of an electron of spin σ', where t is the tunneling amplitude and $D_{\alpha\sigma'}$ is density of states for electrons of spin σ' in the lead α at the corresponding chemical potential μ_α. Due to the particular choice of the arbitrary phase of the 7 particle ground states, $\omega_{\alpha\sigma}$ is real and does not depend on the orbital quantum number l. It depends instead on the bias and gate voltage through the energy of the 6,7-ground and 8 particle states. In Figure 5 the black curve depicts $\omega_{L\sigma}$ as a function of the bias in absence of polarization: the frequencies corresponding to the two spin species coincide and thus vanish at the same bias. The condition

$$\omega_{L\sigma} = 0 \tag{8}$$

determines the bias at which the current is completely blocked. In fact, at that bias the effective Hamiltonian contains only the projection of the angular momentum in the direction of the right lead (the drain) and the density matrix corresponding to the full occupation of the 7 particle R-antisymmetric state ($\rho = |\psi_{R,a}\rangle\langle\psi_{R,a}|$) is the stationary solution of eq 3. As we leave the blocking bias the effective Hamiltonian contains also the projection of the angular momentum in the direction of the left lead and the R-antisymmetric state is no longer an eigenstate of H_{eff}. The corresponding density matrix is not a stationary solution of (3) and current flows through the system. The $L \leftrightarrow R$ symmetry of the system implies, for negative biases, the blocking condition $\omega_{R\sigma} = 0$.

All-electric-spin control is achieved, in an ISET, only in the presence of ferromagnetic leads (or more generally

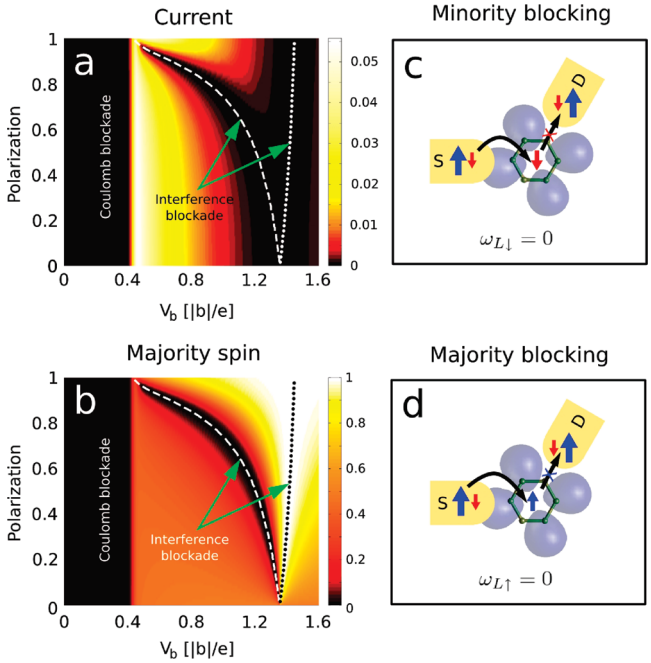

Figure 4. Spin control. Panel a. Current (in units of eΓ) through the benzene ISET vs bias and polarization at the $6 \rightarrow 7$ electron transition. Panel b. Population of the majority spin 7 particle state. The two zero current lines at high bias correspond to the maximum or minimum population of the 7 particle majority spin state and thus identify the spin state of the trapped electron on the molecule. Panels c and d. Schematic representation of the spin selective blocking corresponding to the dashed (c) and dotted (d) lines of panels a and b.

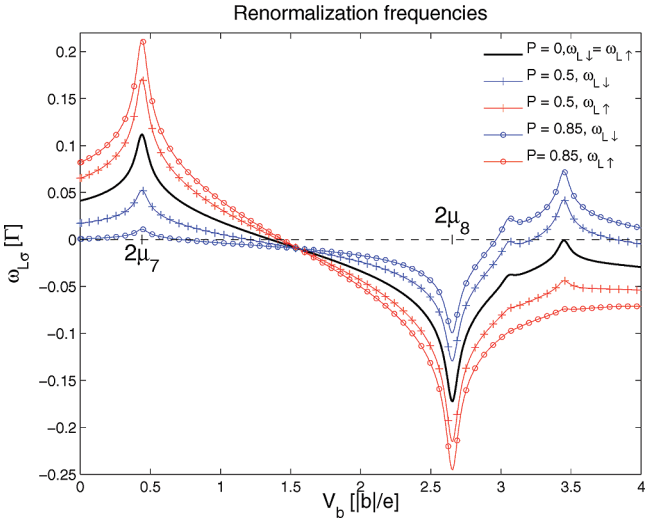

Figure 5. Blocking condition. Renormalization frequencies $\omega_{L\sigma}$ of a benzene ISET as function of the bias and for different lead polarizations. The current blocking condition $\omega_{L\sigma} = 0$ is fulfilled at different biases for the different spin states. $\mu_N = E_{N_g} - E_{N-1_g}$.

a spin injection source) and with exchange interaction on the system, i.e., an interaction which yields a singlet−triplet splitting on the isolated system. By manipulating (7) it is possible to show that the frequency splitting $\omega_{\alpha\uparrow} - \omega_{\alpha\downarrow}$ is proportional to the polarization in the α lead but vanishes in the absence of exchange interaction on the system capable to lift the singlet−triplet degeneracy of the 6 and 8 particle states (see the Supporting Information). In Figure 5 we show the frequencies $\omega_{L\sigma} = 0$ vs bias voltage also for finite values of the polarization P calculated for the benzene ISET, where exchange splitting is ensured by the Coulomb interaction on the system. The interference blocking conditions $\omega_{L\sigma} = 0$ for the $L \rightarrow R$ current are satisfied at different biases for the different spin species. The dotted and dashed lines in Figure 4 are the representation of the relations $\omega_{L\uparrow} = 0, \omega_{L\downarrow} = 0$ as a function of the bias and polarization, respectively.

The distance between the two blocking biases is of the same energy scale of the addition energy $\Delta E = \mu_8 - \mu_7$, as can be seen in Figure 5. In fact, even if the splitting in the renormalization frequencies is of order Γ_L, the distance between the two points in which the up and the down renormalization frequencies vanish depends on the particular dependence of those frequencies on bias. Their dependence is roughly linear in the interesting region (Figure 5) and with a slope given approximately by $\Gamma_L/\Delta E$. The bias splitting corresponding to a frequency splitting of order Γ_L is thus in the same energy scale of the addition energy.

The realization of a triple dot ISET with injection of spin-polarized carriers is feasible even if experimentally demanding. We suggest graphene for the realization of the triple-dot system due to the possibility of easily evaporating ferromagnetic leads and to the intrinsically low spin−orbit coupling. Graphene has been already successfully contacted with ferromagnetic leads,[26] while the possibility of defining mesoscopic structures in graphene sheets electrostatically[25] or by etching[27] has also already been demonstrated. For these reasons we think that the realization of the proposed all-electrical spin control in ISETs in graphene devices is perhaps the most promising even if still experimentally challenging. Spin injection in semiconductor heterostructures is at least as challenging, and the relevance of intrinsic spin−orbit effect also represents a drawback. On the other hand the high control reached in heterostructure fabrication should not be forgotten, such that also semiconducting triple dots are possible candidates for ISETs.

In previous studies[11] we have shown that the interference current blocking does not depend on the perfect symmetry of the system but rather relies on the existence of quasi-degenerate states in which the energy splitting is smaller than the tunneling coupling to the source and drain leads. In the proposed structures the degeneracy is associated with the rotational symmetry and it has the advantage of a simple geometrical realization of the interference conditions (2). Nevertheless the effect is more general and any other structure exhibiting orbital degeneracy is a good candidate for an ISET.

Acknowledgment. We acknowledge financial support by the DFG under the programs SFB689, SPP1243.

Supporting Information Available: System Hamiltonian, the generalized master equation, matrix form of the operator L_α, and the spin splitting of the renormalization frequencies. This material is available free of charge via the Internet at http://pubs.acs.org.

References

(1) Young, T. Experiments and calculations relative to physical optics. *Philos. Trans. R. Soc. London* **1804**, *94*, 12–48.
(2) Jönsson, C. Elektroneninterferenzen an mehreren künstlich hergestellten Feinspalten. *Z. Phys.* **1961**, *161*, 454–474.
(3) Merli, P. G.; Missiroli, G. F.; Pozzi, G. On the statistical aspect of electron interference phenomena. *Am. J. Phys.* **1976**, *44*, 306–307.
(4) Arndt, M.; et al. Wave-particle duality of C_{60} molecules. *Nature* **1999**, *401*, 680–682.
(5) Yacoby, A.; Heiblum, M.; Mahalu, D.; Shtrikman, H. Coherence and phase sensitive measurements in a quantum dot. *Phys. Rev. Lett.* **1995**, *74*, 4047–4050.
(6) Gustavsson, S.; Leturcq, R.; Studer, M.; Ihn, T.; Ensslin, K. Time-Resolved Detection of Single-Electron Interference. *Nano Lett.* **2008**, *8*, 2547–2550.
(7) Cardamone, D. V.; Stafford, C. A.; Mazumdar, S. Controlling quantum transport through a single molecule. *Nano Lett.* **2006**, *6*, 2422–2426.
(8) Ke, S.-H.; Yang, W.; Baranger, U. Quantum-interference-controlled molecular electronics. *Nano Lett.* **2008**, *8*, 3257–3261.
(9) Quian, Z.; Li, R.; Zhao, X.; Hou, S.; Sanvito, S. Conceptual molecular quantum phase transistor based on first-principles quantum transport calculations. *Phys. Rev. B* **2008**, *78*, 113301.1–4.
(10) Begemann, G.; Darau, D.; Donarini, A.; Grifoni, M. Symmetry fingerprints of a benzene single-electron transistor: Interplay between Coulomb interaction and orbital symmetry. *Phys. Rev. B* **2008**, *77*, 201406(R).1-4; **2008**, *78*, 089901(E).1.
(11) Darau, D.; Begemann, G.; Donarini, A.; Grifoni, M. Interference effects on the transport characteristics of a benzene single-electron transistor. *Phys. Rev. B* **2009**, *79*, 235404.
(12) Wolf, S. A.; et al. Spintronics: A spin-based electronic vision for the future. *Science* **2001**, *294*, 1488–1495.
(13) Awschalom, D. D.; Flatte, M. E. Challenges for semiconductor spintronics. *Nat. Phys.* **2007**, *3*, 153–159.
(14) Ohno, H.; et al. Elecric-field control of ferromagnetism. *Nature* **2000**, *408*, 944–946.
(15) Golovach, V. N.; Borhani, M.; Loss, D. Electric-dipole-induced spin resonance in quantum dots. *Phys. Rev. B* **2006**, *74*, 165319.1–10.
(16) Levitov, L.; Rashba, E. Dynamical spin-electric coupling in a quantum dot. *Phys. Rev. B* **2003**, *67*, 115324.1–5.
(17) Debald, S.; Emary, C. Spin-orbit-driven coherent oscillations in a few-electron quantum dot. *Phys. Rev. Lett.* **2005**, *94*, 226803.1–4.

(18) Walls, J. Parametric spin excitations in lateral quantum dots. *Phys. Rev. B* **2007**, *76*, 195307.1–16.
(19) Nowack, K. C.; Koppens, F. H. L.; Nazarov, Yu. V.; Vandersypen, L. M. K. Coherent control of a single electron spin with electric fields. *Science* **2007**, *318*, 1430–1433.
(20) Hauptmann, J. R.; Paaske, J.; Lindelof, P. E. Electric-field-controlled spin reversal in a quantum dot with ferromagnetic contacts. *Nat. Phys.* **2008**, *4*, 373–376.
(21) The corresponding eigenvalue depends on the symmetry of the atomic (quantum dot) wave function with respect to the molecular (artificial molecule) plane: $\hbar$ or 0 for symmetric or antisymmetric wave fuctions, respectively.
(22) Wunsch, B.; Braun, M.; König, J.; Pfannkuche, D. Probing level renormalization by sequential transport through double quantum dots. *Phys. Rev. B* **2005**, *72*, 205319.1–9.
(23) Schultz, M. G.; von Oppen, F., Quantum Transport through Nanostructures with Orbital Degeneracies arXiv:0812.1491v2.
(24) Braun, M.; König, J.; Martinek, J. Theory of transport through quantum-dot spin valves in the weak-coupling regime. *Phys. Rev. B* **2004**, *70*, 195345.1–12.
(25) Molitor, F.; Dröscher, S.; Güttinger, J.; Jacobsen, A.; Stampfer, C.; Ihn, T.; Ensslin, K. Transport through graphene double dots. *Appl. Phys. Lett.* **2009**, *94*, 222107.
(26) Tombros, N.; Jozsa, C.; Popinciuc, M.; Jonkman, H. T.; van Wees, B. J. Electronic spin transport and spin precession in single graphene layers at room temperature. *Nature* **2007**, *448*, 71–574.
(27) Eroms, J. Weiss, D. Weak Localization and Transport Gap in Graphene Antidot Lattices, arXiv:0901.0840.

NL901199P

Supplementary material for ”All-electric-spin control in interference single electron transistors”

Andrea Donarini,* Georg Begemann, and Milena Grifoni

Theoretische Physik, Universität Regensburg, 93040 Regensburg, Germany

E-mail: Andrea.Donarini@physik.uni-regensburg.de

The system Hamiltonian

The Hamiltonian that describes both systems represented in Fig. 1 reads

$$\begin{aligned} H_{\rm sys} = & \xi_0 \sum_{i\sigma} d^\dagger_{i\sigma} d_{i\sigma} + b \sum_{i\sigma} \left(d^\dagger_{i\sigma} d_{i+1\sigma} + d^\dagger_{i+1\sigma} d_{i\sigma} \right) \\ & + U \sum_i \left(n_{i\uparrow} - \tfrac{1}{2} \right) \left(n_{i\downarrow} - \tfrac{1}{2} \right) \\ & + V \sum_i \left(n_{i\uparrow} + n_{i\downarrow} - 1 \right) \left(n_{i+1\uparrow} + n_{i+1\downarrow} - 1 \right), \end{aligned} \tag{1}$$

where $d^\dagger_{i\sigma}$ creates an electron of spin σ in the p_z orbital of carbon i or in the ground state of the quantum dot i and $i = 1, \ldots, 6(3)$ runs over the six carbon atoms (three quantum dots) of the system. Moreover $n_{i\sigma} = d^\dagger_{i\sigma} d_{i\sigma}$. The effect of the gate is included as a renormalization of the on-site energy $\xi = \xi_0 - eV_{\rm g}$ ($V_{\rm g}$ is the gate voltage) and we conventionally set $V_{\rm g} = 0$ at the charge neutrality point. The parameters that we have used are $b = -2.5eV$, $U = 10eV$, $V = 6eV$.

The generalized master equation

We describe the dynamics of the system with a generalized master equation (GME) for the reduced density matrix ρ. This equation is obtained from the Liouville equation for the full density matrix as a perturbation to the lowest non vanishing order in the coupling to the leads by tracing out the leads degrees of freedom. A generic formulation of the GME for a SET in presence of degeneracies or quasi-degeneracies can be found elsewhere *e.g.*[1] We concentrate here on the range of gate and bias voltages at which the dynamics is restricted to transitions involving the $|6_g 00\rangle$ and $|7_g \ell\sigma\rangle$ many particle states of the benzene ISET.

The seven particle states are spin and orbital degenerate. The general theory of the GME would require a priori to keep a full 4x4 density matrix describing the 7 particle subspace. In presence of parallel polarized leads, though, the coherences between different spin degrees of freedom can be neglected since spin is always conserved by the electrons while travelling through the device. The GME can thus be written in terms of the nine variables collected in the 1x1 matrix ρ^{6_g} and

the two 2x2 matrices $\rho^{7_g\sigma}$ with $\sigma = \uparrow, \downarrow$. Due to the rotational symmetry of the system it is more convenient to refer to another set of variables, namely to describe the dynamics in terms of the occupation probabilities W_6, $\mathrm{W}_{7\sigma}$ and the expectation values of the different projections of the angular momentum for the system. The new set of variables is:

$$\begin{aligned}
\mathrm{W}_6 &= \rho^{6_g}, \\
\mathrm{W}_{7\sigma} &= \mathrm{Tr}\{\rho^{7_g\sigma}\}, \\
\mathrm{L}_{\alpha\sigma} &= \mathrm{Tr}\{L_\alpha \rho^{7_g\sigma}\}, \\
\mathrm{L}_{z\sigma} &= \mathrm{Tr}\{L_z \rho^{7_g\sigma}\}.
\end{aligned} \tag{2}$$

The operator L_z is the generator of the set of discrete rotations around the axis perpendicular to the plane of the benzene molecule that bring the molecule into itself and can be written within the 7 particle Hilbert space spanned by the vectors $|7_g \ell \sigma\rangle$ as $L_z = -\hbar|\ell|\sigma_z$, where σ_z is the third Pauli matrix. The operator L_α generates, in the same space, the discrete rotations around the axis in the molecular plane and passing through the center and the atom closest to the contact α. Finally, the dynamics for the variables introduced in Eq. (2) is given by the equations:

$$\begin{aligned}
\dot{\mathrm{W}}_6 =& 2\sum_{\alpha\sigma} \Gamma_{\alpha\sigma} \left[-f^+_\alpha(\Delta E)\mathrm{W}_6 + f^-_\alpha(\Delta E)\mathrm{L}_{\alpha\sigma} \right], \\
\dot{\mathrm{W}}_{7\sigma} =& 2\sum_{\alpha} \Gamma_{\alpha\sigma} \left[f^+_\alpha(\Delta E)W_6 - f^-_\alpha(\Delta E)\mathrm{L}_{\alpha\sigma} \right], \\
\dot{\mathrm{L}}_{\alpha\sigma} =& -2\Gamma_{\alpha\sigma} f^-_\alpha(\Delta E)\mathrm{L}_{\alpha\sigma} + 2\left\{ \Gamma_{\alpha\sigma} f^+_\alpha(\Delta E) + \Gamma_{\bar\alpha\sigma} f^+_{\bar\alpha}(\Delta E)\cos^2[|\ell|(\phi_\alpha - \phi_{\bar\alpha})] \right\} \mathrm{W}_6 \\
& + \Gamma_{\bar\alpha\sigma} f^-_{\bar\alpha}(\Delta E)\sin^2[|\ell|(\phi_\alpha - \phi_{\bar\alpha})]\mathrm{W}_{7\sigma} - \Gamma_{\bar\alpha\sigma} f^-_{\bar\alpha}(\Delta E)(\mathrm{L}_{\alpha\sigma} + \mathrm{L}_{\bar\alpha\sigma}) + \frac{\sin[2|\ell|(\phi_\alpha - \phi_{\bar\alpha})]}{4}\omega_{\bar\alpha\sigma}\mathrm{L}_{z\sigma}, \\
\dot{\mathrm{L}}_{z\sigma} =& -\sum_{\alpha} \Gamma_{\alpha\sigma} f^-_\alpha(\Delta E)\mathrm{L}_{z\sigma} - 2\tan[|\ell|(\phi_L - \phi_R)](\omega_{L\sigma} - \omega_{R\sigma})(\mathrm{W}_{7\sigma} - \mathrm{L}_{L\sigma} - \mathrm{L}_{R\sigma}) \\
& - 2\cot[|\ell|(\phi_L - \phi_R)](\omega_{L\sigma} + \omega_{R\sigma})(\mathrm{L}_{L\sigma} - \mathrm{L}_{R\sigma}),
\end{aligned} \tag{3}$$

where $\Gamma_{\alpha\sigma} = \Gamma^0_{\alpha\sigma}|\langle 6_g 00|d_{\alpha\sigma}|7_g \ell\sigma\rangle|^2$ is the tunnelling rate at the lead α involving the ground states with 6 and 7 particles. Terms describing sequential tunnelling from and to the lead α are

proportional to the Fermi functions $f^+_\alpha(x) := f(x-\mu_\alpha)$ and $f^-_\alpha(x) := 1 - f^+_\alpha(x)$, respectively, and $\Delta E = E_{6g} - E_{7g} + eV_g$ where E_{6g} and E_{7g} are the energies of the 6 and 7 particle ground states. Finally with $\bar{\alpha}$ we mean the lead opposite to the lead α. By using the expression $|\ell|$ (to be substituted with 2 for the $6 \to 7$ particle transition) we maintained the generality of the equations. The replacement $|\ell| = 2 \to 1$ and the appropriate redefinition of ΔE is enough to treat the $6 \to 5$ transition. Another important generalization concerns the position of the leads. The para ($\phi_L - \phi_R = \pi$) and ortho ($\phi_L - \phi_R = \pi/3$) configuration are also treated within the same equations. In particular one can see that all the terms containing the renormalization frequencies drop from the equations in the para configuration and that the equations for the ortho and meta configuration coincide.

Matrix form of the operator L_α

The explicit form of L_α is given in Eq. (6). We give here its derivation. It is convenient, for this purpose, to choose the arbitrary phases of the states $|7_g \ell \sigma\rangle$ in such a way that the rotation of π around the axis passing through a reference atom M and the center of the molecule transforms $|7_g \ell \sigma\rangle$ into $-|7_g - \ell \sigma\rangle$. In other terms

$$\exp(i\pi \tfrac{L_M}{\hbar}) = -\sigma_x, \tag{4}$$

where σ_x is the first Pauli matrix. The relation is in fact an equation for L_M and the solution reads:

$$L_M = \frac{\hbar}{2} \begin{pmatrix} 1 & 1 \\ 1 & 1 \end{pmatrix}. \tag{5}$$

Eventually we obtain L_α by rotation of L_M in the molecular plane, namely:

$$L_\alpha = e^{-\frac{i}{\hbar}\phi_\alpha L_z} L_M e^{\frac{i}{\hbar}\phi_\alpha L_z} = \frac{\hbar}{2} \begin{pmatrix} 1 & e^{i2|\ell|\phi_\alpha} \\ e^{-i2|\ell|\phi_\alpha} & 1 \end{pmatrix}, \tag{6}$$

where ϕ_α is the angle of which we have to rotate the molecule to bring the reference atom M into the position of the contact atom α.

The spin splitting of the renormalization frequencies

The spin splitting of the renormalization frequencies is obtained from Eq. (7). By introducing the average bare rate $\Gamma = \frac{\Gamma^0_{\alpha\uparrow}+\Gamma^0_{\alpha\downarrow}}{2}$, for simplicity equal in both leads, and using the fact that benzene is paramagnetic we get:

$$\begin{aligned}\omega_{\alpha\uparrow}-\omega_{\alpha\downarrow} = 2\Gamma P_\alpha \frac{1}{\pi}\sum_{\{E\}} \\ \Big[&\langle 7_g \ell\uparrow|d_{M\uparrow}|8\{E\}\rangle\langle 8\{E\}|d^\dagger_{M\uparrow}|7_g-\ell\uparrow\rangle p_\alpha(E-E_{7_g}) \\ +&\langle 7_g \ell\uparrow|d^\dagger_{M\uparrow}|6\{E\}\rangle\langle 6\{E\}|d_{M\uparrow}|7_g-\ell\uparrow\rangle p_\alpha(E_{7_g}-E) \\ -&\langle 7_g \ell\uparrow|d_{M\downarrow}|8\{E\}\rangle\langle 8\{E\}|d^\dagger_{M\downarrow}|7_g-\ell\uparrow\rangle p_\alpha(E-E_{7_g}) \\ -&\langle 7_g \ell\uparrow|d^\dagger_{M\downarrow}|6\{E\}\rangle\langle 6\{E\}|d_{M\downarrow}|7_g-\ell\uparrow\rangle p_\alpha(E_{7_g}-E)\Big],\end{aligned} \tag{7}$$

where one appreciates the linear dependence of the spin splitting on the lead polarization P_α. The first and the third term of the sum would cancel each other if the energy of the singlet and triplet 8 particle states would coincide. An analogous condition, but this time on the 6 particle states, concerns the second and the fourth terms. For this reason the exchange interaction on the system is a necessary condition to obtain spin splitting of the renormalization frequencies and thus the full all-electric spin control.

References

(1) Darau, D., Begemann, G., Donarini, A., and Grifoni, M., Interference effects on the transport characteristics of a benzene single-electron transistor, *Phys. Rev. B* **79**, 235404 (2009).